U.S. DEPARTMENT
OF COMMERCE

TECHNOLOGY
ADMINISTRATION

National Institute
of Standards and
Technology

NISTIR 5568

Carbon Monoxide Production in Compartment Fires – Reduced-Scale Enclosure Test Facility

Nelson P. Bryner
Erik L. Johnsson
William M. Pitts

NISTIR 5568

Carbon Monoxide Production in Compartment Fires - Reduced-Scale Enclosure Test Facility

Nelson P. Bryner, Erik L. Johnsson, and William M. Pitts

December 1994
Building and Fire Research Laboratory
National Institute of Standards and Technology
Gaithersburg, MD 20899

U.S. Department of Commerce
Ronald H. Brown, *Secretary*
Technology Administration
Mary L. Good, *Under Secretary for Technology*
National Institute of Standards and Technology
Arati Prabhakar, *Director*

Ordering

Copies of this document are available from the National Technical Information Services, 5285 Port Royal Road, Springfield, Virginia 22161, at (800) 553-6847 or (703) 487-4650.

Abstract

The formation of carbon monoxide during room or compartment fires has been investigated using natural gas fires burning within a reduced-scale enclosure (RSE), an 0.98 m x 0.98 m x 1.46 m (w x h x d) room with a single door opening centered in the front wall. This series of 125 fires ranging in heat release rate (HRR) from 7 to 650 kW and global equivalence ratio (ϕ_g) from 0.2 to 4.2, respectively, has demonstrated that the upper layer is nonuniform in temperature and gas species, and that upper-layer oxygen is depleted for underventilated fires with high-temperature upper layers. For fires having HRR exceeding 400 kW ($\phi_g > 2$), carbon monoxide concentrations of up to 3.5 percent have been observed in the front portion of the upper layer. Carbon monoxide concentrations in the rear were consistently lower being on the order of 2.0 percent for $\phi_g > 2$. While oxygen concentrations approached zero in both the front and rear of the upper layer for underventilated burning conditions, temperatures were generally 200 °C to 300 °C higher in the front of the upper layer than in the rear. Both the high temperatures and high carbon monoxide concentrations in the front of the upper layer are consistent with oxygen being transported directly into the upper layer as well as entering through the fire plume for the large fires. This oxygen appears to react with unburned fuel to form carbon monoxide, instead of being fully oxidized to carbon dioxide. As the unburned fuel is oxidized, additional energy release occurs which provides an explanation for the higher temperatures observed in the front of the RSE. The exact mechanism for transporting oxygen directly into the front portion of the upper layer is not yet understood.

The results of these RSE fires clearly indicate that higher levels of carbon monoxide can be generated in post-flashover scenarios than suggested by earlier laboratory hood experiments or earlier enclosure studies designed to generate a stable two-layer structure. Current fire models do not adequately simulate the temperature and gas species nonuniformities nor the high levels of carbon monoxide.

Table of Contents

Table of Contents cont'd.

List of Figure Captions

List of Figure Captions cont'd.

List of Figure Captions cont'd.

List of Figure Captions cont'd.

List of Figure Captions cont'd.

List of Figure Captions cont'd.

List of Tables

1.0 Introduction

In 1991 over 27,000 injuries and 4855 deaths [1] were caused by fires in the United States. Recent studies attribute a large percentage of fire injuries and deaths to the products of combustion such as smoke, heat, and carbon monoxide (CO). Smoke and poisonous gases often cause victims to become disoriented, lost, and incapacitated before being overcome by heat or a lack of oxygen. Carbon monoxide has been implicated as a major toxicant by investigations [2,3,4,5] which indicate that more than one half of all fire victims have fatal levels of carboxyhemoglobin in their blood. In an effort to understand how and why carbon monoxide is produced in fires, the Building and Fire Research Laboratory (BFRL) at the National Institute of Standards and Technology (NIST) initiated a project to study the production of carbon monoxide in fires [6,7]. The Carbon Monoxide Production and Prediction (CMPP) study includes nine fundamental and thirteen engineering components. Once a greater understanding is available of how and why toxic levels of carbon monoxide are produced, carbon monoxide production models will be formulated. The incorporation of these production models into realistic fire models, such as HAZARD I [8], will allow strategies to be developed for reducing the number of deaths caused by carbon monoxide.

Previous idealized studies have provided insight into carbon monoxide production by considering the interaction between the fire plume and the upper layer in two-layer compartment fires. Three of the most extensive studies, Beyler [9,10,11], Toner et al. [12], and Morehart et al. [13,14], allowed fires burning in an open laboratory to mix and interact with a heated layer of combustion gases which were collected and contained by hood systems. All three investigations demonstrated that the carbon monoxide levels in the upper layer increase as the upper layer becomes underventilated. Although somewhat fuel dependent, the upper-layer concentrations of CO generally tended to level off at about 2%. Whereas Toner et al. burned only natural gas,

Morehart et al. studied natural gas, ethylene, and propylene fires utilizing a hood which allowed the injection of air directly into the upper layer. Beyler's experiments involved a wider range of liquid, solid, and gaseous fuels including propane, propene, hexanes, toluene, ethanol, and acetone. Beyler examined propane gas fires with theoretical heat release rates ranging from 8 to 32 kW. Beyler collected the combustion gases within an insulated 1 m diameter x 0.48 m deep hood (0.38 m^3). Burning much larger fires, Toner et al. studied natural gas fires with calculated heat release rates ranging from 20 to 200 kW. Using a larger hood system than Beyler, Toner et al. employed a 1.2 x 1.2 x 1.2 m hood (1.7 m^3) to contain the combustion products. Morehart et al. also burned natural gas in fires ranging from 41 to 67 kW, but collected the effluent in the largest hood system. Initially, Morehart et al. employed a non-insulated 1.8 x 1.8 x 1.2 m deep hood (3.9 m^3). Later, in an attempt to increase the upper-layer temperatures to match those of Toner et al., Morehart et al. insulated the outside of the hood. As the additional insulation increased the upper-layer temperature, the concentrations of carbon monoxide also increased slightly.

The temperature of the upper layer began to emerge as a key factor in the production of carbon monoxide. Toner et al. recorded the highest layer temperatures, approximately 600 °C for natural gas, as well as the highest carbon monoxide concentrations, about 2.3%. The higher temperatures of Toner et al. seemed to point towards a temperature dependent kinetic mechanism which might allow higher concentrations (>2%) of carbon monoxide to be generated.

In a re-creation of a 1987 townhouse fire which killed three people in Sharon, Pennsylvania, Levine and Nelson [15] recorded carbon monoxide levels of 8% in the upper layer. These concentrations were much higher than the levels observed in the hood experiments. Levine and Nelson hypothesized that the conditions typically encountered in a post-flashover room, such as the high temperature, low oxygen levels, and fuel-rich stoichiometry, might prove instrumental in producing the high concentrations of carbon monoxide.

It is important to characterize the fire conditions where high levels of carbon monoxide were being generated. The CMPP study endeavors to combine theoretical and experimental components to help understand the fire phenomena allowing the concentration of carbon monoxide to reach levels higher than those observed in the hood experiments.

This report focuses on one of the experimental components, the design, construction and operation of a reduced-scale enclosure (RSE) fire facility. This enclosure is designed to model important experimental characteristics of a fire located within a compartment and provides a convenient experimental platform for the investigation of the layer uniformity, temperature profiles, carbon monoxide production and burnout, and validation of mixing and species production models. For the studies reported here, natural gas is the fuel for burns with heat release rates (HRRs) ranging from 7 kW to 650 kW. Igniting a natural gas fire of greater than 150 kW within the RSE creates post-flashover conditions with flames extending 0.5 to 1.5 m out of the doorway and upper layer temperatures exceeding 600 °C. The temperatures inside the RSE and the CO, CO_2, and O_2 concentrations inside and outside the enclosure are measured at different elevations and positions as the heat release rates are varied.

2.0 Experimental

2.1 Design

The reduced-scale enclosure is designed to be a 40% scale model of a standard room proposed for adoption by the ISO [16] and ASTM [17] for full-scale fire tests. Since the standard room is 2.44 m wide x 2.44 m tall x 3.66 m deep, the RSE internal dimensions are 0.98 m wide x 0.98 m tall x 1.46 m deep (Figure 1). A 0.76 m wide x 2.03 m tall doorway is specified for the

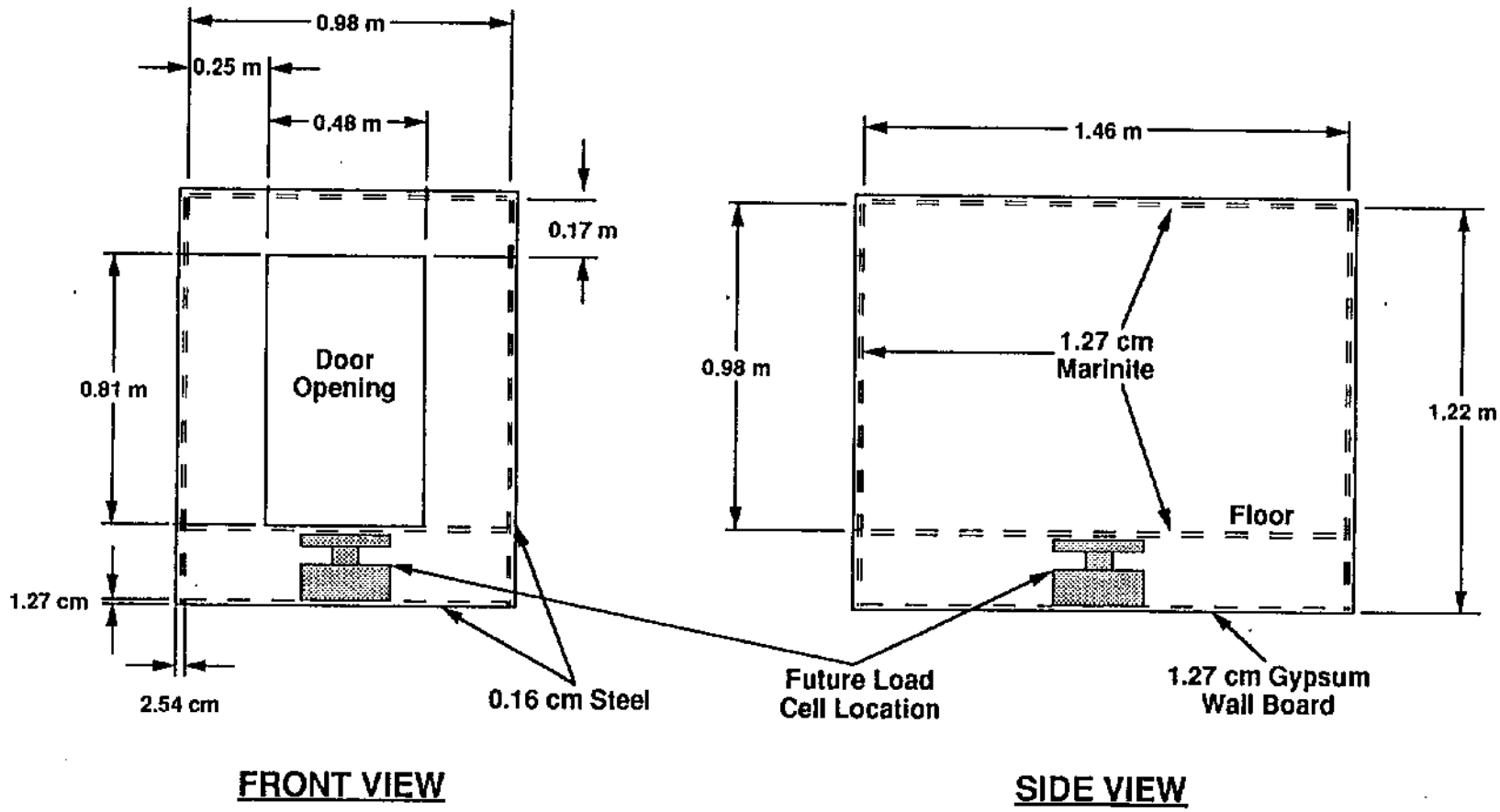

Figure 1. Front and side views of reduced-scale enclosure.

ISO/ASTM test room. The area of the doorway is scaled according to the $Ah^{1/2}$ enclosure ventilation scaling parameter where A is the total area of the ventilation opening and h is the height of the opening [18,19,20,21, and Appendix A]. This results in a 0.48 m wide x 0.81 m tall door for the RSE.

The standard room specifications require the test compartment to be either a framed or a concrete block structure. These requirements were relaxed for the RSE. A rigid steel cage provides a stable framework for the RSE. To reduce the possibility of air leakage into the finished room, the steel frame is lined with steel sheets (Figure 2). Since the ASTM test room doorway wall is lined with calcium-silicate board, it was decided to line the RSE with two layers of calcium-silicate board. A false floor constructed of calcium-silicate board is located 23 cm above the steel-lined floor. The space below the false floor allows for the positioning of a load cell for solid fuel burns which are planned in future (Figure 1). The front and rear walls and frames are removable to allow easy relining of the enclosure.

2.2 Construction

The reduced-scale enclosure was fabricated by in-house machine and welding shops. The steel cage was constructed from 0.64 cm thick x 7.62 cm wide angle stock. The open-ended frame was lined with 0.16 cm thick steel sheets (Figure 2). The front and rear end frames were fabricated from 0.64 cm thick x 10.16 cm wide steel stock. After being assembled, the side walls, ceiling, and front and rear ends of the enclosure were then lined with two layers of 1.27 cm thick Marinite I*, a common calcium-silicate board. The calcium-silicate lining was originally designed to be press-fitted,

*Certain commercial equipment, instruments, or materials are identified in this report to specify adequately the experimental procedure. Such identification does not imply recommendation or endorsement by the National Institute of Standards and Technology, nor does it imply that the materials or equipment identified are necessarily the best available for the purpose.

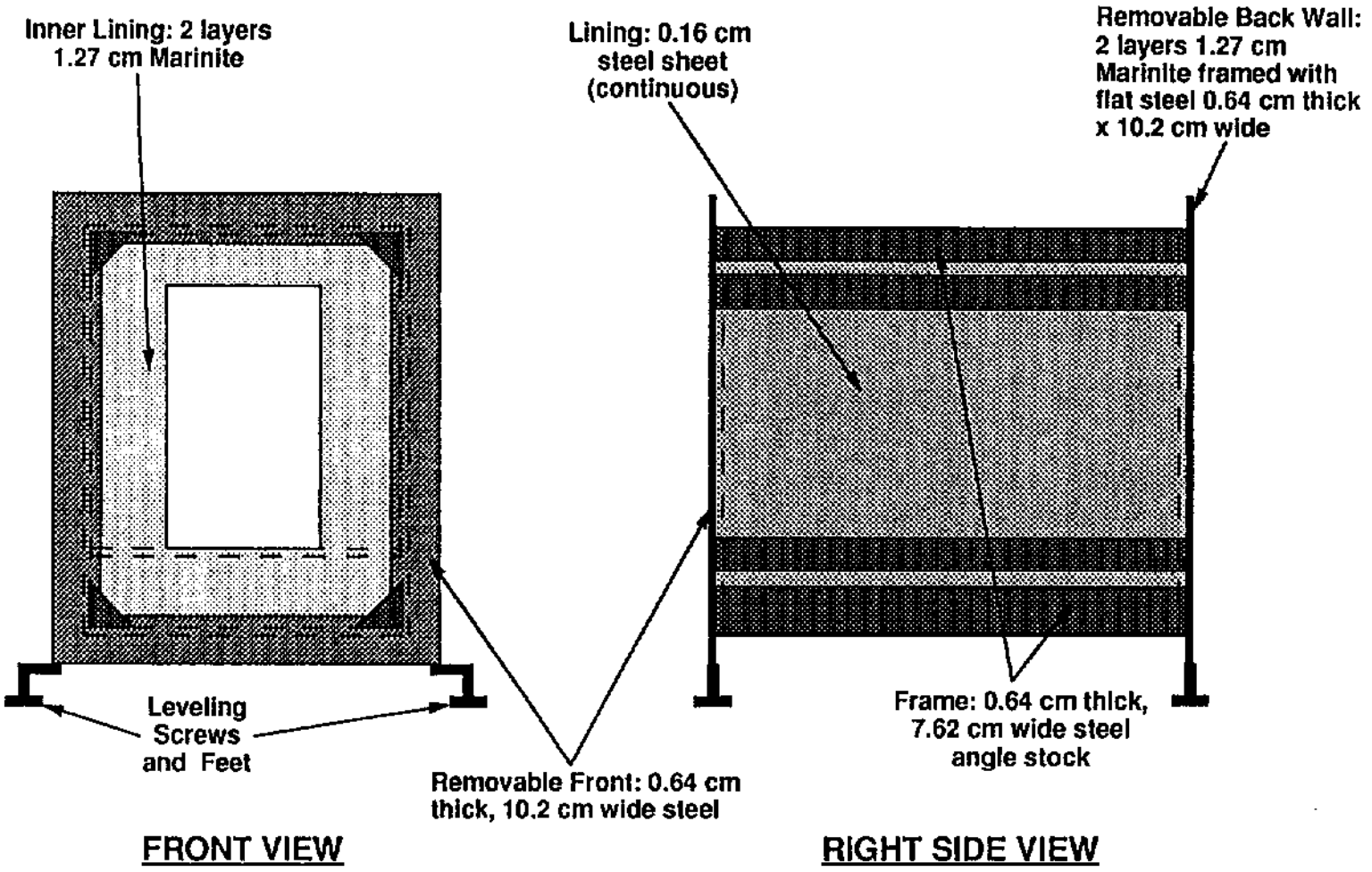

Figure 2. Support frame and steel lining of reduced-scale enclosure.

ie. no screws, into the steel frame in order to reduce the possibility of air leakage, either into or out of the enclosure. The lower floor located below the false Marinite floor was lined with 1.27 cm thick gypsum wall board since it was not exposed to the fire. After installing the 1.27 cm thick Marinite false floor and clamping on the front and back walls, the RSE was positioned under the Furniture Calorimeter (Figure 3) [22,23] located in BFRL's large-scale burn facility, Building 205. Leveling screws and steel wheels, which were welded onto the steel frame, allowed for easy positioning of the RSE.

A set of preliminary burns were performed in the RSE. The Marinite ceiling collapsed after the third natural gas burn. The relatively dense (740 kg/m^3) Marinite ceiling was unable to support its weight over the 0.96 m span. It first cracked and then fell down. Six bolts and washers were added to provide additional support for the ceiling (Figure 4). While these bolts did require drilling through the steel lining which had been designed to prevent air infiltration, each bolt hole was carefully sealed with RTV Silicon Rubber to ensure the integrity of the steel lining. A second series of three natural gas burns resulted in the failure of the side walls of the enclosure. Apparently without the weight of the ceiling to hold the walls in place, the walls worked loose and collapsed. An additional ten bolts and washers, five for each side wall, were added to support the inner layer of Marinite I (Figure 4). These bolt holes were also sealed to maintain an air-tight enclosure. After several additional gas burns, the false floor also began to sag and crack. When the enclosure was relined, three pieces of Marinite were inserted between the false floor and lower floor to support the false floor. The additional support prevented any further sagging and cracking.

A 15.2 cm diameter natural gas burner was normally positioned in the middle, front to back and side to side, of the enclosure (Figure 5). Three adjustable legs supported the glass-bead filled burner 15.2 cm above the Marinite floor. A 1.27 cm diameter black-steel pipe was used to fuel the burner. It was positioned on top of the false floor and extended out the center of the doorway. The

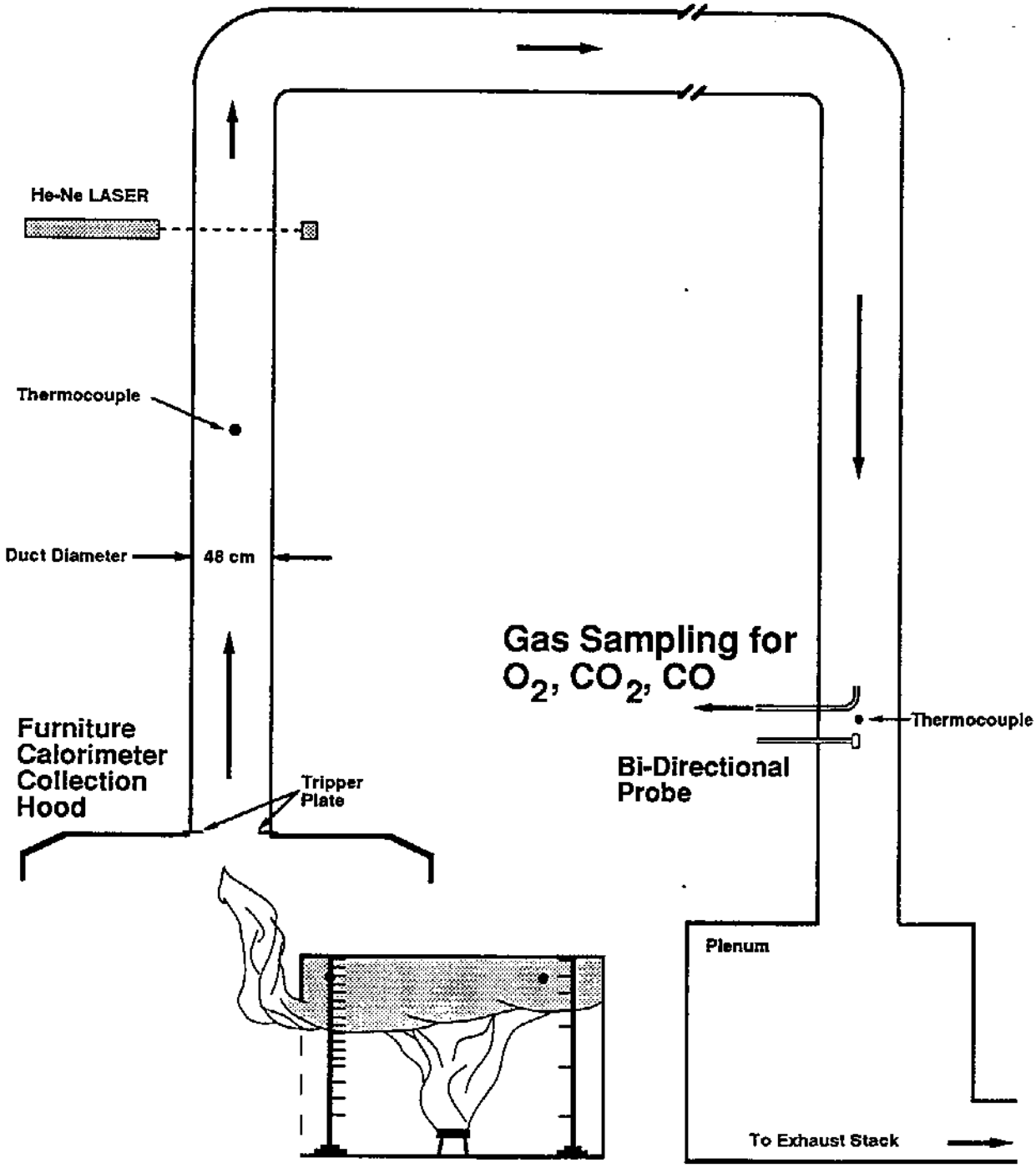

Figure 3. Overall view of reduced-scale enclosure positioned under the Furniture Calorimeter Test Facility.

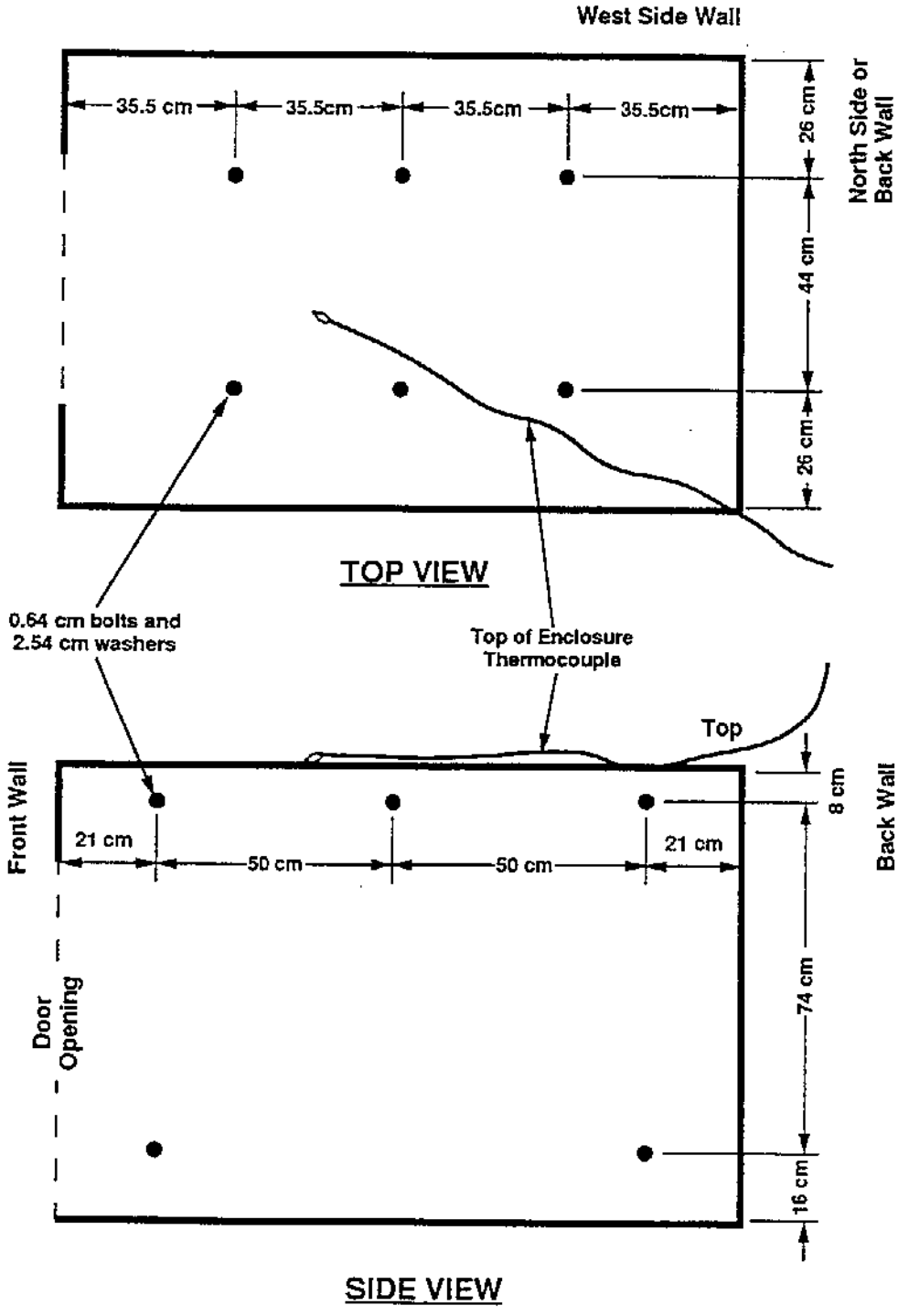

Figure 4. Location of Marinite lining retention bolts.

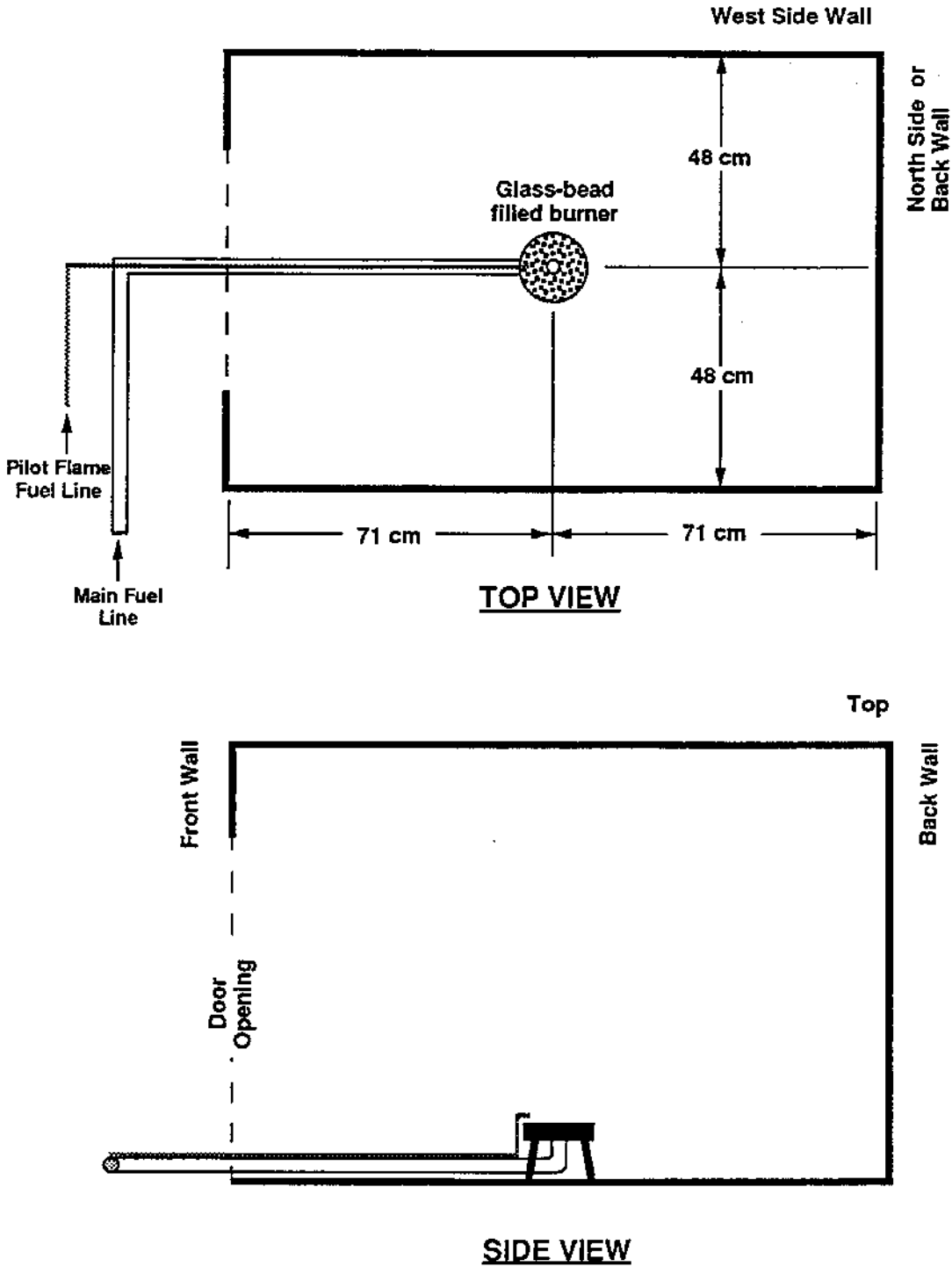

Figure 5. Natural gas burner, fuel line, and pilot flame located within the reduced-scale enclosure.

steel supply pipe was 1.5 m long to allow the burner to be positioned anywhere within the enclosure. A 0.64 cm diameter copper line for a pilot light was installed next to the fuel delivery pipe. The end of the copper tubing was positioned approximately 2.54 cm above and 1.27 cm into the burner. While the other end of the pilot light supply line was connected to a small cylinder of propane, the main gas line was plumbed to flow rate metering instrumentation.

2.3 Instrumentation

2.3.1 Thermocouples

Two thermocouple trees were utilized to monitor temperatures within the enclosure and one tree of aspirated thermocouples was used to track temperatures across the doorway. One of the trees was located in a rear corner while the other was located in a front corner (Figure 6). For all the burns the front tree was positioned 20.3 cm from the front wall and 20.3 cm from the side wall. The rear tree was usually located 20.3 x 20.3 cm from the side and rear walls, but for a limited number of burns the rear tree was positioned 30.5 x 30.5 cm from the side and rear walls. The rear thermocouple tree was relocated further away from the wall in order to investigate possible boundary layer effects. One inside tree consisted of seven thermocouples located 8, 24, 44, 56, 68, 80, and 97 cm above the floor. The other internal tree consisted of 17 thermocouples positioned 8, 24, 40, 44, 48, 52, 56, 60, 64, 68, 72, 76, 80, 84, 88, 92, 97 cm above the floor. For most of the burns, the 17 thermocouple tree was positioned in the front of the enclosure and the 7 thermocouple tree was located in the rear. For a limited number of burns, the tree assignments were reversed. The aspirated tree was positioned in the middle of the doorway and thermocouples were located 8, 23, 38, 53, 69, and 79 cm above the floor. Each thermocouple was fabricated by spot-welding two Chromel-Alumel 0.51 mm diameter wires together using a Weldmatic 1026C Thermocouple Welder.

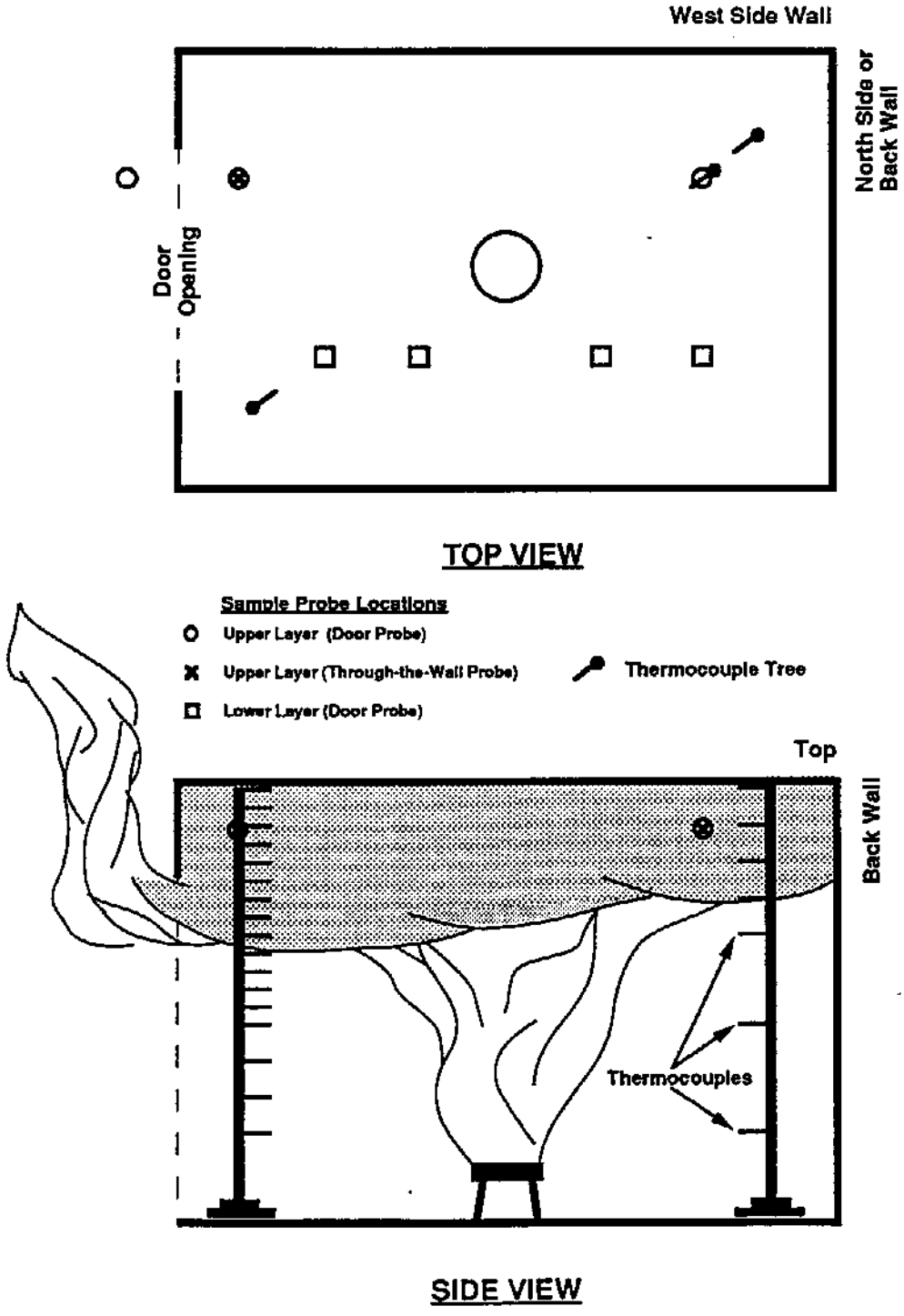

Figure 6. Thermocouple tree locations within the reduced-scale enclosure.

The enclosure top-surface temperature was monitored during and after a burn using a single Chromel-Alumel thermocouple positioned on the outer surface of the steel enclosure top. While this measurement was not intended as a quantitative determination of the RSE temperature, it did provide a general measure of enclosure wall temperature. Since pre-burn top-surface temperatures were about 25 °C to 28 °C, successive burns were not initiated until the enclosure cooled sufficiently to drop the top-surface temperatures to 25 °C to 28 °C.

2.3.2 Sampling Probes

Gaseous combustion products were sampled using four different probes at various positions inside and outside of the enclosure and in the exhaust stack of the Furniture Calorimeter. There were insufficient gas analyzers to measure CO, CO_2, and O_2 levels for all five probes simultaneously. During each burn, at least two probes were sampling from the exhaust stack and within the enclosure, but an additional probe was often positioned at a second location within the RSE. The exhaust-duct sampling probe was fabricated from a 30.5 cm long piece of 0.95 cm diameter copper tubing. A 90-degree bend was placed 7.6 cm from the tip of the probe. This uncooled probe was then positioned on the centerline with the tip opening directed into the flow of the exhaust duct (Figure 3). The probe was installed far downstream of the collection hood to allow the combustion gases to mix thoroughly before being sampled.

The combustion gases inside and outside the enclosure were sampled using four probes of three designs: a) two 191 cm long uncooled double-walled stainless steel probes, b) a 48 cm long uncooled double-walled stainless steel probe, and c) a 167 cm long water-cooled steel outer wall and stainless-steel inner wall probe. For the early series of gas fires, a 191 cm single uncooled double-walled probe was used to sample the upper-layer gases within the enclosure. Inserted through the doorway, this probe was long enough to reach all points within the enclosure. After an additional

set of gas analyzers was obtained, a second long uncooled double-wall probe was constructed. With both probes operational, two locations within or outside the RSE could be simultaneously monitored. Since both probes were uncooled, there was concern about the combustion gases reacting within the sample probe as the gases were transported to the analyzers. When each of the uncooled long probes sampled in the upper layer, the tip and approximately 15 cm of tubing were located within the hot upper-layer combustion gases, after which the probe then angled down passing through the interface between the upper and lower layers before emerging out the doorway. Particularly for the fuel-rich fires, there was often a flame sheet observed at the layer-interface location. Thus, there was a possibility that the sampled gases were being heated significantly as the gases were drawn through the portion of the probe in the flame sheet. In order to avoid having the probe pass through the flame sheet, access holes, front and rear, were drilled through the side wall, through which a 48 cm-long double-walled probe was then inserted. This probe was essentially a shortened version of the longer uncooled probes. The shorter probe could be positioned in the upper layer near the ceiling in either the front or rear of the RSE. Combustion gases extracted via this "through-the-wall" probe did not pass through a flame sheet on the way to the gas analyzers.

While the short through-the-wall probe addressed flame sheet concerns, the sampled combustion gases were still hot and possibly reacting until the gases reached the cold traps used to remove water. Other researchers, including Seery and Zabielski [24], Orloff et al.[25], and Schoenung et al. [26] have used cooled and/or low pressure probes to quench combustion gases in sampling probes. A water-cooled version of the long uncooled probes was fabricated. The water jacket around the sample tube successfully cooled the sample gases from 800 to 1000 °C (600 kW heat-release-rate fire) at the tip to approximately 100 °C at the base of the probe. Such a temperature reduction should be sufficient to quench all chemical reactions.

The two 191 cm uncooled sample probes were fabricated using 304 stainless steel tubing. Each probe was constructed by inserting a 0.95 cm diameter (OD) tube inside a 1.27 cm diameter (OD) tube (Figure 7). While both the inner and outer tubes were 167 cm in length, the tubes were offset by 24 cm to allow for the positioning of a thermocouple near the tip and installation of valves at the base. A Chromel-Alumel thermocouple formed from two 0.51 mm diameter wires welded together was threaded between the two stainless steel tubes and positioned near the sample probe tip to monitor gas temperature.

For the 167 cm-long water-cooled sample probe, a 2.13 cm diameter (OD) galvanized steel pipe formed the outer cylinder with a 0.95 cm (OD) 304 stainless-steel tube 167 cm long forming the inner tube (Figure 8). Water was circulated through the annular area between the cylinders via tee fittings near the probe base and tip. Inlet water temperatures were typically 18 °C and a 600 kW heat-release-rate fire produced water exit temperatures of approximately 60 °C for flow rates of 3.0 l/min of water. A Chromel-Alumel thermocouple similar to the one mounted in the uncooled long probe was positioned 10.2 cm from the tip and centered in the inner tube. The thermocouples wires exited through a second tee in the sample line.

For the short uncooled probe, two 45.7 cm lengths of 304 stainless steel tubing, 1.27 and 0.95 cm diameter, were fabricated into a sample probe for through-the-wall sampling (Figure 9). Except for being shorter, the through-the-wall probe was similar to the long uncooled probe. A slight curvature or bend was added to the short probe to allow it to sample close to the ceiling. A Chromel-Alumel thermocouple was located 10.2 cm from tip. As in the long uncooled probes, the thermocouple wire was routed out through the annular area between the tubes.

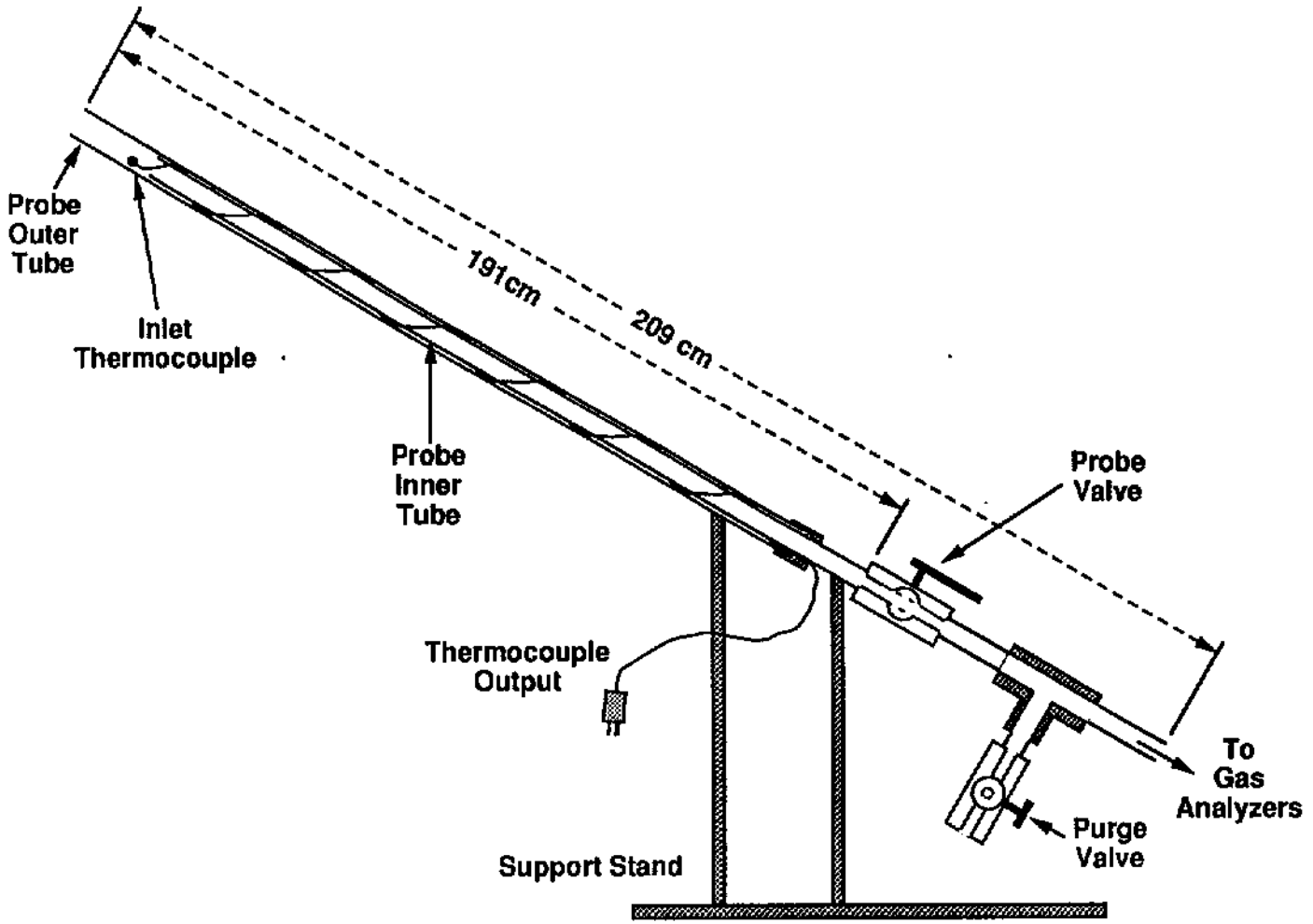

Figure 7. Uncooled through-the-door sample probe.

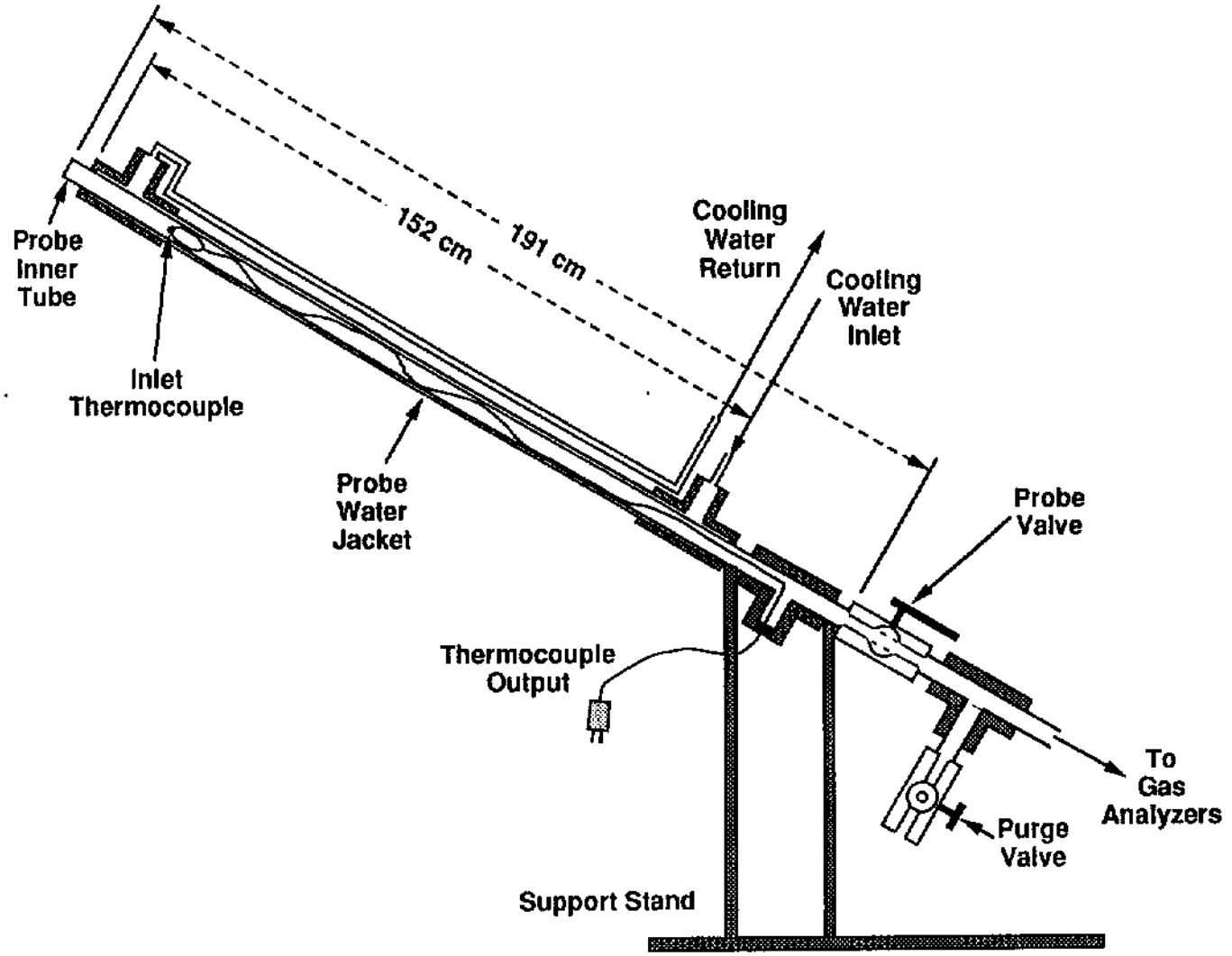

Figure 8. Water-cooled through-the-door sample probe.

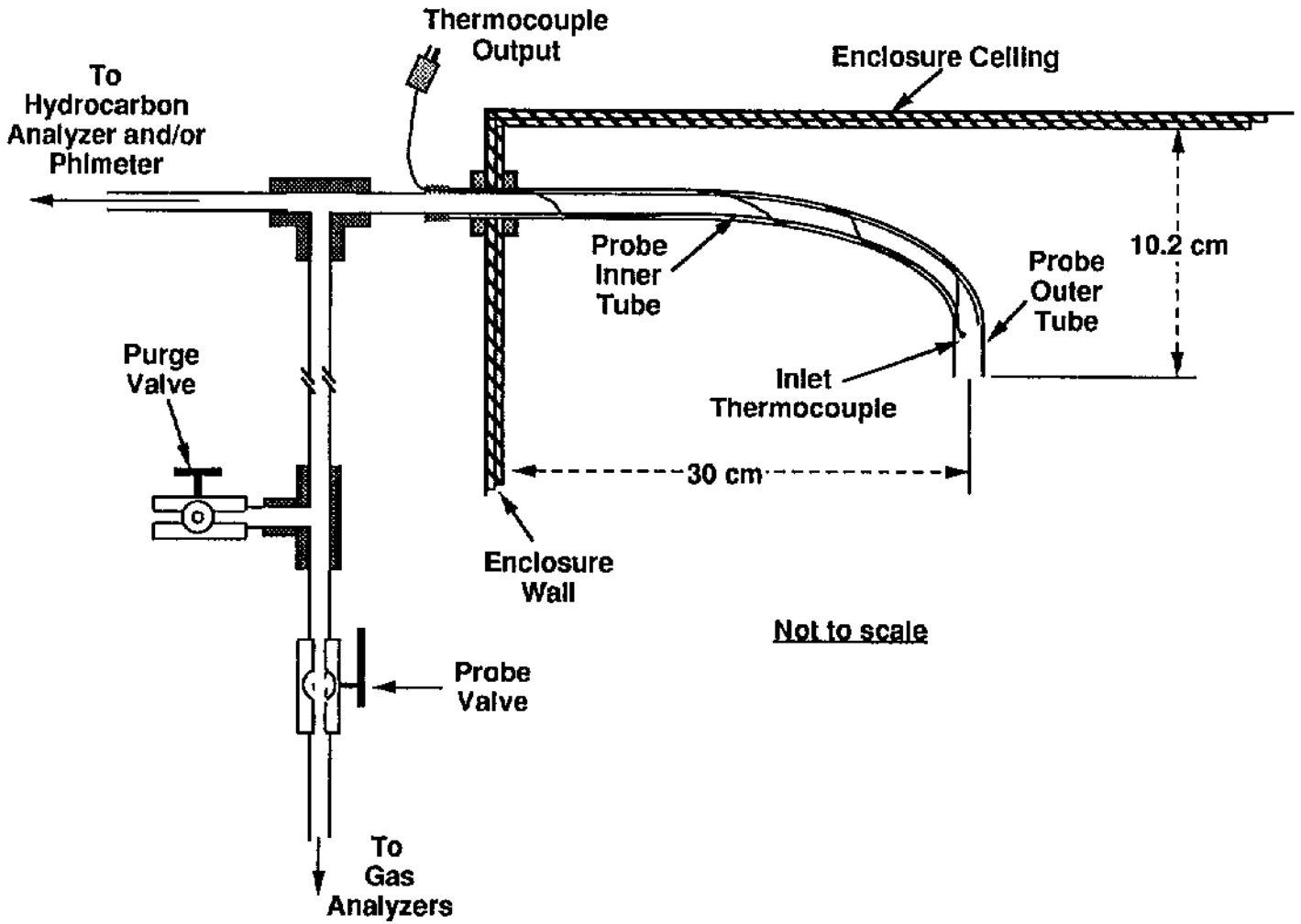

Figure 9. Short, uncooled, through-the-wall sample probe.

2.3.3 Sample Lines

Each sample probe was connected to a series of three cold traps via a set of valves and 5 m of 0.95 cm (OD) diameter soft copper tubing (Figure 10). Diaphragm pumps were used to draw gases through the probes for conditioning and sampling. The ball valves at the base of the enclosure probes allowed for leak-testing of sample lines, timing of delays between probes and analyzers, and purging of the sample lines. For leak-testing, a cylinder of span gas, a gas of analyzed composition, was introduced into the tee at the probe base. With the sample pump on, span gas pressure was adjusted until excess span gas flowed out of the probe tip. An air leak into the sample line resulted in the dilution of the span gas and lowered the concentration recorded by the gas analyzer. The integrity of the sample lines (i.e. no air leaks) was verified each time the gas analyzer measured the full or undiluted span gas concentration.

After completion of a successful leak-test and before disconnecting the span gas, the sample delay time was measured. This is the time required for the combustion products to travel between the probe and the gas analyzers. Since each group or bank of gas analyzers employed a different system composed of a sample probe, sample line, and cold traps, each analyzer bank had a different delay time. These time delays were incorporated into the data reduction algorithm to allow each analyzer bank to be placed on the same time line. Typically, the same span gas pressures and flow rates used for the leak-test were used for measuring the delay times. The process of determining the sampling delays began with the recording of background levels with the span gas off and the sample pump pulling air through the probe, lines, and cold trap. At time zero the span gas valve was opened and the span gas began to flood the sample lines with an excess flowing out the probe tip. The times at which each analyzer bank began to respond and the time required to reach full span-gas concentration were recorded. This process of obtaining backgrounds and measuring delay times was usually repeated three times to allow the initial response time and full concentration time to be

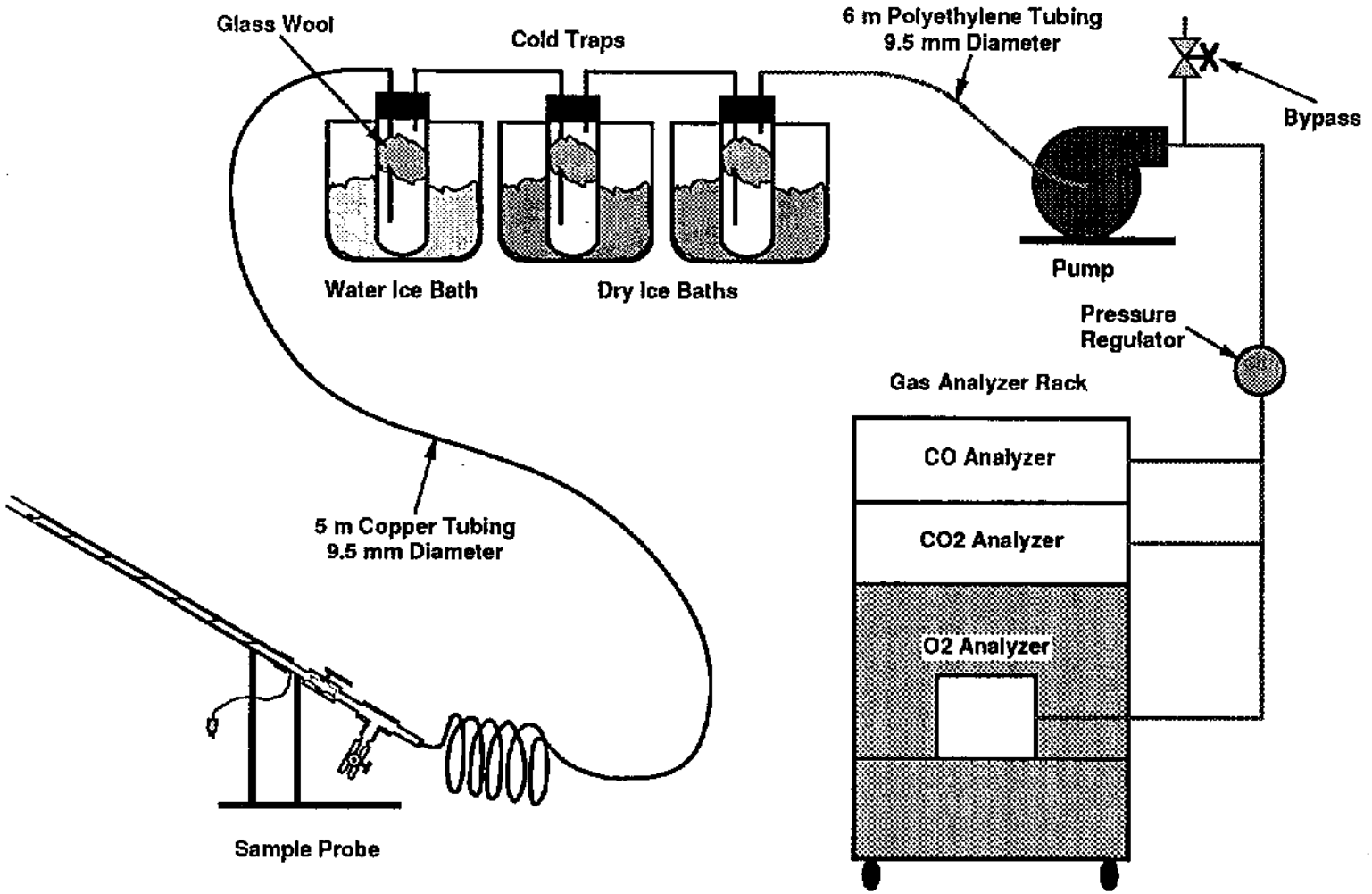

Figure 10. Gas sampling and conditioning equipment.

averaged. The ball valves and tee combination also allowed water and particulate material to be purged out of each sample line and probe. After every other burn, the sample lines were disconnected at the cold trap and any accumulated ice was removed. In addition to removing the ice, the particulate filter media, 8 micrometer diameter glass fibers, was replaced. High pressure air, approximately 550 kPa, was introduced into the sample line connection at the trap. With the probe tip valve closed the condensation and soot were blown out the tee. After the sample line was cleared, the probe valve was opened and the tee valve closed. The high pressure air was then used to blow out the probe tip. Most of the soot and all of the water were blown out of the tee in order to ensure that water and soot did not cover the thermocouple bead.

For each sample line a pair of dry-ice traps were initially employed to remove water from the gas sample. Occasionally, after a pair of high heat release fires (500+ kW), sufficient water accumulated and froze in a trap to cause the glass to fracture. To prevent this, an additional cold trap using water ice was inserted into each of the enclosure sample lines before the dry ice traps to condense some of the water before the gases reached the dry ice traps (Figure 10). This modification prevented further fracturing of the traps.

2.3.4 Gas Analyzers

During each burn, instrumentation monitored the concentrations of carbon monoxide, carbon dioxide, and oxygen in the RSE as well as the exhaust stack. Typically the analyzers were grouped in a rack or bank of three instruments including a CO, a CO_2, and an O_2 meter. One rack was dedicated to the exhaust stack sample probe and another bank was assigned to the sample probe in the enclosure. As the project advanced, additional instrumentation was incorporated to upgrade older, less reliable gas analyzers, to provide a second rack for sampling within the enclosure, and to allow preliminary measurements of total unburned hydrocarbons and local equivalence ratio. The

sampling system also permitted bag samples to be collected for off-line analysis by gas chromatography.

During the early phases of the project, both the carbon monoxide analyzers and the carbon dioxide instruments were Mine Safety Appliance Model 303 LIRA non-dispersive infrared analyzers. The LIRAs employ Luft-cell technology and are dual optical pathlength instruments. Since dual-pathlength analyzers have both a sample path and a reference path, they have a potential to drift. As the LIRA analyzers began to suffer operational problems due to their advanced age, they were phased out and new Maihak DEFOR analyzers were placed in service. These Maihak instruments had several advantages over the older analyzers. The DEFOR analyzers are also non-dispersive infrared analyzers, but utilize a single optical path design which offers less potential for drift. While the older LIRAs have a single range of 0 to 10% carbon monoxide analyzers, the DEFORs have dual ranges of 0 to 2% and 0 to 10%. The low range allows better resolution for low concentrations while automatic range switching allows the higher range to be available when required. Analog outputs from the LIRAs were non-linear, thus requiring additional data analysis while the signals from the DEFORs were linearized. Flow rates to the LIRAs were 3 l/min at approximately 34.5 kPa (5 psi). The sample pumps were designed to maintain at least 34.5 kPa and a pressure relief device bled off excess pressure. The DEFOR analyzer flow rates were set at 1.5 l/min and the sample gases were regulated at 20.7 kPa (3 psi). For the DEFOR instruments, a bypass valve was located after the pump and before the pressure regulator to vent excess gas.

Each instrument rack included a Servomex 1100 or Taylor 580A oxygen analyzer. Both models use the paramagnetic properties of oxygen to determine the concentration of oxygen in the sample gas when compared to a reference gas. In these experiments filtered room air was used as the reference gas. While the Taylor instruments do not utilize barometric pressure compensation, the newer Servomex analyzers do automatically compensate for changes in ambient atmospheric

pressures. The Taylor analyzers were operated at flow rates of 3 l/min at 20.7 kPa and the Servomex instruments were operated at 0.6 l/min at 490 PA.

A total unburned hydrocarbon analyzer, a Rosemount Analytical Model 402A, was connected to the uncooled through-the-wall probe for later burns. This instrument uses a small hydrogen burner and a flame-ionization detector (FID) to monitor unburned hydrocarbon species. The sample line between the probe and the instrument was heated to prevent condensation of heavier hydrocarbon species. Methane was used to calibrate the analyzer before each burn. Since soot or particulate carbon interferes with the FID, it was necessary to filter the gas sample before it reached the FID. By calibrating the sample flow rate through the unburned hydrocarbon analyzer and by weighing the filter before and after each burn, a rough measure of the soot concentration was obtained.

A second instrument, dubbed the phi-meter, was also connected to the short uncooled probe. The phi-meter was designed and developed at BFRL by Babrauskas et al. [27] to make local measurements of the equivalence ratio. The equivalence ratio, often denoted by the Greek letter phi, ϕ, is defined as the ratio of mass derived from fuel to that from air normalized by the stoichiometric fuel-to-air ratio required for complete combustion. Since the fuel-to-air ratio was only sampled at one specific location, the tip of the probe, the phi-meter provided only the local equivalence ratio, ϕ_ℓ. Various types of equivalence ratios have been utilized by other researchers [9,11-13,28,29, and 30]. The phi-meter continuously adds oxygen to a small sample stream of hot combustion gases. The sample gases mixed with the oxygen are pulled through a platinum wire gauze in a high-temperature tube furnace, where the unburnt fuel and products of incomplete combustion are completely oxidized. Three oxygen concentration measurements were required to determine the equivalence ratio: the oxygen concentration in ambient air, the oxygen concentration with added oxygen while sampling ambient air, and the oxygen concentration while sampling the combustion products. The first two oxygen concentrations correspond to "zero" and "span" type measurements.

Babrauskas et al. derived the relationships between the three oxygen concentration measurements and the equivalence ratio. The phi-meter typically sampled gases drawn from the same short uncooled probe as the total unburned hydrocarbon analyzer.

Combustion gases were analyzed off-line for hydrogen for a limited number of later burns by collecting grab-bag samples. A tee, which was inserted after the pump but before the gas analyzers, allowed the filling of 2 liter Tedlar sample bags. During a designated burn, several bags were filled, time of collection recorded, and sealed. Later, the bags were analyzed using a HP 5890 Gas Chromatograph with a 183 cm long by 0.32 cm diameter stainless steel column packed with washed Poropak N of mesh size 80/100. The chromatograph utilized a thermal conductivity detector and used nitrogen as the carrier gas. This was the same type column utilized by Morehart et al.[12] for measuring hydrogen in flame gases.

2.3.5 Gas Flow Metering

Natural gas at a pressure of 103.4 kPa was plumbed through a set of valves, a diaphragm test meter (DTM), a rotameter, pressure gauges, and a pressure regulator (Figure 11). Composition, specific gravity, and heat of combustion for the natural gas were obtained by contacting the local gas supplier (Appendix B). The mass-flow rate of natural gas was calculated from the DTM and the rotameter. Since the DTM is a volume displacement device, the mass-flow rate was calculated for a specific pressure, temperature, and volume by recording the period required to flow a known volume. The rotameter is a mass-momentum device and the calculations of the flow rate are more complex. Relationships provided by the manufacturer [31,32] were used to calculate the mass flow rate (Appendix C). Three rotameters, 0 to 50, 1 to 200, and 0 to 850 l/min, were necessary to cover the range of flow rates for the fire sizes investigated. The rotameter provided a visual method to monitor continuously the flow rate via the position of the ball float on the coarse scale. This

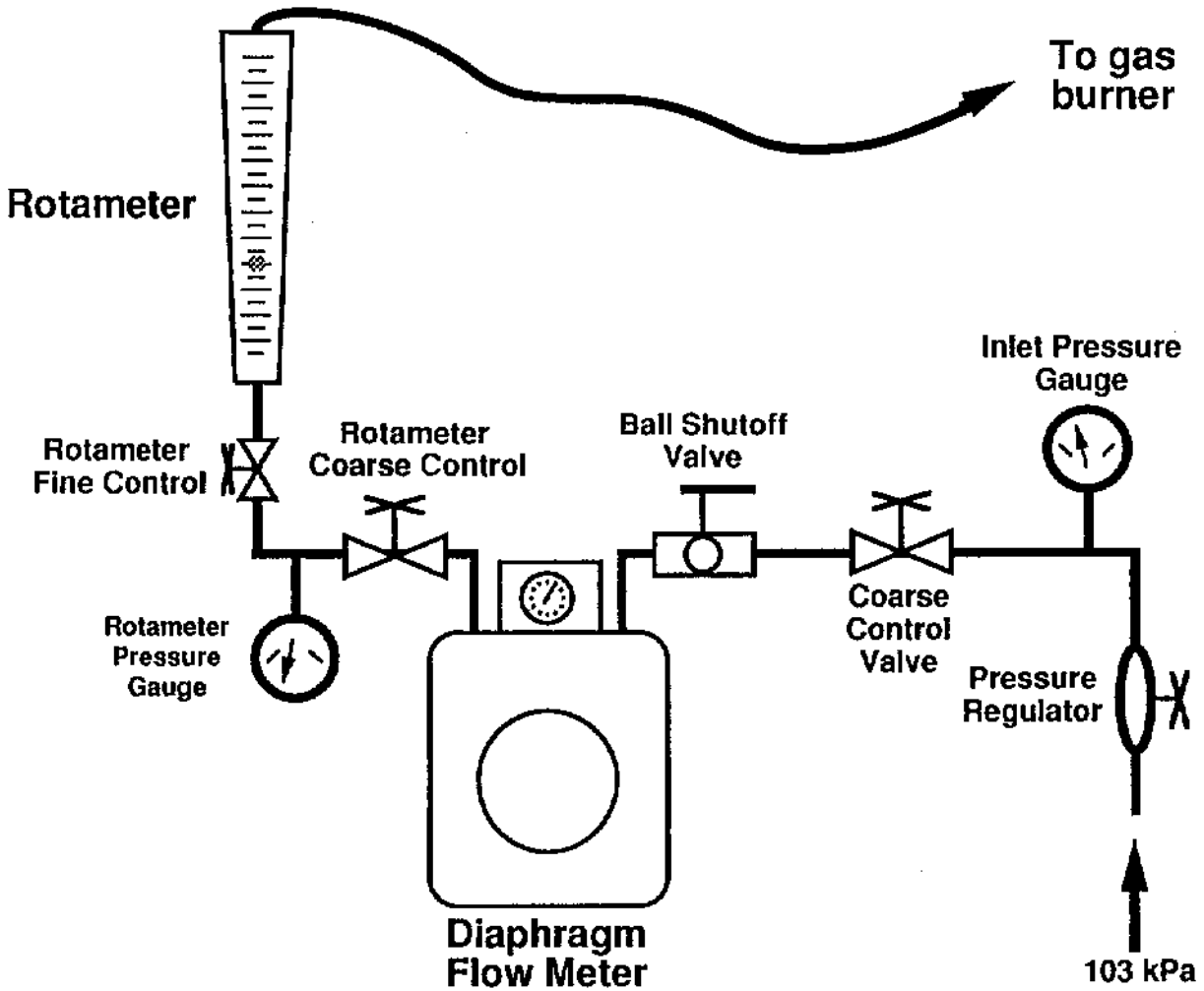

Figure 11. Natural gas flow rate metering equipment.

instantaneous visual reading allowed quick adjustment to a specific flow rate, but was not as reproducible or accurate as the DTM. Since the DTM required 10 to 180 seconds (depending on the fire size) to displace the desired volume, the DTM provided an integrated sum over the entire timed period. The time delay necessary to obtain the integrated DTM value made it very difficult to use the DTM to make fine adjustments to the flow.

Flow rate was coarsely set using a primary flow control valve and then fine tuned with the rotameter needle valve while observing the position of the rotameter float. During a typical fire, 4 or 5 timed DTM volumes, either 70, 140, or 280 l, were recorded. The rotameter float position and pressure drop across the rotameter were also recorded during the timed volumes. Inlet gas line pressure was recorded and used as the pressure within the diaphragm test meter. The mass rates calculated from the DTM and the rotameter differed by 5 to 30 percent. Most of the uncertainty was attributed to the difficulty in reading the coarse scale on the rotameter and fluctuations in the gas supply pressure (see Uncertainty Analysis in Section 3.11). For the early fires, inlet pressure for the natural gas sometimes varied over a range of 13.8 to 20.7 kPa during a single burn. A pressure regulator was later installed in the supply line to minimize the inlet pressure fluctuations.

2.3.6 Pressure Transducer

The pressure differential across the enclosure door was monitored using a Datametrics Barometer with a 0 to 1330 Pa range. While one side of the pressure cell was open to ambient pressure, the other side was connected via 0.64 cm copper tubing to the pressure probe tip inside the enclosure. The pressure probe tip entered through the front wall on the east side of the door and was positioned 2.54 cm into the room at a position 2.54 cm above the floor.

2.3.7 Flashover Tests

A qualitative test, which was loosely patterned after the crumpled newsprint flashover test of the ASTM room [17], was used as a crude measure of the thermal radiation levels on the enclosure floor. The time required to ignite two crumpled balls of paper and a flat sheet of paper were recorded. Two sheets of 21.6 cm x 27.9 cm white bond paper were crumpled into balls and placed on the floor 30.5 cm from the burner center. One sheet was compacted rather loosely, while the second sheet was packed rather tightly. In addition to these two balls, referred to as less crumpled (LC) and more crumpled (MC), a 7.6 cm x 21.6 cm piece of white bond paper was positioned 21.6 cm x 21.6 cm from the east and south walls and held flat by four pennies. Although the radiation never reached levels high enough to melt solid copper pennies, the radiation levels were high enough to deform or partially melt copper-plated zinc pennies. Copper and zinc have melting points of approximately 1100 and 420 °C, respectively.

2.4 Sample Probe Locations

Combustion gases were sampled at two "standard" locations within the upper layer and one location just outside the doorway (Figures 12 and 13). For a limited number of fires, the lower layer was sampled at four locations (Figure 14) and the upper layer was mapped vertically (Figure 15) in the front of the enclosure and horizontally (Figure 16). The RSE was positioned so that the wall with the door opening was the south wall. As one stood facing the doorway and looking into the enclosure, most of the gas sampling was done on the left or west side of the enclosure at either the front or rear corners of the upper layer. The front location was 10 cm inside the door or south wall, 29 cm from the west wall, and 10 cm down from the ceiling. The rear location was 29 cm x 29 cm x 10 cm from the north, west, and ceiling, respectively. The probe location in the flame sheet outside

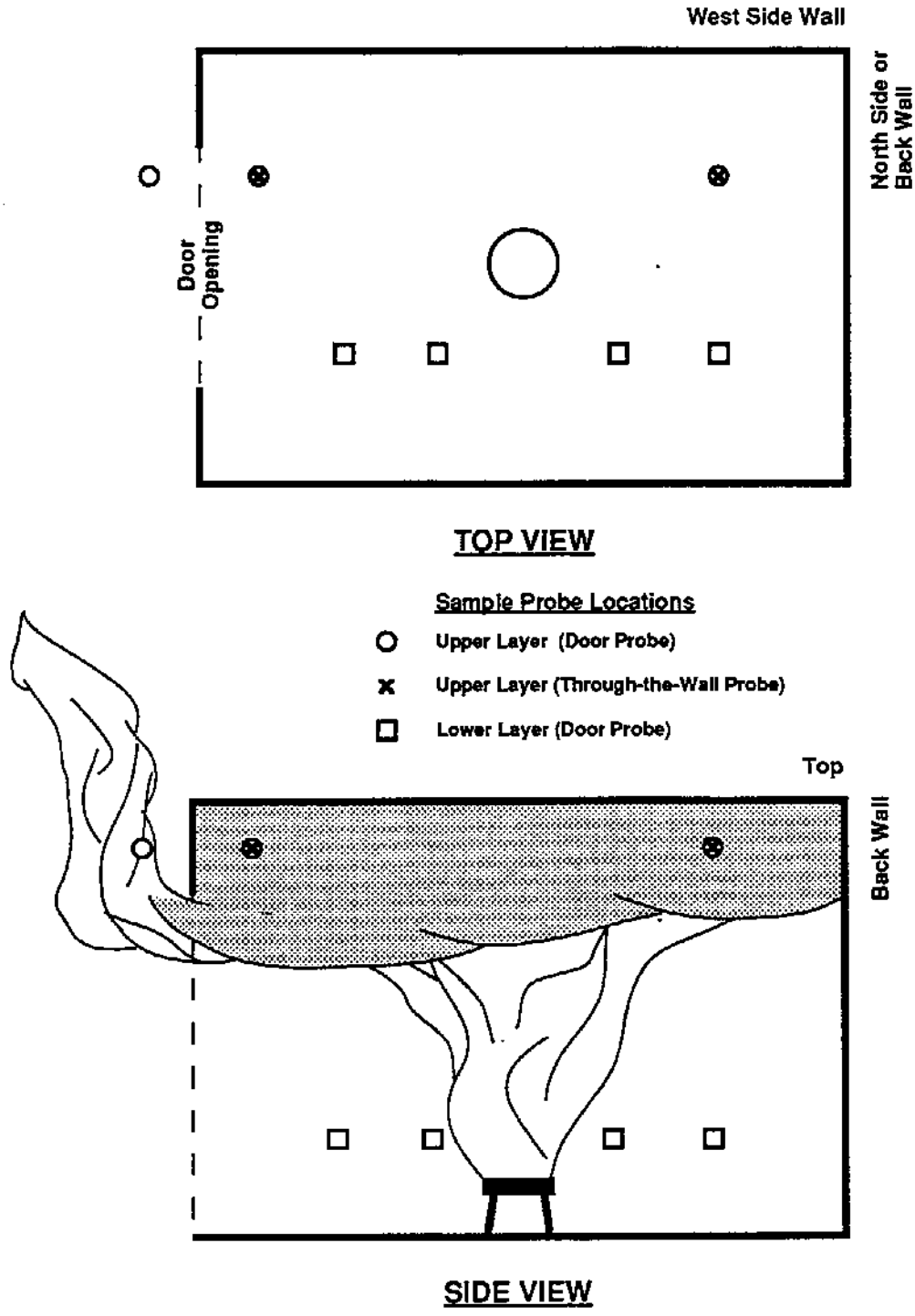

Figure 12. Probe locations for sampling gases in reduced-scale enclosure.

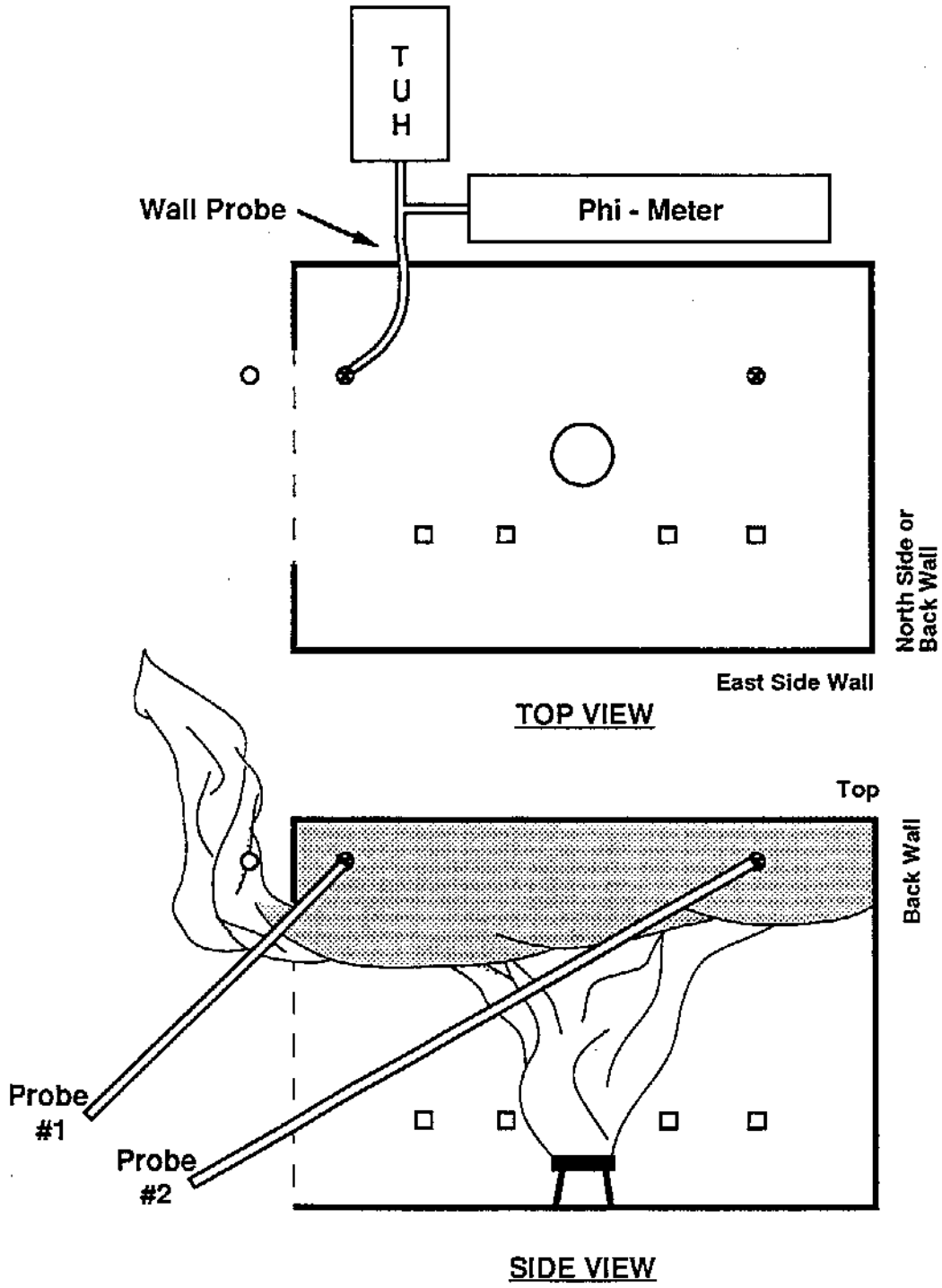

Figure 13. Probes sampling upper-layer gases.

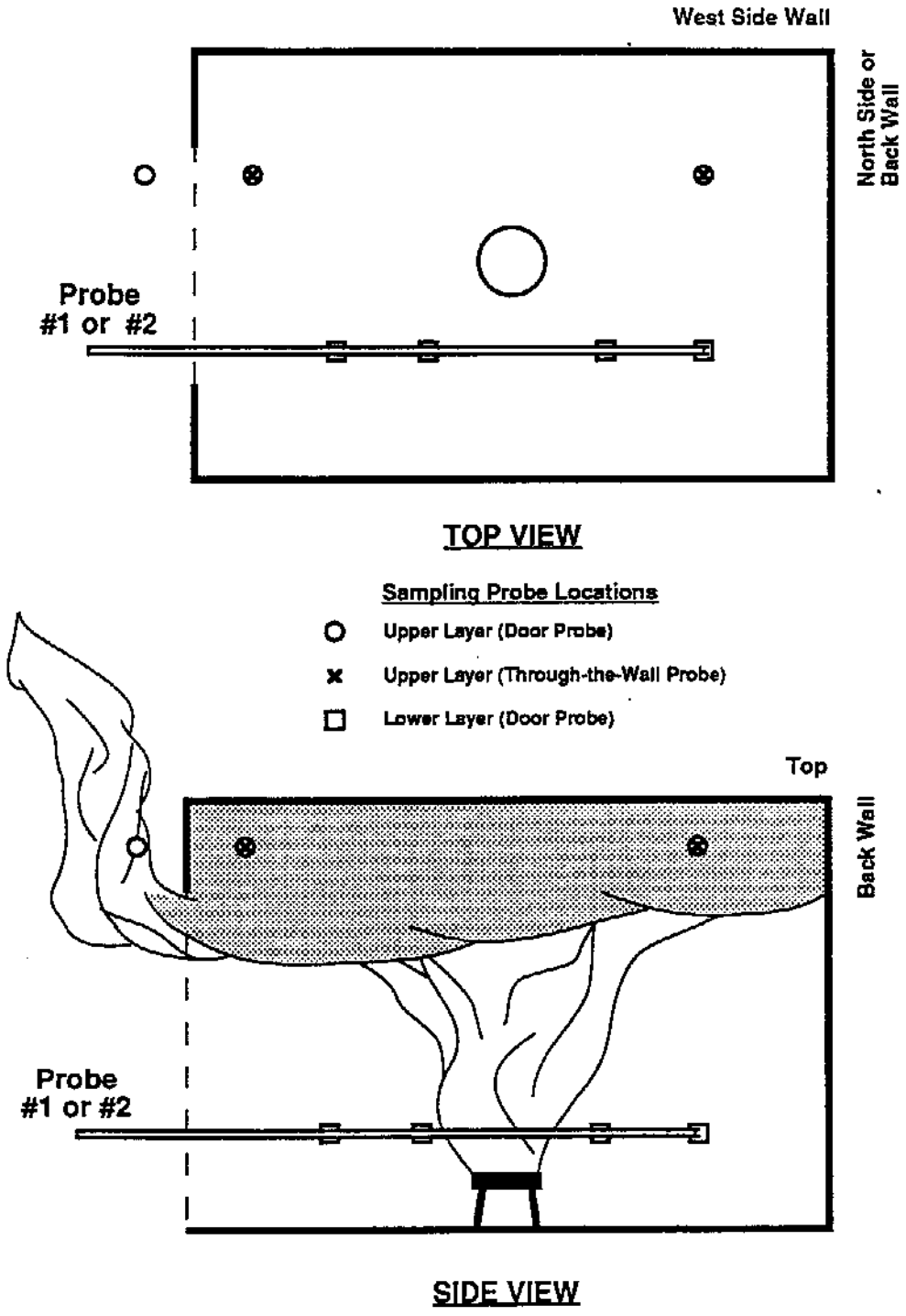

Figure 14. Probes sampling gases in lower layer of reduced-scale enclosure.

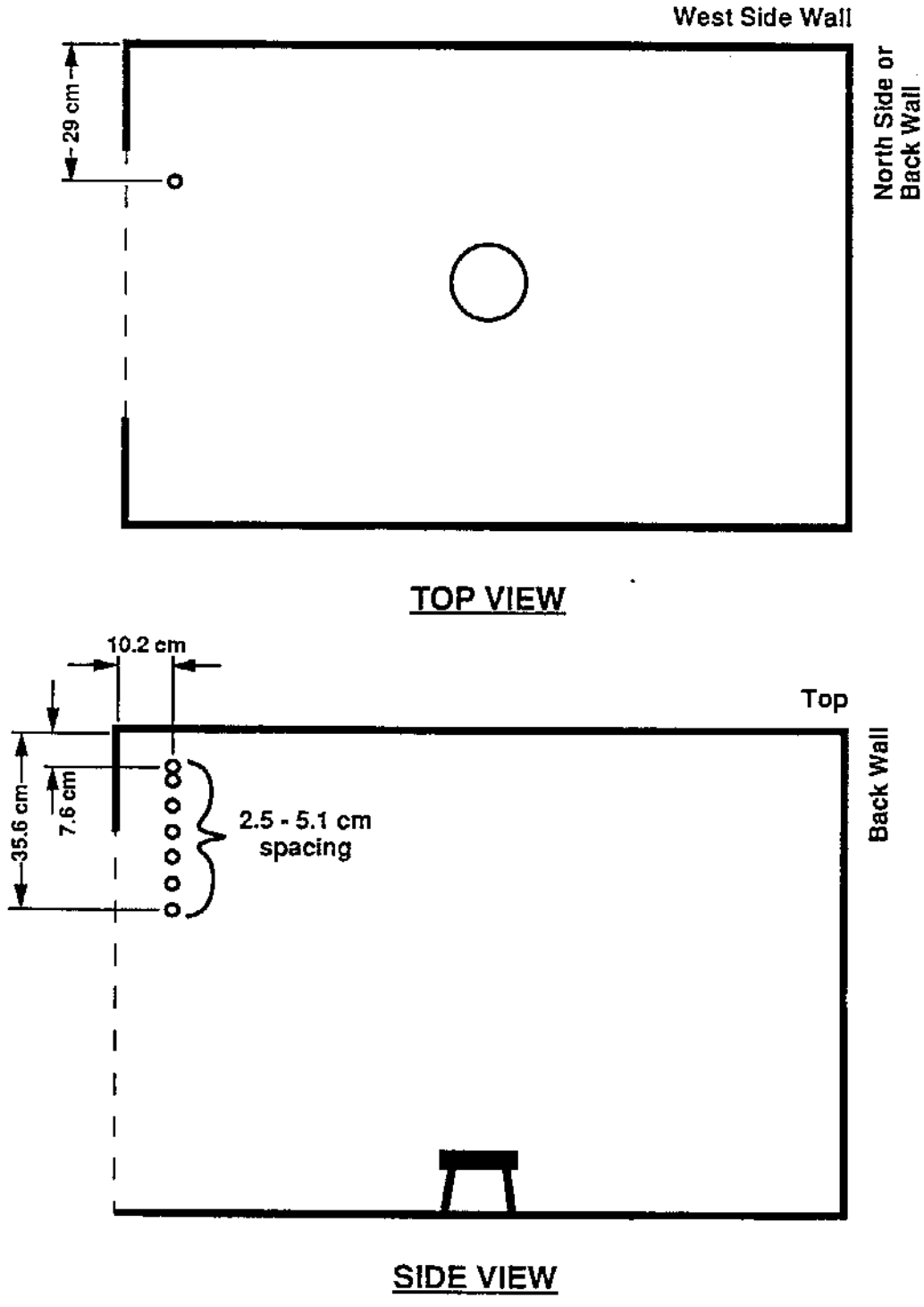

Figure 15. Vertical mapping sample locations.

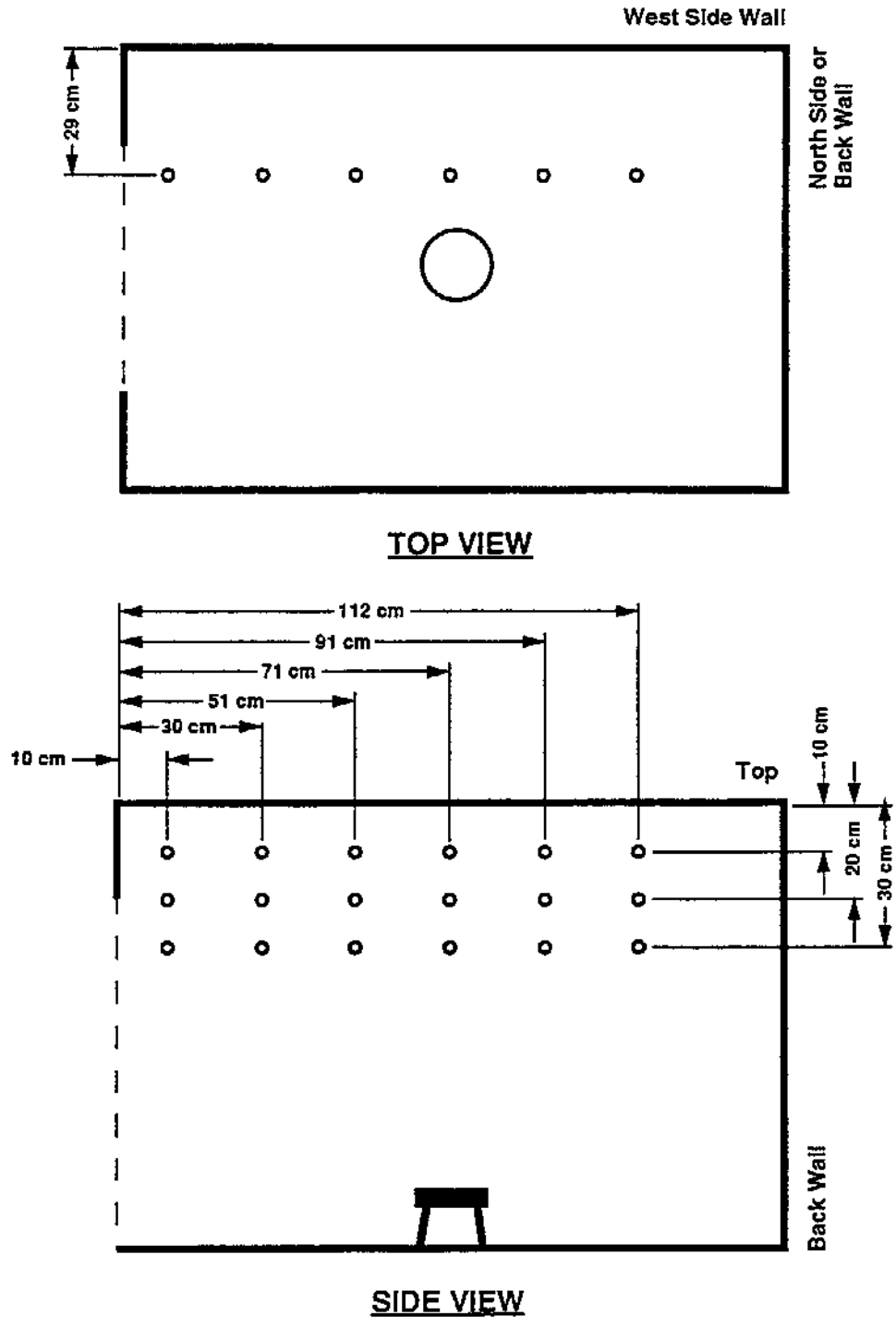

Figure 16. Horizontal mapping sample locations.

the door was the same distance from the enclosure ceiling and west wall, 10 cm and 29 cm respectively, but was located 10 cm from the south wall.

While the uncooled through-the-wall probe sampled at only two positions, the front and rear corners; both the cooled and uncooled long probes were positioned at many locations inside and one location outside the enclosure. The long probes could also be moved to different locations during a single fire. In this way it was possible to sample or map gas concentrations at multiple locations, typically the same distance from two surfaces, but a variable distance from a third surface. For example, during a vertical mapping run, the probe was positioned 10 cm x 29 cm from south and west walls, but adjusted to positions located 10, 15.2, 20.3, 25.4, 30.5, 35.6, and 40.6 cm from the ceiling (Figure 15). During a horizontal mapping run, the probe was located 10 cm from the ceiling and 29 cm from the west wall, but moved 112, 91, 71, 51, 30, and 10 cm from the south or front wall. Separate horizontal mappings were conducted at 10, 20, 30 cm from the ceiling. Typically, the probe remained at each location for 2 minutes before it was moved to the next position. Usually, either the through-the-wall probe or a second long probe was sampling continuously from a stationary location to monitor whether the fire changed significantly during the course of a mapping run. Another check of whether fire conditions changed was to start the mapping probe next to a stationary probe, move the mapping probe away from the stationary probe for eight sample locations, but return the mapping probe to its initial position as the ninth or last location on the mapping run.

2.5 Data Acquisition, Reduction, and Plotting

2.5.1 Overview

The data acquisition system recorded 55 channels of data from each fire and stored the values in a data (RSE92XX.DTA) file (Figure 17). The raw data was transferred to an IBM-XT computer and then processed into temperatures, flow rates, gas concentrations, etc. using the RAPID data

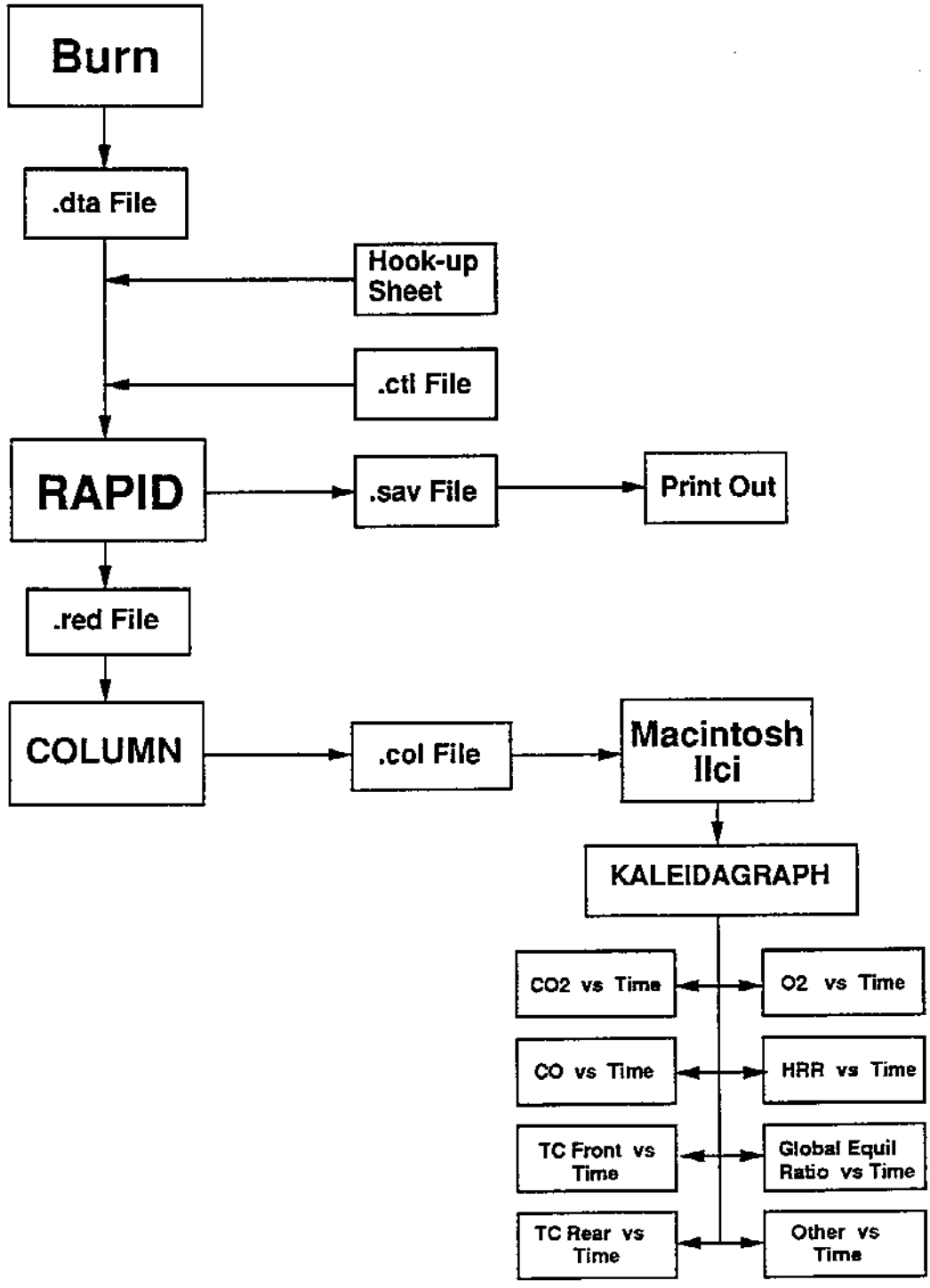

Figure 17. Flowchart of data reduction, analysis, and plotting.

reduction software [33,34]. The reduced data sets from RAPID were saved in output files (RSE92XX.SAV and RSE92XX.RED). One of these output files (RSE92XX.RED) was then processed using the COLUMN reformatting program into a columnar file (RSE92XX.COL) for export to a Macintosh IIci computer. Standard sets of plots were generated with commercial software on the Macintosh.

2.5.2 Data Acquisition

The data acquisition system consisted of a Hewlett-Packard HP9630 computer, HP3460 scanner box, and a HP3454A digital voltmeter. The system used the 24-bit resolution of the digital voltmeter to convert voltage signals to digital values. The data system scanned 20 channels of signals from instruments and 35 channels of thermocouple outputs. The thermocouple data were converted to temperatures before being stored in the data file. The interval for a scan of all channels was set to 10 seconds allowing six scans per minute.

An example of a data file is shown in Appendix D. The first line or header identified the test, fuel, heat release rate, and date. The data from each complete scan were stored as a unit or record in the data file. Each data record identified the date, time, and type of scan on the first line, and listed each channel number followed by its voltage or temperature. The first data records, usually five scans, contained the zero or background scans of all data channels. Following the zero scans were the full range or span scans, typically five to ten records, necessary to establish the range of the gas analyzers. The number and ranges of the gas analyzers determined whether five or ten scans were necessary for the span scans. After completing the necessary zero and span scans, the data system was ready to begin collecting data during a fire. Typically, two minutes of background data were collected before the natural gas fire was ignited. During each fire the system temporarily accumulated the data records in a data file on the computer hard disk drive. After each fire was

completed, an additional two minutes of background data were collected. The data file was transferred to an IBM-XT computer which was subsequently used to save the data on floppy disks.

2.5.3 Data Reduction

Before the data reduction process began, the raw .DTA file was inspected for unusual voltages that might represent reversed polarity, an open circuit, or a malfunctioning instrument. If more than one set of span scans was required for a test, the span data for the instruments requiring the additional scans were inspected for the span value. Since RAPID only allows for automatic reading of one set of span scans, the additional spans had to be inserted manually into the .CTL file. Each raw data file was assigned a file name with a suffix of .DTA, e.g. RSE9201.DTA, was the raw data for fire 9201. For each fire an instrument hook-up sheet described the channel assignments for all instruments and thermocouples (Appendix E). These channel descriptions included calibration constants and conversion factors for the gas instrumentation and the location of each thermocouple.

Reduction of the data was accomplished using the RAPID software developed at NIST. RAPID is a collection of FORTRAN subroutines used to convert voltages from thermocouples and typical fire research instrumentation to meaningful physical values and useful combinations of these values. While the subroutines, such as DELAY, TC, and GAS%, are described very briefly in this report, the subroutines are completely documented in the RAPID software package [33,34]. RAPID utilizes a user-customized control (.CTL) file (Appendix F) in conjunction with the raw data (.DTA) file to generate two output files, .SAV and .RED. The .CTL file started with a brief documentation of the date, fuel, fire size, and burner position. The next section of the file assigned instruments to each channel and described them. A command line was used to specify which records in the .DTA file were documentation, zero, span, and data records. The next section contained the commands necessary to convert the voltages to physical quantities such as gas concentration and temperature.

The following section manipulated the physical quantities to generate combinations that were of interest. A final section contained additional "data channels" that were created by the reduction process.

The section responsible for basic conversion of voltages had several components. The GAS% subroutine was used to specify the gas analyzers as to type, whether the zeroes and scans were in the zero and scan records or what the hand calculated values were, and what concentrations of span gases were used. The COMPUTE subroutine, which can calculate arithmetic expressions, was used for gas analyzers with dual ranges. For the Maihak dual-range analyzers, the range or scale was recorded by the range marker channels that monitored each of these instruments. The DELAY subroutine was applied to the probe and exhaust stack channels to correct the time lines for the period required for samples to travel to the analyzers from the enclosure.

The VELOCITY and PRESSURE subroutines along with appropriate calibration information were used to convert raw data to forms having the proper units. Since the data acquisition system automatically converted the thermocouple voltages into temperatures as the data was collected, the TC subroutine simply identified each block of channels used to store the temperature data. The SMOOTH command was applied to the front thermocouple tree channels due to fluctuations observed in the temperatures at this location. These fluctuations were not observed in the rear thermocouple data. We speculate that these fluctuations were cause by turbulence near the doorway. The SMOOTH subroutine replaced each data point with one generated by a seven-point smoothing algorithm.

The next section of the .CTL file combined physical measurements to provide fire properties. The first set of subroutines utilized MASS-FLOW-3, HEAT-RATE, and INTEGRATE to determine the instantaneous heat release rate and cumulative heat release from the exhaust stack measurements of CO and CO_2. Data from the bi-directional velocity probe and the thermocouple located in the

exhaust stack were used by MASS-FLOW-3 to calculate the total mass flow. Using the exhaust-stack oxygen concentration and the total mass flow, HEAT-RATE computed the total heat release rate via oxygen calorimetry. INTEGRATE summed the instantaneous values to provide cumulative values of heat release or mass flow.

CO and CO_2 yields (g/g) were calculated using GAS-FLOW, COMPUTE, and INTEGRATE commands on exhaust stack CO and CO_2 data with reference to the average fuel flow rate. The GAS-FLOW subroutine computed the mass flow rate for each gas species by utilizing the gas species concentration and the total mass flow rate through the exhaust stack. The mass flow rate of fuel provided by the diaphragm test meter was calculated using the commercially available Excel software package. The yields of CO and CO_2 involved a COMPUTE statement which ratioed the mass flow rate of each species to the total mass flow rate. Additional COMPUTE commands were used on CO and CO_2 data to generate the molar CO/CO_2 ratios.

The global equivalence ratio was calculated using the MASS-FLOW2 and COMPUTE subroutines. Periodic natural gas analyses were coupled with the records of experimental flow rates to generate the stoichiometric air flow rate and the average fuel flow rate for each fire. The actual air flow into the enclosure was required in addition to the actual fuel flow and stoichiometric air flow rates. This was accomplished by modification of the original RAPID MASS-FLOW2 subroutine to calculate the neutral plane at the door using the algorithm suggested by Janssens and Tran [35]. The method utilizes the doorway and front enclosure temperature profiles to calculate static pressure gradients across the doorway [36]. The sum of the mass inflow through the door and fuel mass flow was matched to the outflow through the door. This was achieved by matching the integrals representing the flows due to the pressure gradients by varying the location of the neutral plane. After the neutral plane providing mass conservation was located, the mass flow rate into the enclosure was recalculated and combined with the fuel flow rate measurement and air flow rate

required for stoichiometric burning in a COMPUTE statement to calculate the global equivalence ratio. The local equivalence ratio was calculated with a COMPUTE statement from oxygen concentrations generated by the phi-meter.

The .SAV file which was generated by RAPID was useful for inspection of the converted data which was listed with respect to time for each channel. If RAPID executed without errors, important data channels in the .SAV file were inspected for reasonable values and trends. If an unusual case was found, the specific channel was reinspected in the .DTA file to determine if a poor zero or span was overlooked. After questionable data was understood, the file was re-reduced, columnized, and plotted. The .SAV file also documents the process by which the values were computed through the .CTL file commands. The .RED file was an abbreviated listing of the data and served as the source file for the COLUMN program. This program reformatted the reduced data in matrix form with channel titles over each column and time in the first column. The resulting .COL files were exported to a Macintosh IIci for plotting.

2.5.4 Data Plotting

For each test, a standard set of data plots was generated in order to provide a handy visual record of the results. The first step in creating the plots was to convert the .COL file from IBM-XT format to a form compatible for use on an Apple Macintosh computer. This conversion process used Apple File Exchange software. Kaleidagraph, a spreadsheet and graphing software package, was used for display and plotting of the data. This graphing package allows previous plots to be used as templates upon which new sets of data can be plotted. This feature was very helpful in efficiently plotting the 9 to 12 "standard" plots generated for each fire.

The basic plots for each test were sets of data versus time consisting of CO, CO_2, and O_2 concentrations, front temperature profiles, rear temperature profiles, heat release rate, and

equivalence ratio. These were plotted for every fire and were the "standard" plots by which tests were compared for reproducibility.

Additional plots that were not always produced were the molar CO/CO_2 ratio, front and rear temperatures comparison, and the sum of CO and CO_2 concentrations. The temperature comparison was helpful in visualizing the layer thickness and temperature differences between the front to the back of the enclosure. The sum of CO and CO_2 was used as a doublecheck of analyzer performance by comparing the sum against the theoretical maximum that could be achieved. Of the 125 fires, only four fires exceeded, and then only slightly, the theoretical maximum total of CO and CO_2.

Averages of the major parameters of each fire were put into a separate file and plotted versus average heat release rate and global equivalence ratio. This resulted in a series of summary plots for all tests such as CO versus heat release rate, CO_2 versus global equivalence ratio, etc. Also, typical temperature traces versus time were plotted from fires of different sizes on the same plot to show relative differences.

2.6 Gas Concentrations

The oxygen, carbon monoxide, and carbon dioxide analyzers measured the gas concentrations on an Orsat or dry basis. Since water vapor, carbon monoxide, and carbon dioxide all absorb radiation in the infrared portion of the electromagnetic spectrum, it was necessary to remove the water vapor to prevent interference with the non-dispersive infrared photometry technique employed by the LIRA and DEFOR analyzers. Water does not interfere significantly with the Servomex oxygen analyzers which utilize the paramagnetic properties of oxygen molecules. Running separate sample lines, valves, regulators and pumps for just the oxygen measurements was not considered a practical option. In order to eliminate the interference for the LIRA and DEFOR instrumentation, the sample gases were pulled through cold traps to remove all water vapor. The cold traps also

condensed any heavy organic species with low vapor pressures. The filter media within each cold trap removed soot particulates. Reporting the gas concentrations as dry volume percents allowed the data to be examined before making approximations or corrections for the removed water.

Toner et al. [12] and Morehart et al. [13] employed gas chromatography to analyze their combustion gases and reported gas concentrations on a wet basis. To allow comparison with these studies, the dry-basis measurements were converted to wet volume percents. The conversion was implemented by assuming that the formation of each mole of carbon dioxide also resulted in the generation of two moles of water,

$$CH_4 + 2O_2 \rightarrow CO_2 + 2H_2O. \qquad (1)$$

This assumption was also utilized by Roby and Beyler [37] when they presented their gas concentrations on a wet basis. Once the total number of moles of water was calculated, the oxygen, carbon monoxide, and carbon dioxide concentrations were corrected. These wet concentrations were plotted in a manner similar to the dry concentrations. After completing the data reduction for each fire, individual plots of oxygen, carbon monoxide, and carbon dioxide wet concentrations were generated. Following a series of fires, summary plots combined the data from multiple burns for comparison purposes.

After the water concentration was computed and after the oxygen, carbon monoxide, and carbon dioxide concentrations were corrected, an oxygen balance was completed and then nitrogen was assumed to be present in a ratio of 3.79:1, nitrogen to oxygen. Percentages of H_2O, O_2, CO, CO_2, and N_2 were summed and subtracted from 100 percent. The difference, referred to as residual combustion gases, consisted of all the other combustion products, including, but not limited to, unburned hydrocarbons, soot, and hydrogen.

2.7 Natural Gas Fire Operation

The reduced-scale enclosure was positioned under the Furniture Calorimeter hood in the BFRL Large Scale Burn Facility. The enclosure was centered under the hood east to west, but was pushed to the north or rear of the hood (Figure 18). This location allowed the effluent from the RSE to be exhausted into the calorimeter hood. After leveling the enclosure, the gas burner, pilot light, and thermocouple trees were placed inside. The sample probes were connected to the sample lines and the tip of each probe positioned at the desired location within the room. If the fire was to be recorded on videotape, the camera and monitor were setup. The data system was initialized, data files were opened, and scanning interval was set.

Before each fire, the gas analyzers, velocity probe, and pressure transducer were checked for proper performance at low (zero) and high (span) points. The analyzers were zeroed by pumping nitrogen through each instrument. Turning off the Furniture Calorimeter exhaust fan allowed the velocity probe and the pressure transducer to be zeroed. While zeroing the gas analyzers, the thermocouples were checked for electrical continuity. After recording at least five scans of zero data with the computer, span gases were pumped through the analyzers and the exhaust fan was started. After allowing the analyzers to respond to the span gases and the velocity probe to register full exhaust duct flow, five span scans were recorded with the computer.

If an analyzer, probe, transducer, or thermocouple appeared to be malfunctioning, the instrument was double-checked at this point and repaired. Occasionally, when an instrument or thermocouple could not be repaired quickly, it was necessary to postpone the fire, but if the instrument was not deemed critical, then the fire proceeded without the malfunctioning instrument.

After successfully zeroing and spanning the instrumentation, the data system was reset to scan continuously every 10 seconds. The top-surface temperature of the RSE was recorded on the operation sheet (Appendix G). The videotape and a stopwatch were started and background data

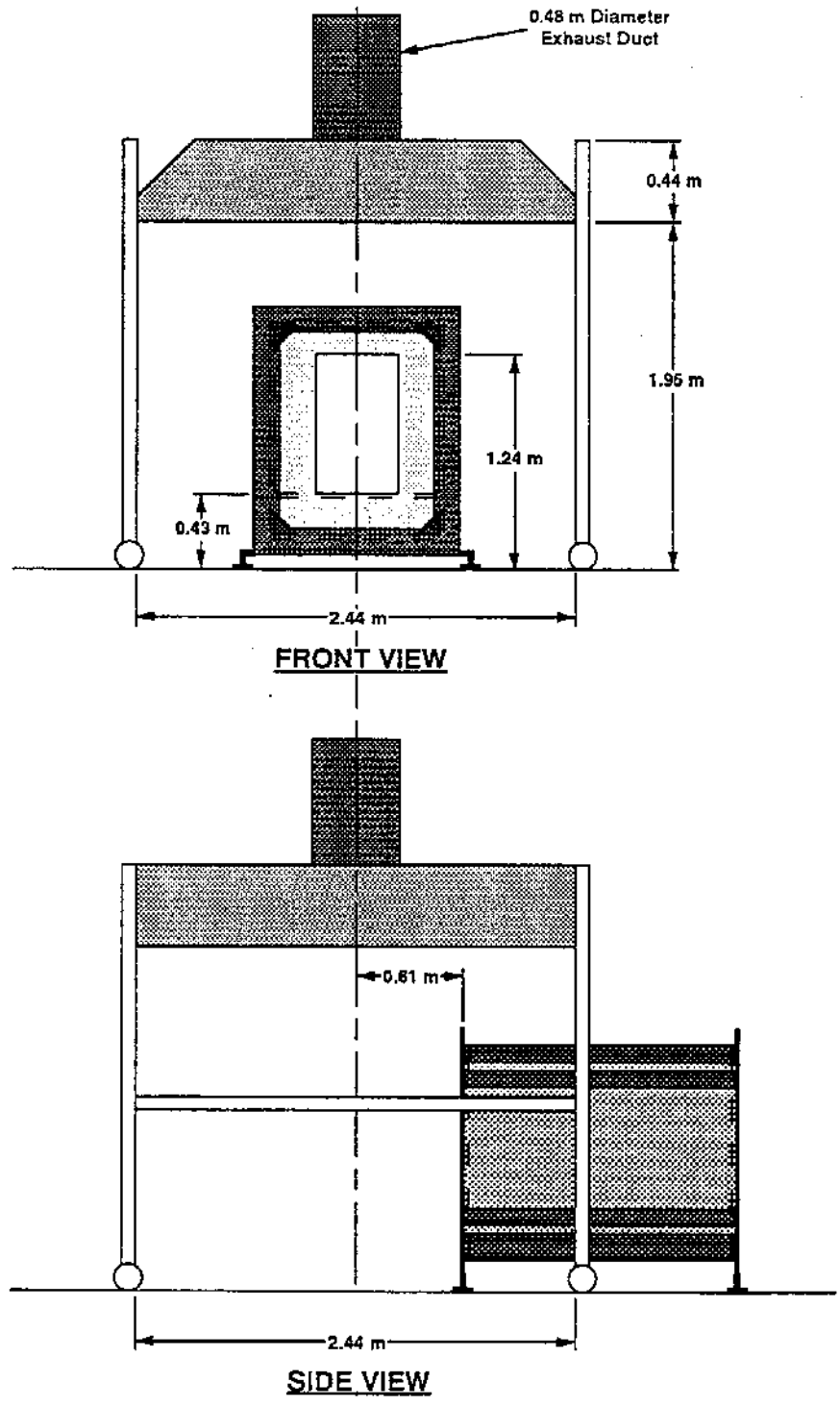

Figure 18. Reduced-scale enclosure positioned under Furniture Calorimeter hood.

was collected, typically for 60 seconds or 6 scans. At 45 seconds, the propane flow for the pilot flame on the gas burner was started and at 60 seconds a propane torch ignited the pilot flame. Another 60 seconds of background data was collected with the pilot light burning. Approximately 30 seconds after the pilot flame was ignited, the natural gas line was pressurized up to 103 kPa. After two minutes of background, one without the pilot flame and one with the pilot, a ball valve was opened and the natural gas flowed to the burner and was ignited by the pilot flame. After ignition, the pilot flame was turned off and the natural gas flow-control valves were quickly adjusted to achieve the required gas-flow rate. After setting the gas-flow rate, the diaphragm test meter was used to time the displacement of either 70 l, 140 l, or 280 l. The largest volume was used to time the higher flow rates while the smaller volumes were employed in timing the lower gas-flow rates. Gas-line pressures and rotameter readings were also recorded. Approximately one minute after ignition, the burning natural gas fires appeared visually to reach a steady burning state. A fire typically lasted 15 minutes with the enclosure top-surface temperature and gas-flow data being recorded every 3 to 5 minutes. The top-surface temperature of the RSE was observed to increase throughout all of the fires indicating that conduction of energy through the walls never reached a steady state. If the sample probes were being moved, longer fire times were necessary to allow the probes to reach steady state at each specified location. The longest fires were approximately 30 minutes in duration.

After the planned burn time was completed, the natural gas flow was interrupted and the residual natural gas was allowed to burn. Before all the natural gas was consumed, the pilot-flame fuel flow was turned on and the pilot flame was reignited to prevent the accumulation of quantities of unburned natural gas within the hot enclosure. After the natural gas was completely burned, the data system was allowed to collect two additional minutes of post-burn background data. The additional background information was used to check instrument operation.

After collecting the post-burn background, the data system was turned off and the data transferred to the IBM-XT. While the data was being transferred, a pair of 56 cm diameter fans were positioned on the front and east side of the enclosure to increase the cooling rate of the room. Usually a minimum of 45 minutes was required before the top surface temperature reached the 25 °C to 28 °C range. Once the box had cooled, another experimental sequence could be initiated. Three or four burns were possible each day.

2.8 Narrow Door Burn Configuration

A limited number of small fires, 7, 10, 15, and 20 kW, were conducted with a 1 cm wide by 81.3 cm tall door. Two pieces of Marinite were clamped over the normal door to achieve the narrower door (Figure 19). These burns were designed to increase the time required for the upper layer to develop and stabilize. This provided a test for a model which assumes the Global Equivalence Ratio concept can be incorporated into a zone fire model to predict carbon monoxide formation [38]. This configuration also resulted in considerably lower upper-layer temperatures than the full-door configuration and provided insights into temperature effects on carbon monoxide formation.

3.0 Results

3.1 Gas Profiles

The oxygen, carbon monoxide, carbon dioxide, and water concentrations (volume percent, wet) were plotted as a function of time for each fire. Examples for 25, 50, 100, 150, 200, 250, 300, 400, 500, and 600 kW fires are shown in Figures 20-38. These plots are typical of gases sampled at

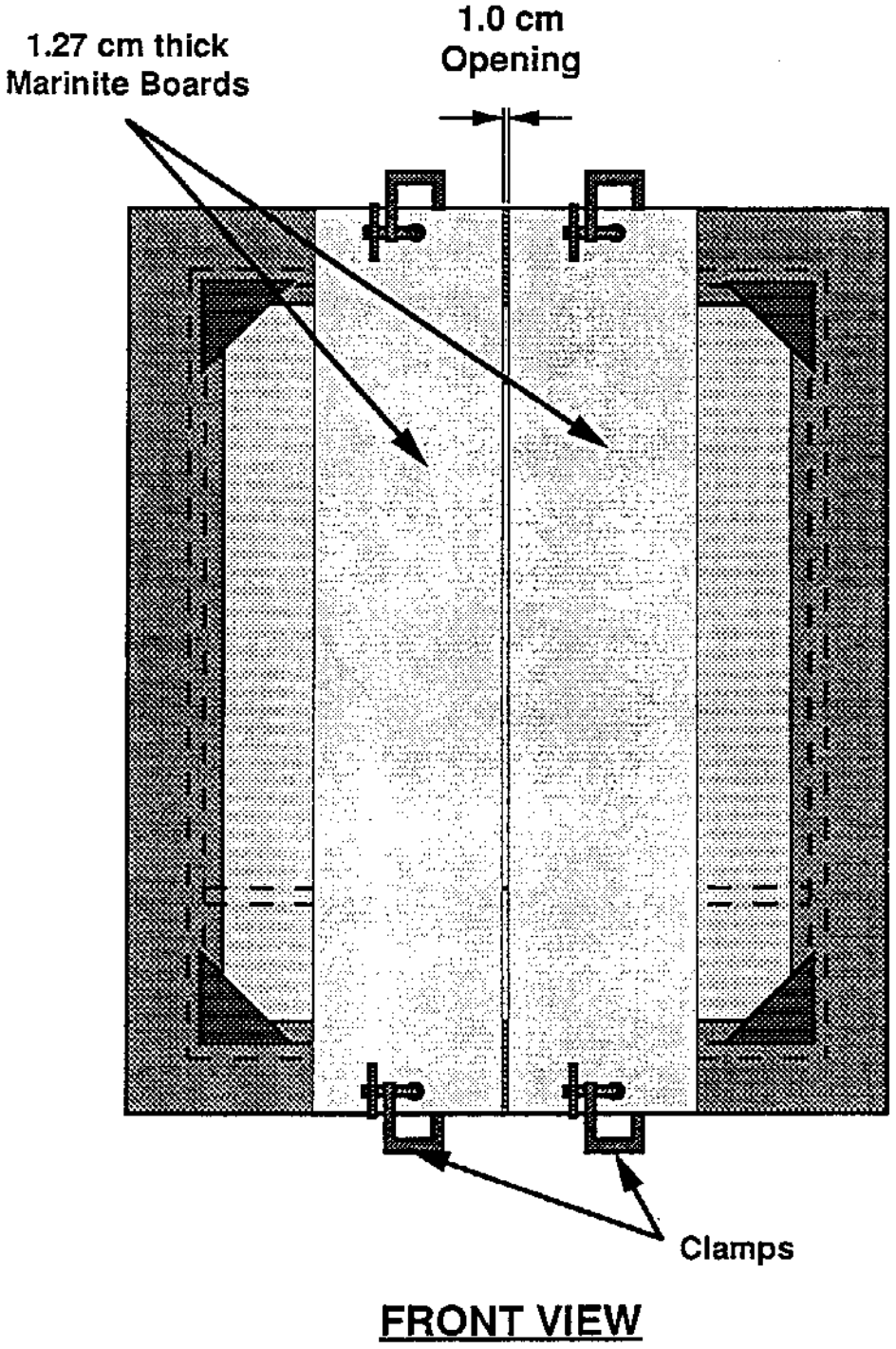

Figure 19. Narrow-door configuration of reduced-scale enclosure.

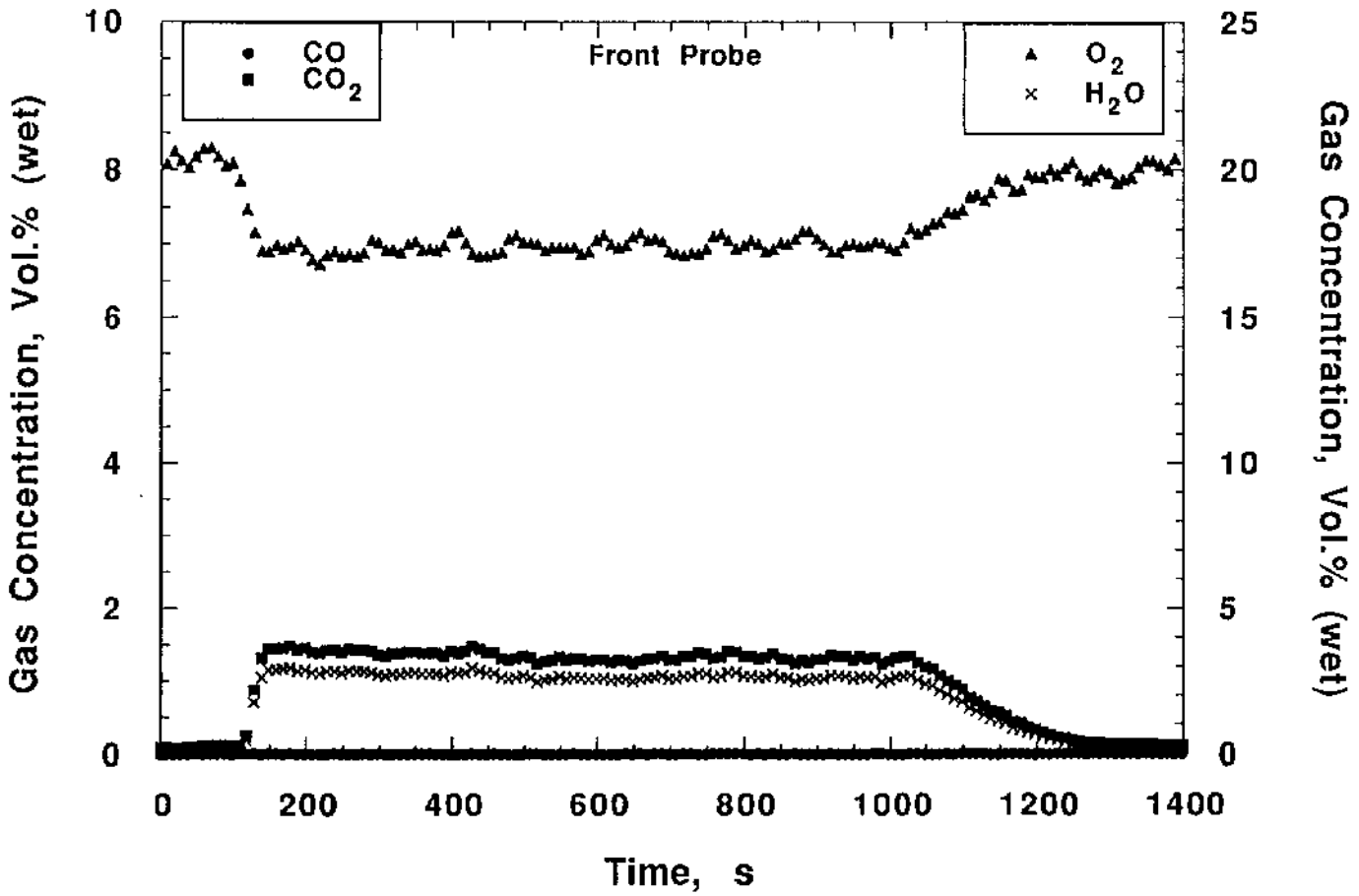

Figure 20. Gas concentrations at front sampling location in upper layer of a 25 kW natural gas fire.

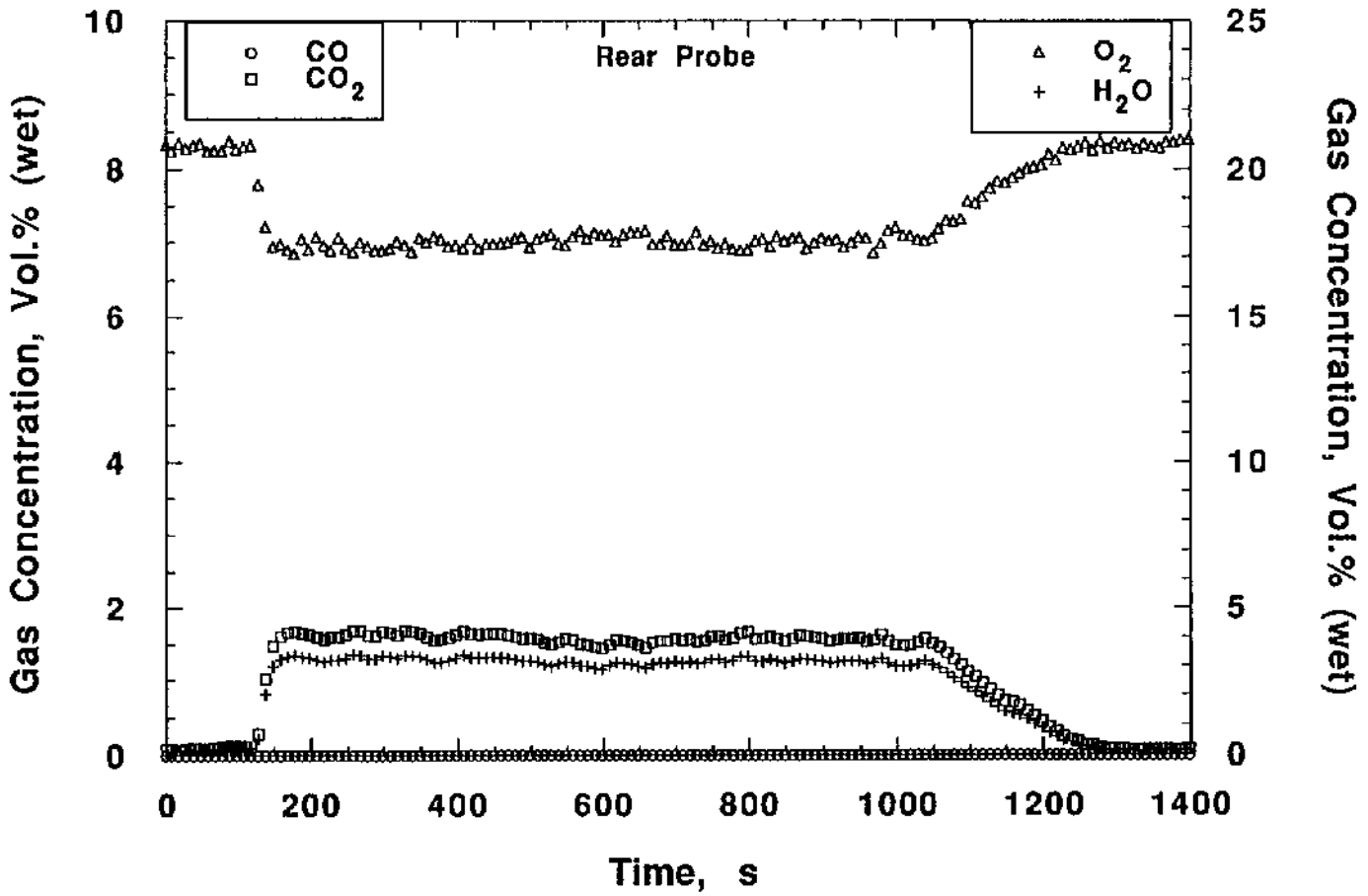

Figure 21. Gas concentrations at rear sampling location in upper layer of a 25 kW natural gas fire.

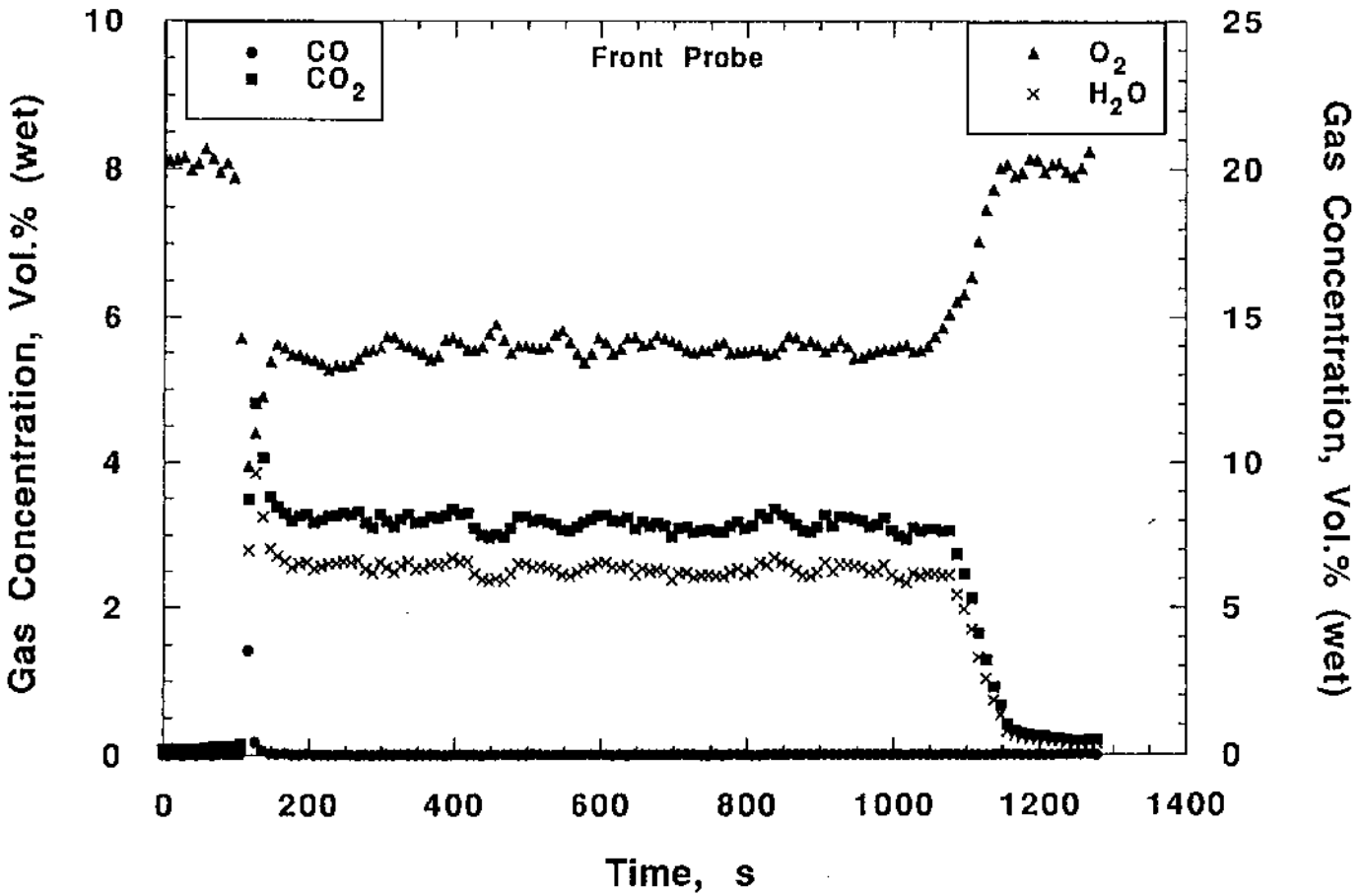

Figure 22. Gas concentrations at front sampling location in upper layer of a 50 kW natural gas fire.

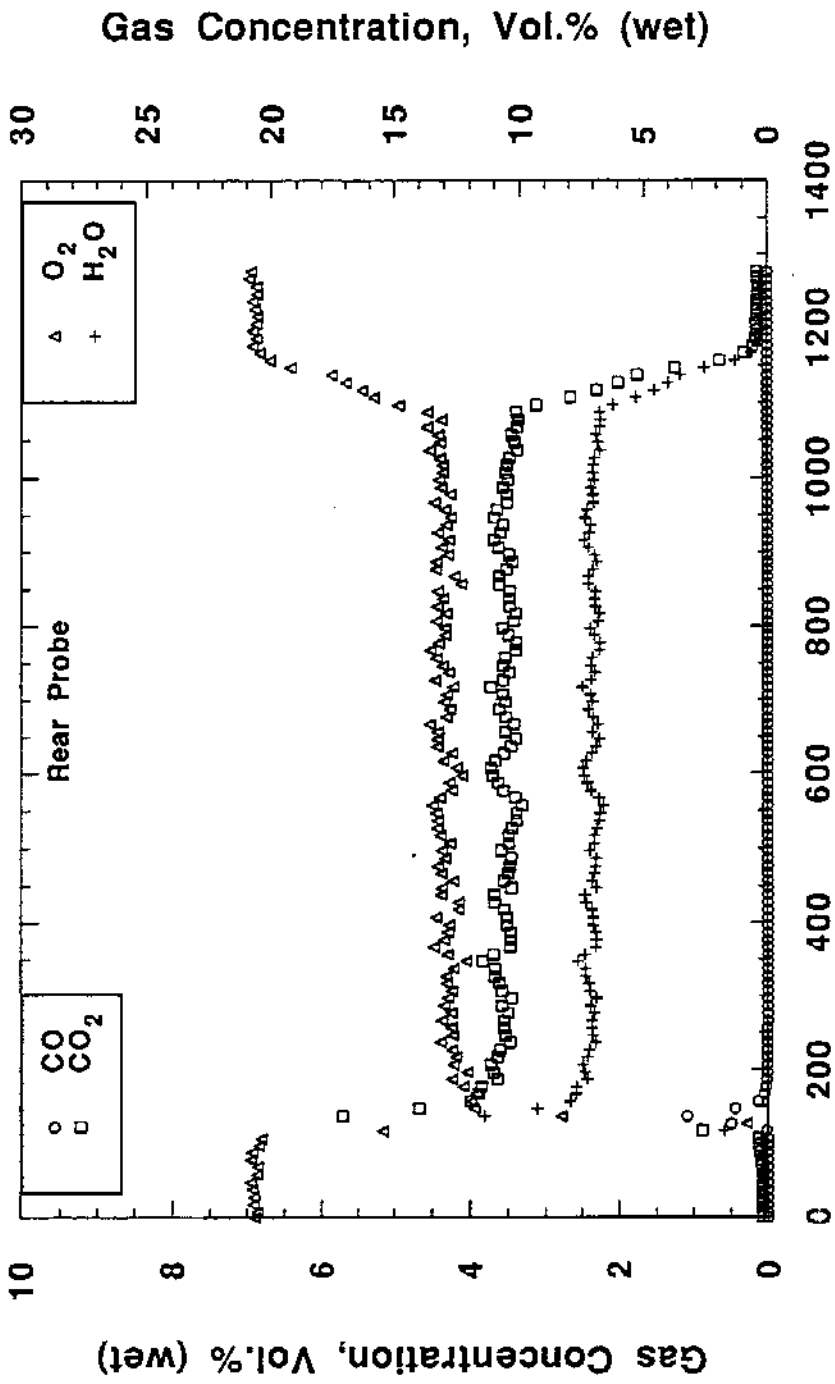

Figure 23. Gas concentrations at rear sampling location in upper layer of a 50 kW natural gas fire.

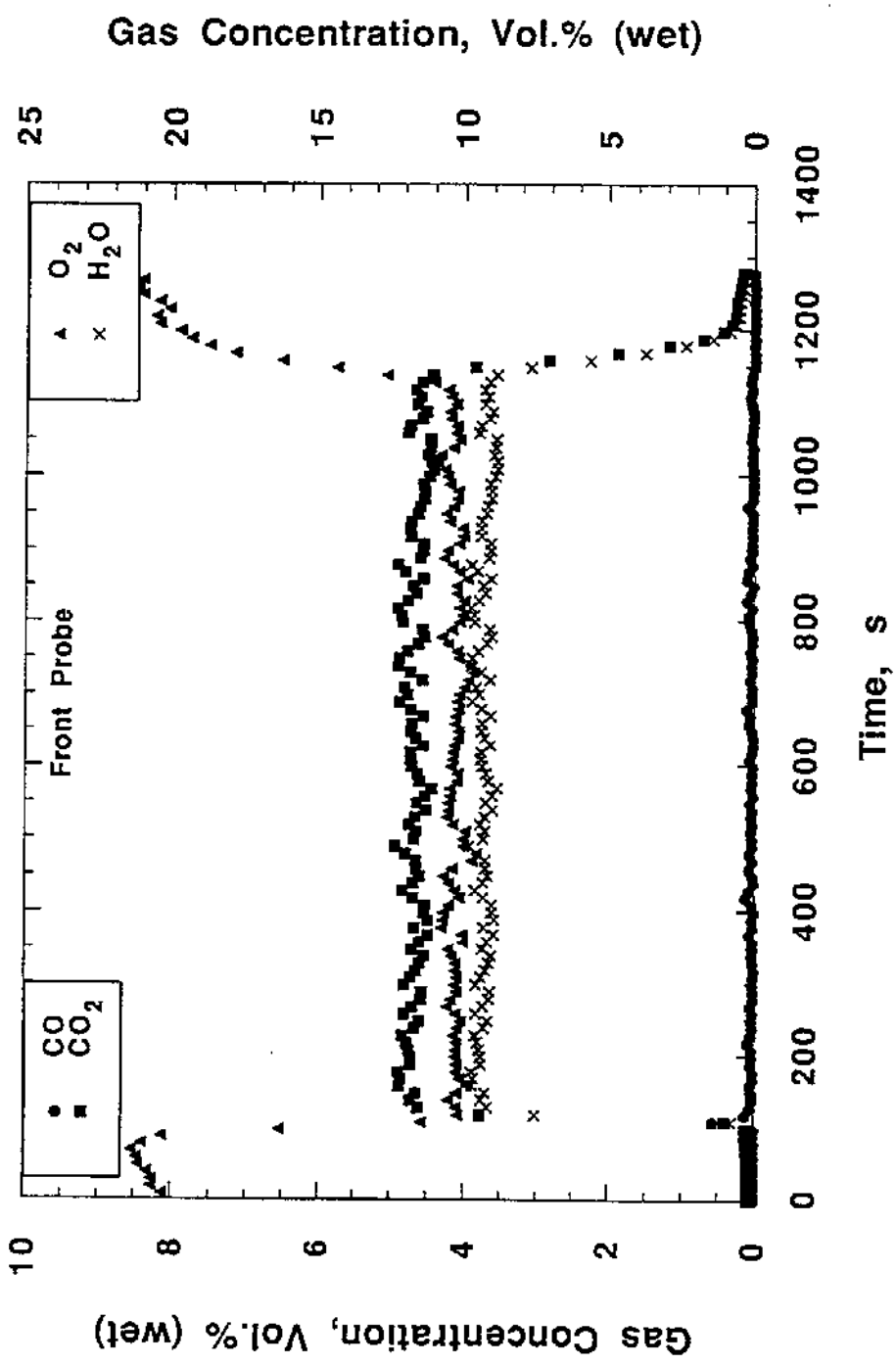

Figure 24. Gas concentrations at front sampling location in upper layer of a 100 kW natural gas fire.

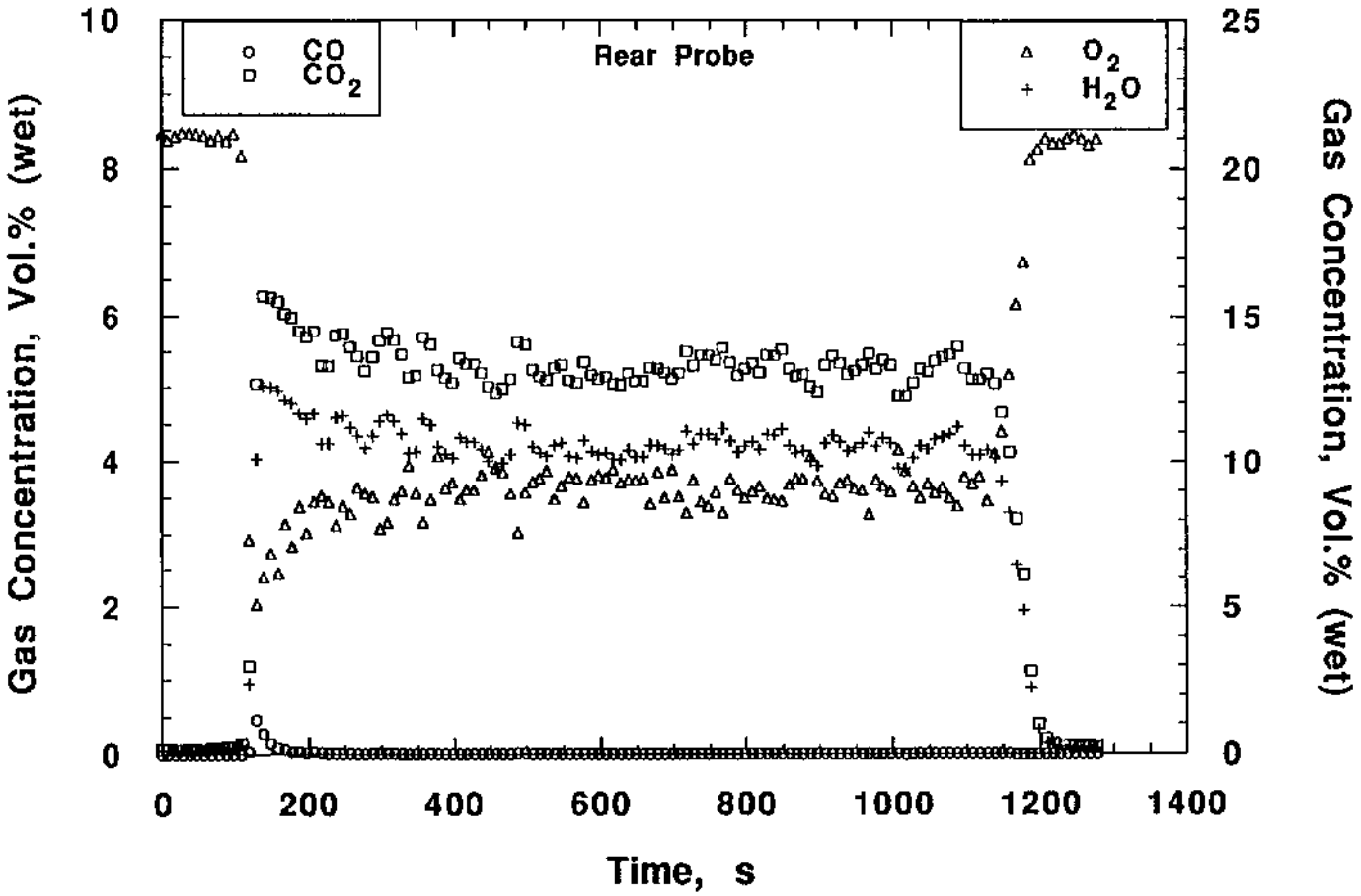

Figure 25. Gas concentrations at rear sampling location in upper layer of a 100 kW natural gas fire.

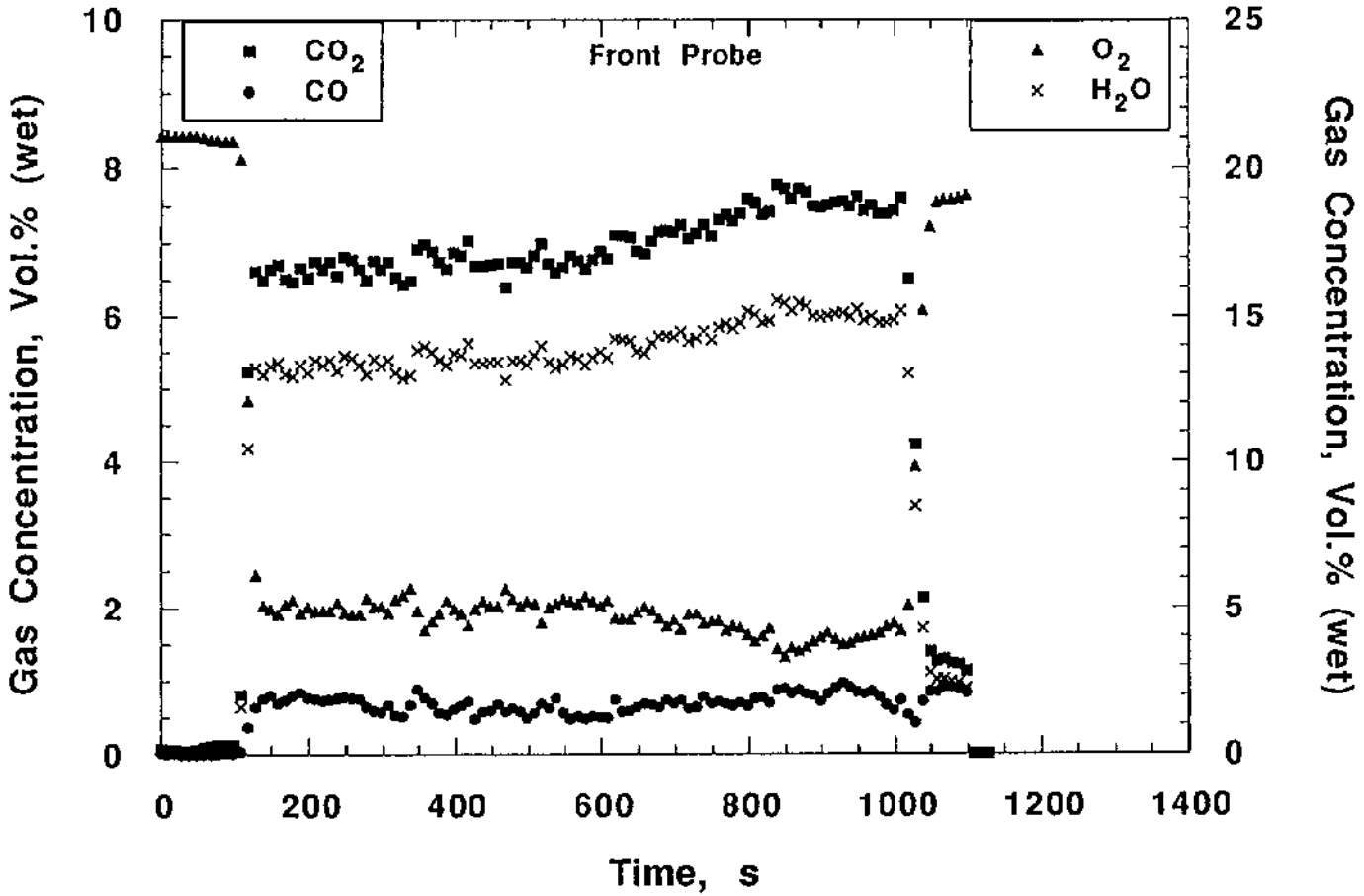

Figure 26. Gas concentrations at front sampling location in upper layer of a 150 kW natural gas fire.

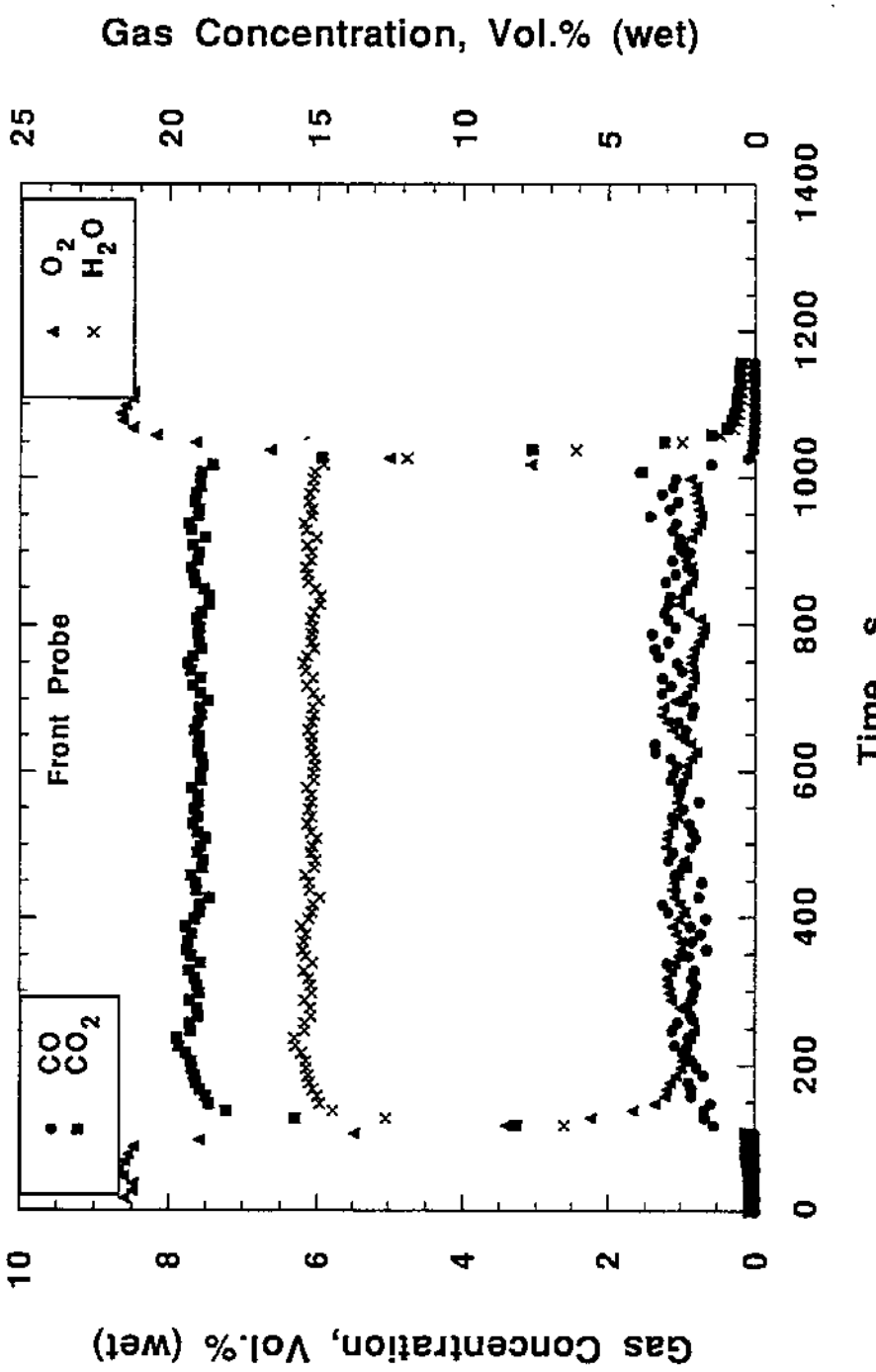

Figure 27. Gas concentrations at front sampling location in upper layer of a 200 kW natural gas fire.

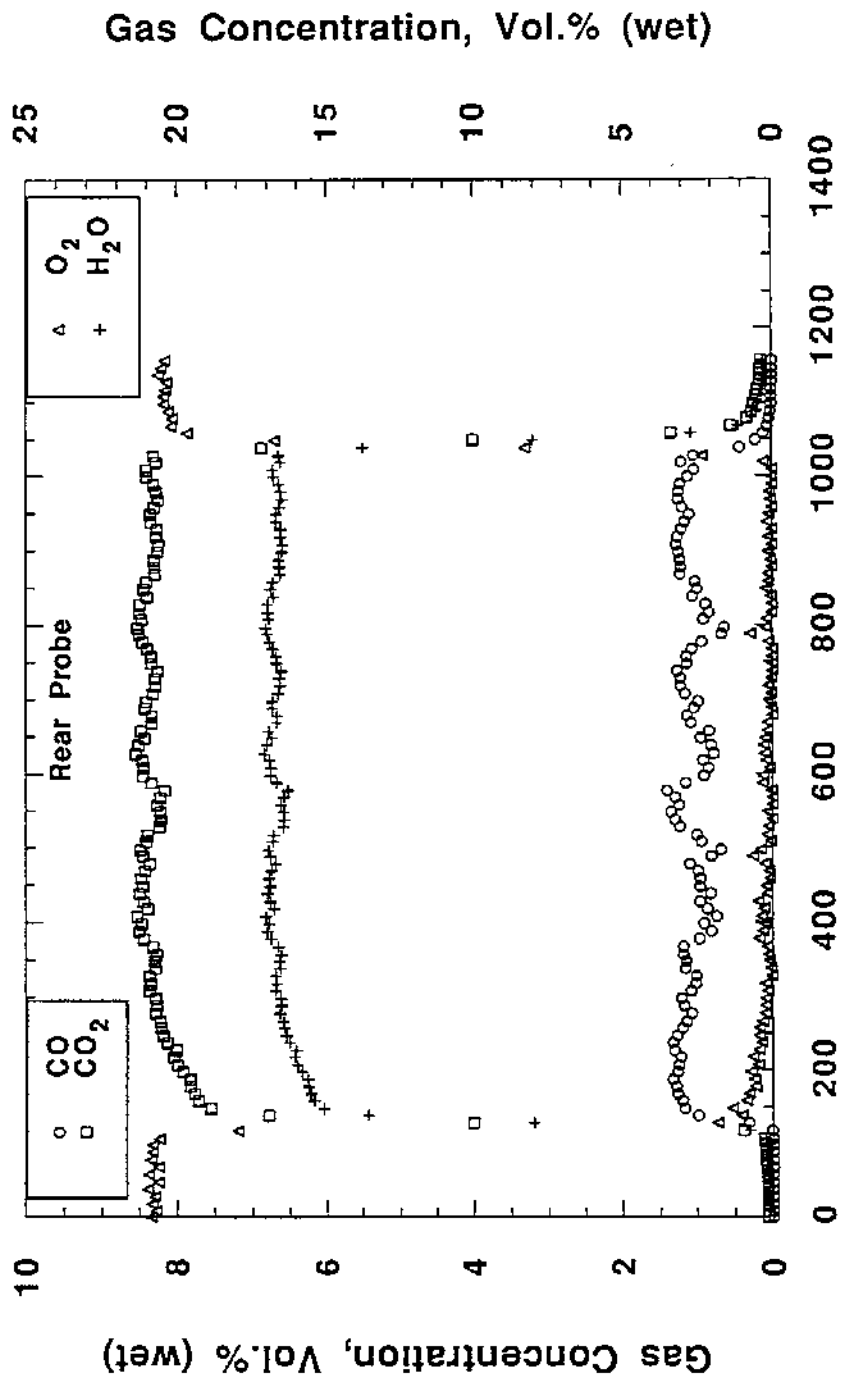

Figure 28. Gas concentrations at rear sampling location in upper layer of a 200 kW natural gas fire.

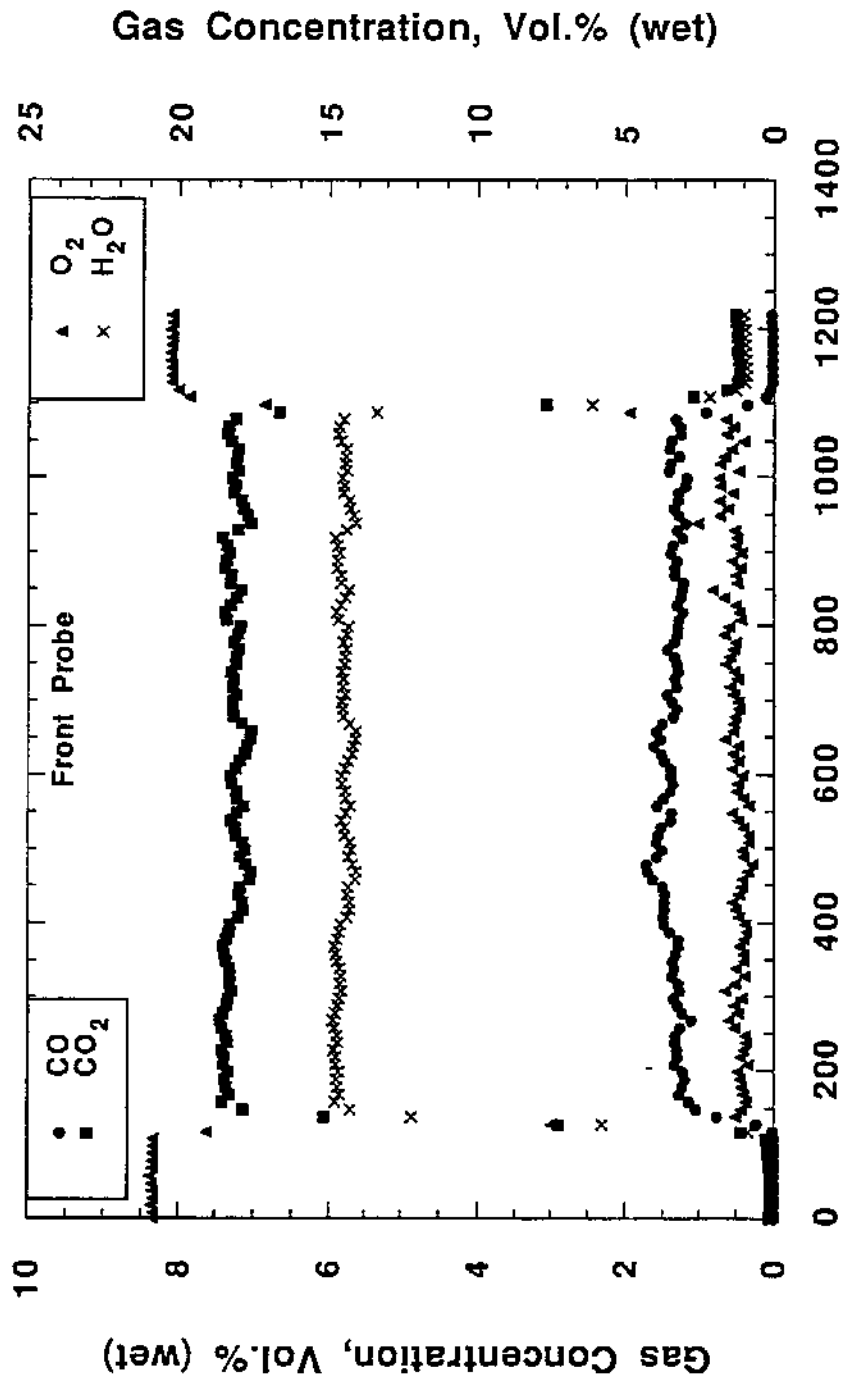

Figure 29. Gas concentrations at front sampling location in upper layer of a 250 kW natural gas fire.

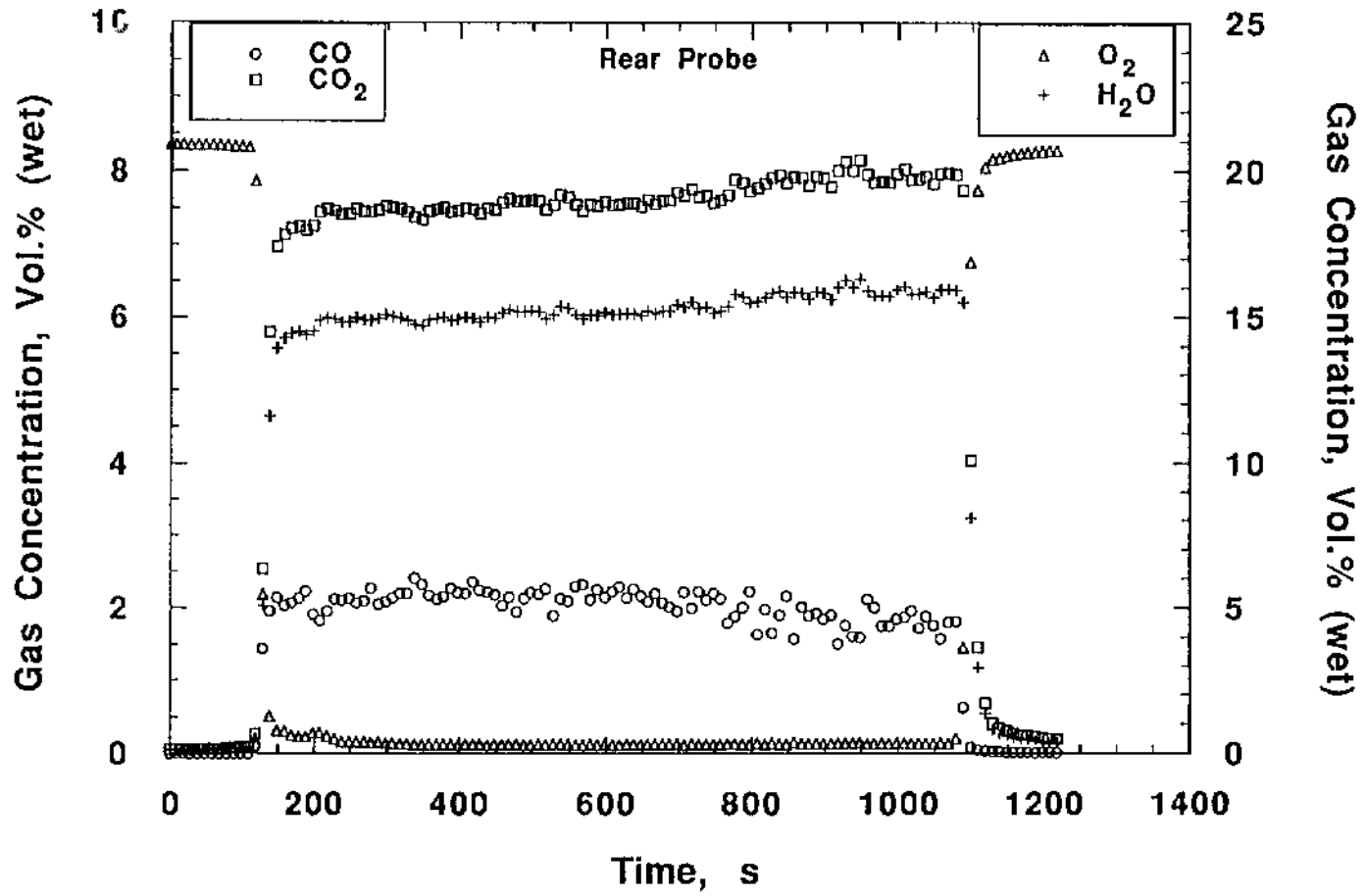

Figure 30. Gas concentrations at rear sampling location in upper layer of a 250 kW natural gas fire.

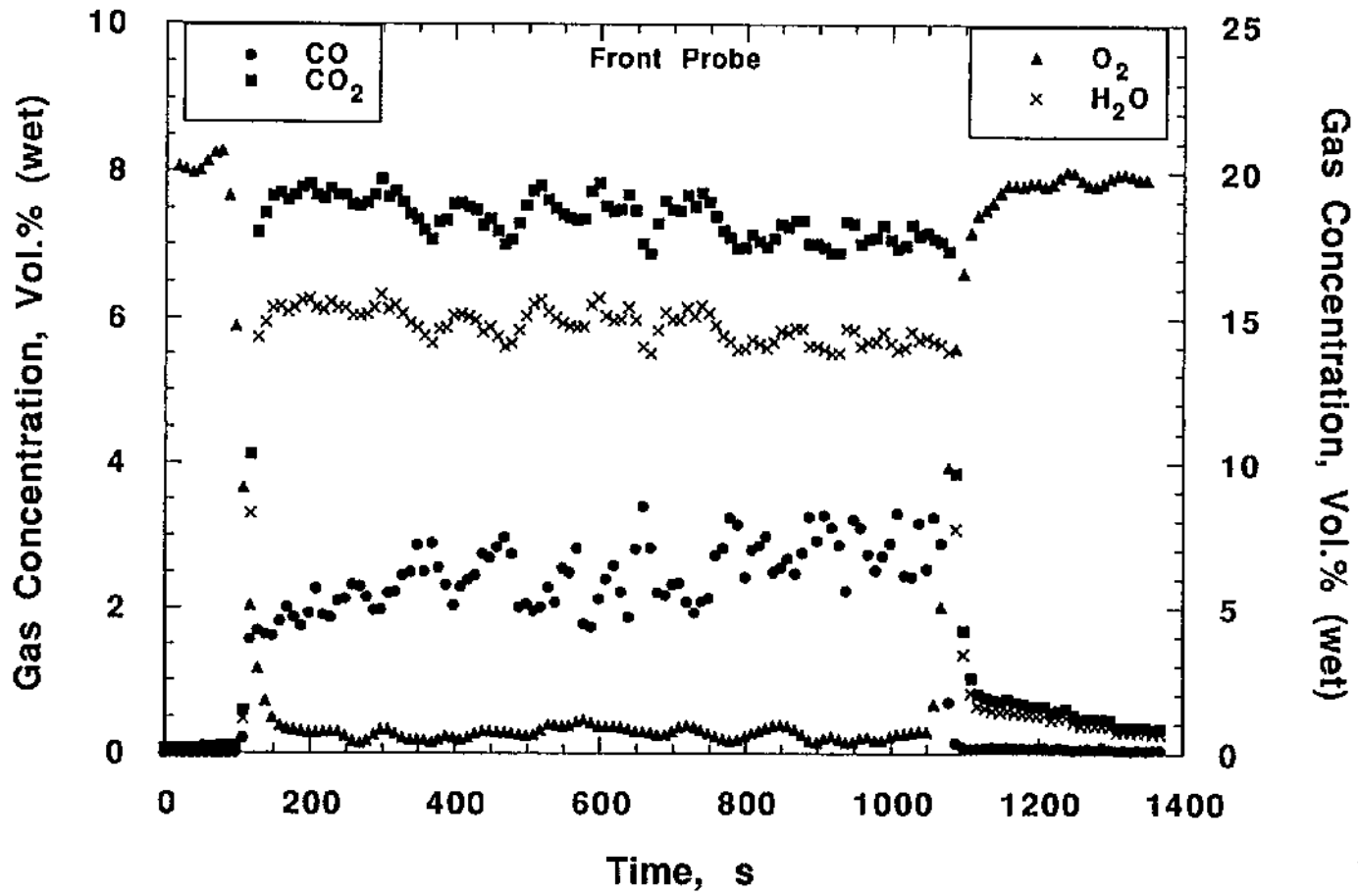

Figure 31. Gas concentrations at front sampling location in upper layer of a 300 kW natural gas fire.

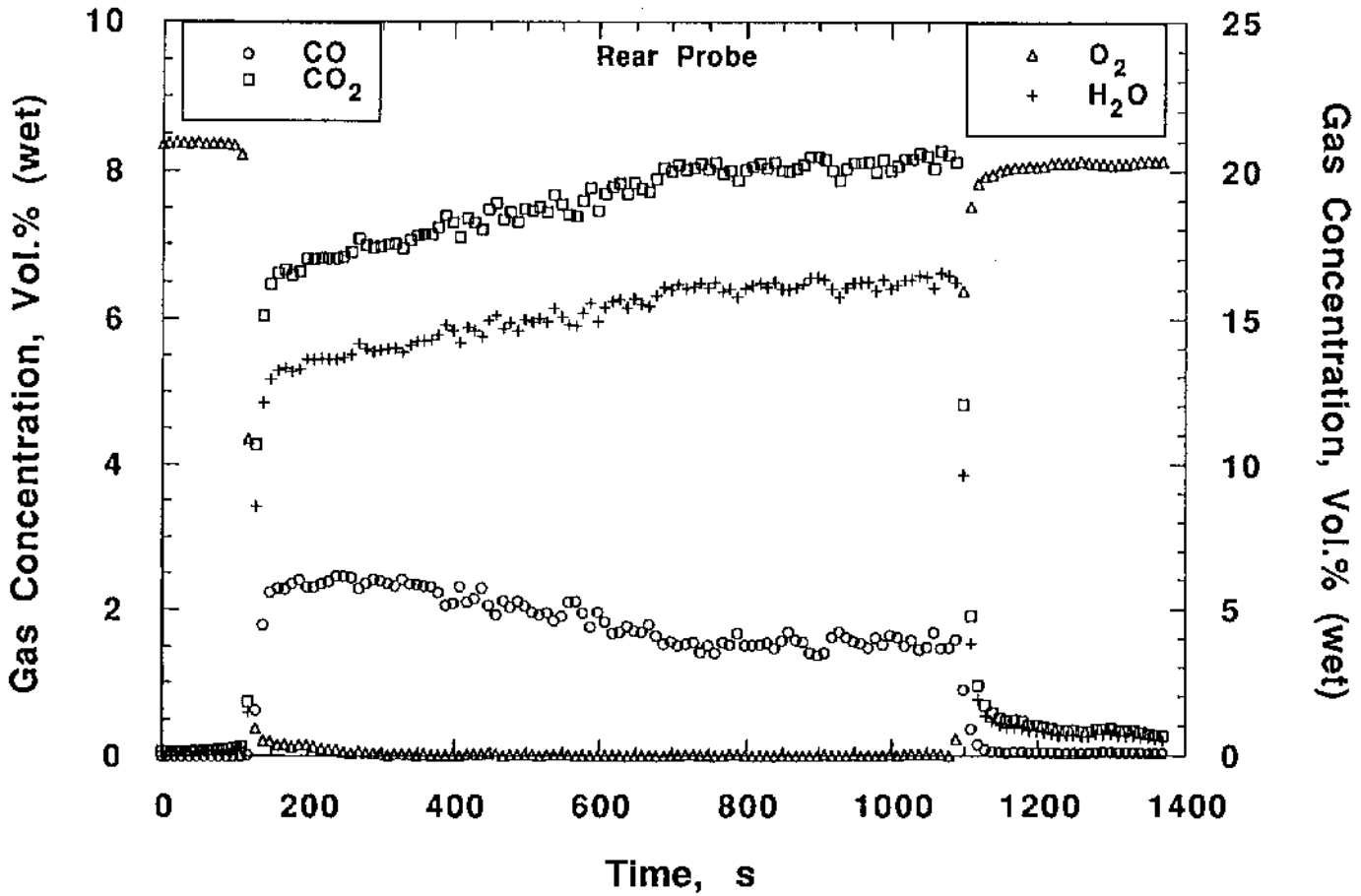

Figure 32. Gas concentrations at rear sampling location in upper layer of a 300 kW natural gas fire.

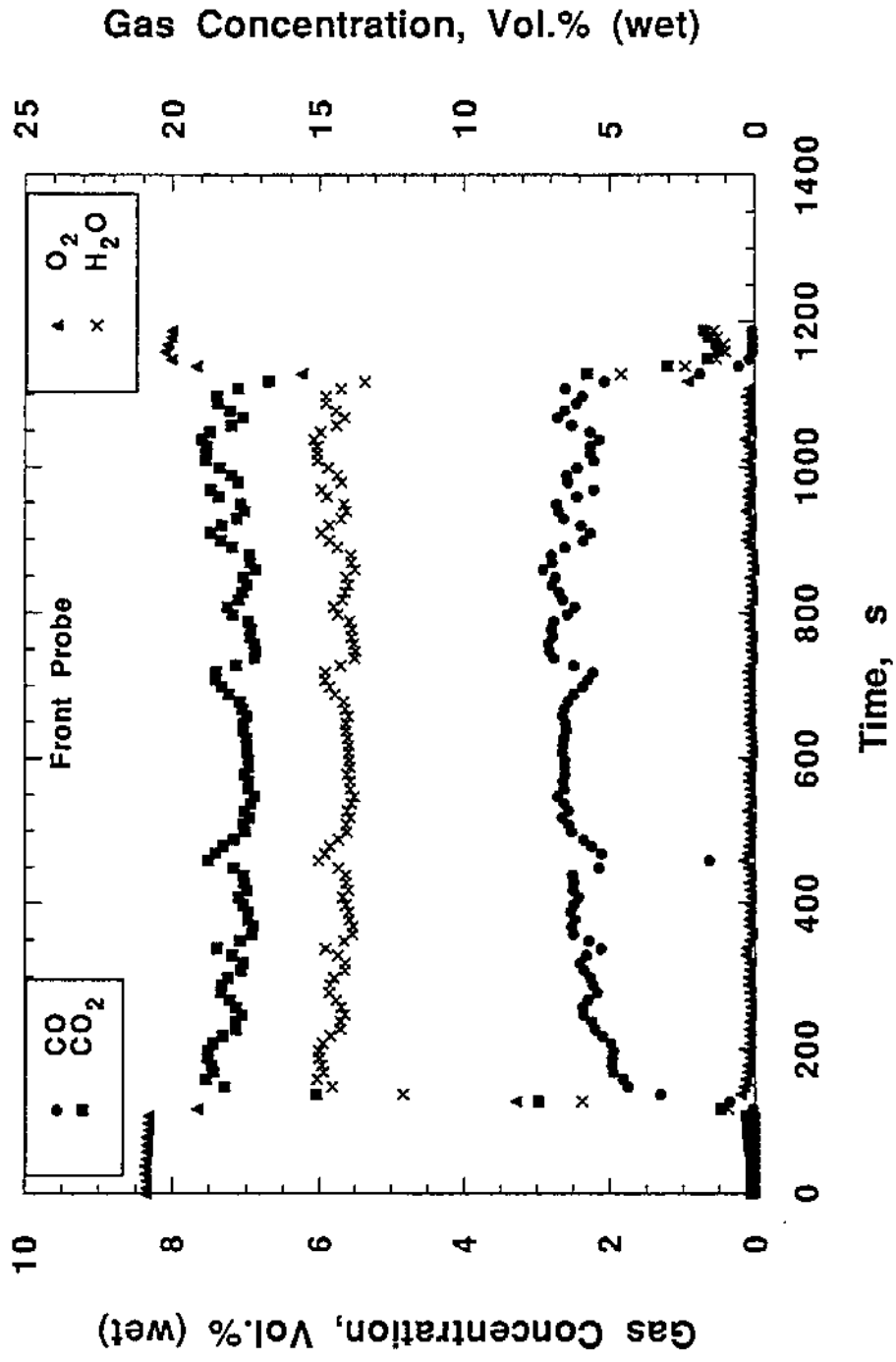

Figure 33. Gas concentrations at front sampling location in upper layer of a 400 kW natural gas fire.

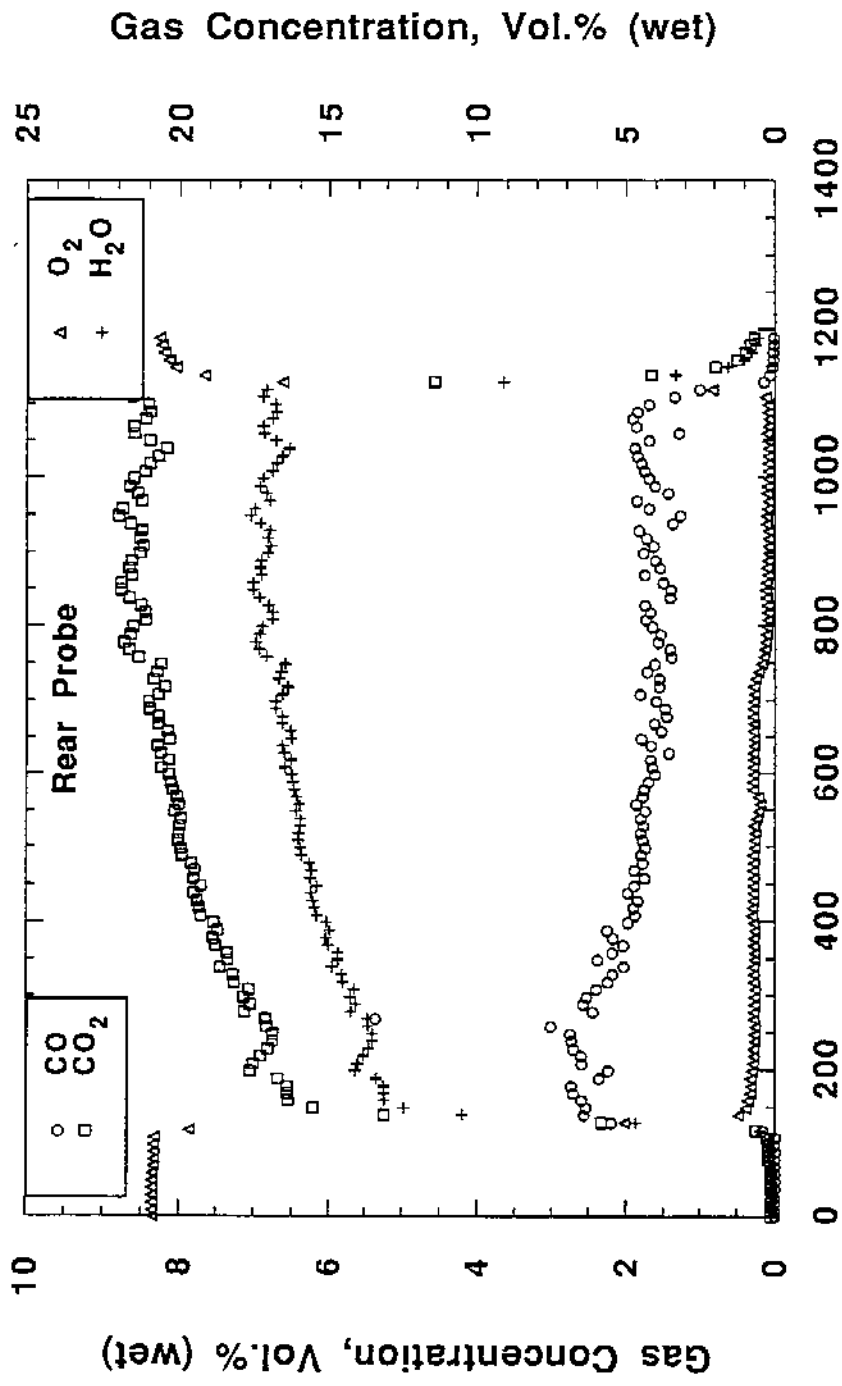

Figure 34. Gas concentrations at rear sampling location in upper layer of a 400 kW natural gas fire.

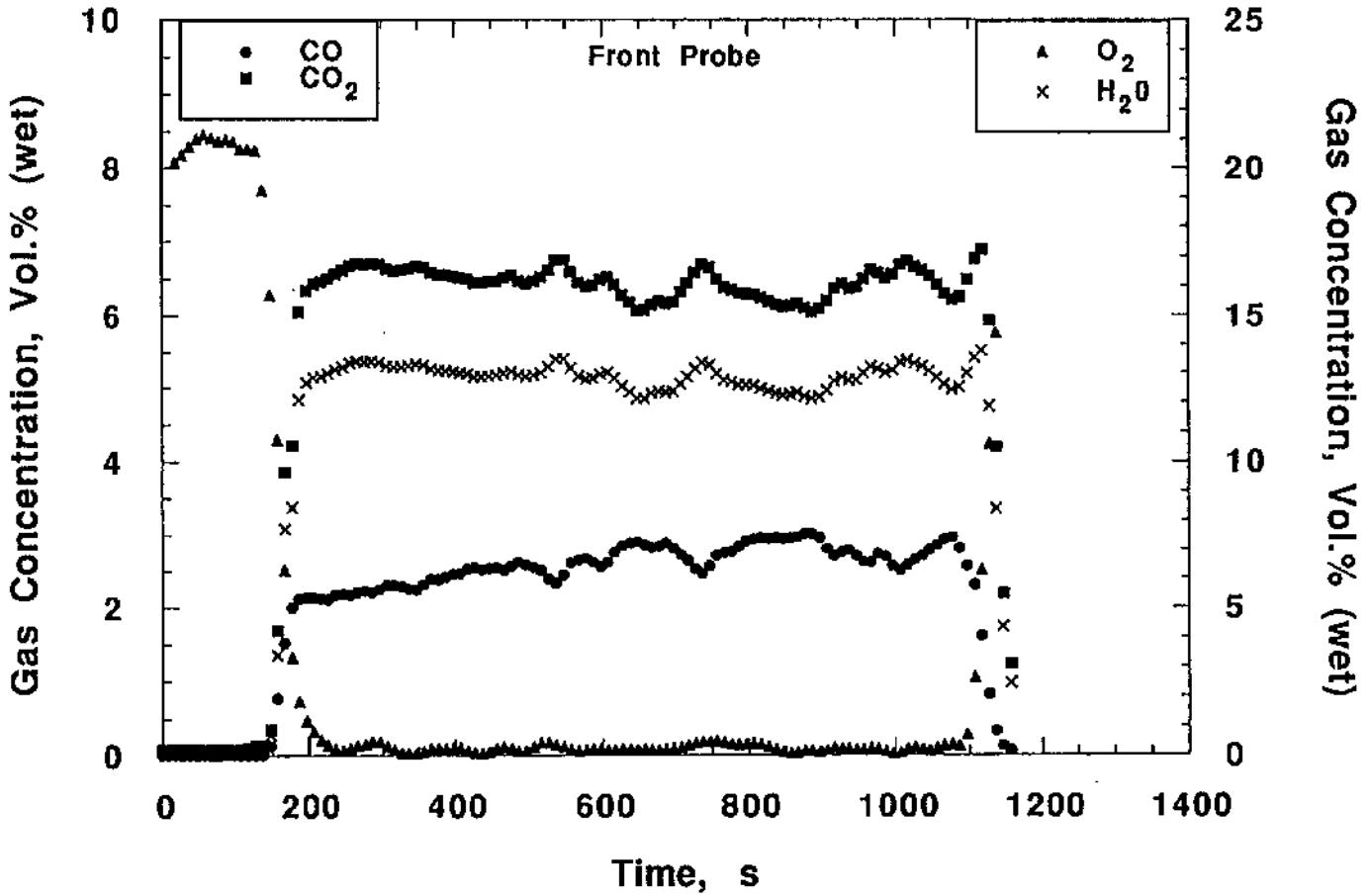

Figure 35. Gas concentrations at front sampling location in upper layer of a 500 kW natural gas fire.

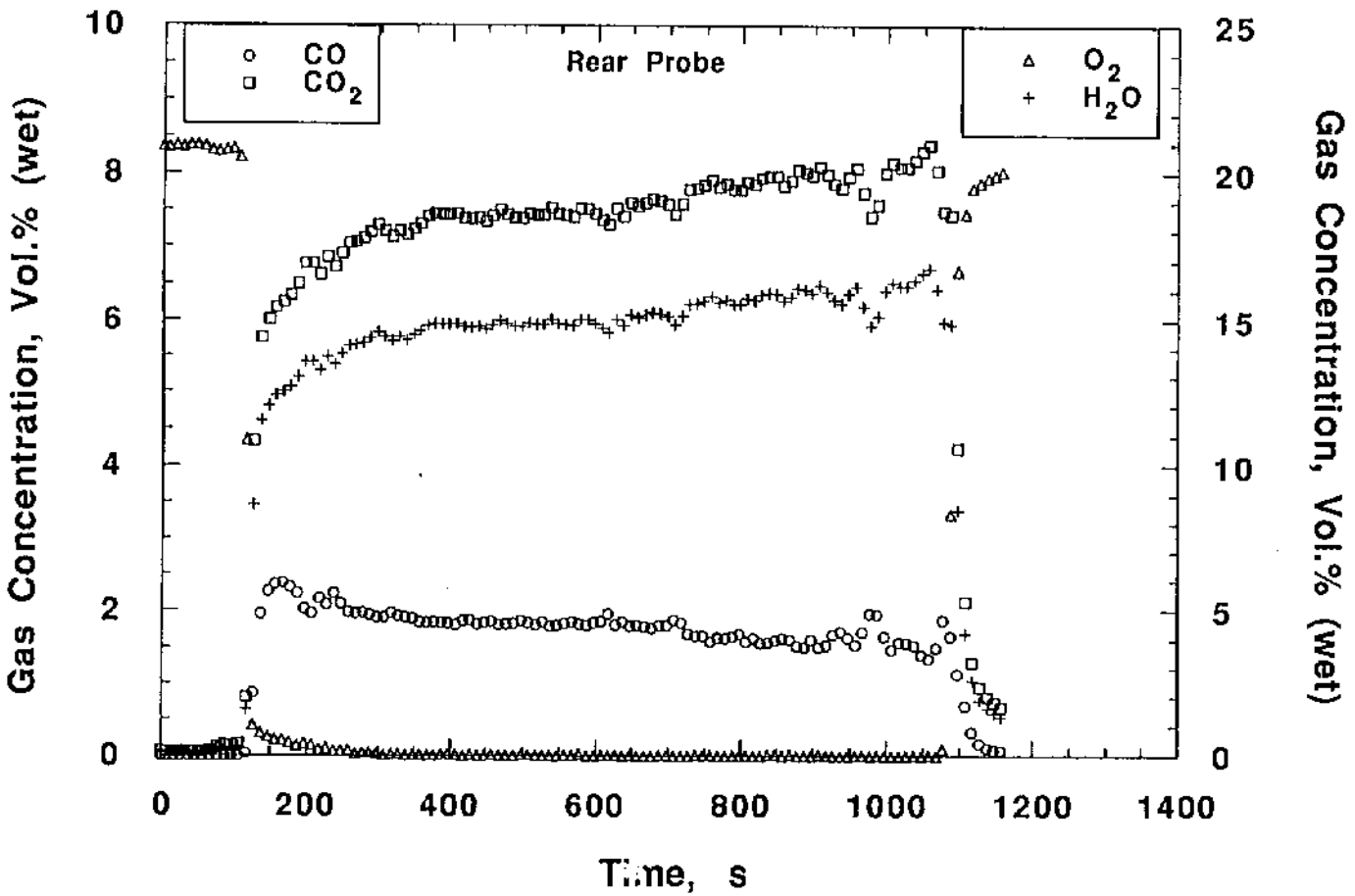

Figure 36. Gas concentrations at rear sampling location in upper layer of a 500 kW natural gas fire.

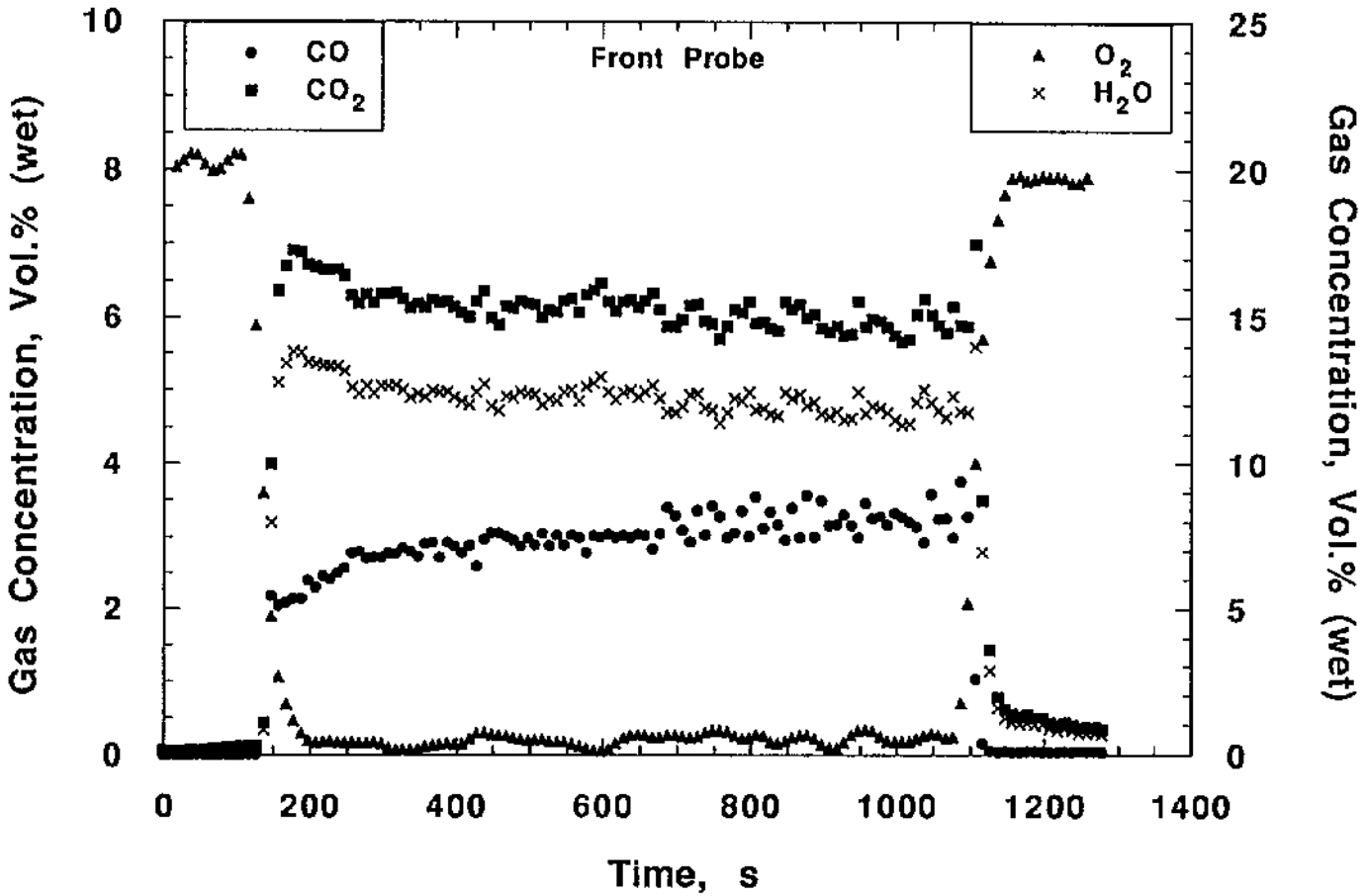

Figure 37. Gas concentrations at front sampling location in upper layer of a 600 kW natural gas fire.

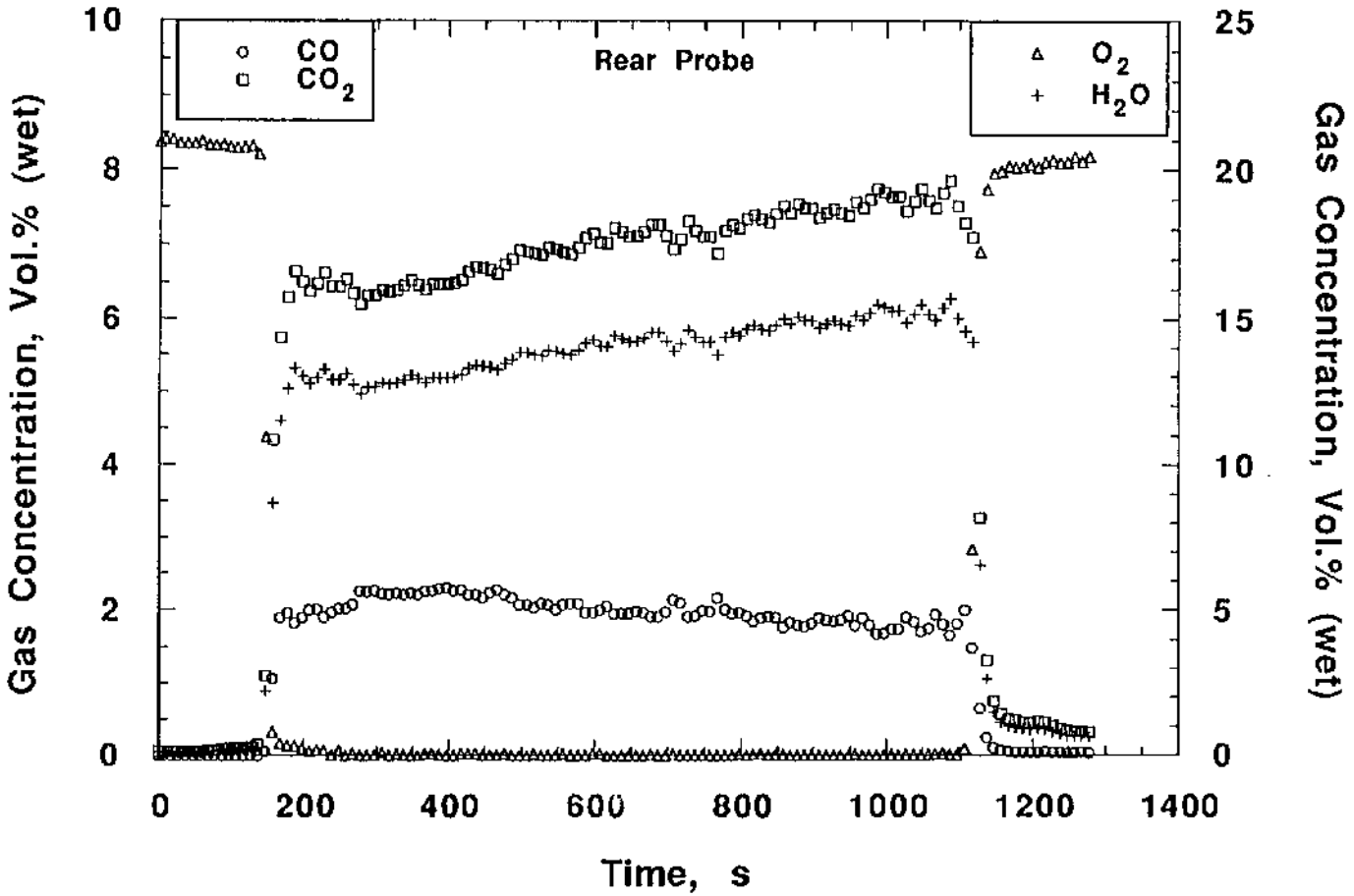

Figure 38. Gas concentrations at rear sampling location in upper layer of a 600 kW natural gas fire.

the front and rear "standard" probe locations for each heat release rate. While this study refers to these concentrations as "front" or "rear", it is not clear how well these two sample locations represent the front and rear of the upper layer. A limited number of vertical and horizontal mapping runs (discussed later in this section) demonstrate that gas species concentrations can vary significantly over very small vertical or horizontal distances within the upper layer. The zone model approach typically assumes that the compartment can be divided into homogeneous zones, upper and lower layers, which are uniform in gas composition. Although the gas concentrations (described later in this section) indicate that the upper layer is not a uniform "zone" either vertically or horizontally, the zone-model terminology of "upper layer" and "lower layer" will be used to refer to the upper and lower sampling locations, respectively. The heat release rate (HRR) which this study uses to characterize a fire includes the combustion which occurs inside the enclosure as well as the burning outside the enclosure.

As the heat release rate is increased, the concentration of oxygen in the upper layer steadily decreases for 25 to 200 kW fires and approaches zero for 200 to 650 kW fires. Typically the steady-state values of oxygen in the upper layer for high heat release rates range from 0.01 to 0.8% with an average of about 0.3%. The difference between oxygen levels in the front and rear of the enclosure is small with the levels in the front appearing to be slightly higher than the rear. This trend of relatively higher oxygen concentration in the front, 10.5% versus 8.5% in the rear, is evident for a 100 kW fire (Figures 24 and 25) which is not ventilation limited, but also appears for underventilated 600 kW fires (Figures 37 and 38) with 0.2% front and zero in the rear of the upper layer. Once an upper layer location becomes depleted of oxygen it remains so until the fire is extinguished. The oxygen concentrations in the front of the enclosure for fire sizes ranging from 25 to 600 kW are plotted as a function of time in Figure 39.

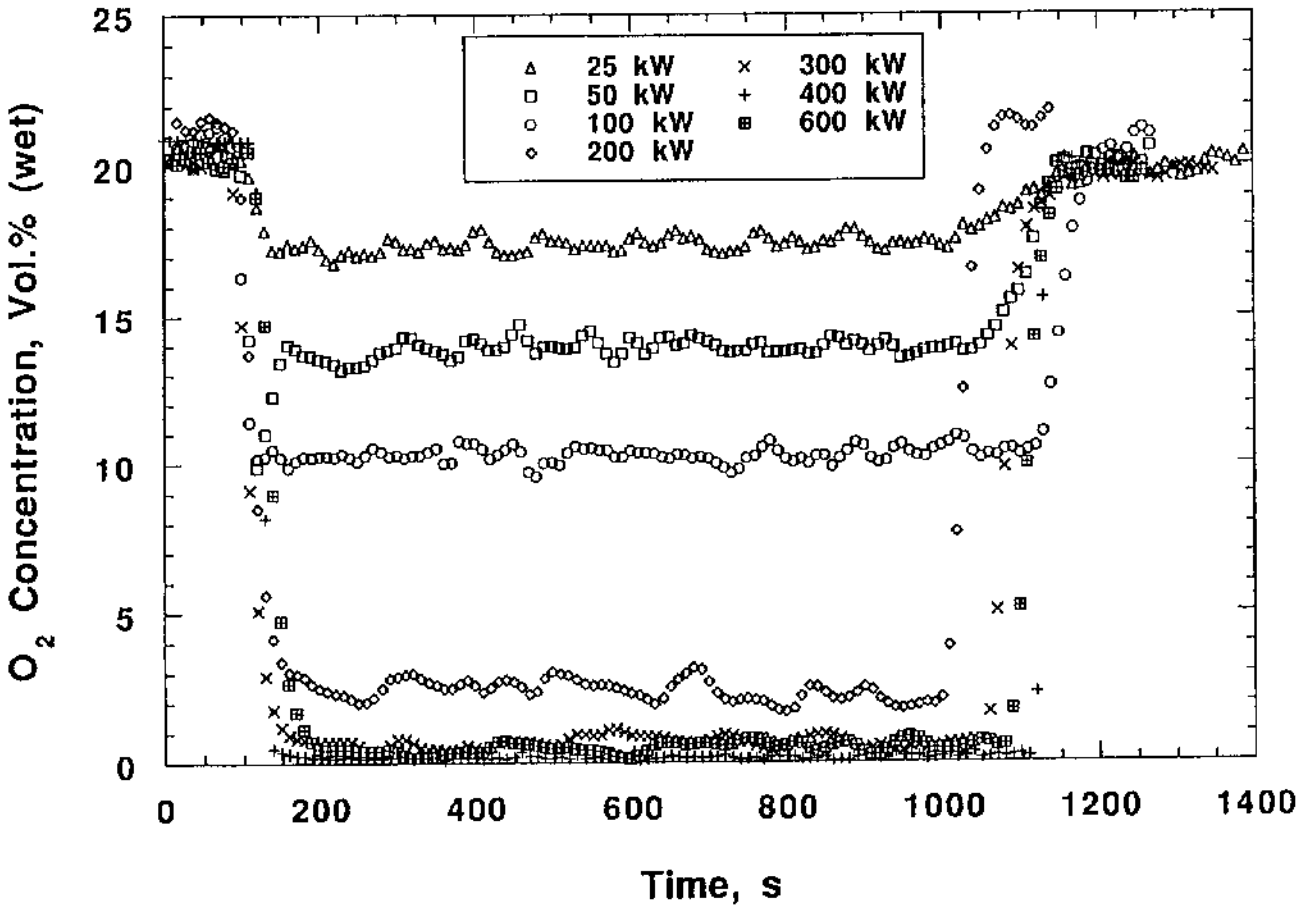

Figure 39. Front upper-layer oxygen concentration for fires with heat release rates ranging from 25 to 600 kW.

Measurements outside the door during two 400 kW fires indicate oxygen concentrations of about 3%. These levels of oxygen just 10.2 cm outside the door and inside the flame sheet, suggest that turbulent mixing is rapidly introducing additional oxygen. All sample locations in the lower layer revealed oxygen concentrations of approximately 20.9%. These concentrations, which are essentially ambient levels, indicate that the lower layer at the height of measurement is entirely fresh air coming through the doorway with little, if any, recirculation of combustion products from the upper layer.

The carbon dioxide concentration (see Figures 20-38) in the upper layer reaches a maximum for about the same heat release rate where the oxygen level first approaches zero. The upper-layer carbon dioxide level increases to a maximum of about 8.5% which was observed in the rear of a 200 kW fire. Gradually, with further increases in HRR, the carbon dioxide concentration decreases, reaching 7.5% for 600 kW fires. Typically, the concentration of carbon dioxide is significantly lower, differences of 0.3 to 1%, in the front when compared to the rear of the enclosure. The carbon dioxide concentration in the front of the enclosure typically reaches peak values after approximately 200 seconds, and then the concentration declines slightly, usually less than 1%. However, the opposite trend or increasing carbon dioxide concentration in the front was observed in the 150 kW fire. In the rear of the enclosure, the carbon dioxide concentration reaches about 80% of its final value in the first 200 seconds and then continues to increase until the end of the fire. The increases with time are much more apparent in the rear of the enclosure than the decreases in the front.

Measurements for the lower-layer sampling points (as shown in Figure 14) demonstrate that the levels of carbon dioxide are extremely low, 0.05 to 0.2%, again indicating that lower layer is essentially fresh incoming air. The carbon dioxide concentrations in the front of the RSE for fire sizes ranging from 25 to 600 kW are plotted as a function of time in Figure 40. The front CO_2 concentrations exceed 7.5% for the 200 kW and 300 kW fires, but drop to around 7% and 6% for the 400 kW and 600 kW fires, respectively. The upper-layer carbon monoxide concentrations begin

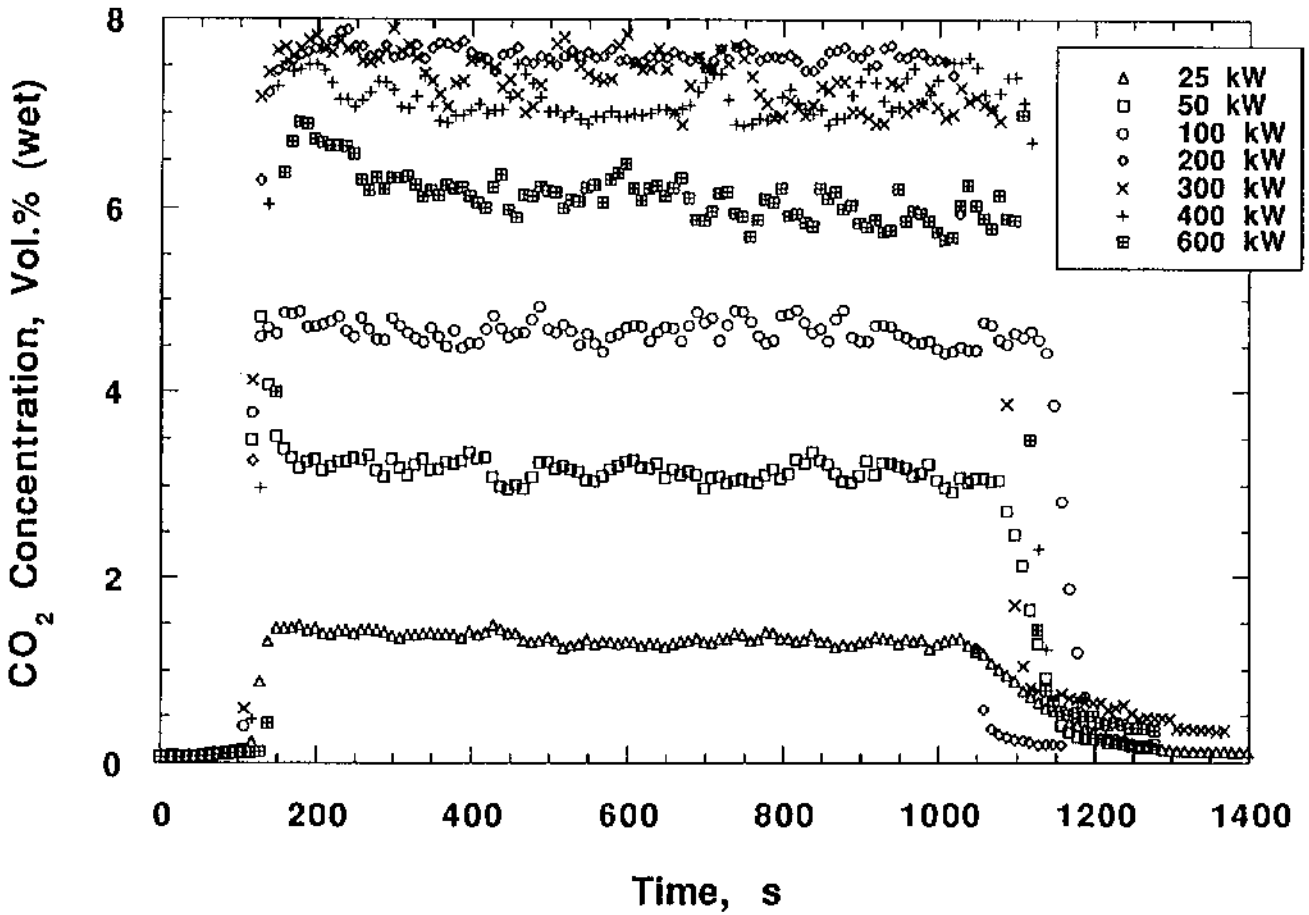

Figure 40. Front upper-layer carbon dioxide concentrations for fires with heat release rates ranging from 25 to 600 kW.

to increase for fires having a HRR of 100 kW and above and reach a peak of 3.5% for 400 and 600 kW fires. While the higher carbon dioxide concentrations appear in the rear of the enclosure, the higher carbon monoxide levels are observed in the front. During many burns the carbon monoxide and carbon dioxide display a strong negative correlation as the concentrations vary with time (e.g., Figure 41). As the carbon dioxide climbs, the carbon monoxide decreases proportionately.

The time variations or trends in the front and rear concentrations of carbon dioxide discussed above are mirrored in the carbon monoxide levels. The carbon monoxide concentration in the front of the enclosure typically reach about 80% of peak values after approximately 200 seconds and then the concentrations increase slightly, usually less than 0.5%. In the rear of the enclosure, the carbon monoxide reach peak values in the first 200 seconds and then the concentrations decrease until the end of the fire. The decreasing trend is much more apparent in the rear of the enclosure than the increasing trend in the front.

Carbon monoxide levels in the lower layer are very low, much like the carbon dioxide concentrations. These concentrations, which are very near background levels, further confirm that the lower layer is essentially fresh air. The carbon monoxide concentrations in the front of the enclosure are plotted as a function of time for fire sizes ranging from 25 to 600 kW in Figure 42. The concentration of water vapor in the upper layer is assumed (see Section 2.6) to be twice the uncorrected carbon dioxide level. The calculated water vapor concentrations peak at about 20% for 200 kW fires. As with the carbon dioxide concentrations, the water tends to decrease slightly for higher HRRs, falling to approximately 16% for 600 kW fires.

The horizontal and vertical mapping plots provide insights into the front-to-rear and top-to-bottom variations in gas concentrations. Horizontal mapping probes sampled (as shown in Figure 16) at different distances from the ceiling, 10 cm, 20 cm, and 30 cm for 400 kW fires (Figures 43 - 51), and 20 cm for a 600 kW fire (Figures 52-54). The overall trend behavior in CO and CO_2

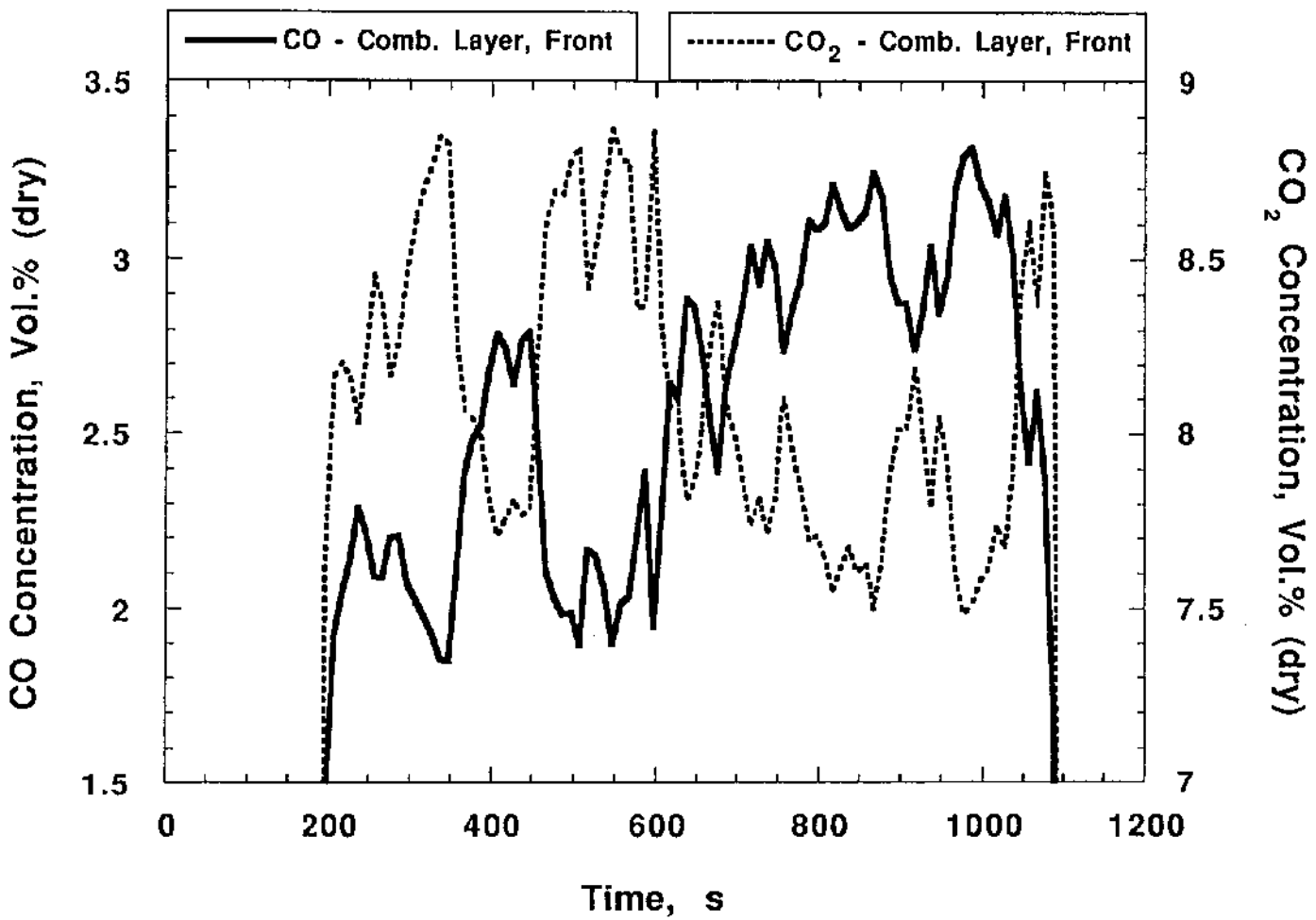

Figure 41. Inverse or "mirror" relationship between carbon monoxide and carbon dioxide concentrations in upper layer. Front sampling location for a 400 kW natural gas fire.

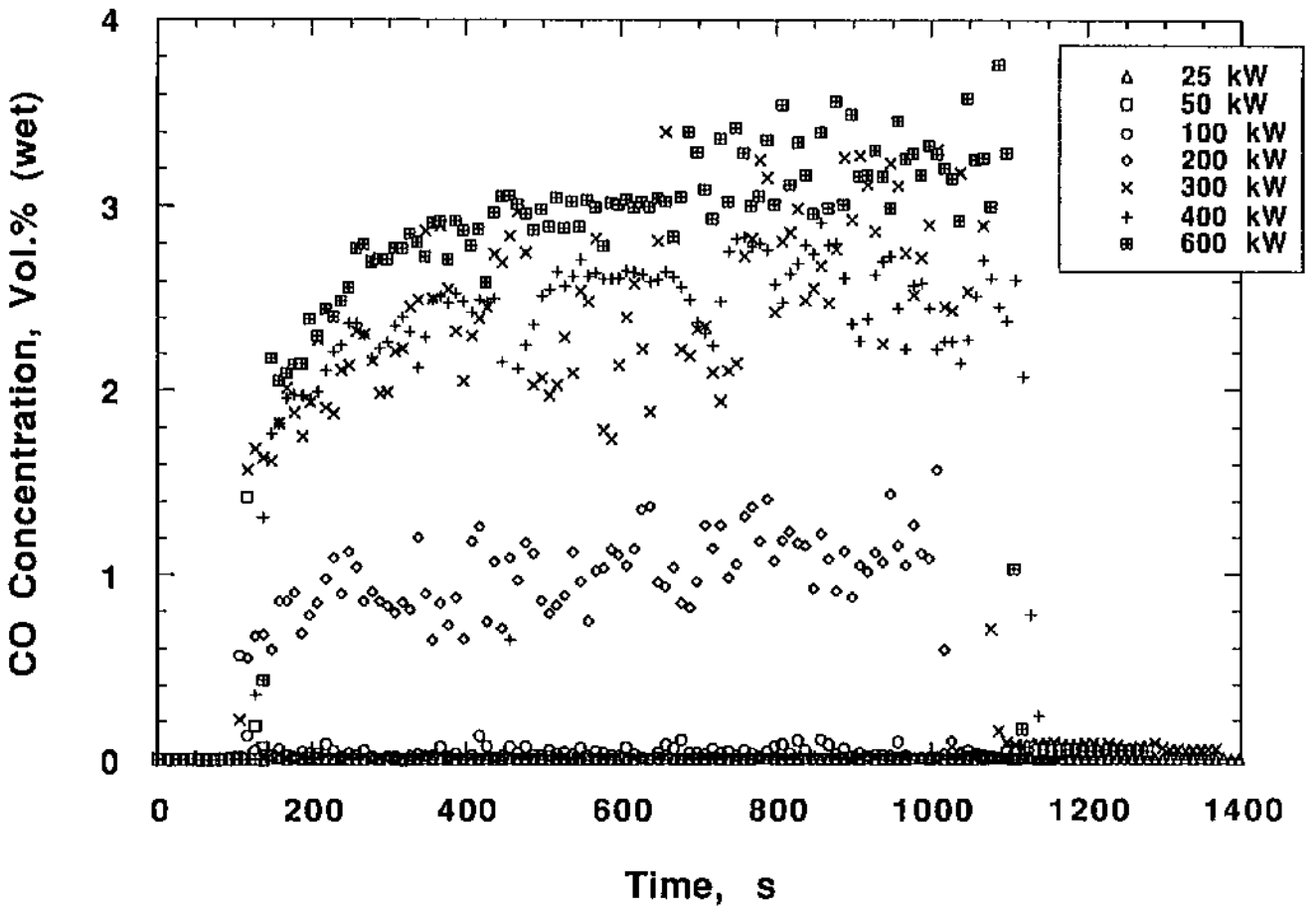

Figure 42. Front upper-layer carbon monoxide concentrations for fires with heat release rates ranging from 25 to 600 kW.

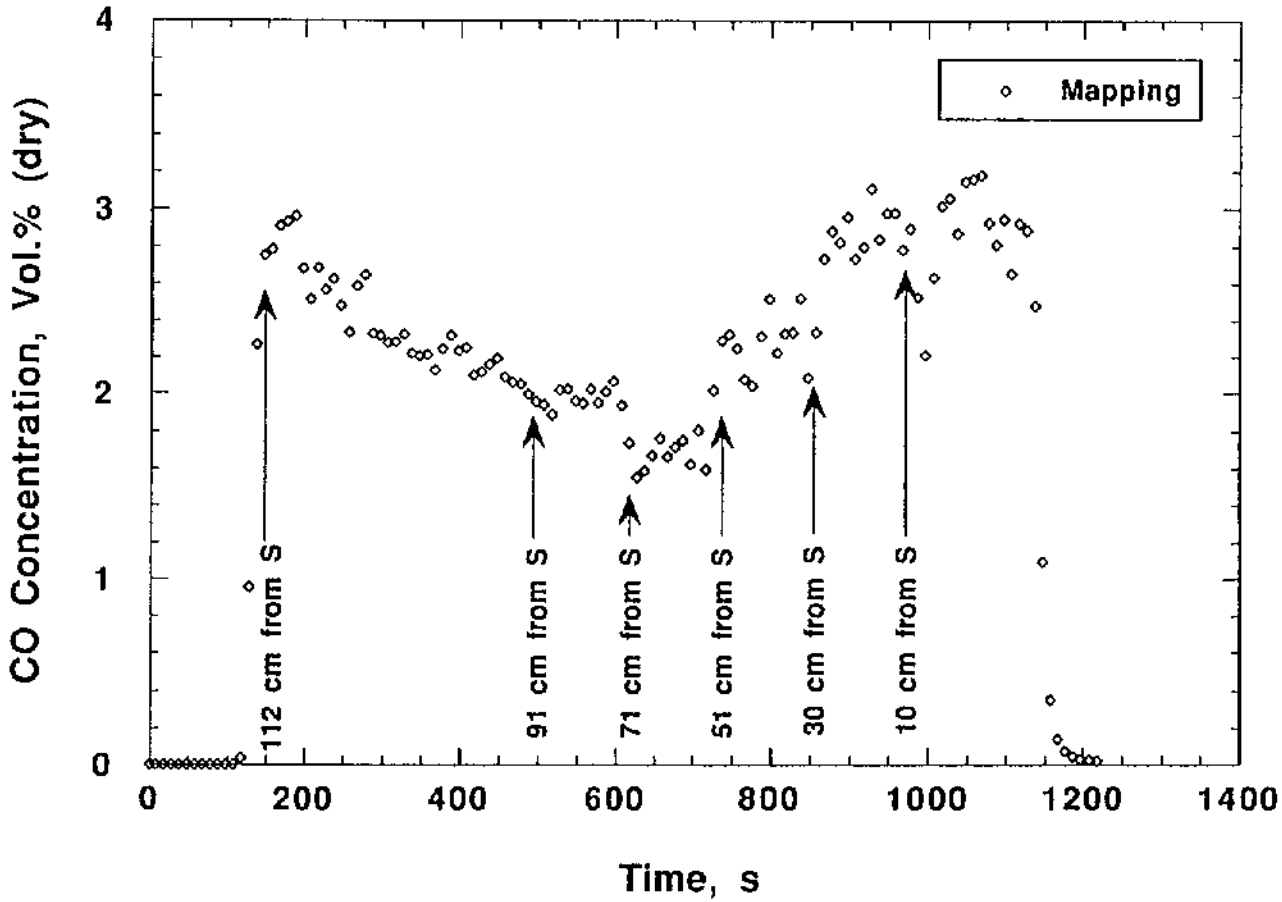

Figure 43. Horizontal mapping of CO concentration 10 cm below ceiling for a 400 kW fire. Mapping probe was moved in a stepwise fashion from the rear to front sampling location. All distances are relative to south (S) or front wall.

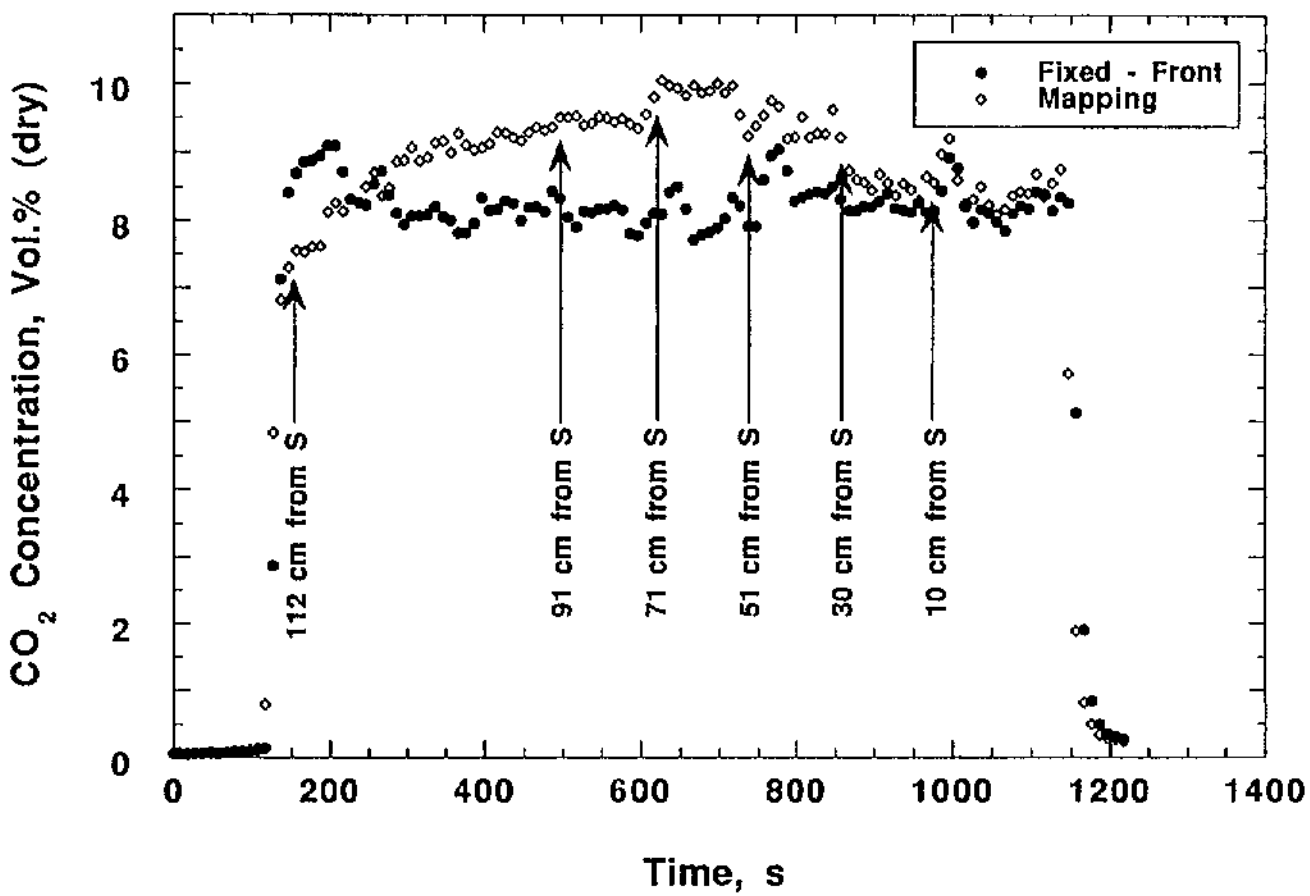

Figure 44. Horizontal mapping of CO_2 concentration 10 cm below ceiling for a 400 kW fire. Mapping probe was moved in a stepwise fashion from the rear to front location. All distances are relative to south (S) or front wall.

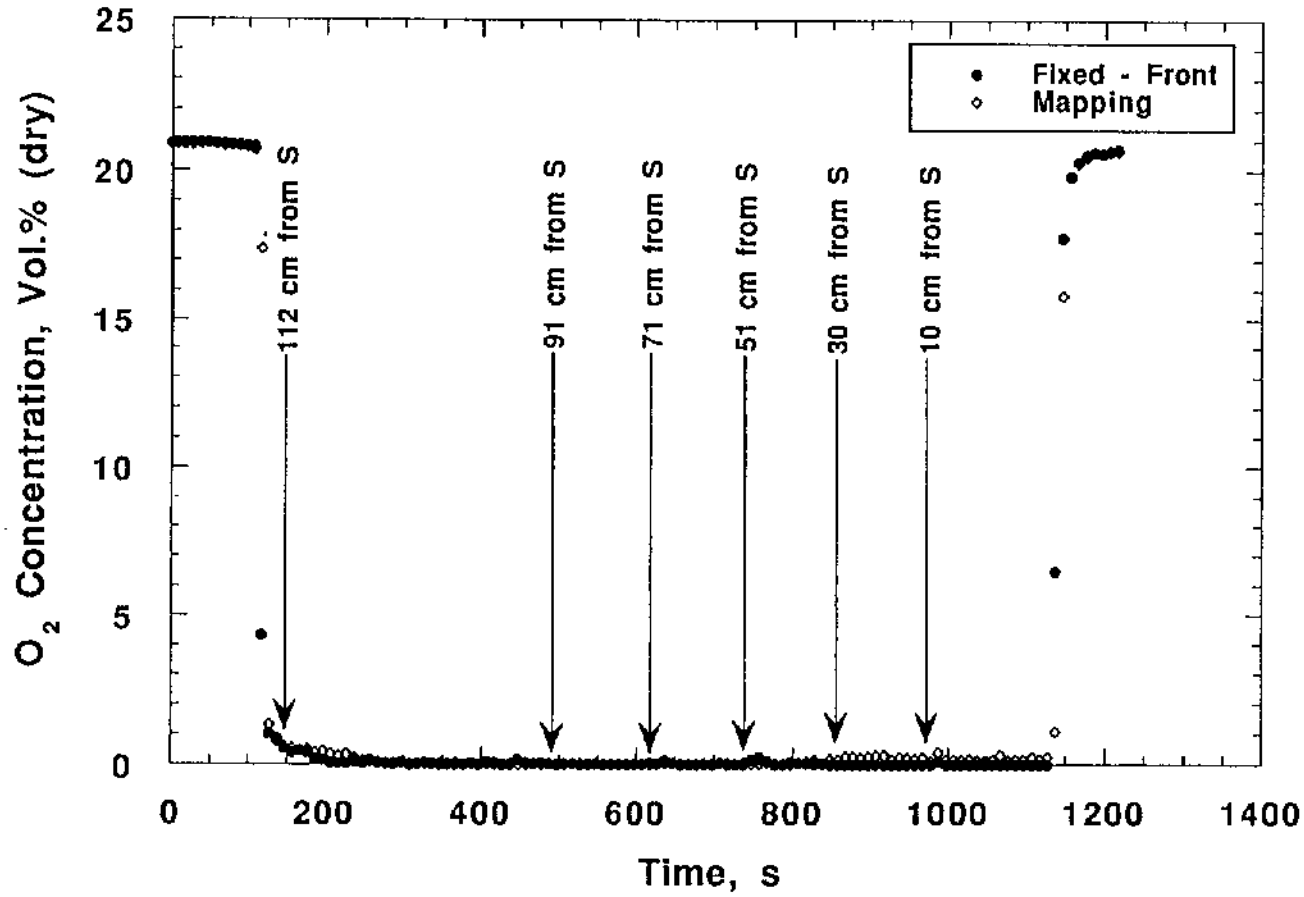

Figure 45. Horizontal mapping of oxygen concentration 10 cm below ceiling for a 400 kW fire. Mapping probe was moved in a stepwise fashion from the rear to front sampling location. All distances are relative to south (S) or front wall.

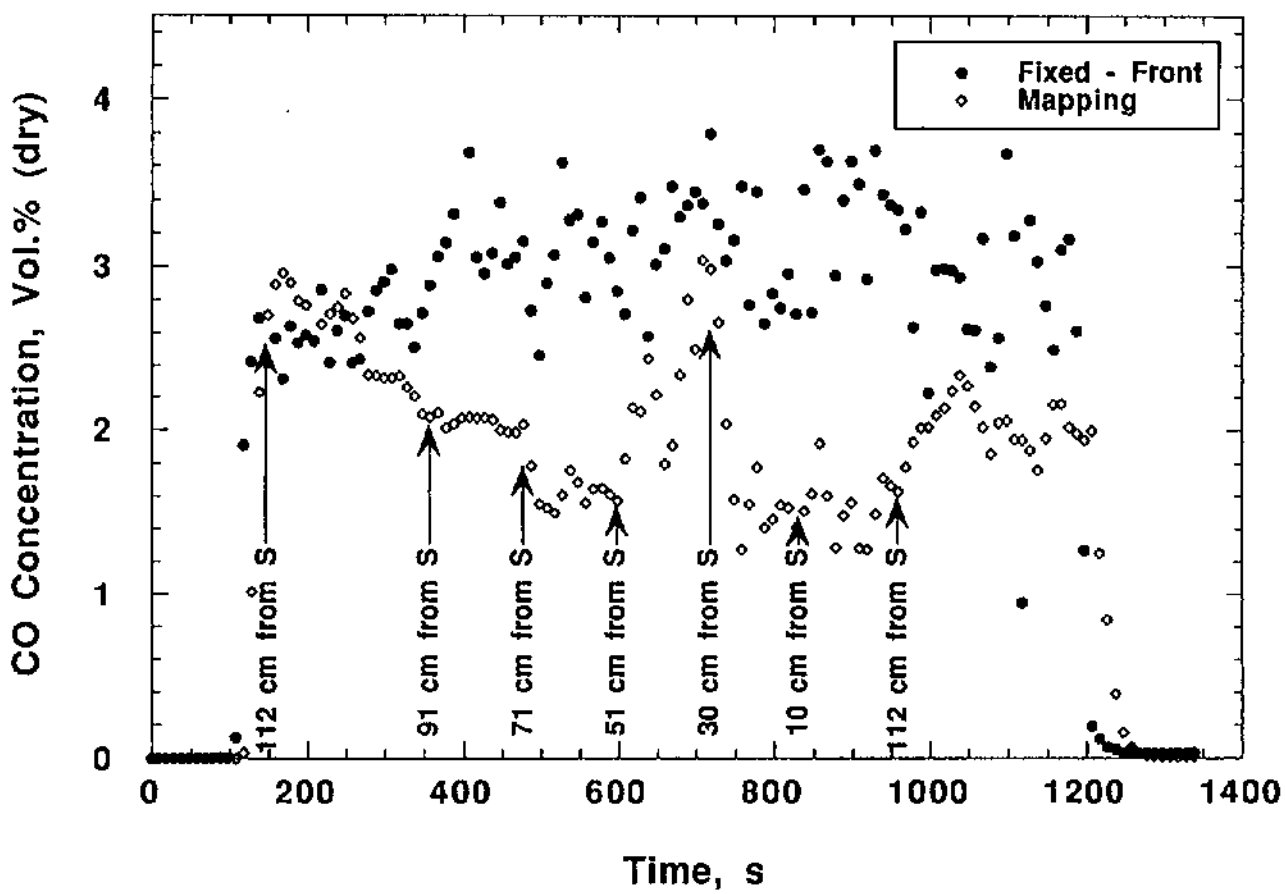

Figure 46. Horizontal mapping of CO concentration 20 cm below the ceiling for a 400 kW fire. Mapping probe was moved in a stepwise fashion from the rear to front sampling location. All distances are relative to south (S) or front wall.

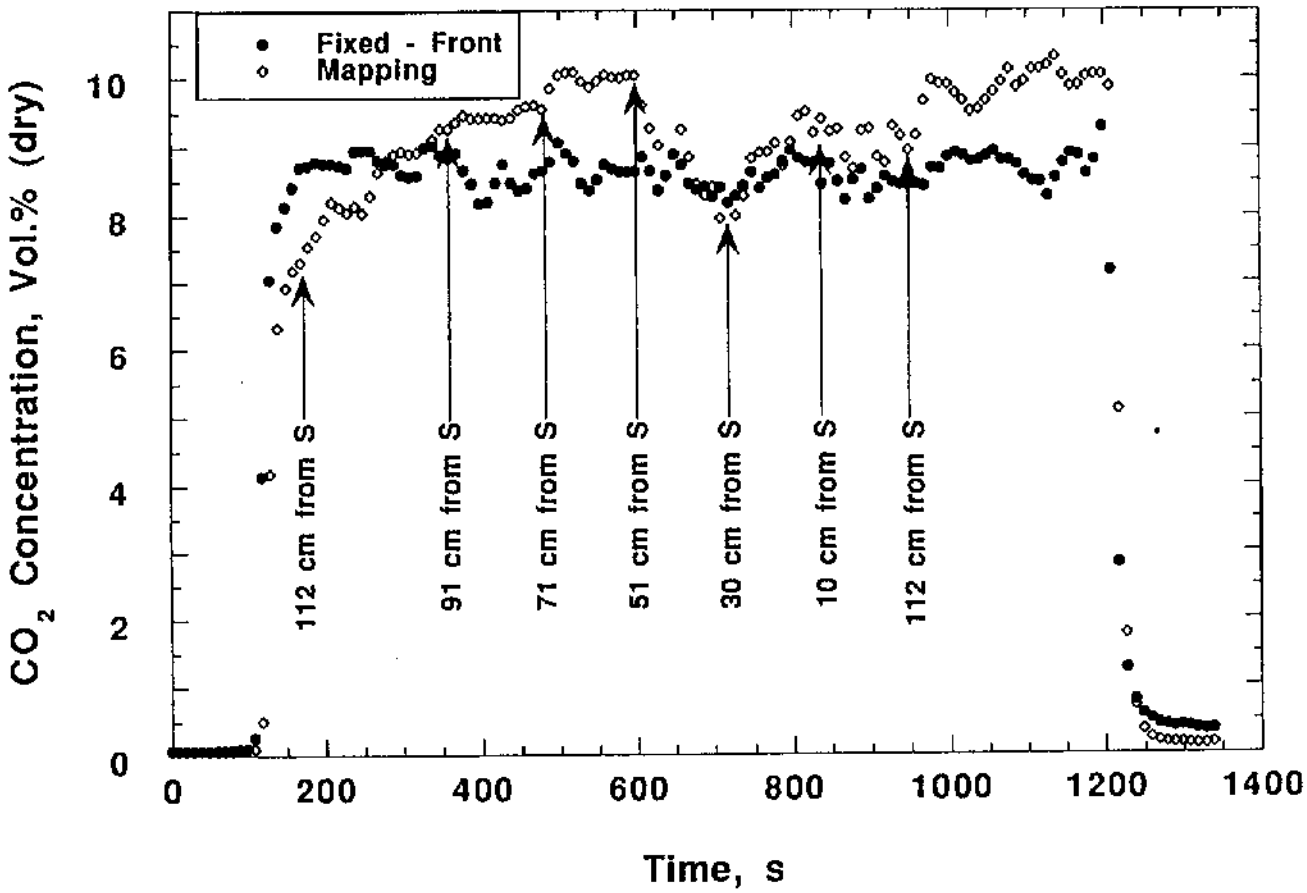

Figure 47. Horizontal mapping of carbon dioxide concentration 20 cm below ceiling for a 400 kW fire. Mapping probe was moved in a stepwise fashion from the rear to front sampling location. All distances are relative to south (S) or front wall.

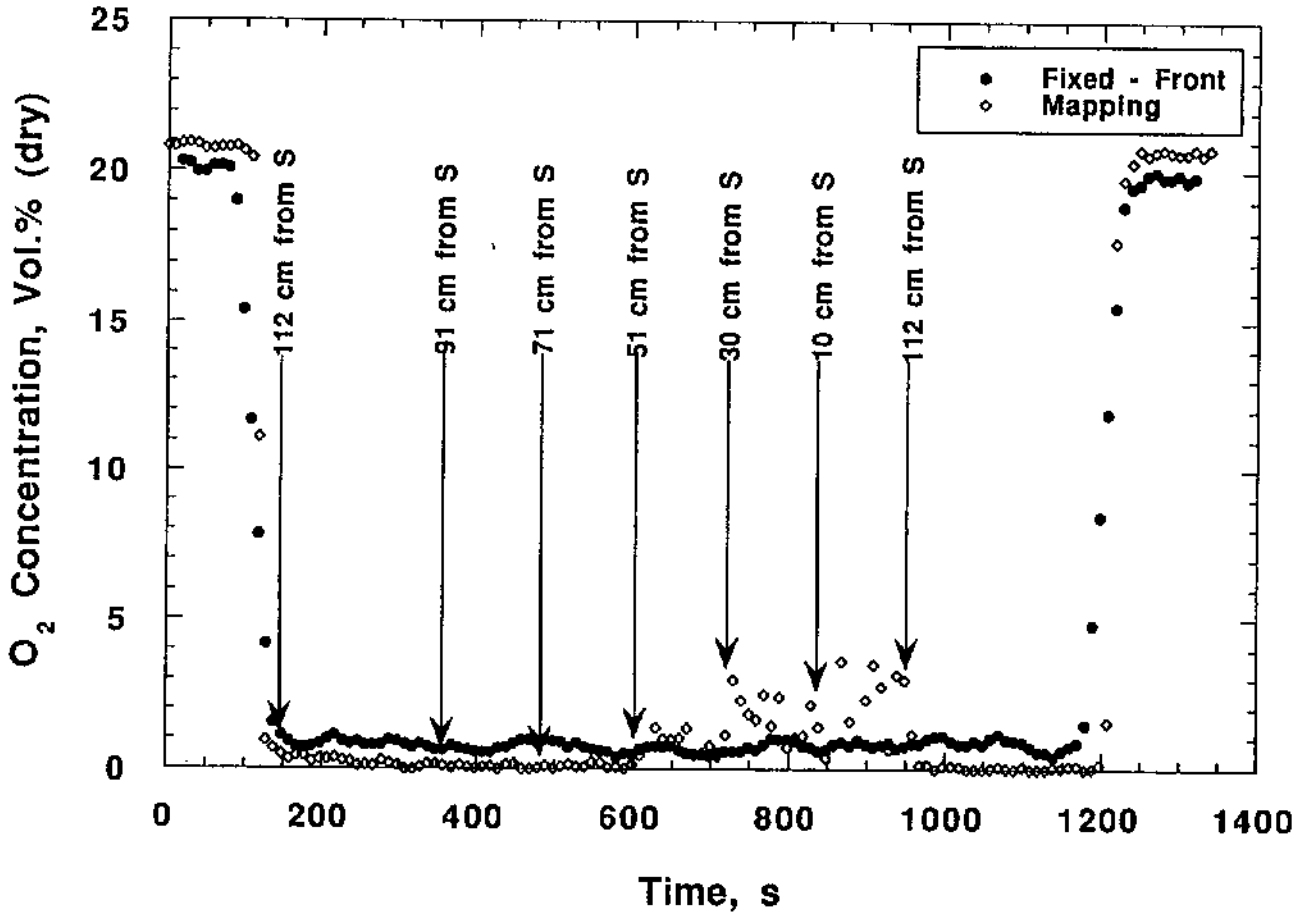

Figure 48. Horizontal mapping of oxygen concentration 20 cm below ceiling for a 400 kW fire. Mapping probe was moved in a stepwise fashion from the rear to front sampling location. All distances are relative to south (S) or front wall.

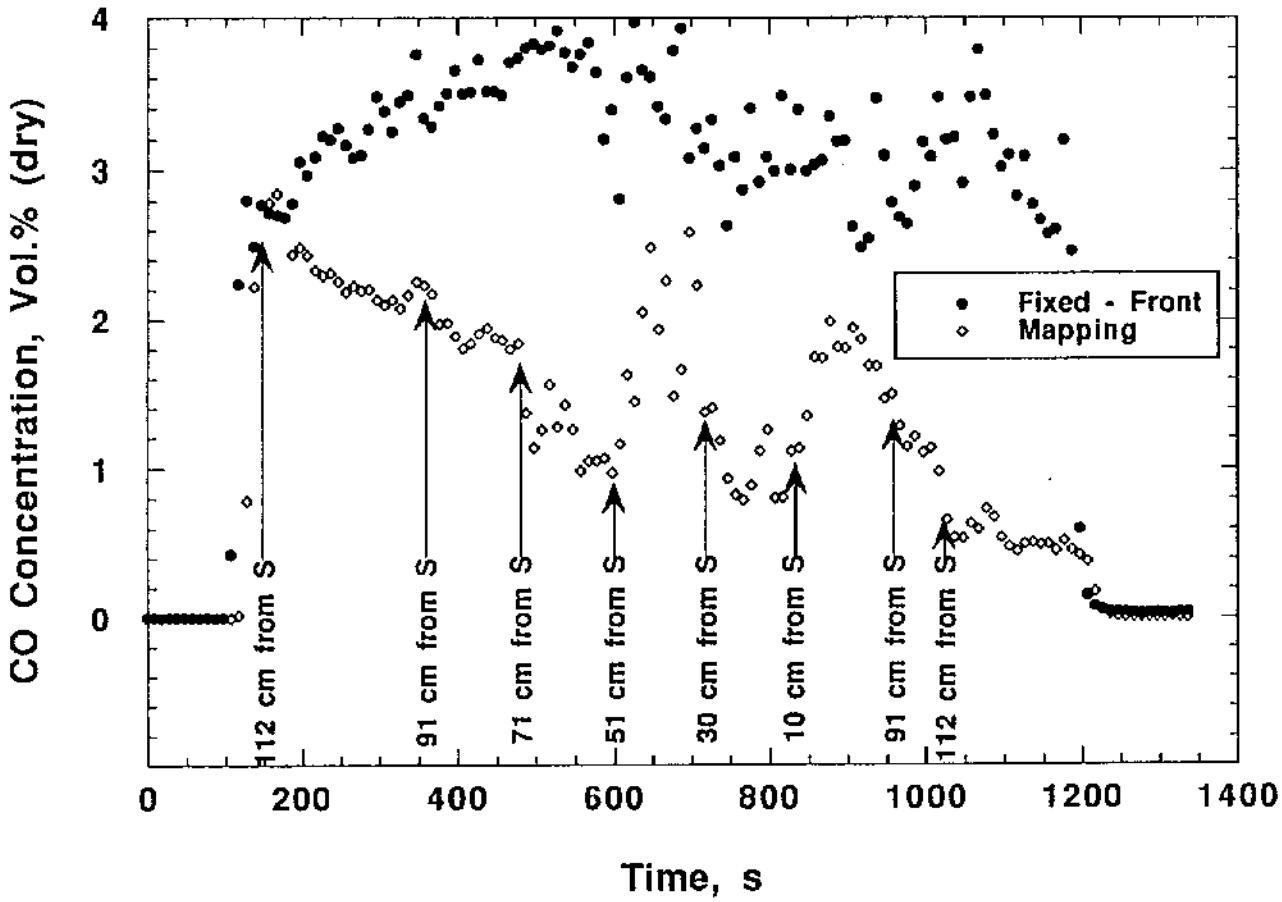

Figure 49. Horizontal mapping of CO concentration 30 cm below ceiling for a 400 kW fire. The mapping probe was moved in stepwise fashion from the rear to front sampling location. All distances are relative to south (S) or front wall.

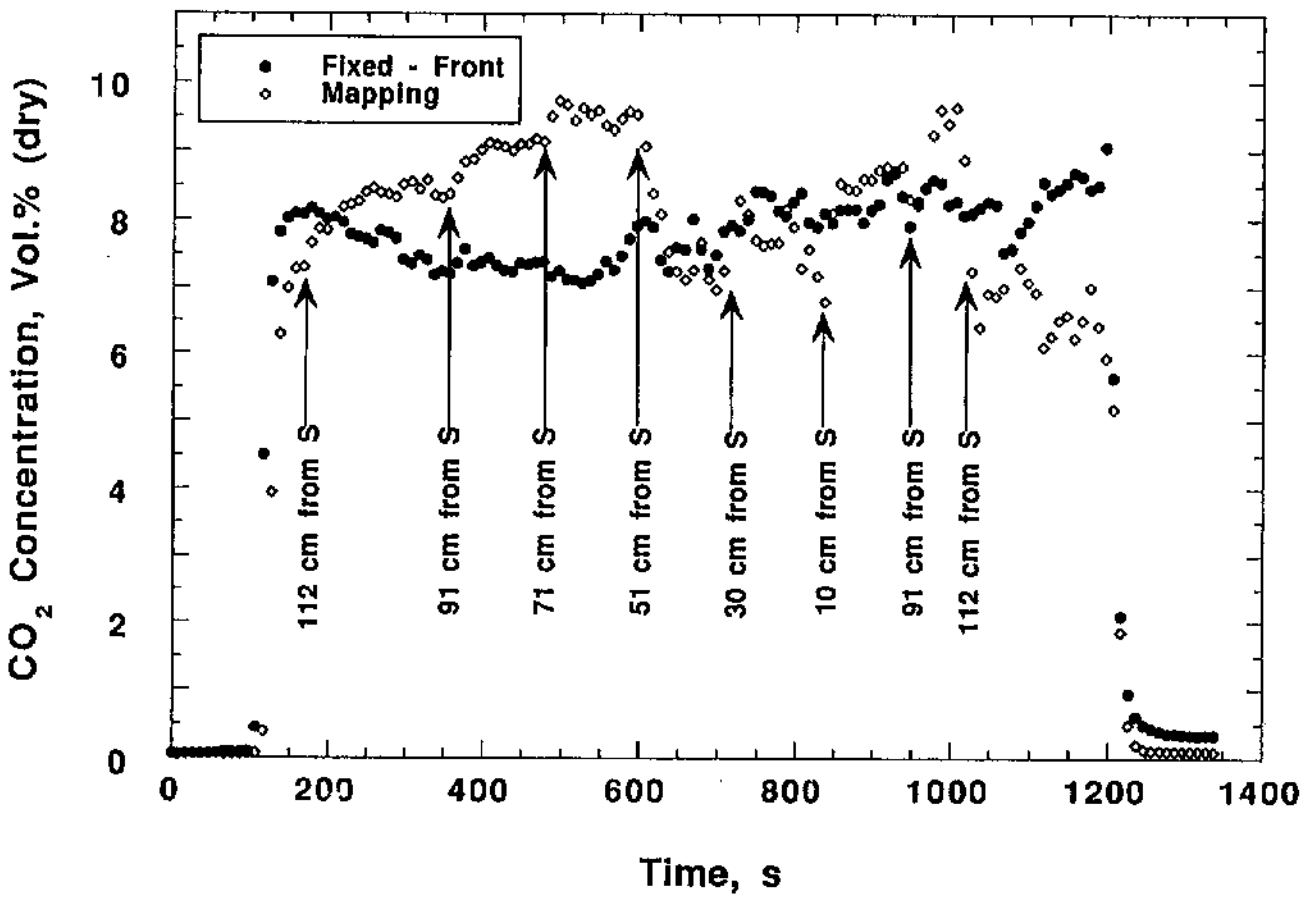

Figure 50. Horizontal mapping of carbon dioxide concentration 30 cm below ceiling for a 400 kW fire. Mapping probe was moved in a stepwise fashion from the rear to front sampling location. All distances are relative to south (S) or front wall.

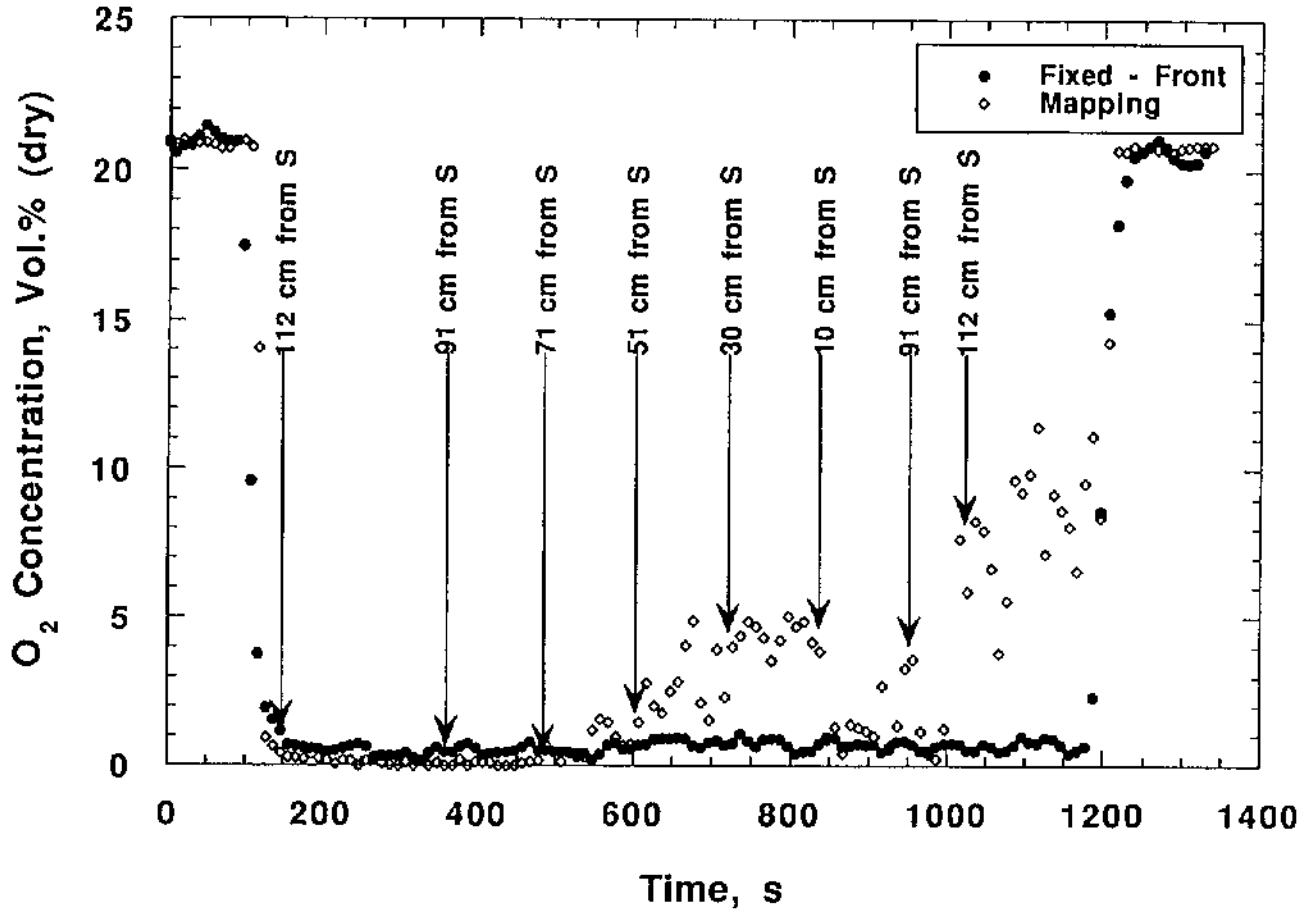

Figure 51. Horizontal mapping of oxygen concentration 30 cm below ceiling for a 400 kW fire. Mapping probe was moved in a stepwise fashion from the rear to front sampling location. All distances are relative to south (S) or front wall.

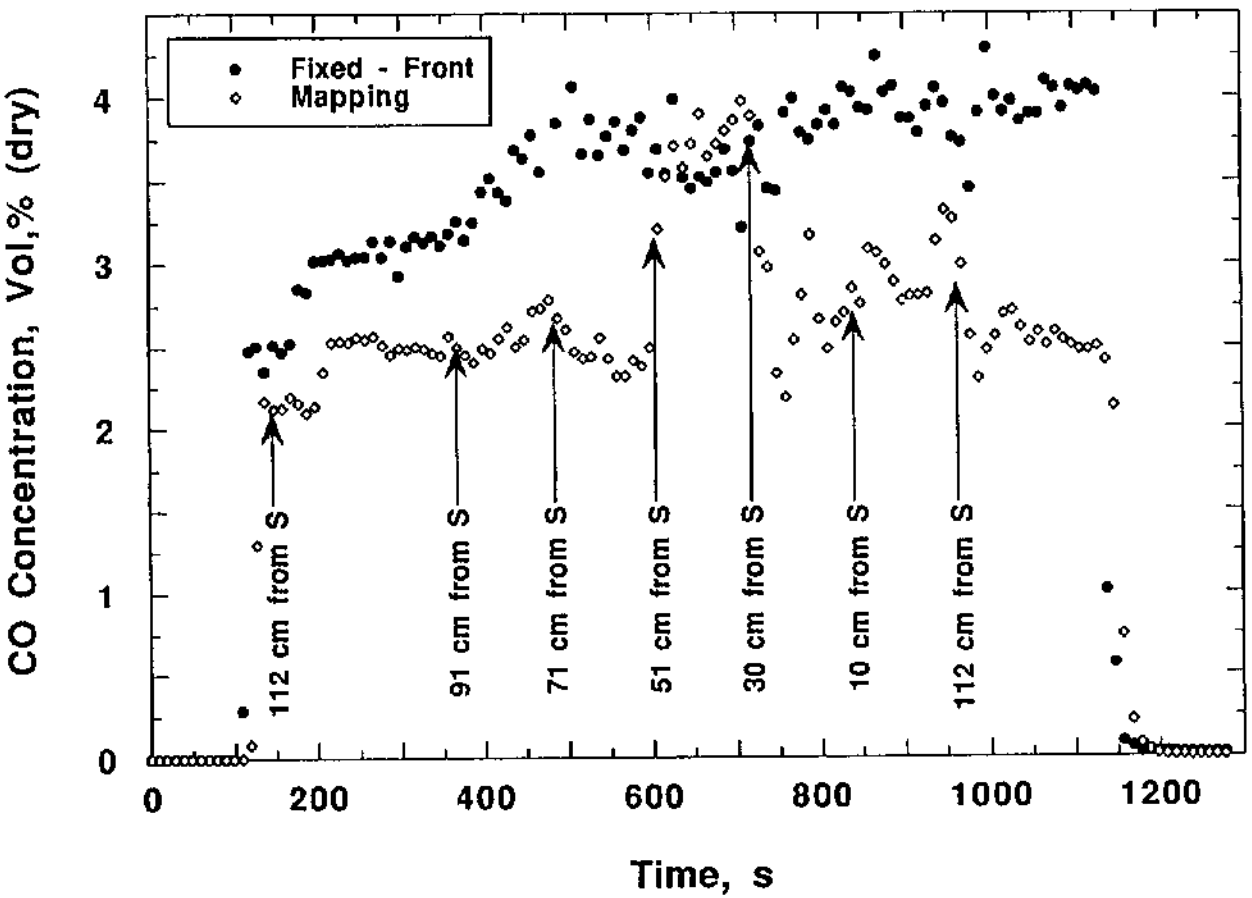

Figure 52. Horizontal mapping of carbon monoxide concentration 20 cm below ceiling for a 600 kW fire. Mapping probe was moved in a stepwise fashion from the rear to front sampling location. All distances are relative to south (S) or front wall.

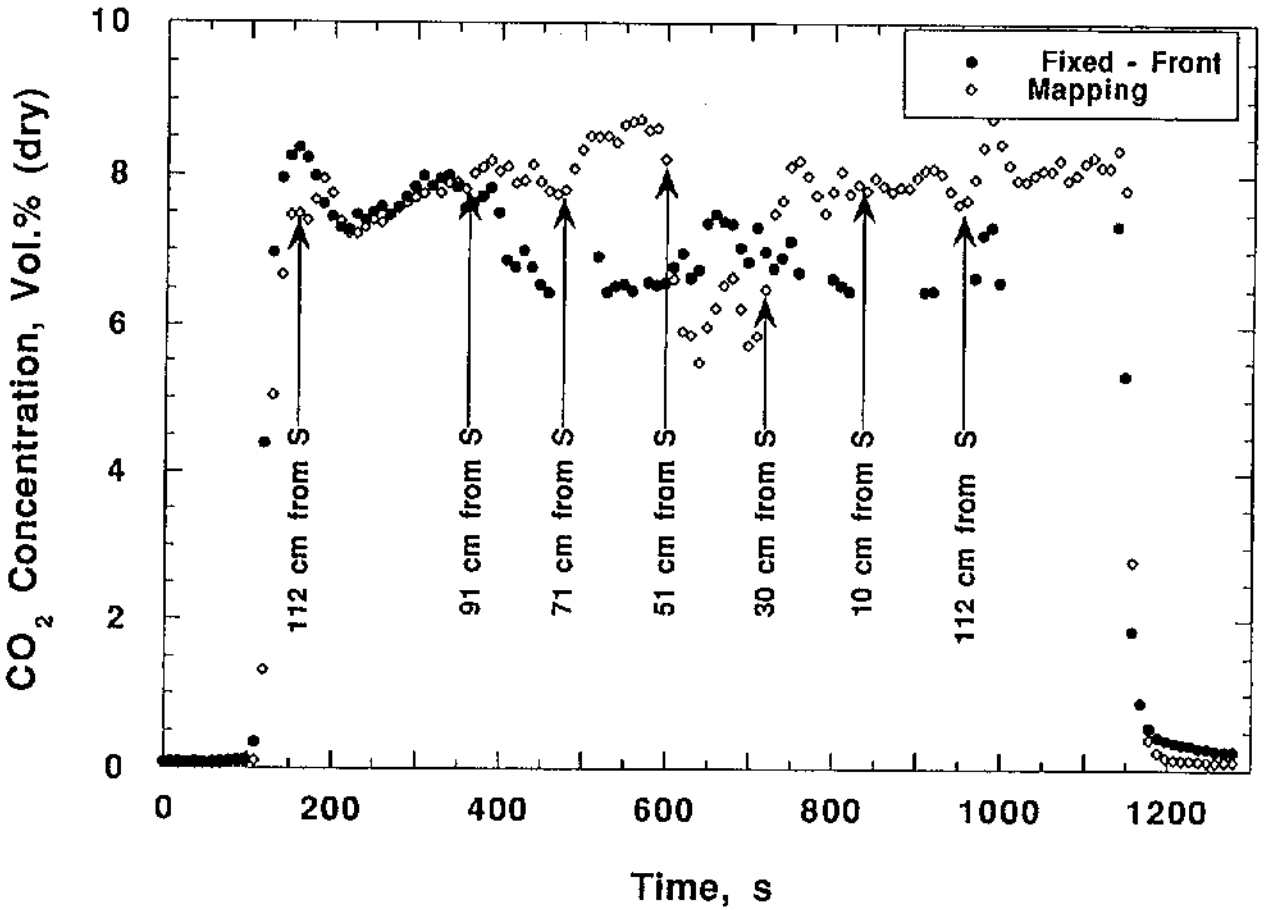

Figure 53. Horizontal mapping of carbon dioxide concentration 20 cm below ceiling for a 600 kW fire. Mapping probe was moved in stepwise fashion from the rear to front sampling location. All distances are relative to south (S) or front wall.

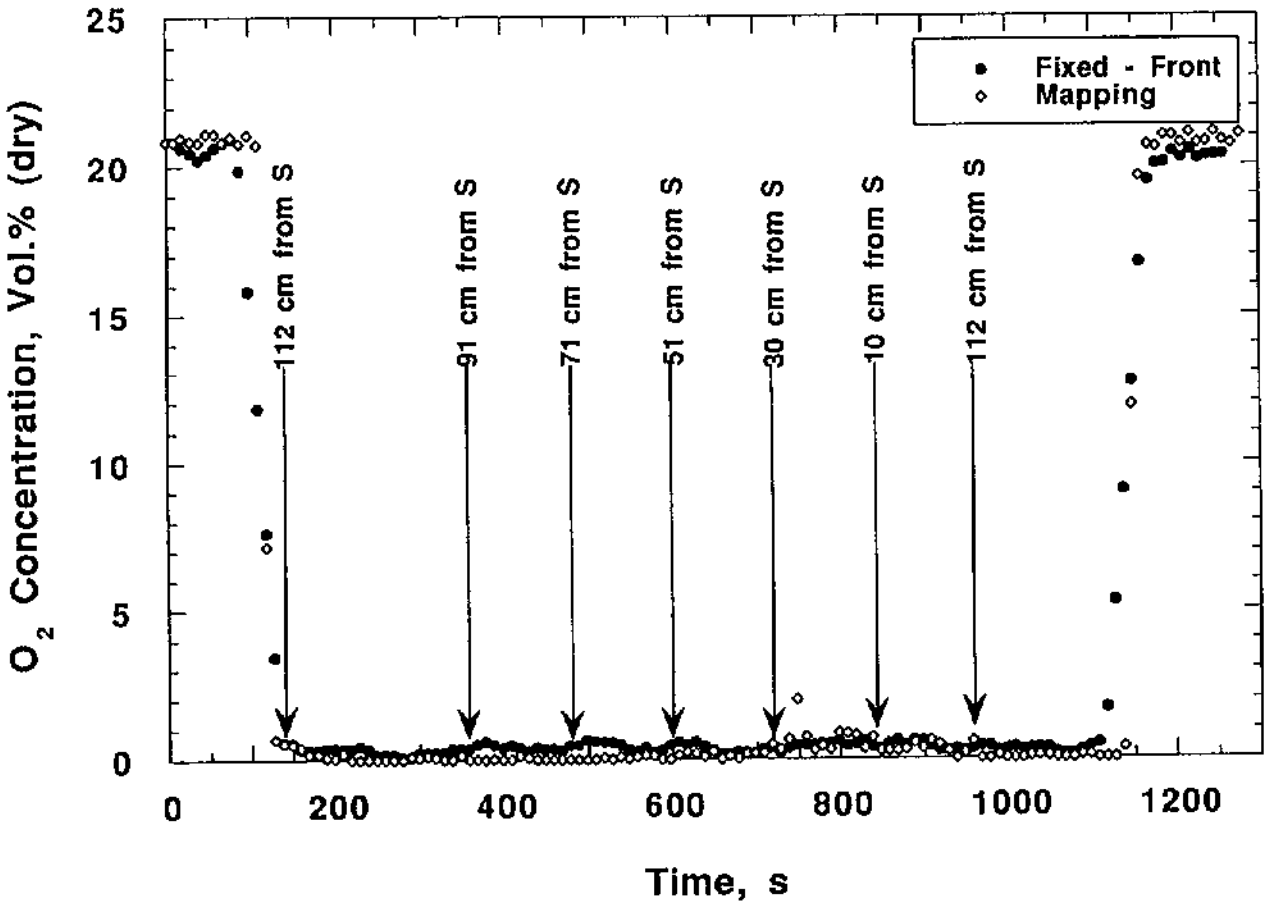

Figure 54. Horizontal mapping of oxygen concentration 20 cm below ceiling for a 600 kW fire. Mapping probe was moved in stepwise fashion from the rear to front sampling location. All distances are relative to south (S) or front wall.

concentrations are also present in the mapping runs and complicate the analysis the gas concentration data. The concentration of gases sampled by the mapping probe depends on both the sampling location and the specific time during the fire when the gases were collected.

Each horizontal run usually began near the north or rear wall and stepped towards the door or front of the enclosure. Typical distances for the sample probe were 112, 91, 71, 51, 30, and 10 cm from the front or south wall. After traversing from the rear to the front, the probe was returned to the starting position in the rear in order to check how the gas concentrations may have changed or drifted over the time required for the mapping run. The fixed-front probe was positioned at the "standard" front location, 10 cm inside the door or south wall, 29 cm from the west wall, and 10 cm down from the ceiling.

By comparing the before and after concentrations of CO at the 112 cm position, the same trends observed and discussed above are exhibited in the rear of the upper layer. Early in the fire, the CO reaches its peak value and declines while the probe is at its initial location, 112 cm. After the mapping run when the probe is returned to 112 cm, the CO concentration decreases by 1 - 1.5%. The corresponding trend for the CO_2, where the CO_2 concentrations increase gradually is also present in the 400 kW fires. These trends in the CO and CO_2 concentrations are harder to see in the 600 kW fire. In terms of CO and CO_2, the rear of the upper layer at 20 cm from the ceiling in the 600 kW fire does not appear to change as much as the 400 kW fire.

The horizontal mapping run 30 cm below the ceiling for the 400 kW fire (Figures 49 - 51) also reveals that the rear of the upper layer became thinner or less deep over the course of the fire. When the concentrations at 300 seconds are compared with 1100 seconds, the CO and CO_2 concentrations both decrease while O_2 increases. If CO was being converted to CO_2 (or vice versa) then the CO and CO_2 levels would move in opposite directions. It is important to note that while decreasing and increasing trends were observed in the CO and CO_2 concentrations, the O_2

concentrations remained near zero throughout each fire and exhibited no trend behavior. The increase in O_2 and decrease in CO and CO_2 levels at 112 cm from the front wall are consistent with the layer becoming thinner and gradually diluted with air from the lower layer. It is also consistent with a gradual thinning of the layer that this effect is observed 30 cm from the ceiling but not at 10 cm or 20 cm below the ceiling.

Although the thinning of the rear layer and the overall decreasing (CO) and increasing (CO_2) trends complicate the analysis, the mapping runs do show a region of high carbon monoxide concentration and relatively lower carbon dioxide levels in the upper layer in the front portion of the enclosure. This region first appears when the probe samples 51 cm from the front wall. When the sampling probe is moved to the 31 cm position (Figure 49 or 52), the CO levels generally tend to decrease to the pre-51 cm position levels. The CO levels recorded 10 cm from the ceiling in the 400 kW fire (Figure 43) do not drop but continue to increase as the sampling probe is moved towards the front of the enclosure. The horizontal mapping runs conducted at 10, 20, and 30 cm from the ceiling and 29 cm from the left (looking in the door) wall indicate that this region of high CO is at least 20 cm deep and at least 30 cm wide (assuming left to right symmetry) for the 400 kW fires. The 15.2 cm diameter burner is centered at 73 cm from the front wall. Since the high levels of CO are not recorded until the 51 cm location, the high CO region appears to be located between the burner and the doorway, but is closer to the burner.

The horizontal mapping runs also indicate that additional oxygen is entering the lower portion of the upper layer in the front of the enclosure. While the upper layer remains completely depleted of oxygen 10 cm from the ceiling (Figure 45), at 20 cm (Figure 48) and 30 cm (Figure 51) down from the ceiling, additional oxygen is observed as the sample probe reaches the 51 cm position. The additional oxygen appears intermittently at 20 cm below the ceiling. At 30 cm below the ceiling enough oxygen enters the layer to increase the concentration to 5% between 30 cm and 10 cm from

the front. For the 600 kw fire (Figure 54), there is no indication of oxygen in the upper layer 20 cm below the ceiling.

During each vertical mapping run, a sampling probe was positioned 10 cm inside the doorway (Figure 55-60) and was moved vertically in a stepwise fashion down from the top to the bottom sampling location. Typical locations for the sample probe were 8, 10, 15, 20, 25, 30, and 36 cm from the ceiling. The upper edge of the doorway is located 17 cm from the ceiling. The overall increasing (CO) and decreasing (CO_2) trends observed in the front of the enclosure for other fires and discussed earlier are apparent for the 250 kW and 600 kW fire results shown. The fixed-front probe was positioned at the "standard" front location, 10 cm inside the door or south wall, 29 cm from the west wall, and 10 cm down from the ceiling.

The vertical mapping plots for the 250 kW fire show that as the probe was moved below 10 cm from the ceiling the upper layer concentrations of both CO and CO_2 dropped quickly while the O_2 concentration increased. This suggests that there was significant mixing of upper layer gases and air at this sampling position. The results for the 600 kW mapping run exhibit a much different behavior. Both the CO and CO_2 concentrations remained nearly constant and did not fall off until the probe was moved to the lowest sampling position, 41 cm below the ceiling. Over the same range, oxygen remained uniformly depleted and only began to rise 41 cm below the ceiling. In the 250 kW fire, the CO, CO_2, and O_2 concentrations were consistent with air intruding into the upper layer around 15 cm from the ceiling and essentially diluting the upper layer while in the 600 kW fire only combustion gases were present. It is remarkable that the layer structure was so different for these two fires. The results demonstrate there is a strong relationship between fire size and nonuniformity within the upper layer.

For each of the burns, average gas concentrations for the pseudo-steady burning portion of the experiment have been calculated for the fixed sampling probe locations. The averages were

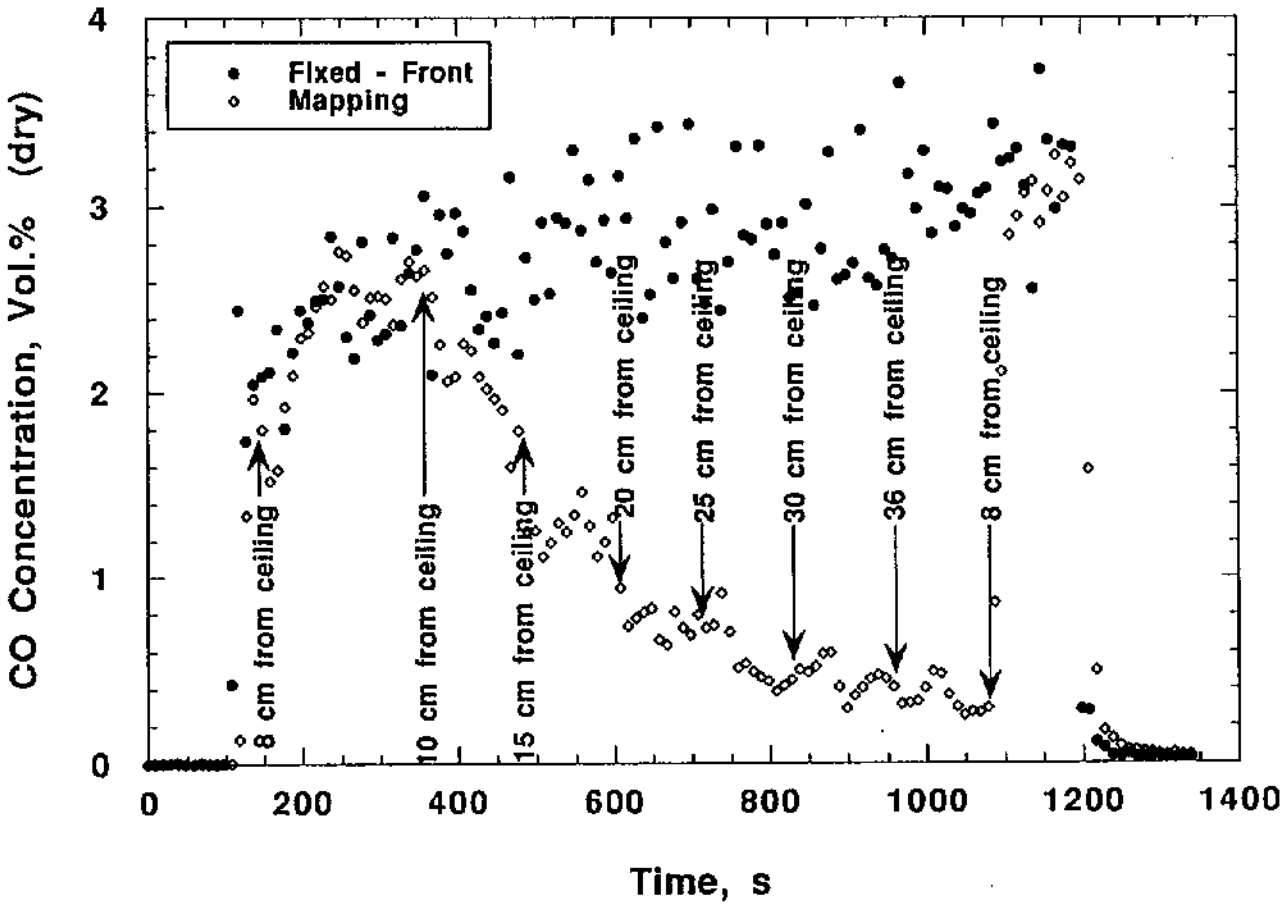

Figure 55. Vertical mapping of CO concentration 10 cm from front wall for a 250 kW fire. While the stationary probe remained at the top location, the mapping probe was moved vertically in a stepwise fashion down from the top to the bottom position.

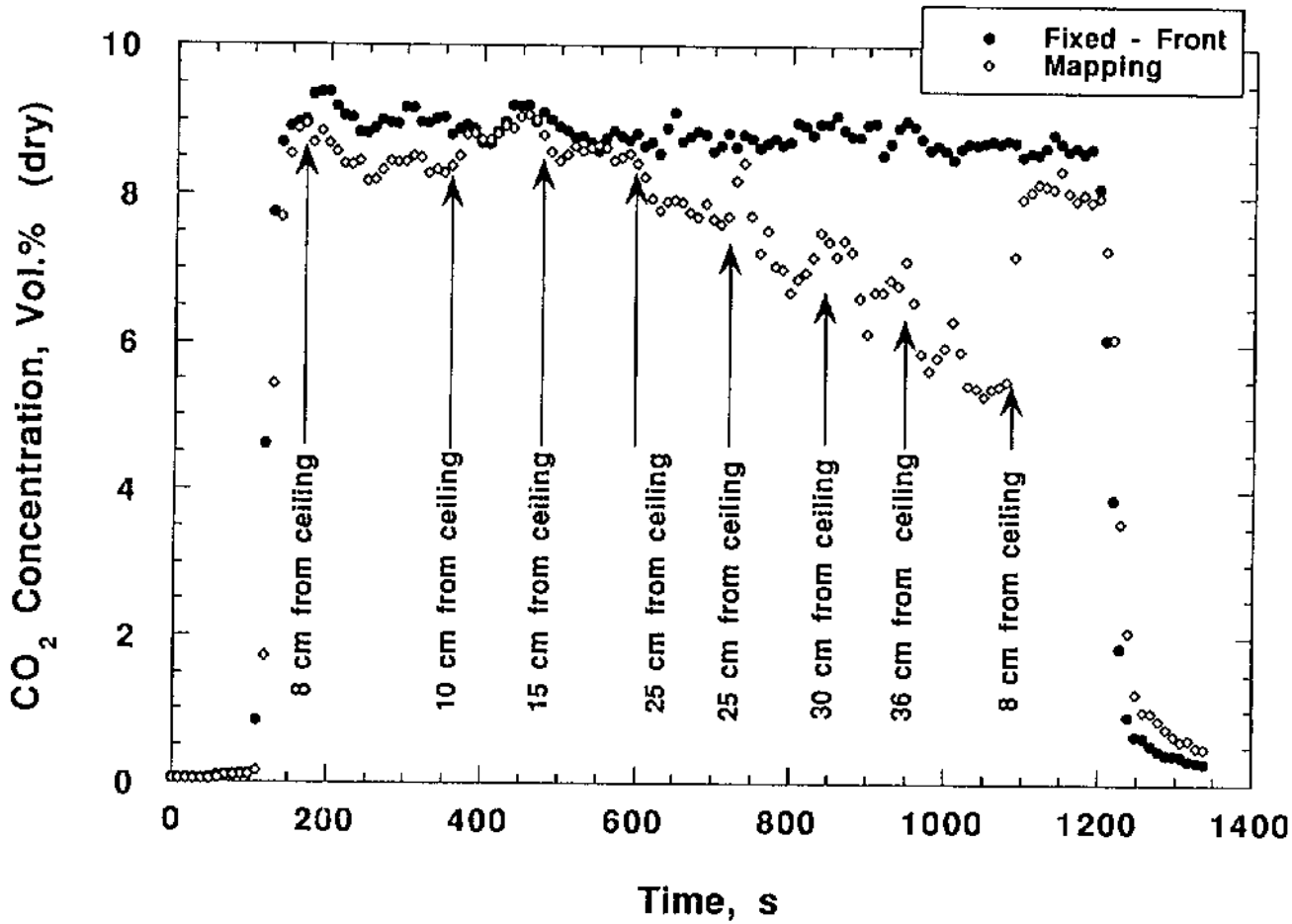

Figure 56. Vertical mapping of CO_2 concentration 10 cm from front wall for a 250 kW fire. While the stationary probe remained at the top location, the mapping probe was moved vertically in a stepwise fashion down from the top to the bottom position.

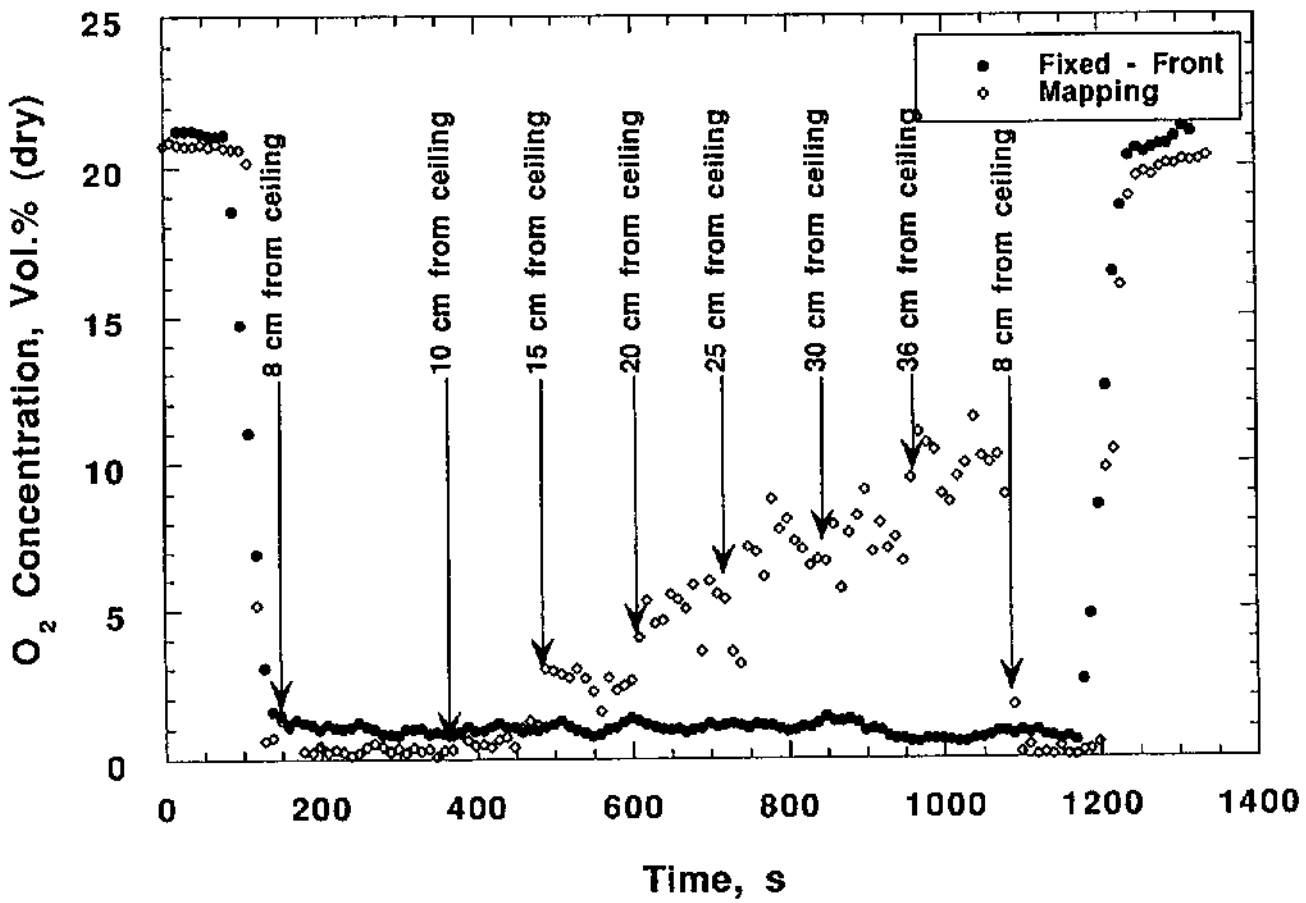

Figure 57. Vertical mapping of O_2 concentration 10 cm from front wall for a 250 kW fire. While the stationary probe remained at the top location, the mapping probe was moved vertically in a stepwise fashion down from the top to bottom sampling location.

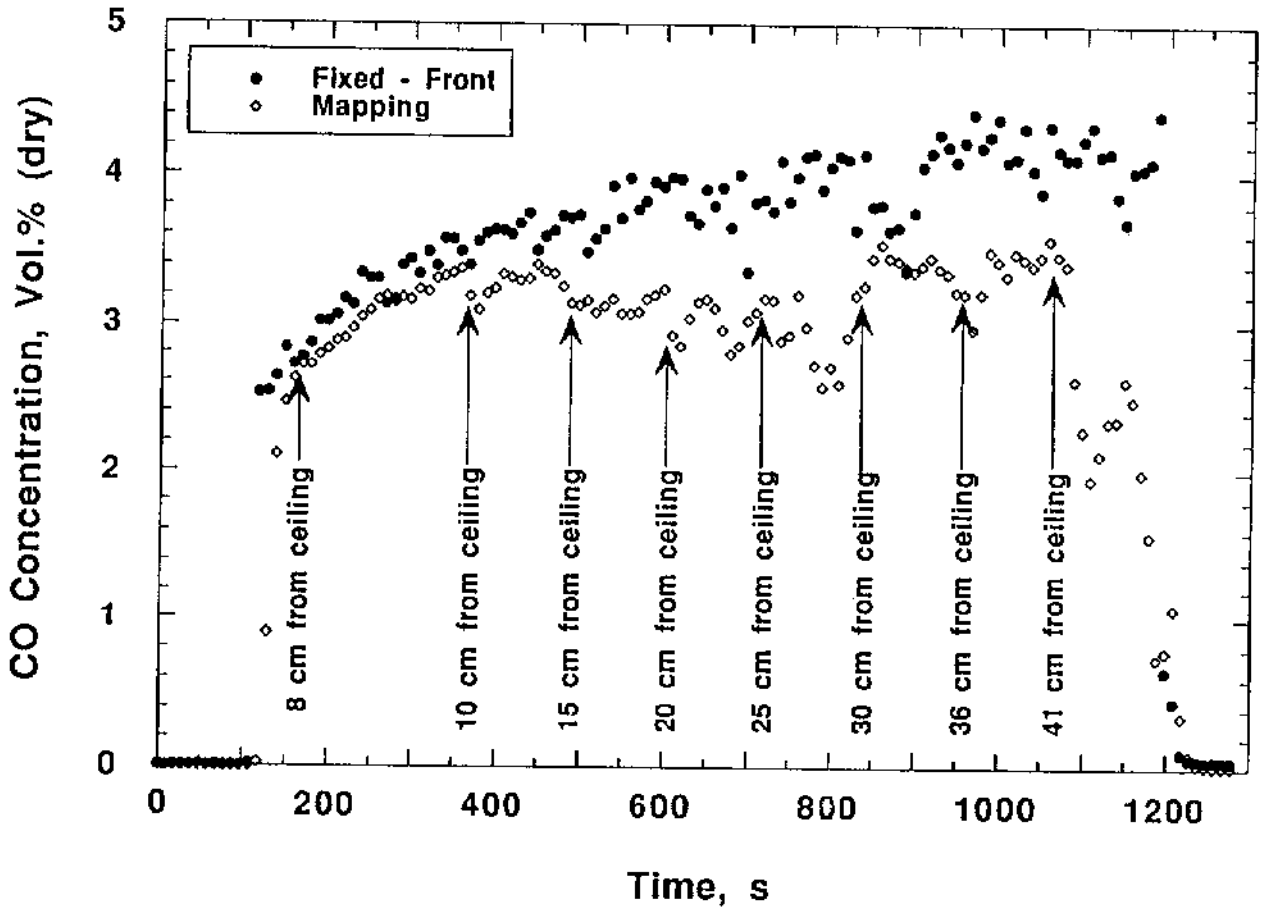

Figure 58. Vertical mapping of CO concentration 10 cm from front wall for a 600 kW fire. While the stationary probe remained at the top location, the mapping probe was moved vertically in a stepwise fashion down from the top to bottom location.

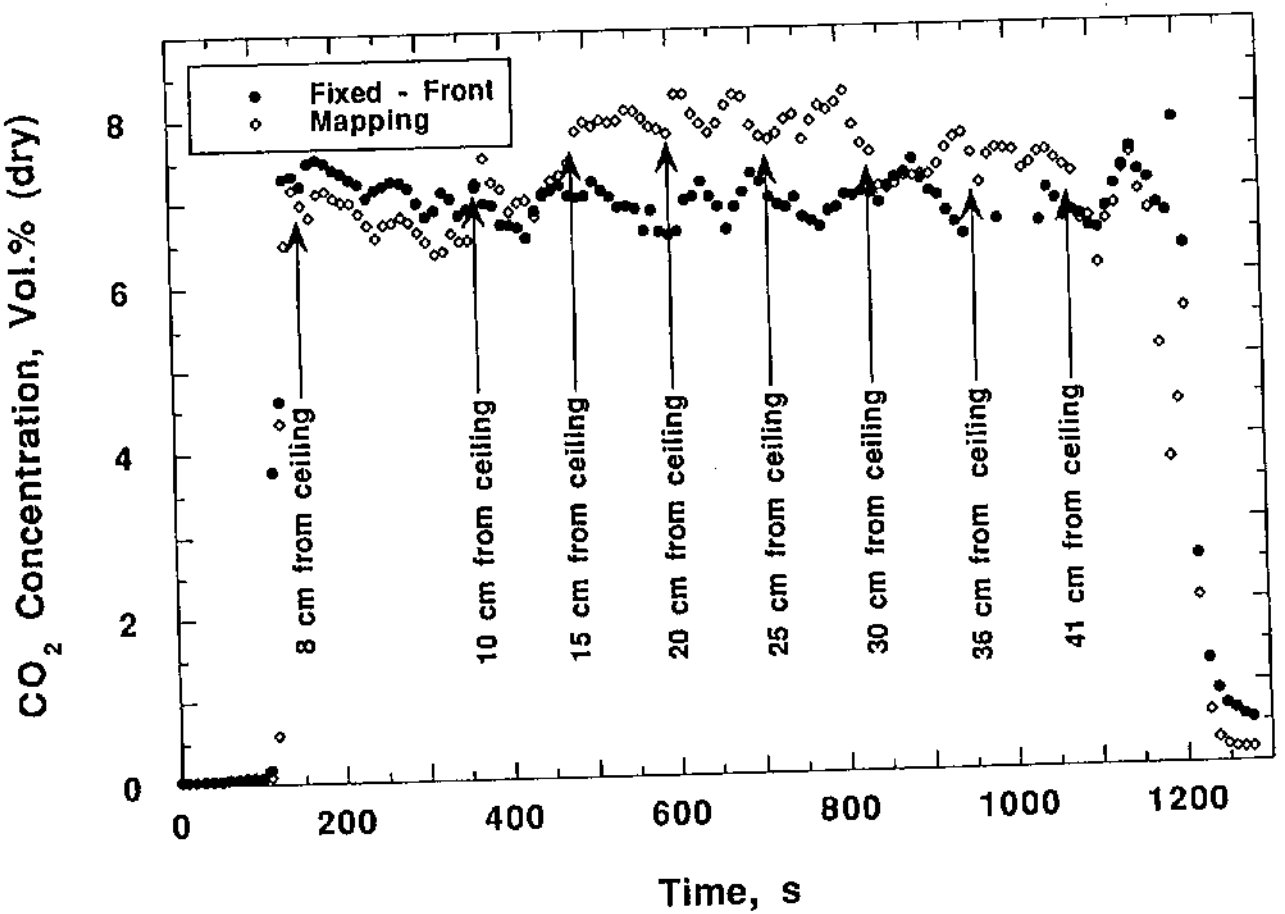

Figure 59. Vertical mapping of CO_2 concentration 10 cm from front wall for a 600 kW fire. While the stationary probe remained at the top location, the mapping probe was moved vertically in a stepwise fashion down from the top to the bottom location.

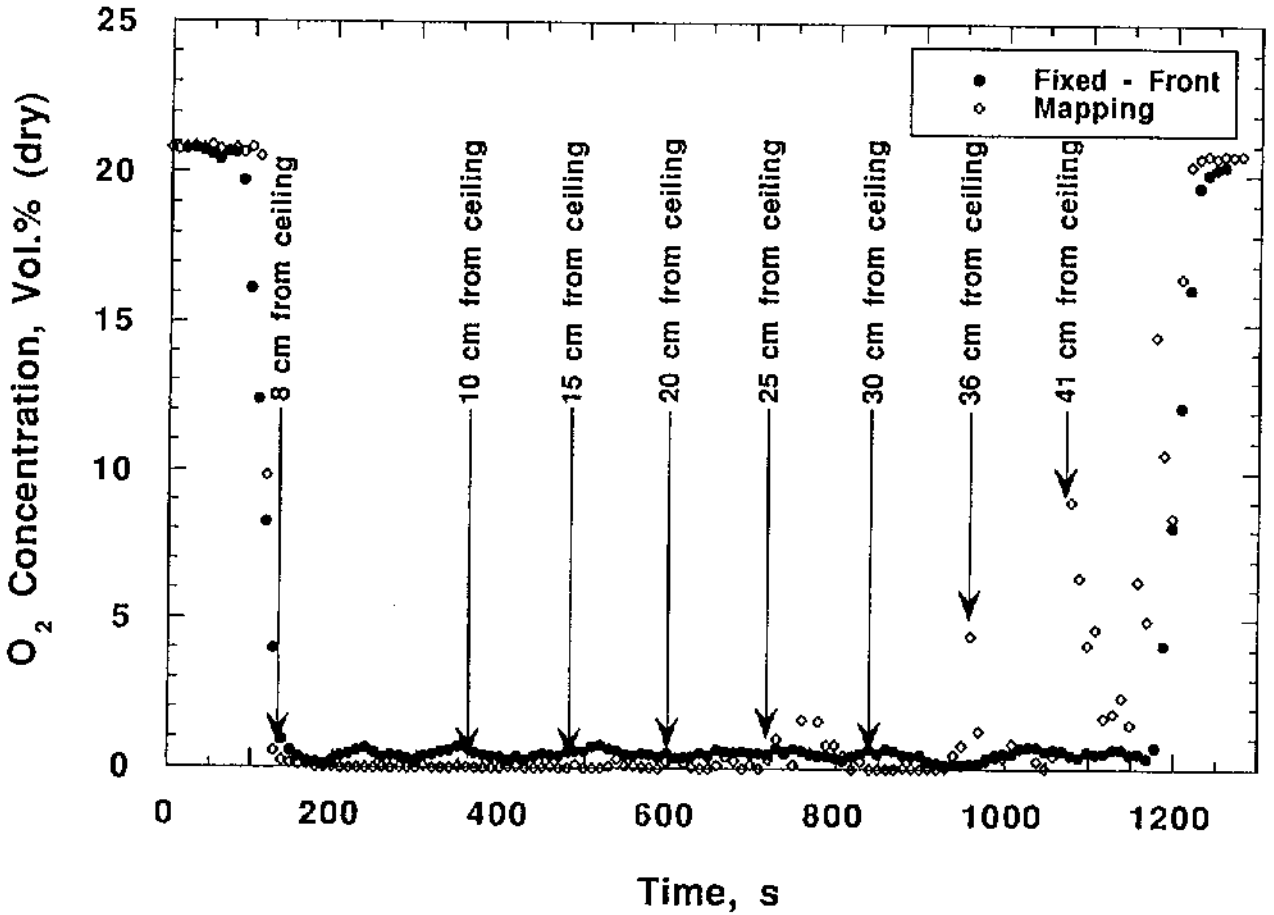

Figure 60. Vertical mapping of O_2 concentration 10 cm from front wall for a 600 kW fire. Mapping probe was moved vertically in a stepwise fashion down from the top to the bottom sampling location.

generated using statistics functions provided by the Kaleidagraph plotting and graphing software. For each burn, a time interval of 600 seconds from 280 to 880 seconds after ignition was chosen for averaging. Due to the 0.1 Hz sampling frequency, each statistical sample consisted of 60 data points. The average wet concentrations for carbon monoxide, carbon dioxide, and oxygen measured at the front and rear positions of the upper and lower layer and outside the door are plotted as a function of HRR in Figures 61-63. The calculated water concentrations as a function of HRR are shown in Figure 64.

Multiple burns at a specific heat release rate were conducted to investigate the reproducibility of the experimental setup. For example, the Marinite lining had to be replaced periodically. Each time the box was relined with new Marinite, the gas burner had to be disconnected and removed. The entire enclosure had to be moved away from the Furniture Calorimeter to allow for the front and rear walls to be removed. A number of 400 and 200 kW burns completed over a span of 18 months are compared in Figures 65 and 66 and indicate that the long-term reproducibility of the fires was quite good.

Another measure of the scatter in the experimental data can be obtained by plotting the residual combustion gases versus heat release rate (Figure 67). As the fuel-to-air ratio exceeds the stoichiometric value, the percentage of residual gases, especially unburned fuel, is expected to increase. Under ideal conditions, when there is just enough oxygen and fuel for stoichiometric burning, the residual gases should approach zero. Qualitatively these expectations are in good agreement with the observed residual combustion gases levels. As the HRR increases, the concentration of residual gases climbs to 20% for a 650 kW fire. For the lowest HRR, the residual gas calculations yield results which lie close to the expected near-zero values.

This difference of 3 to 4% could indicate that the assumption of complete combustion is not correct or could reflect uncertainty in the residual-gas calculations. If the combustion is less than

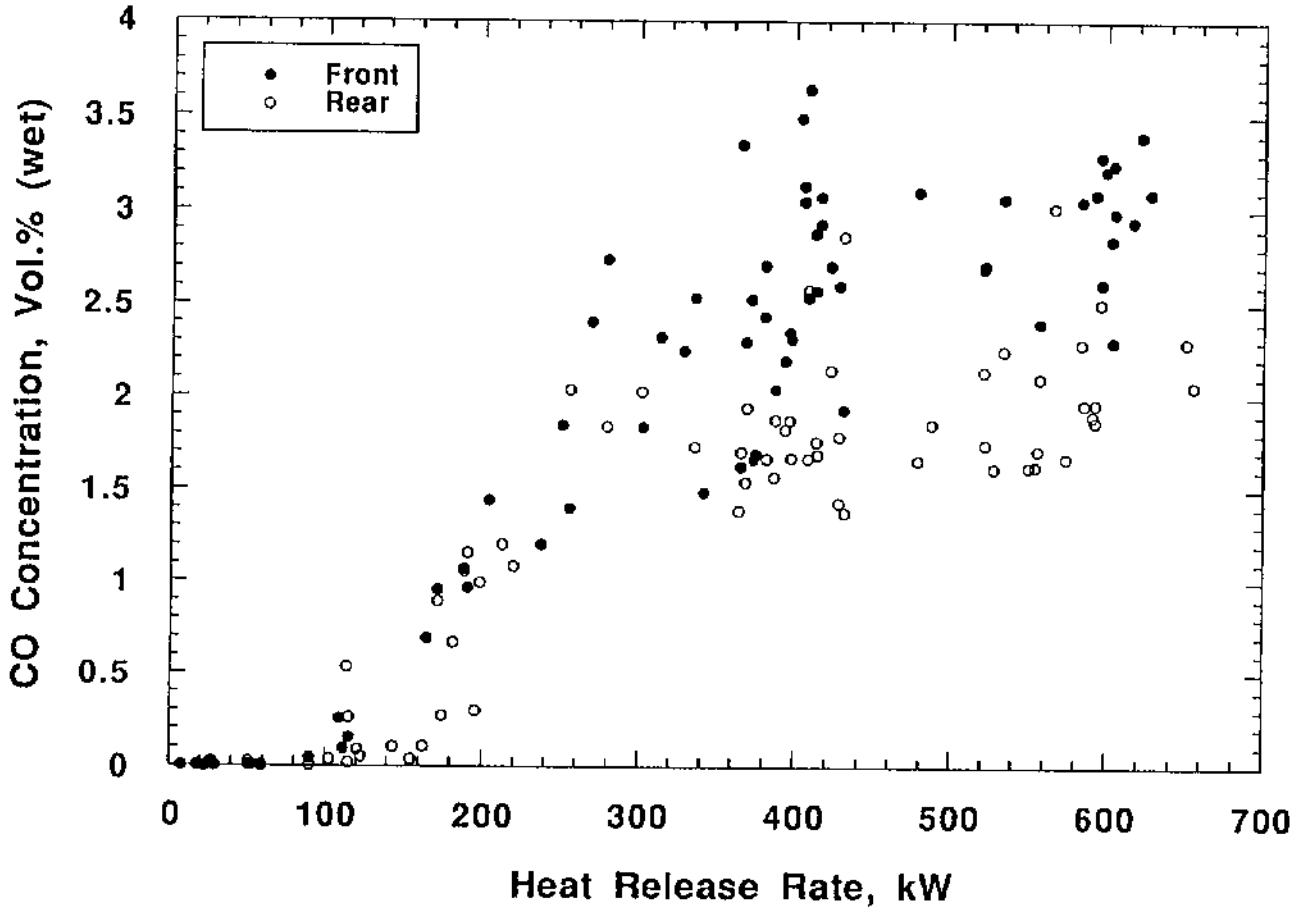

Figure 61. Carbon monoxide concentrations versus heat release rate. Each data point is the average of concentrations recorded between 300 and 900 seconds after ignition. Front and rear sampling locations were 10 cm below the ceiling.

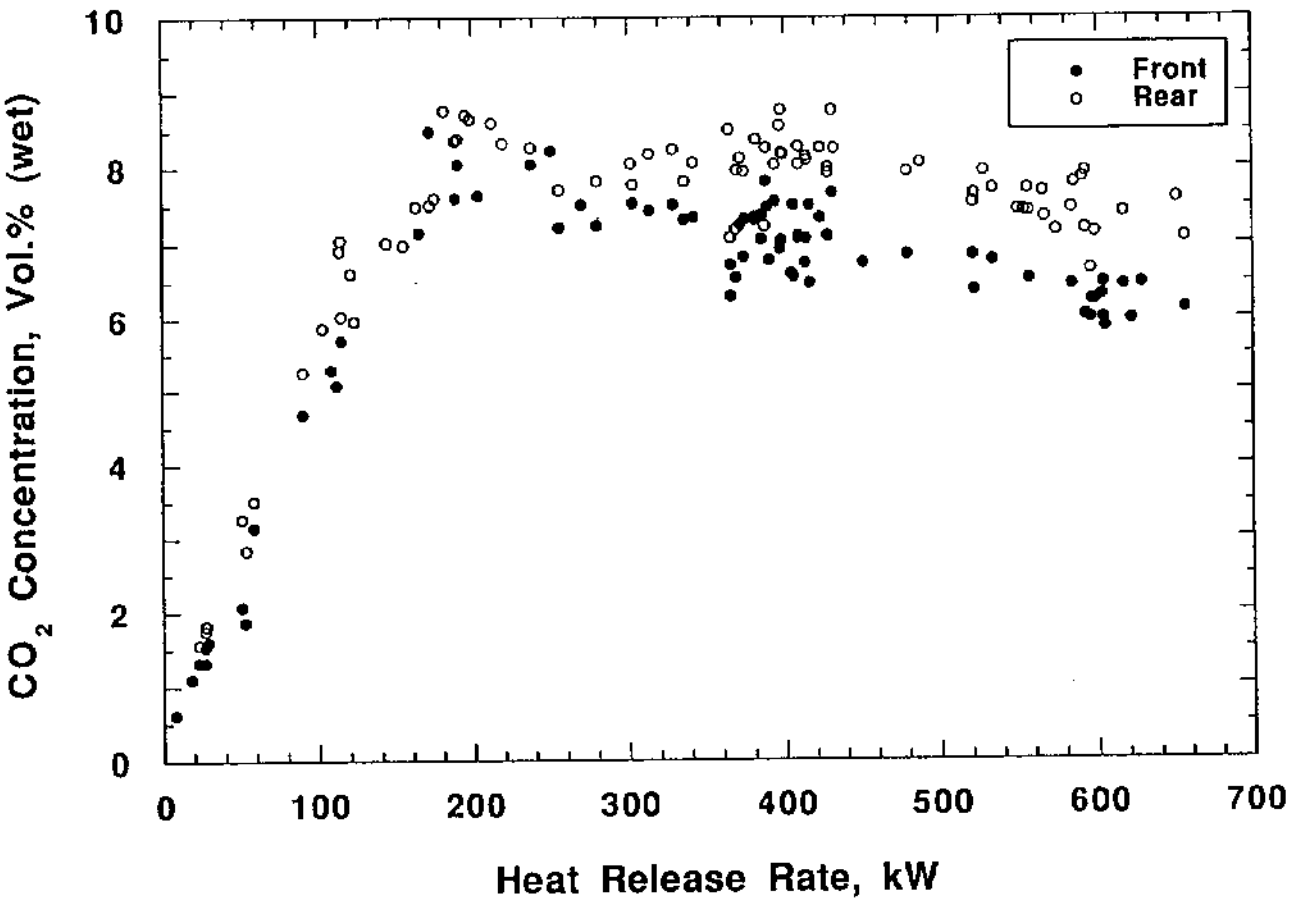

Figure 62. Front and rear carbon dioxide concentrations versus heat release rate. Each data point is the average of concentrations recorded between 300 and 900 seconds after ignition. Front and rear sampling locations were 10 cm below the ceiling.

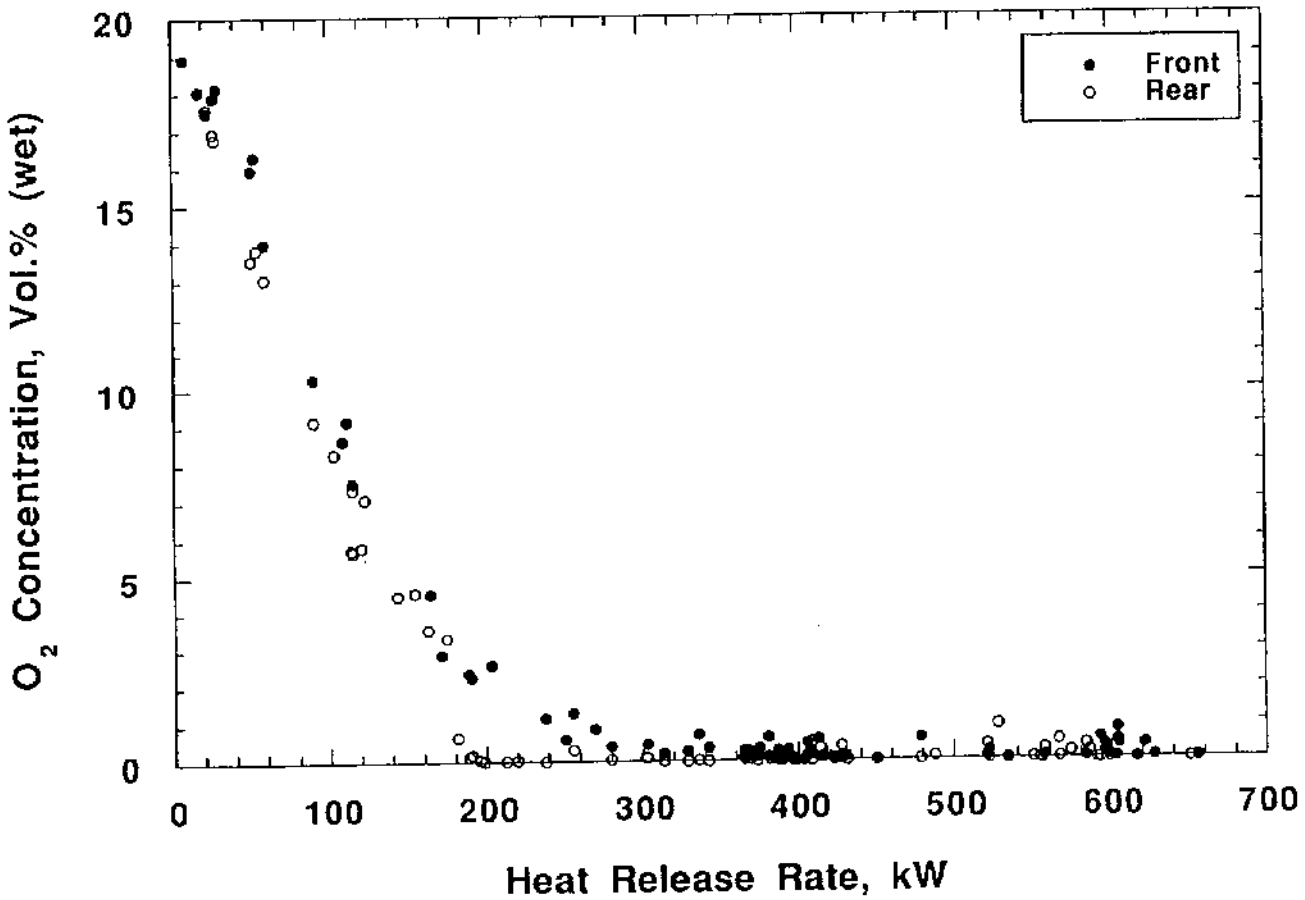

Figure 63. Front and rear oxygen concentrations versus heat release rate. Each point is the average of concentrations recorded between 300 and 900 seconds after ignition. Front and rear sampling locations were 10 cm below the ceiling.

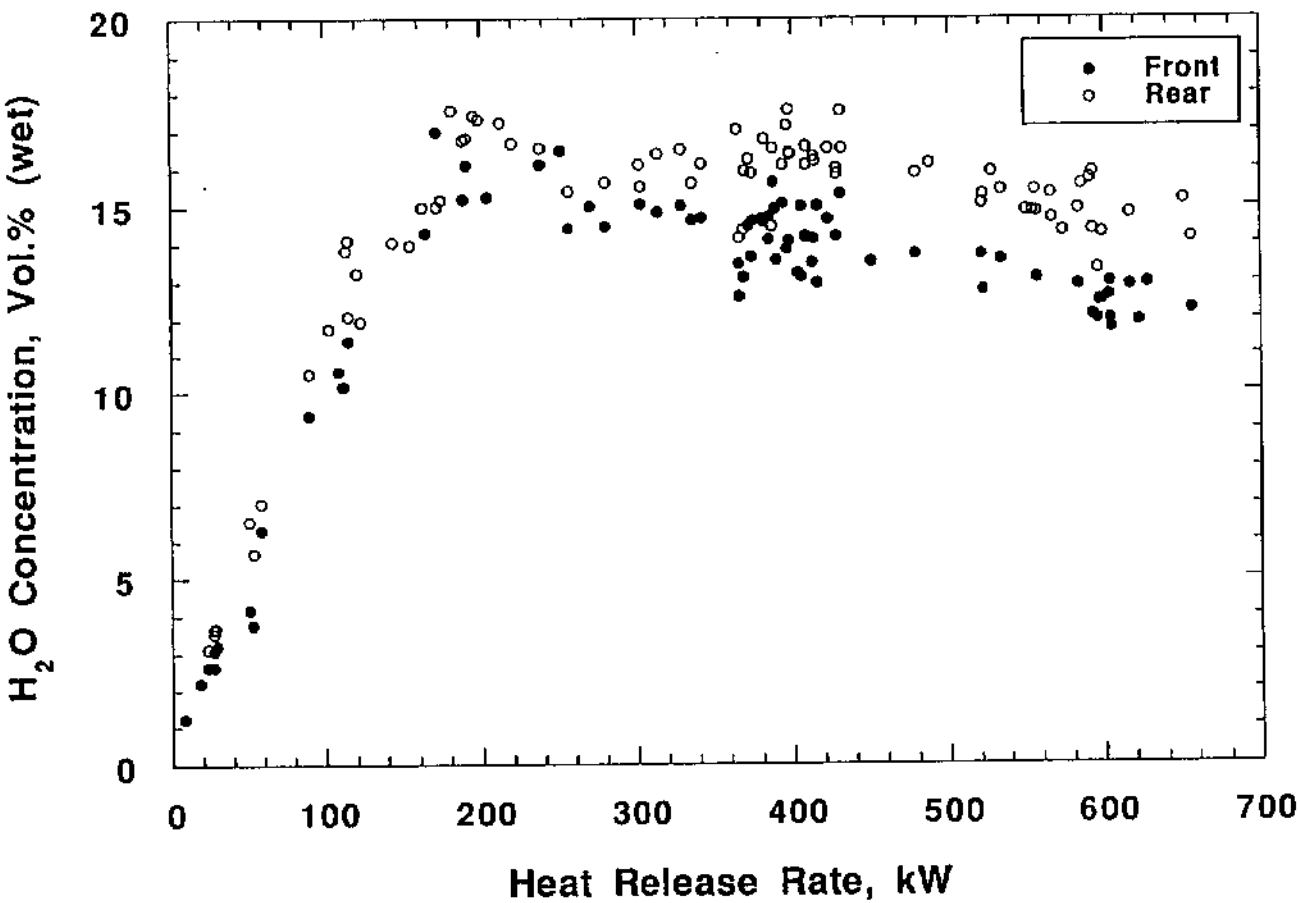

Figure 64. Calculated front and rear water concentrations versus heat release rate. Each data point is the average of concentrations recorded between 300 and 900 seconds after ignition. Front and rear sampling locations were 10 cm below the ceiling.

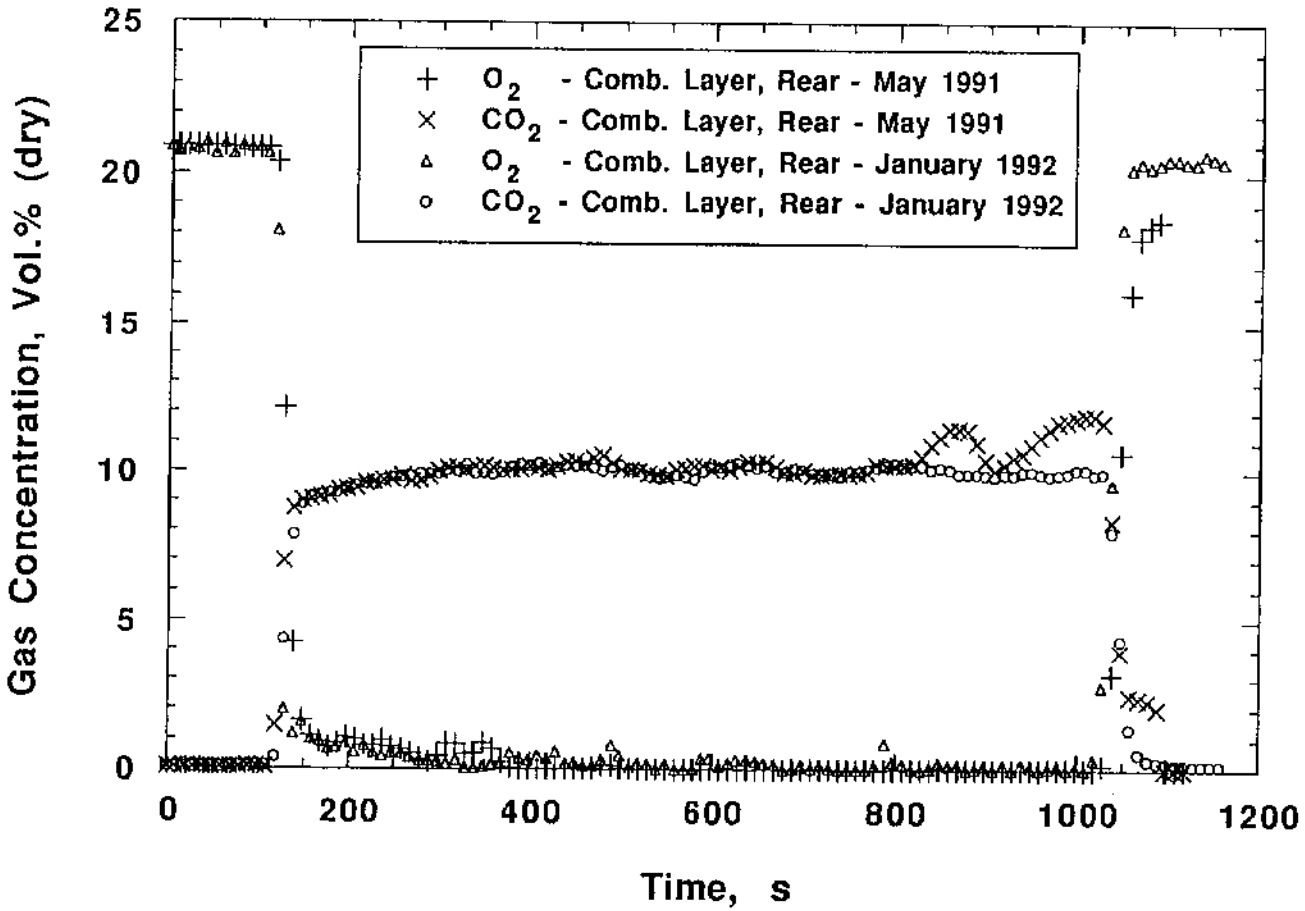

Figure 65. Oxygen and carbon dioxide concentrations for two 200 kW fires demonstrating reproducibility.

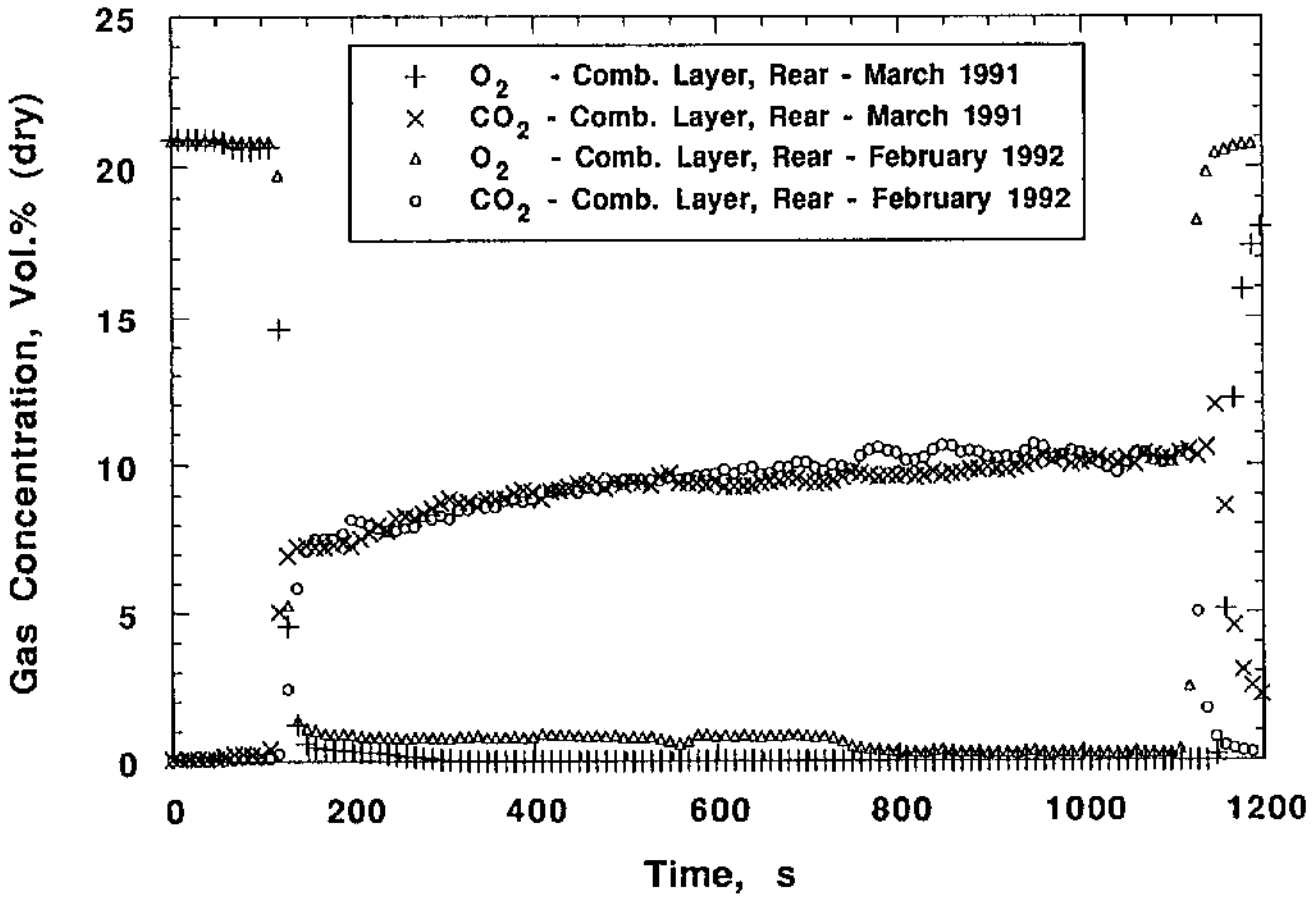

Figure 66. Oxygen and carbon dioxide concentrations for two 400 kW fires demonstrating reproducibility.

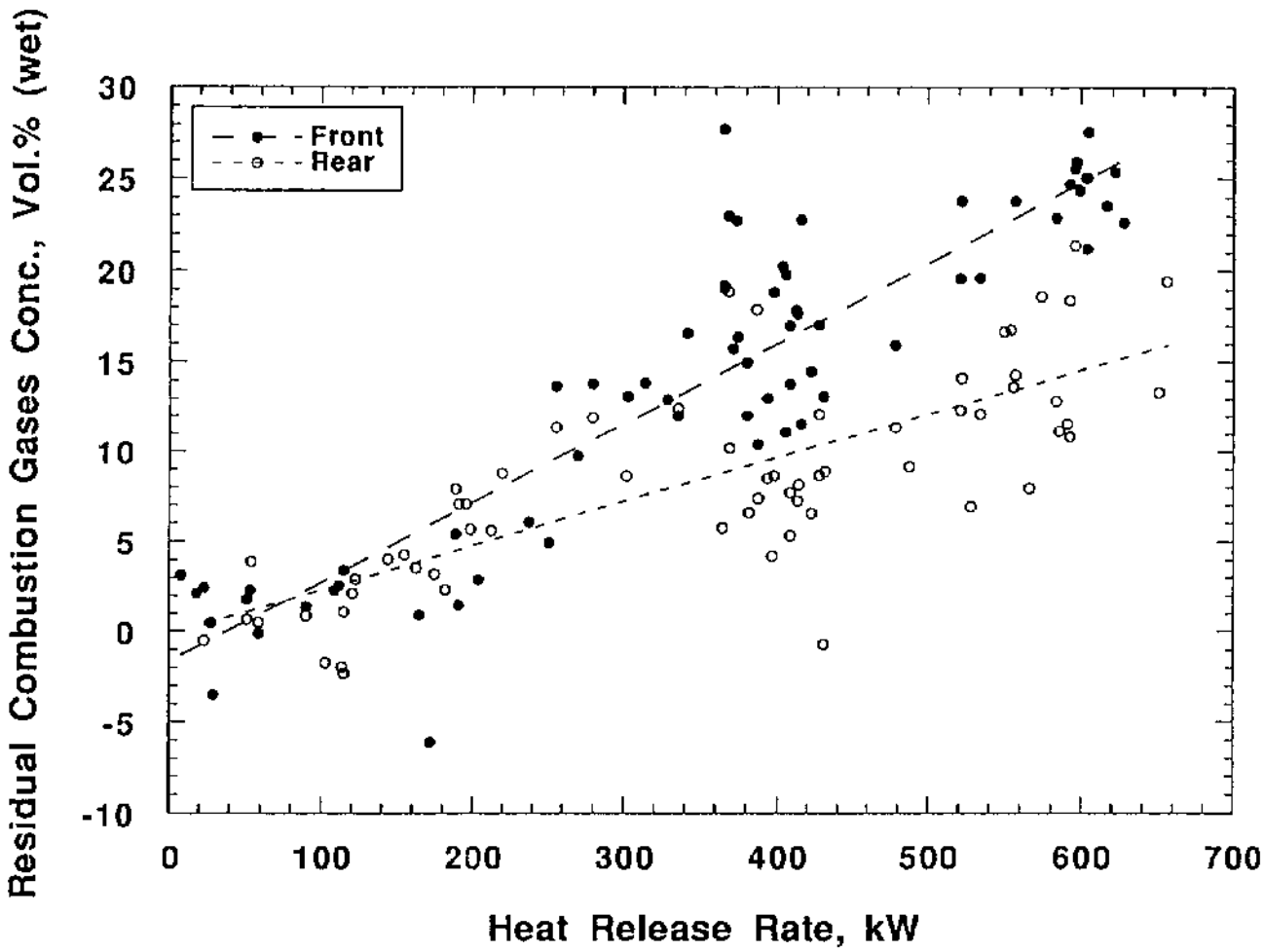

Figure 67. Calculated concentrations of residual gases versus heat release rate. Residual gas concentrations computed by subtracting measured and calculated gas levels from 100 percent.

complete, then intermediate products should be present in measurable concentrations. The gas analyzers only report the levels of CO_2, O_2, CO and sometimes total unburned hydrocarbons. While carbon monoxide is considered to be an intermediate product, the total unburned hydrocarbons include the unburned fuel as well as other products of incomplete combustion. For the lowest HRR, carbon monoxide is present at very low levels - much less than 0.5%. The total-unburned-hydrocarbon analyzer never performed well enough to produce reliable data. The low levels of carbon monoxide indicate that combustion was reasonably complete as expected, but the absence of total unburned hydrocarbons has not been confirmed.

The residual-gas calculations and the water correction are also possible sources of uncertainty. The water concentration is assumed to be twice the CO_2 level and then all the other gas species concentrations are corrected from a dry to wet basis. If this assumption is incorrect, the error is propagated through the other gas concentration calculations. At one stage of the residual-gas concentration algorithm, the moles of oxygen are summed and multiplied by 3.79 to obtain the number of moles of nitrogen. Any error caused by the water-correction assumption is increased by this same factor. Direct measurement of the water concentration in the upper layer would eliminate this source of uncertainty.

Other possible sources of uncertainty are the water and inert gases in the air entrained into the enclosure during a fire. The calculations do not make a correction based on the relative humidity of the combustion air. The calculations also do not consider inert gases, such as argon, which typically are present at slightly less than one percent concentrations [39]. While it is not possible at this time to allocate the uncertainty between the complete-combustion assumption, the residual-gas calculation, and the water or inert content, the uncertainty qualitatively appears to be in the 3 to 4% range.

3.2 Burnout of Carbon Monoxide

The burnout or conversion of carbon monoxide to carbon dioxide occurs quite rapidly once the hot combustion gases exit the enclosure. While the probes within the enclosure sample the upper-layer gases prior to burnout, the Furniture Calorimeter instrumentation monitors the gas concentrations in the exhaust stack (Figure 3) after the gases have mixed with additional external air and had the opportunity to undergo further oxidation. The concentrations of gases within the enclosure can be compared to the exhaust stack levels, but the large volumes of air entrained by the exhaust hood dilute the combustion gases. A better measure of the effect of burnout is to compare the CO/CO_2 ratios observed in the enclosure with those for the exhaust stack. The entrained air will equally dilute the carbon monoxide and carbon dioxide, therefore the ratio will be insensitive to dilution. For a 200 kW fire (Figure 68), the CO/CO_2 ratio in the exhaust stack is reduced from approximately 0.12 in the enclosure front and rear to less than 0.02 which indicates that the hot effluent gases efficiently react with the air available just outside the enclosure to generate carbon dioxide while consuming carbon monoxide. As the fire size is increased to 600 kW (Figure 69), the CO/CO_2 ratio in the stack decreases from about 0.3 (rear) and 0.5 (front) to less than 0.02. The 600 kW fire exhibited higher initial CO/CO_2 ratios than the 200 kW fire because of the larger quantities of CO that are typically generated in higher heat release fires. Although there was more carbon monoxide being produced in the larger fire, the rapid burnout is evident in both cases.

3.3 Temperature Profiles

Temperature profiles from the front and rear thermocouple trees are plotted for representative fires ranging from 20 to 600 kW in Figures 70-87. The thermocouple temperature data

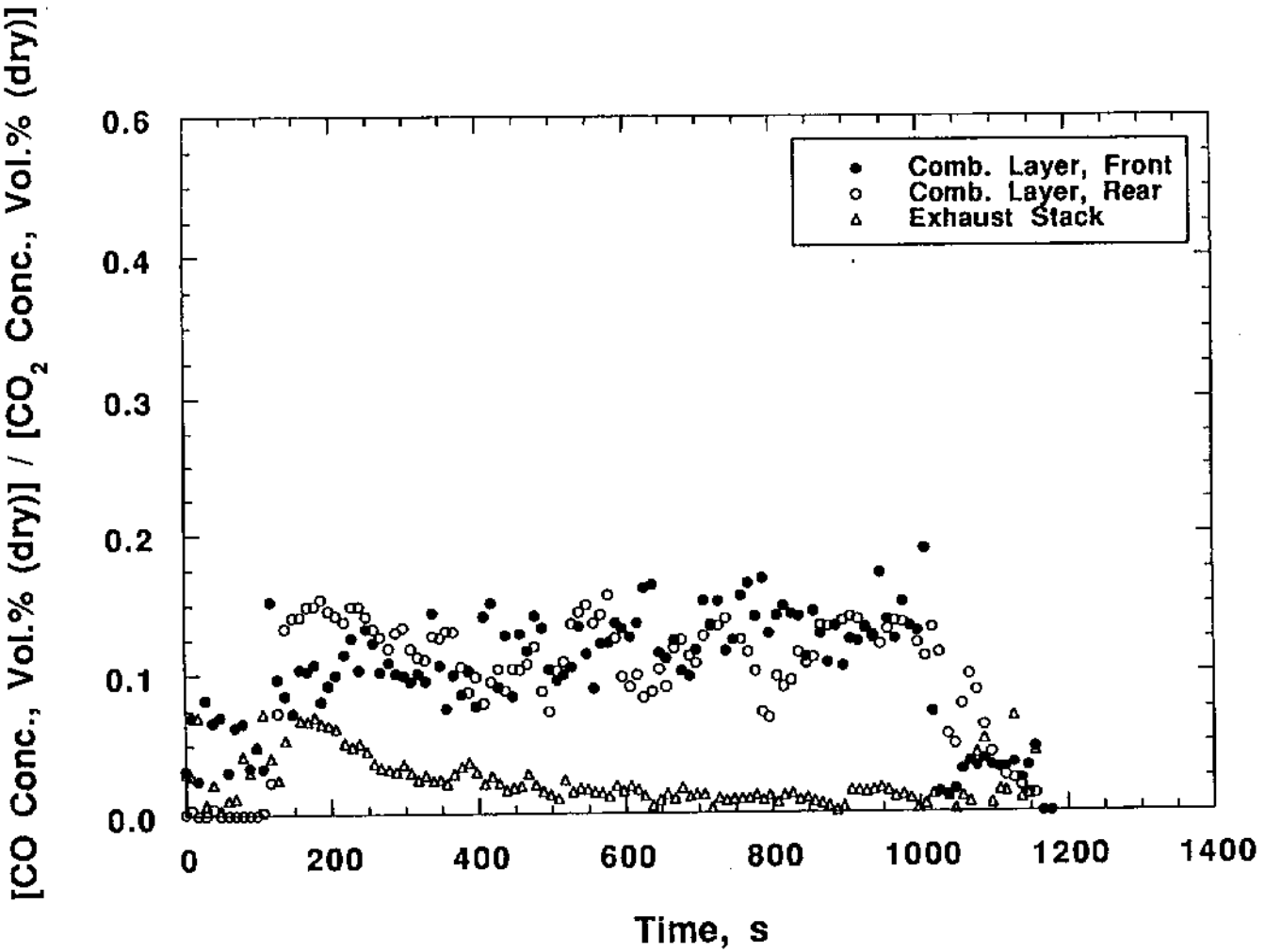

Figure 68. Ratio of carbon monoxide to carbon dioxide in front and rear of enclosure and in exhaust stack for a 200 kW fire.

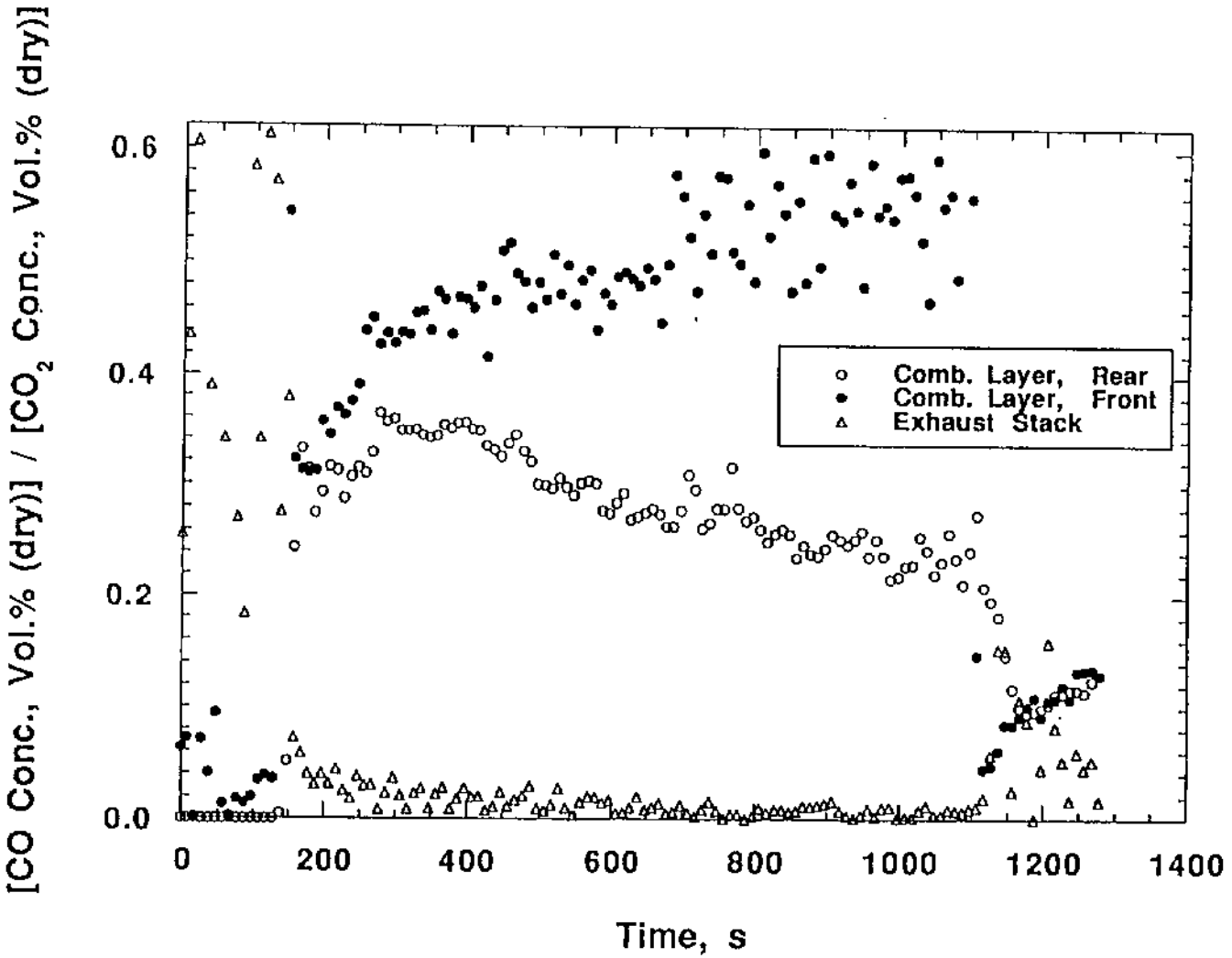

Figure 69. Ratio of carbon monoxide to carbon dioxide in front and rear of enclosure and in exhaust stack for a 600 kW fire.

were not corrected for radiation effects because of difficulties in estimating the appropriate thermocouple-bead size, the view factors of the beads, and the levels of soot adsorbed on the beads.

Temperatures from a thermocouple located 84 cm above the floor are graphed on a single plot (Figure 88) in order to compare the temperature at a single height over a range of different fire sizes. Periodically the reduced-scale enclosure was relined with new Marinite and the thermocouple trees were rewired. Temperatures measured at a specific height, front and rear, are plotted for a pair of medium-sized fires, 200 kW (Figure 89), and two large-sized fires, 600 kW (Figure 90), which were completed over a span of 6 to 8 months. The plots demonstrate that the long-term reproducibility of upper-layer temperatures was quite good.

Most of the fires were conducted with the rear thermocouple tree located 20.3 cm from the west wall and 20.3 cm from the rear wall. However, for a limited number of fires the rear tree was positioned 30.5 x 30.5 cm from the side and rear walls to examine possible boundary layer effects. Measurements at both positions (in different fires) for 400 and 600 kW fires are plotted in Figures 91 and 92. There is not a significant temperature dependence on the distance from the rear wall.

3.4 Global and Local Equivalence Ratios

The global equivalence ratio, (ϕ_g), was defined as the mass in the upper layer derived from the fuel divided by the mass derived from the air normalized by the mass ratio for stoichiometric burning. This ratio was calculated from the mass flow rates for the natural gas and incoming air and using the natural gas analysis to determine the mass ratio at stoichiometric burning. The fuel mass flow rates were computed from the measured volumetric flow rate and the specific gravity of the natural gas. The air mass flow rate into the enclosure was calculated using the method of Janssens and Tran [35] as summarized by Johnsson et al. [36, 39]. By varying the neutral plane height, the method matches the outflow through the door with the combined inflow through the door and fuel

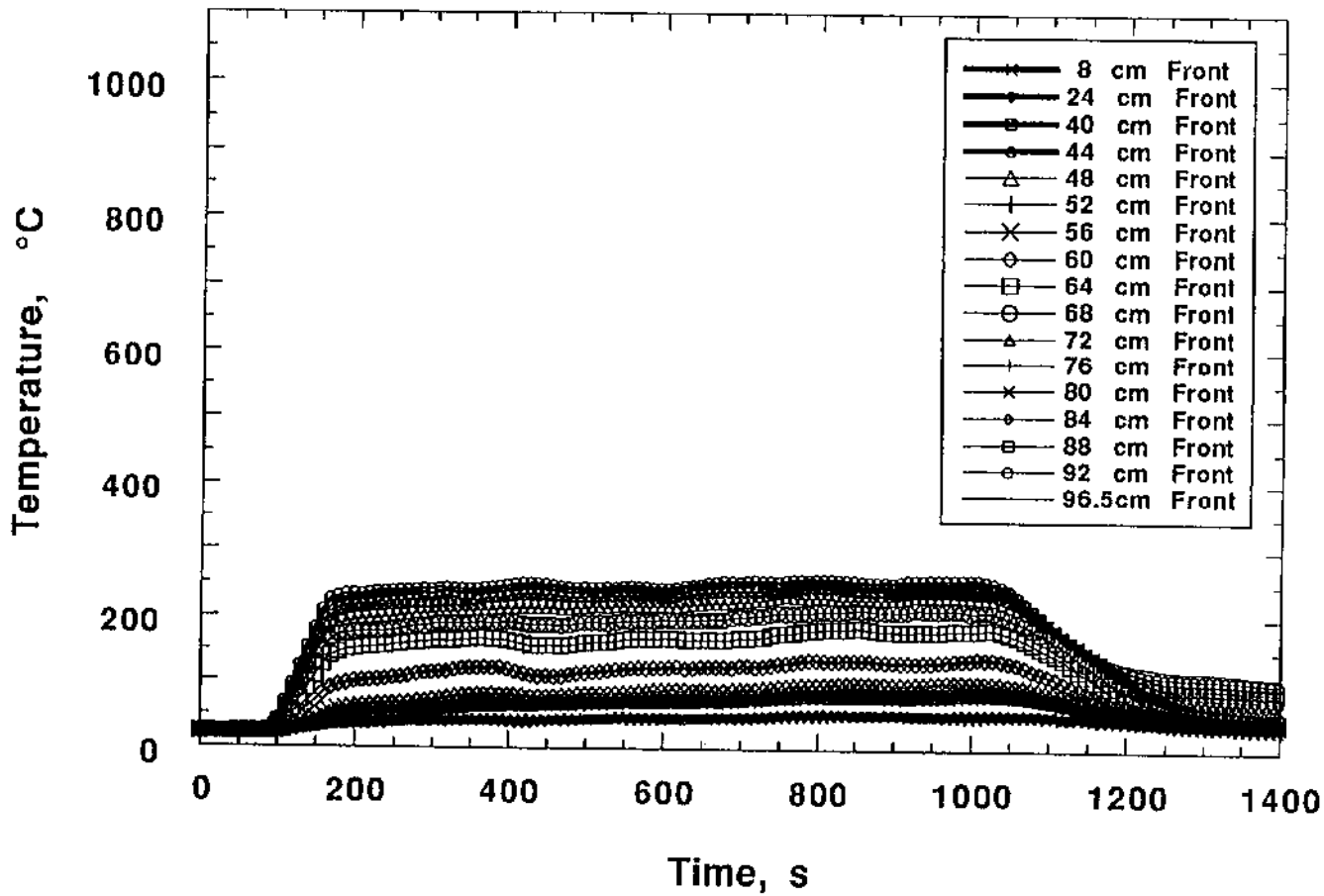

Figure 70. Front thermocouple tree temperature profile for 20 kW fire.

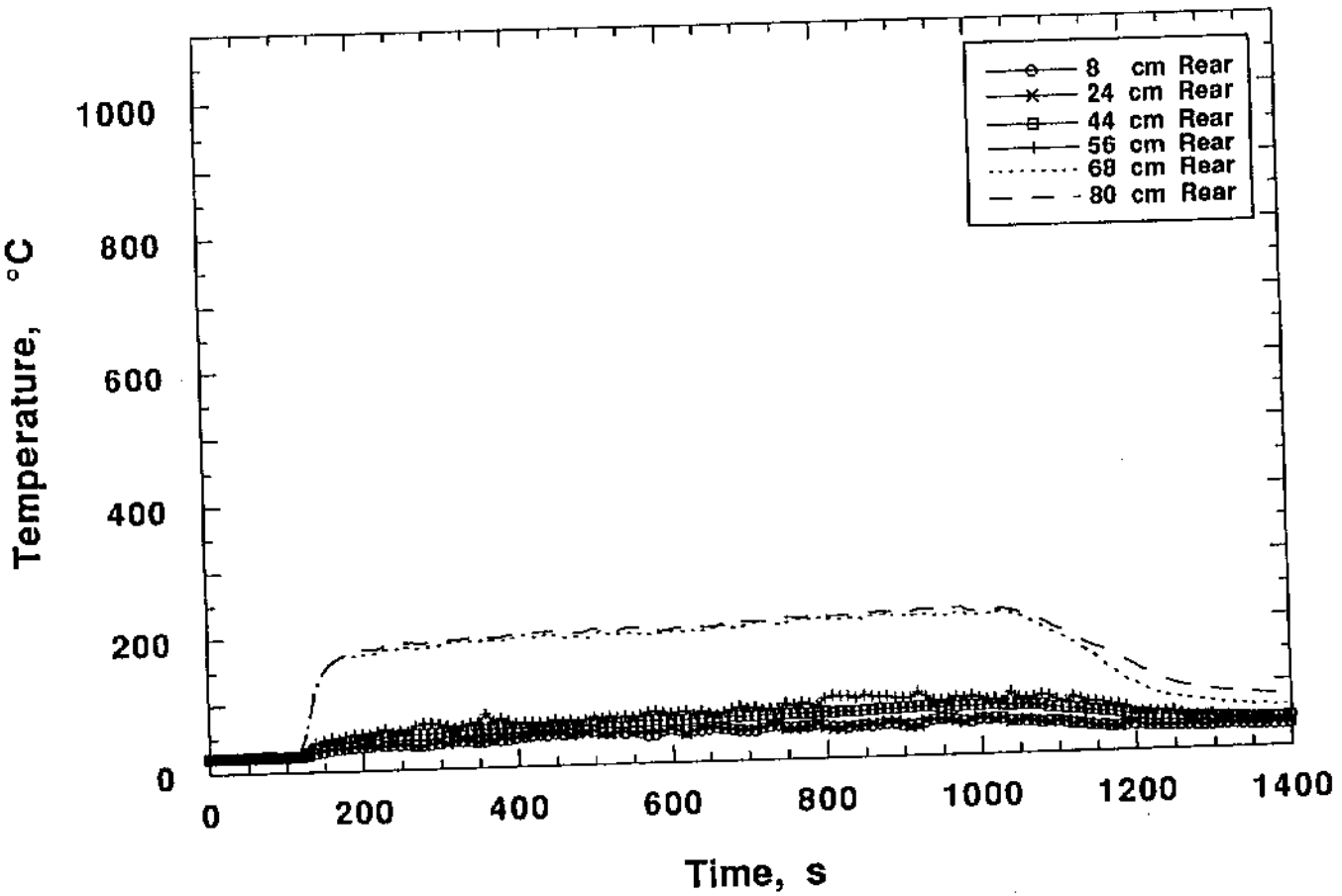

Figure 71. Rear thermocouple tree temperature profile for 20 kW fire.

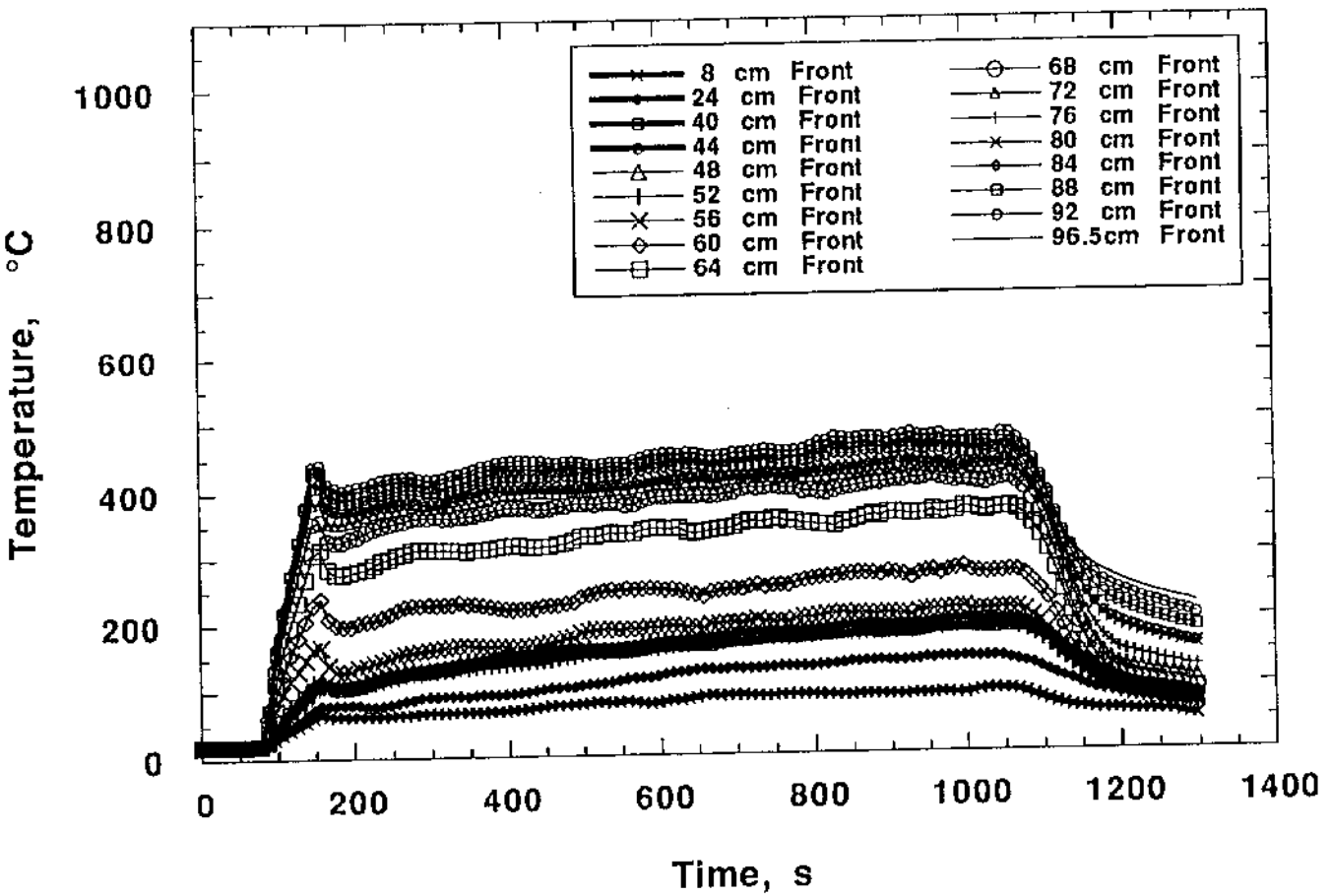

Figure 72. Front thermocouple tree temperature profile for 50 kW fire.

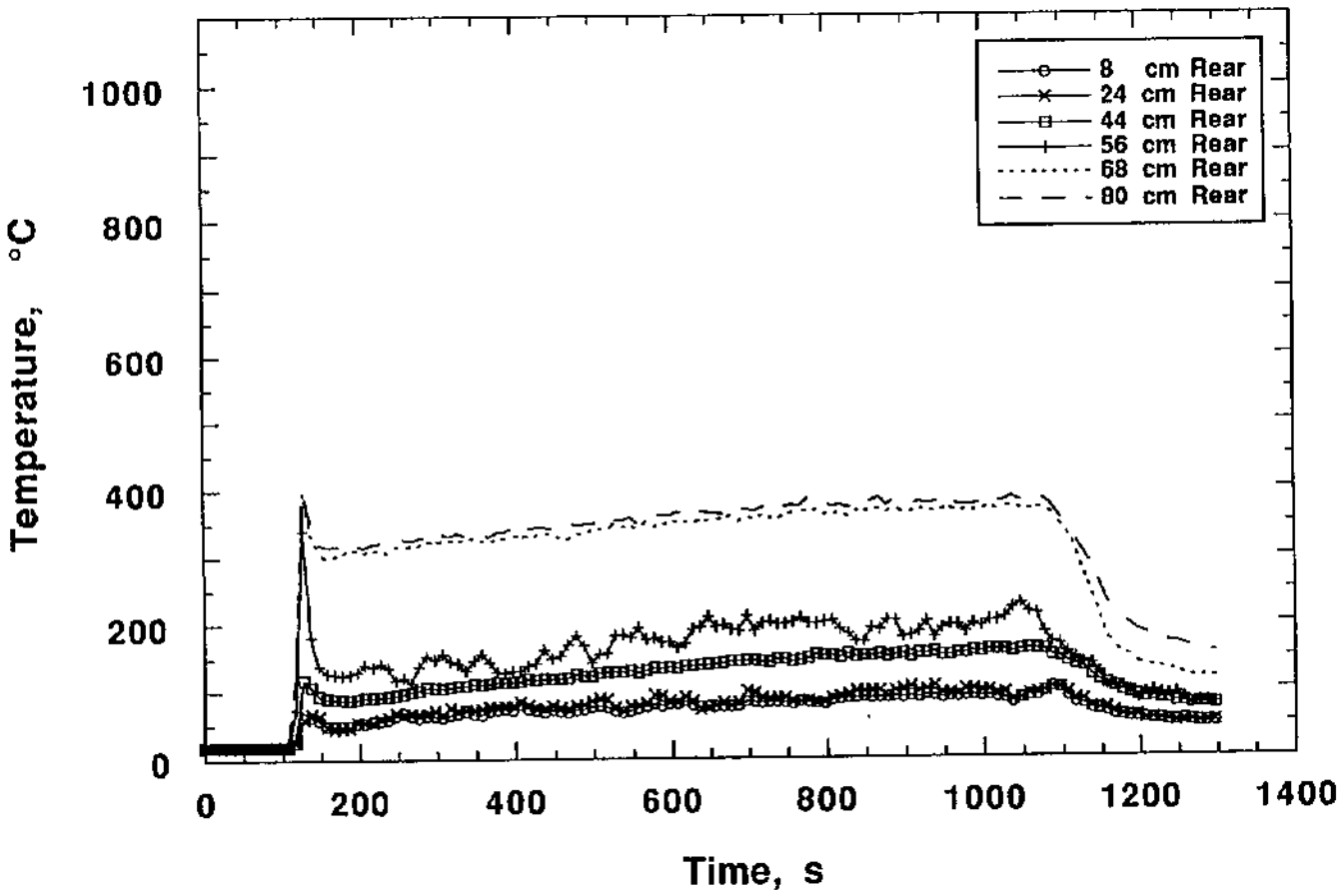

Figure 73. Rear thermocouple tree temperature profile for 50 kW fire.

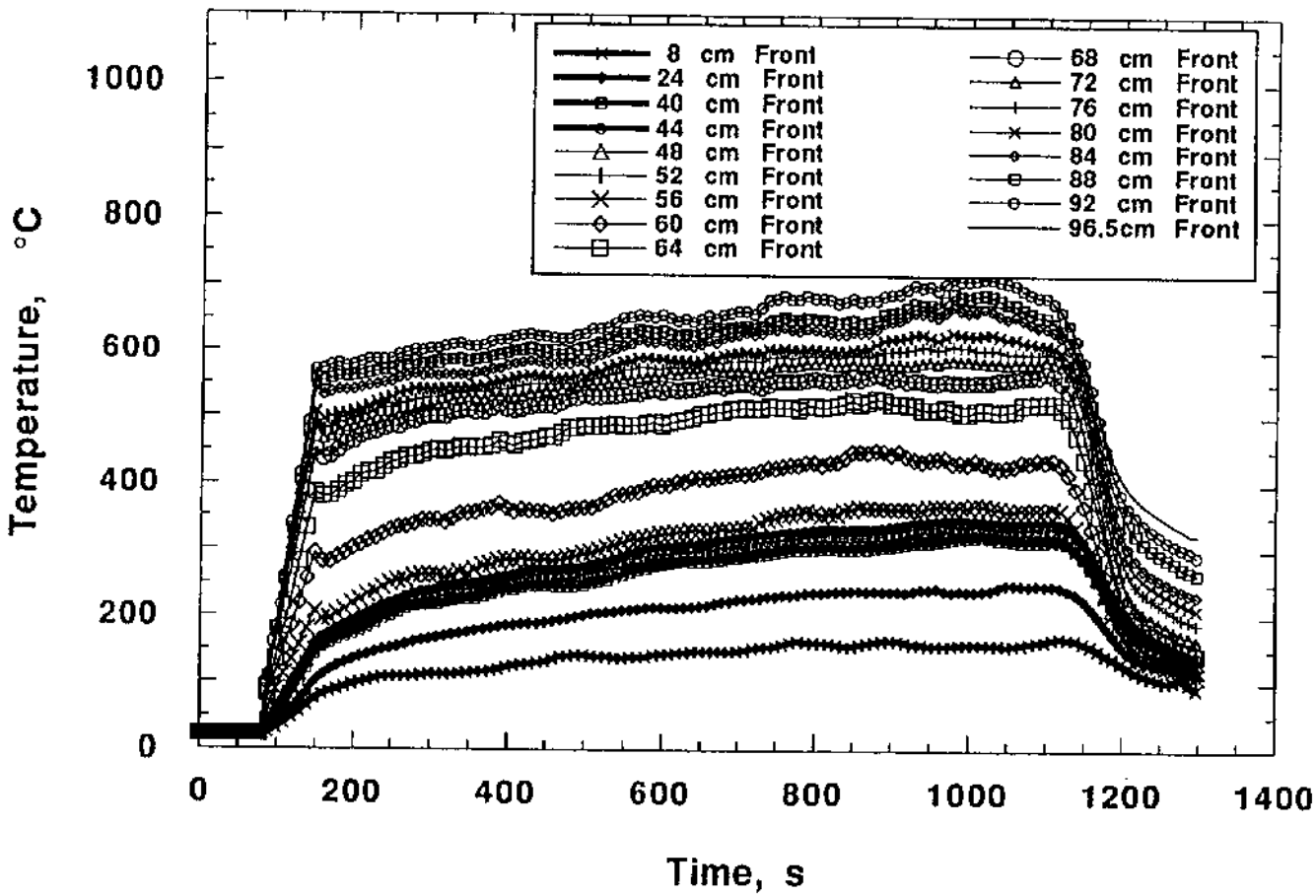

Figure 74. Front thermocouple tree temperature profile for 100 kW fire.

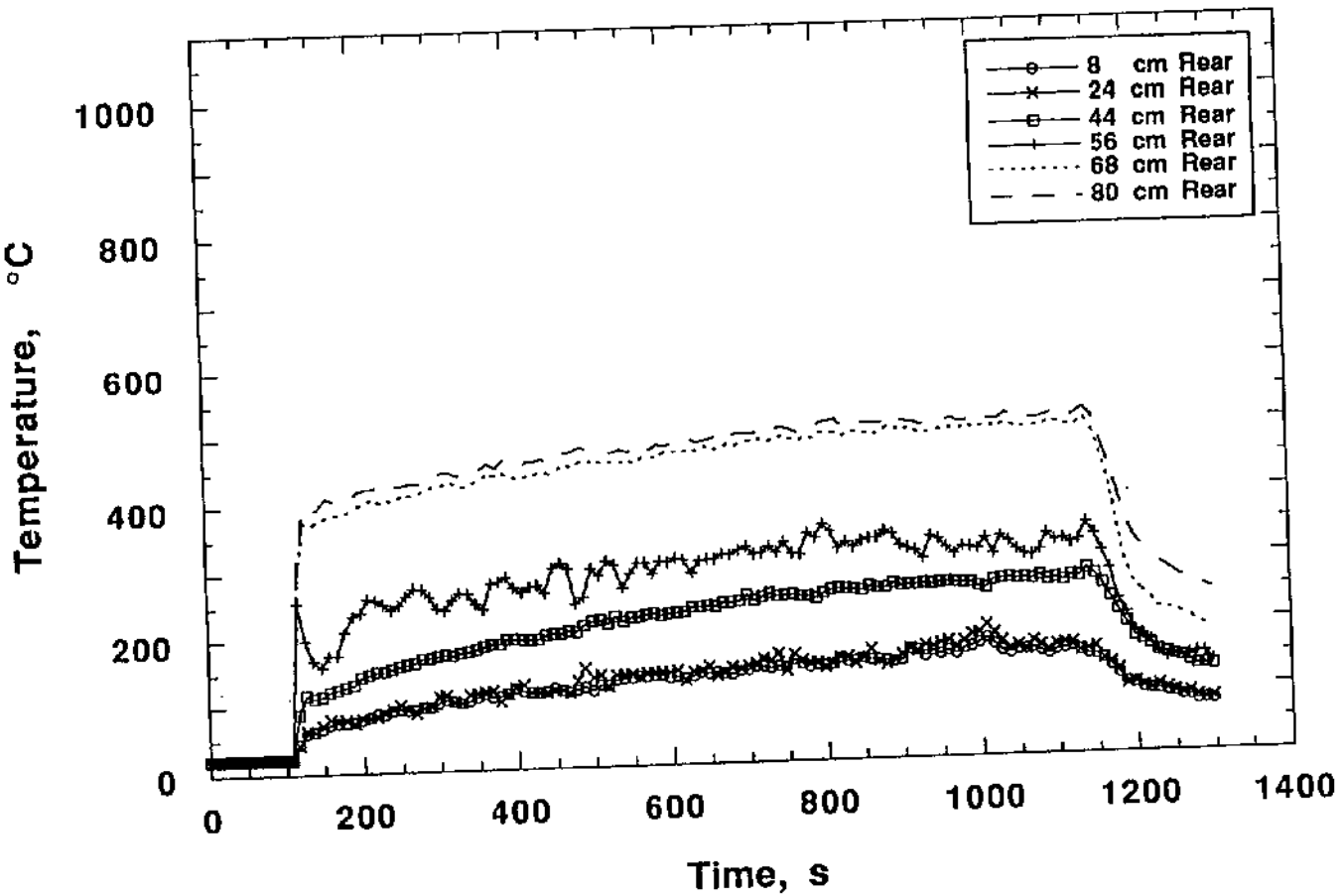

Figure 75. Rear thermocouple tree temperature profile for 100 kW fire.

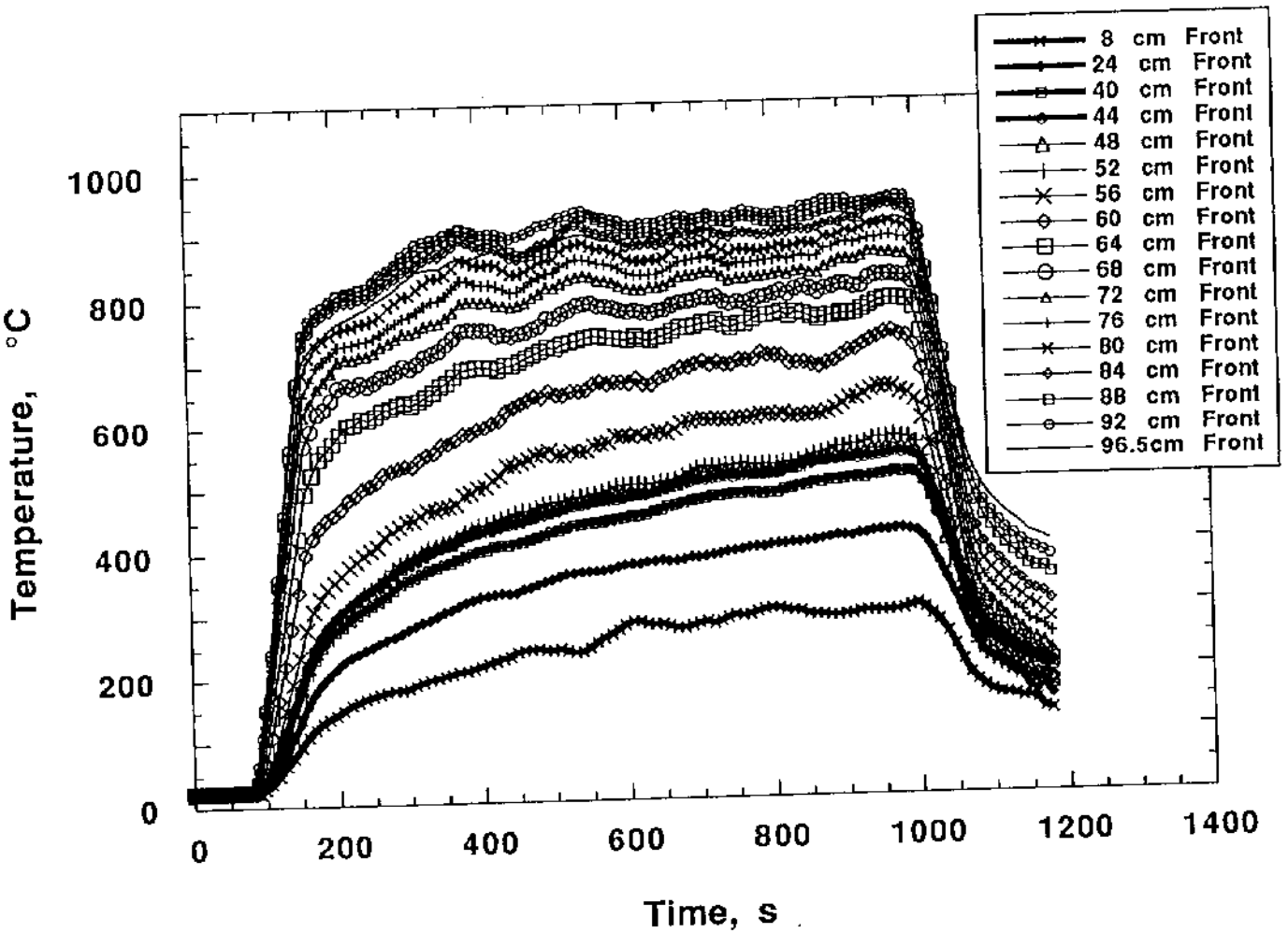

Figure 76. Front thermocouple tree temperature profile for 200 kW fire.

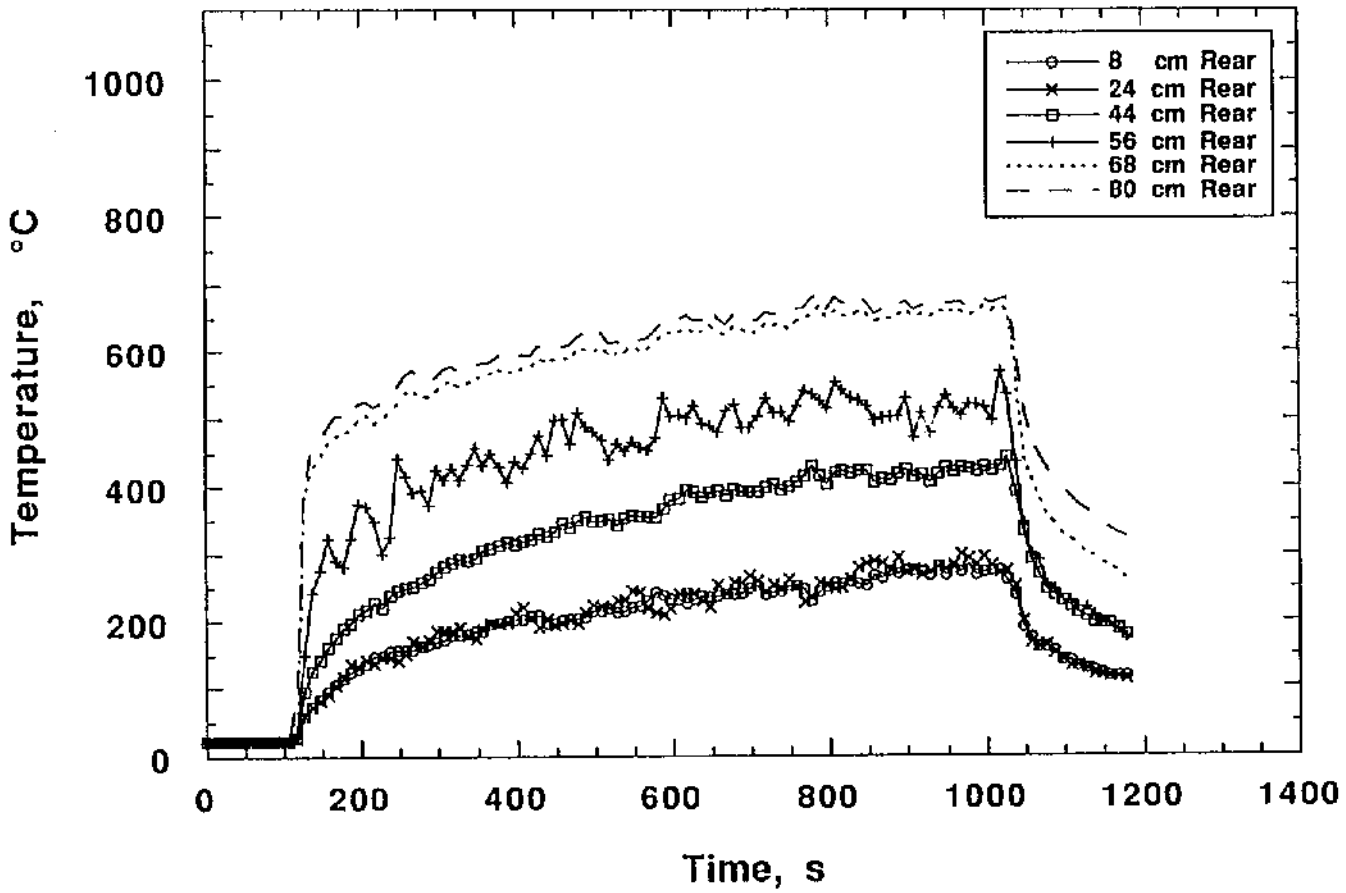

Figure 77. Rear thermocouple tree temperature profile for 200 kW fire.

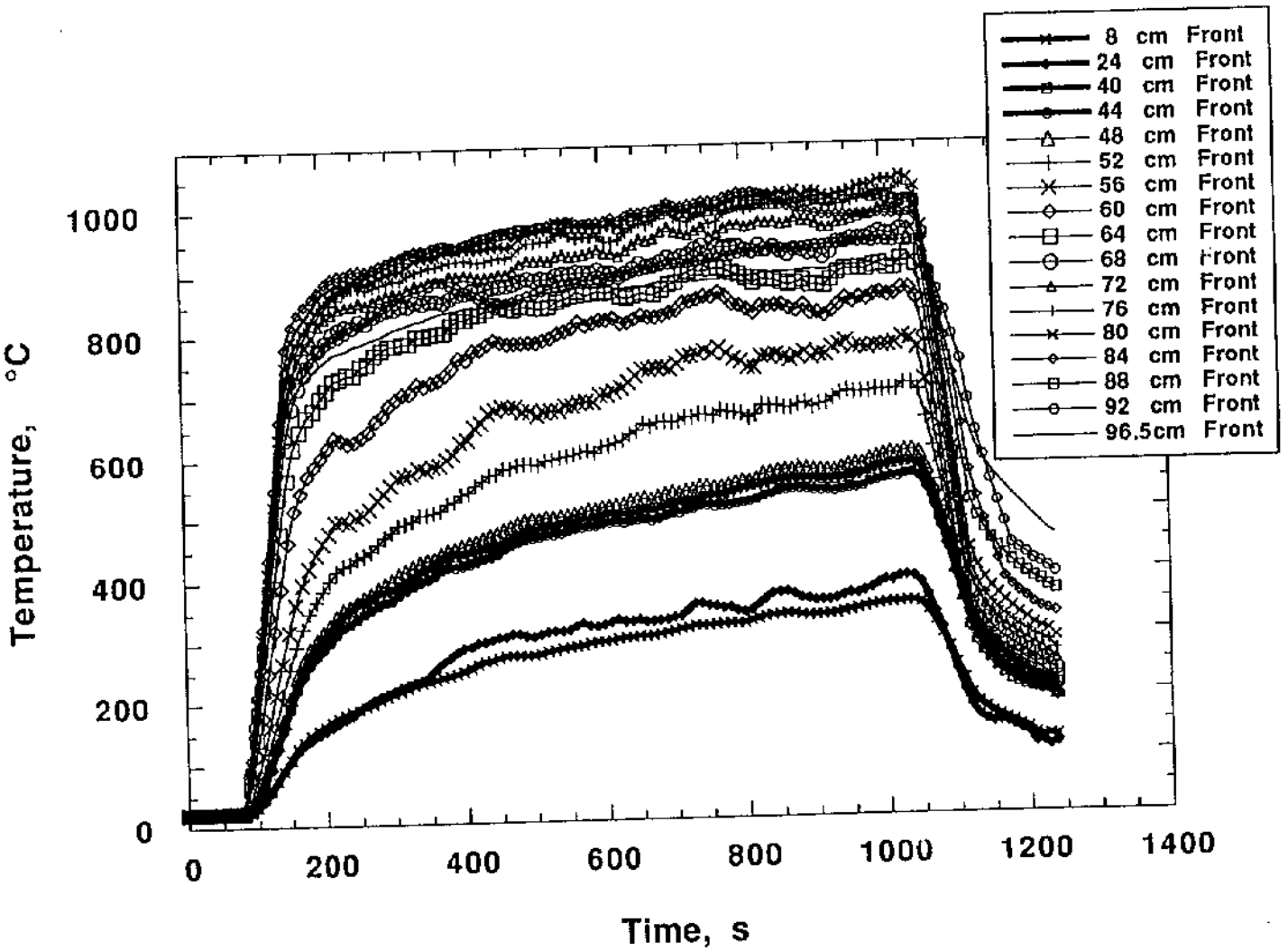

Figure 78. Front thermocouple tree temperature profile for 250 kW fire.

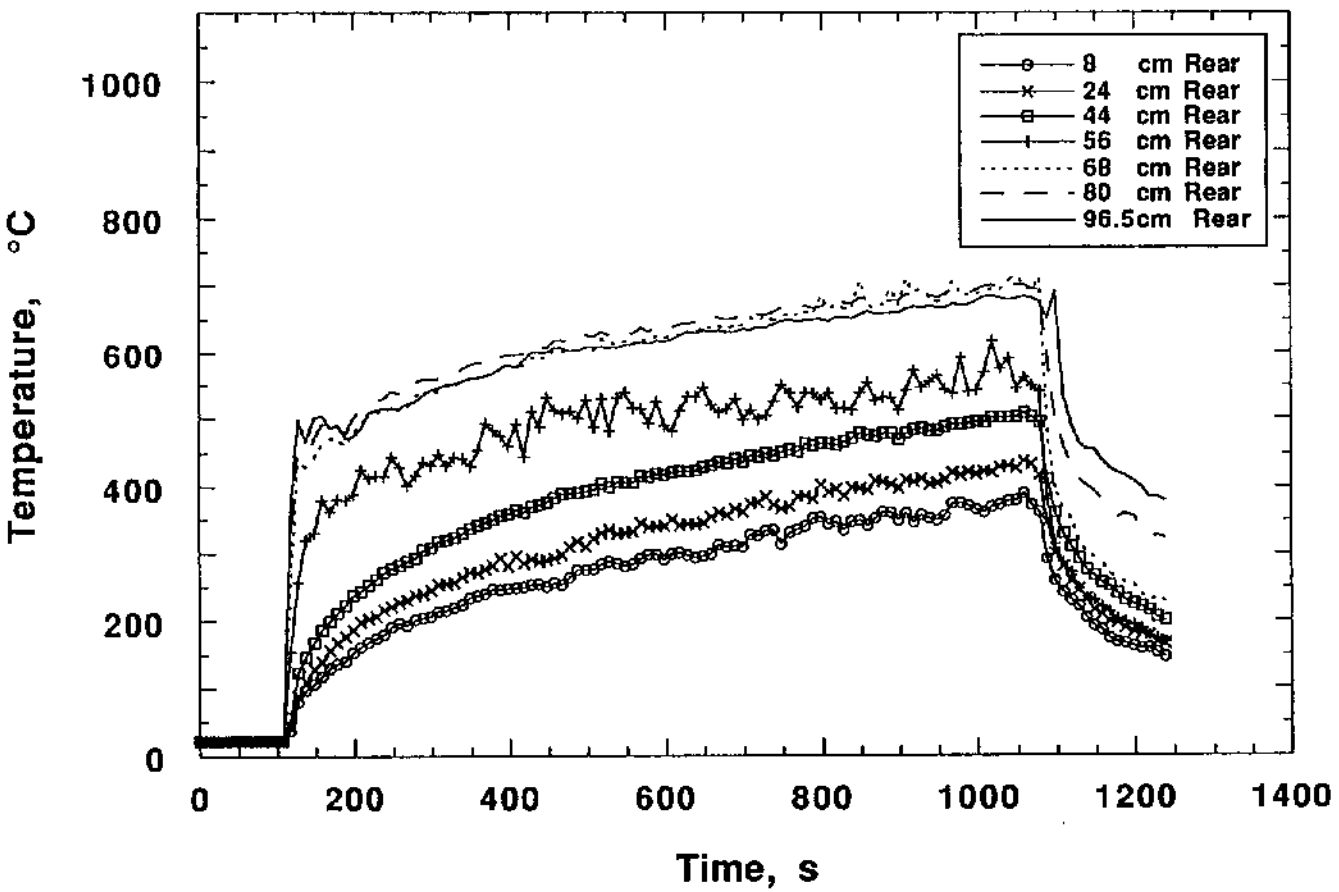

Figure 79. Rear thermocouple tree temperature profile for 250 kW fire.

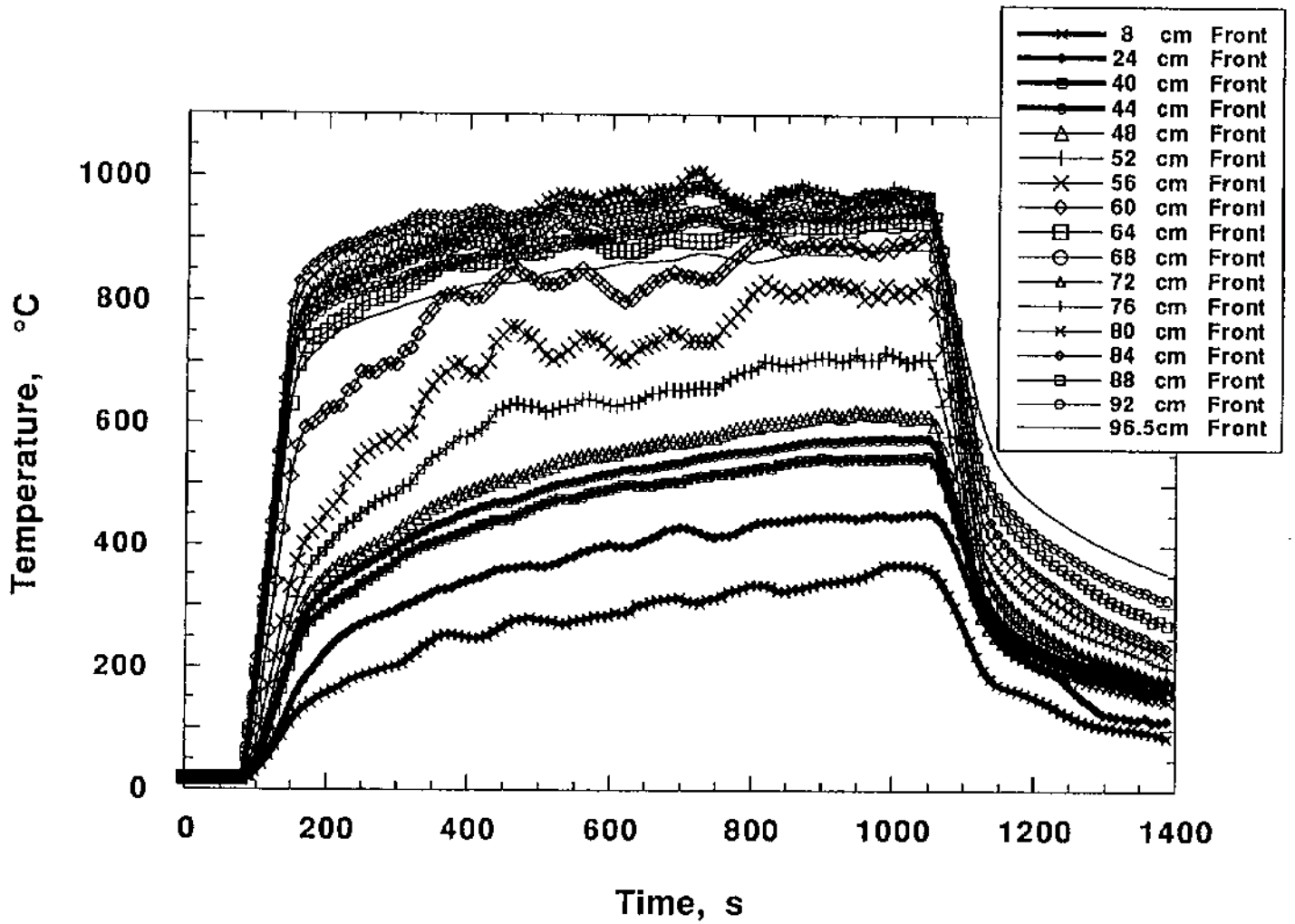

Figure 80. Front thermocouple tree temperature profile for 350 kW fire.

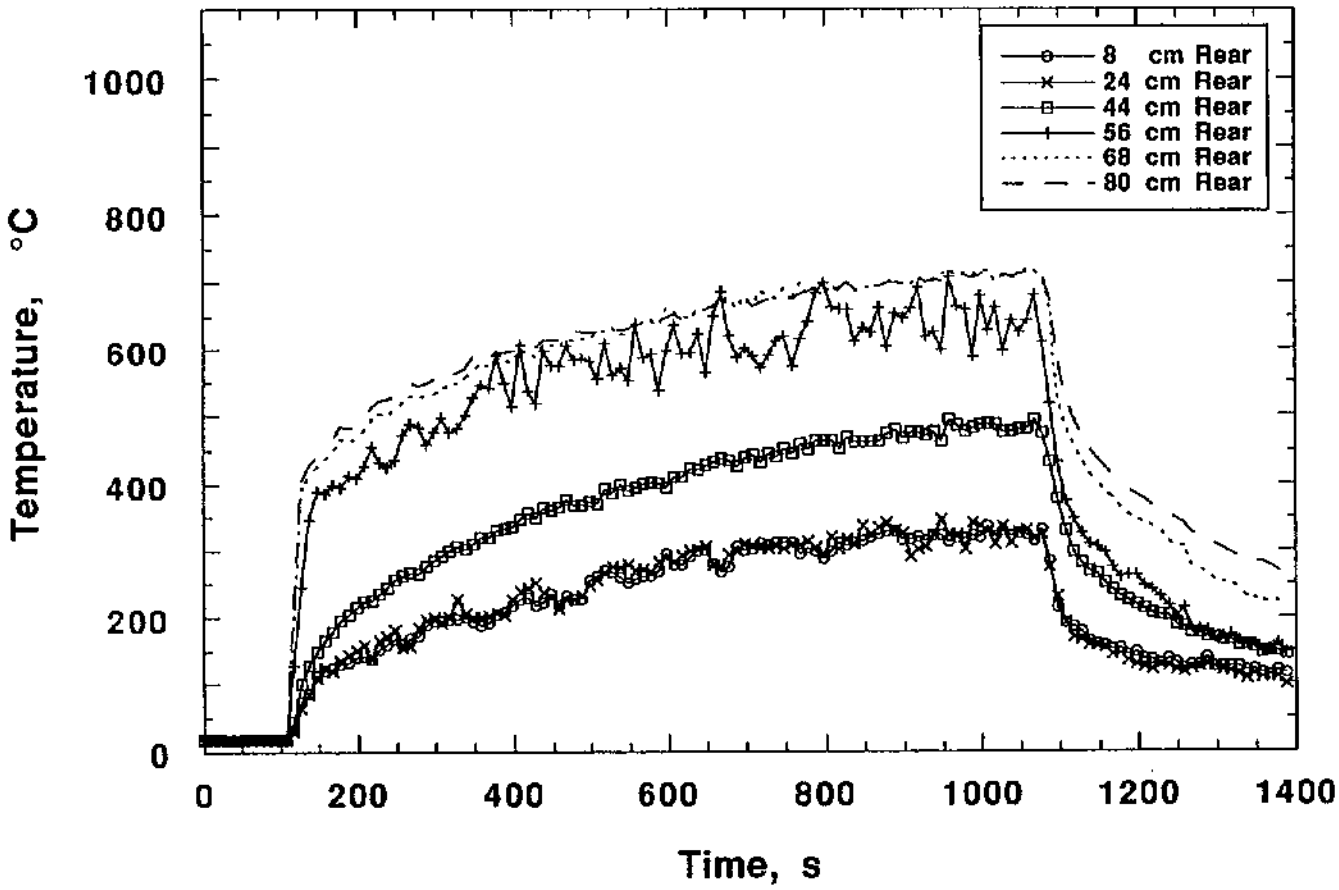

Figure 81. Rear thermocouple tree temperature profile for 350 kW fire.

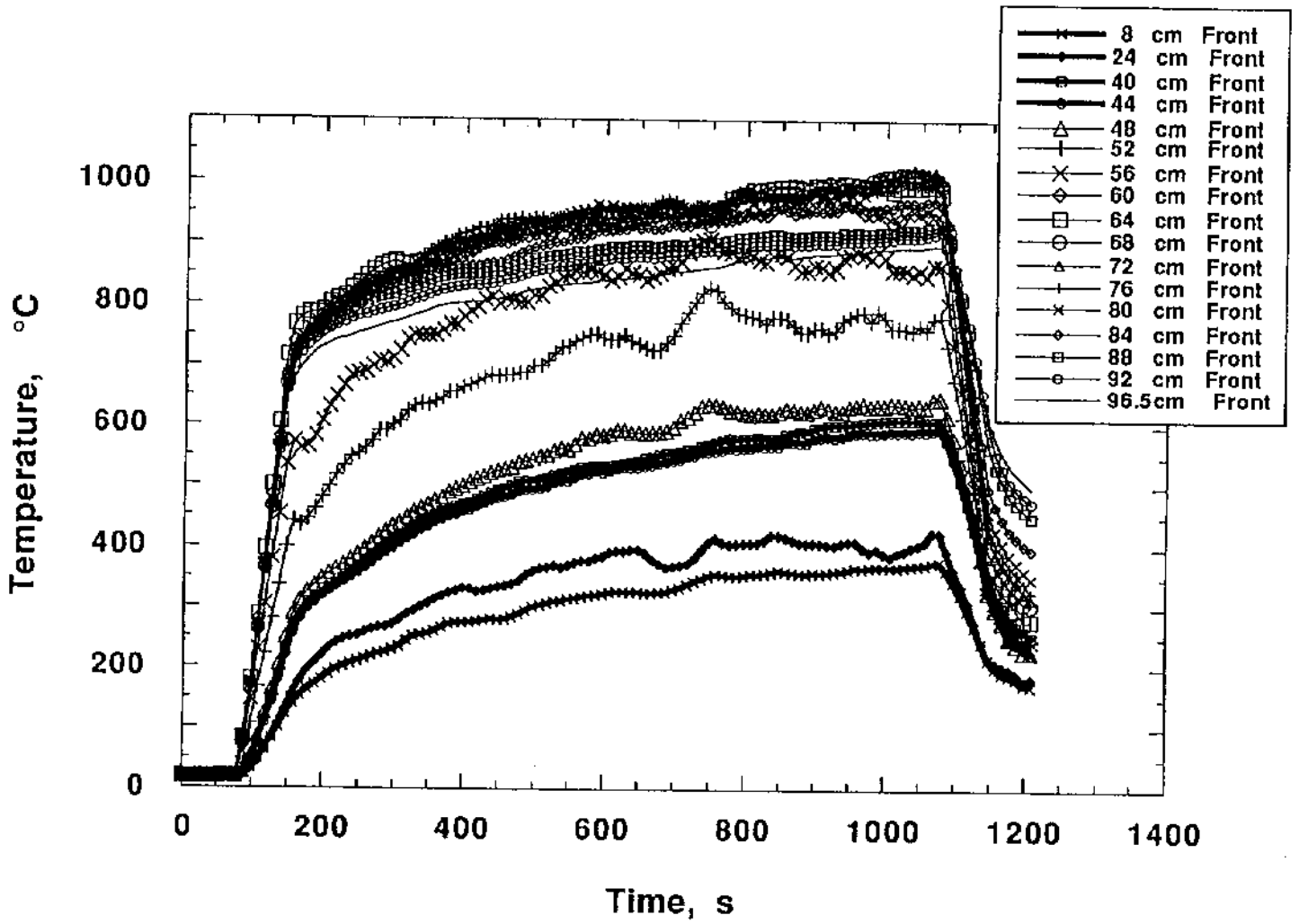

Figure 82. Front thermocouple tree temperature profile for 400 kW fire.

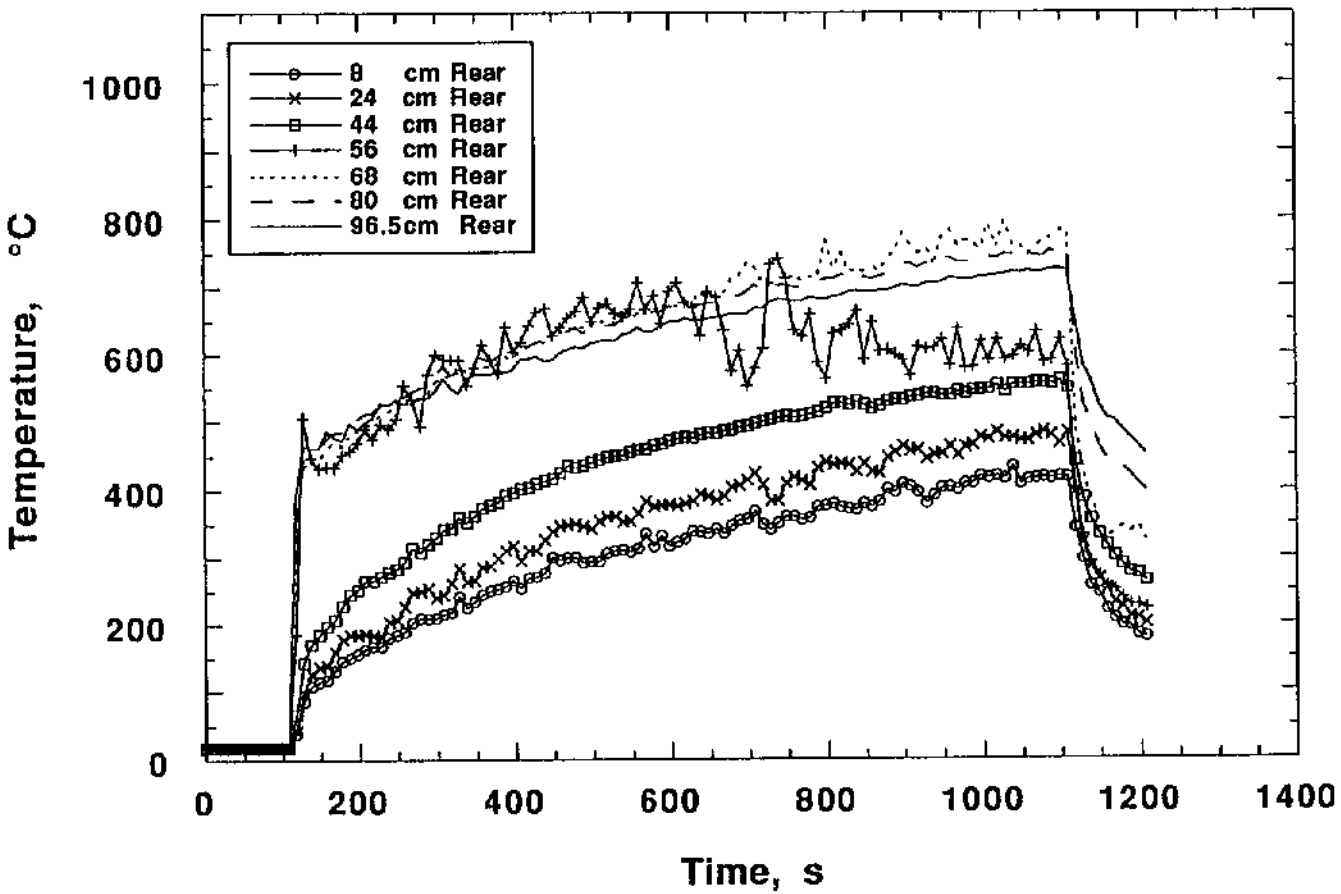

Figure 83. Rear thermocouple tree temperature profile for 400 kW fire.

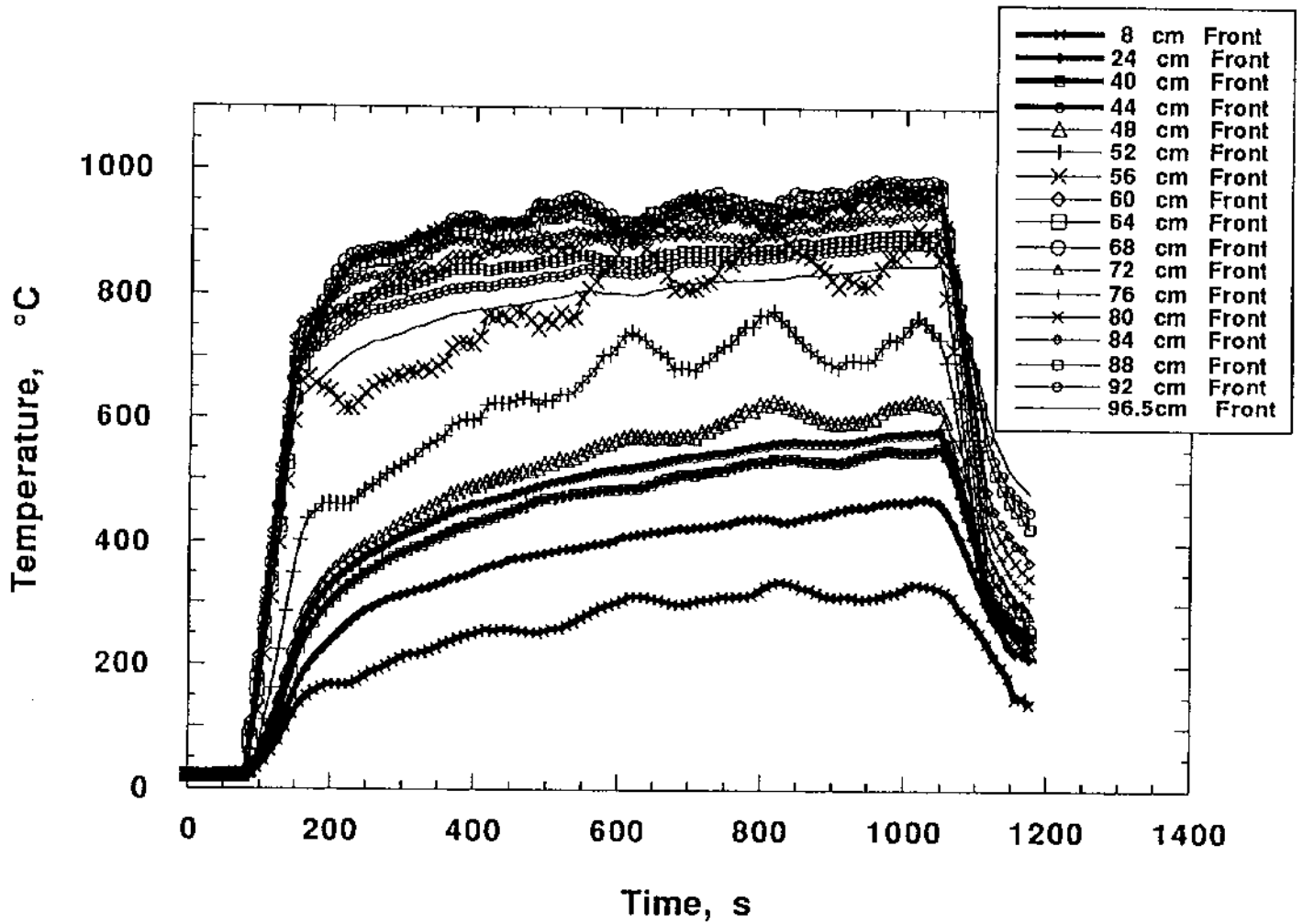

Figure 84. Front thermocouple tree temperature profile for 500 kW fire.

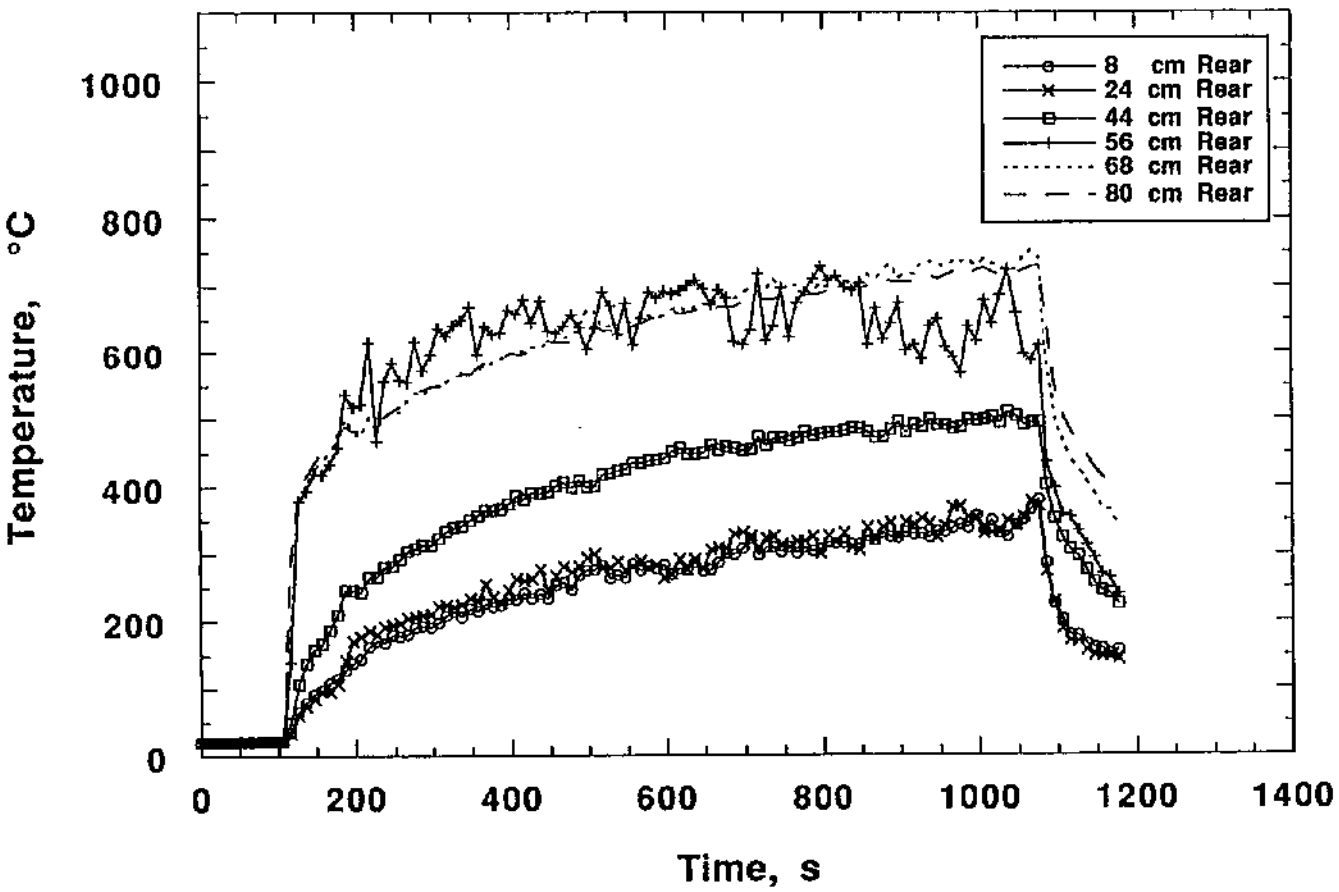

Figure 85. Rear thermocouple tree temperature profile for 500 kW fire.

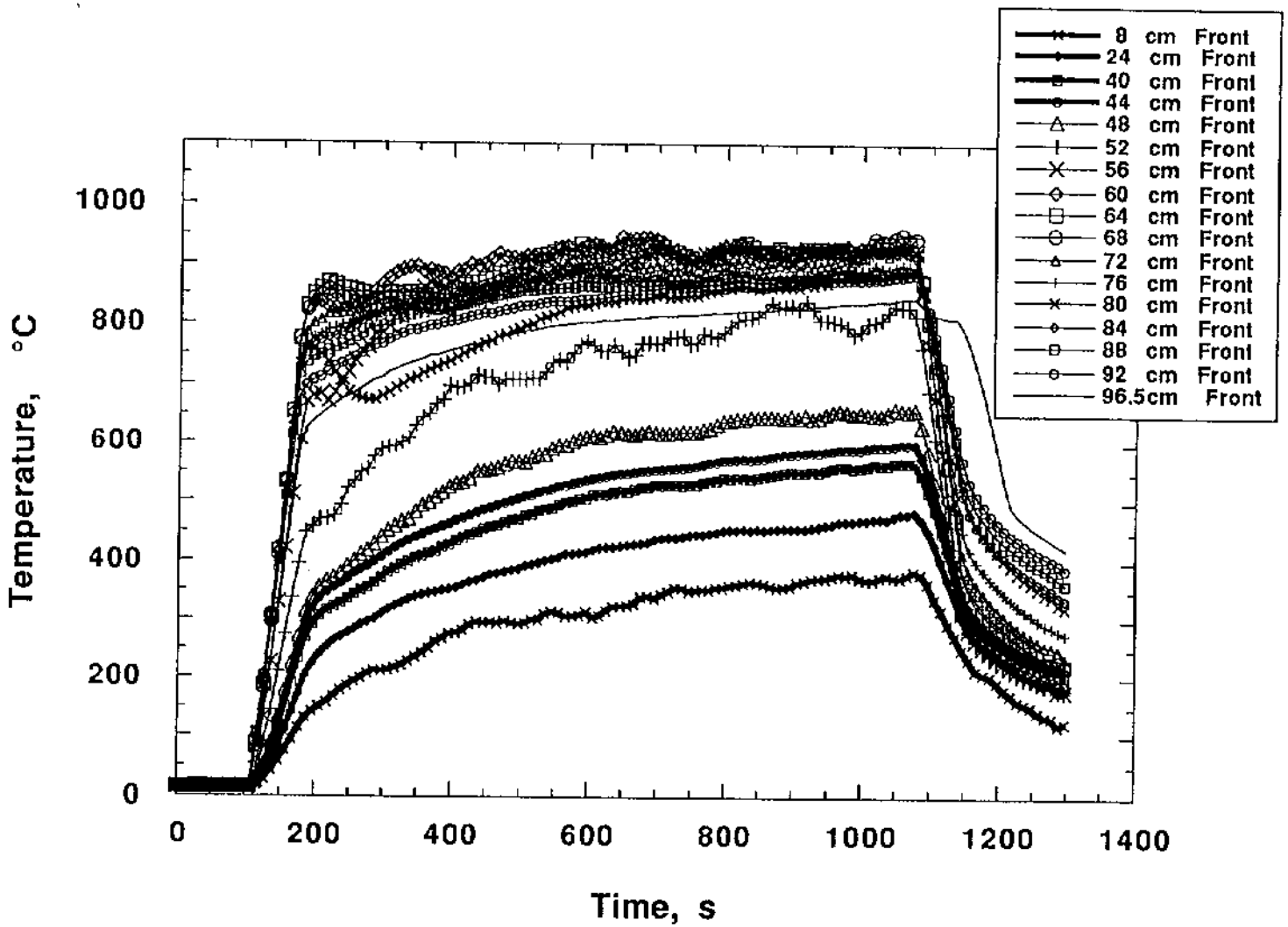

Figure 86. Front thermocouple tree temperature profile for 600 kW fire.

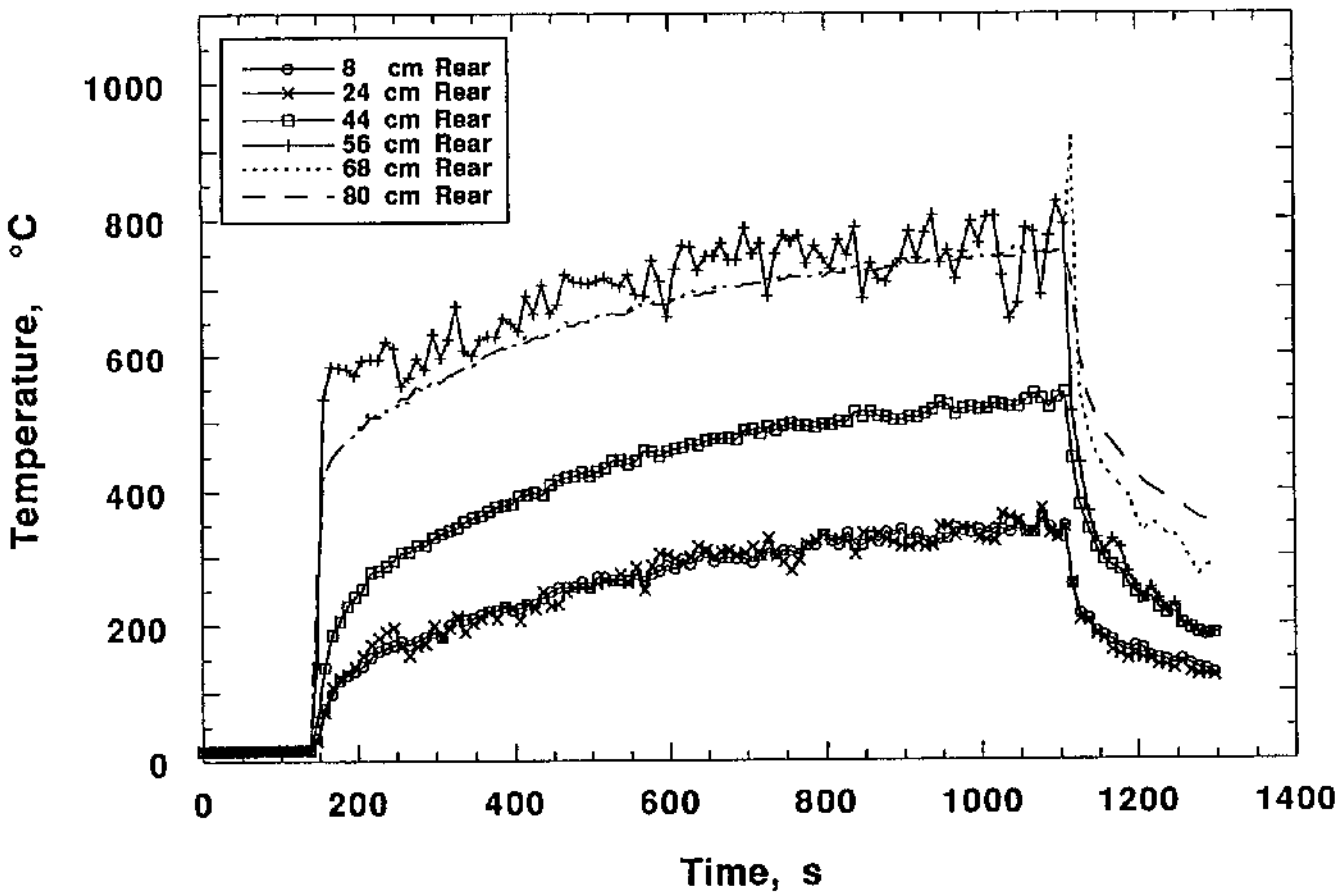

Figure 87. Rear thermocouple tree temperature profile for 600 kW fire.

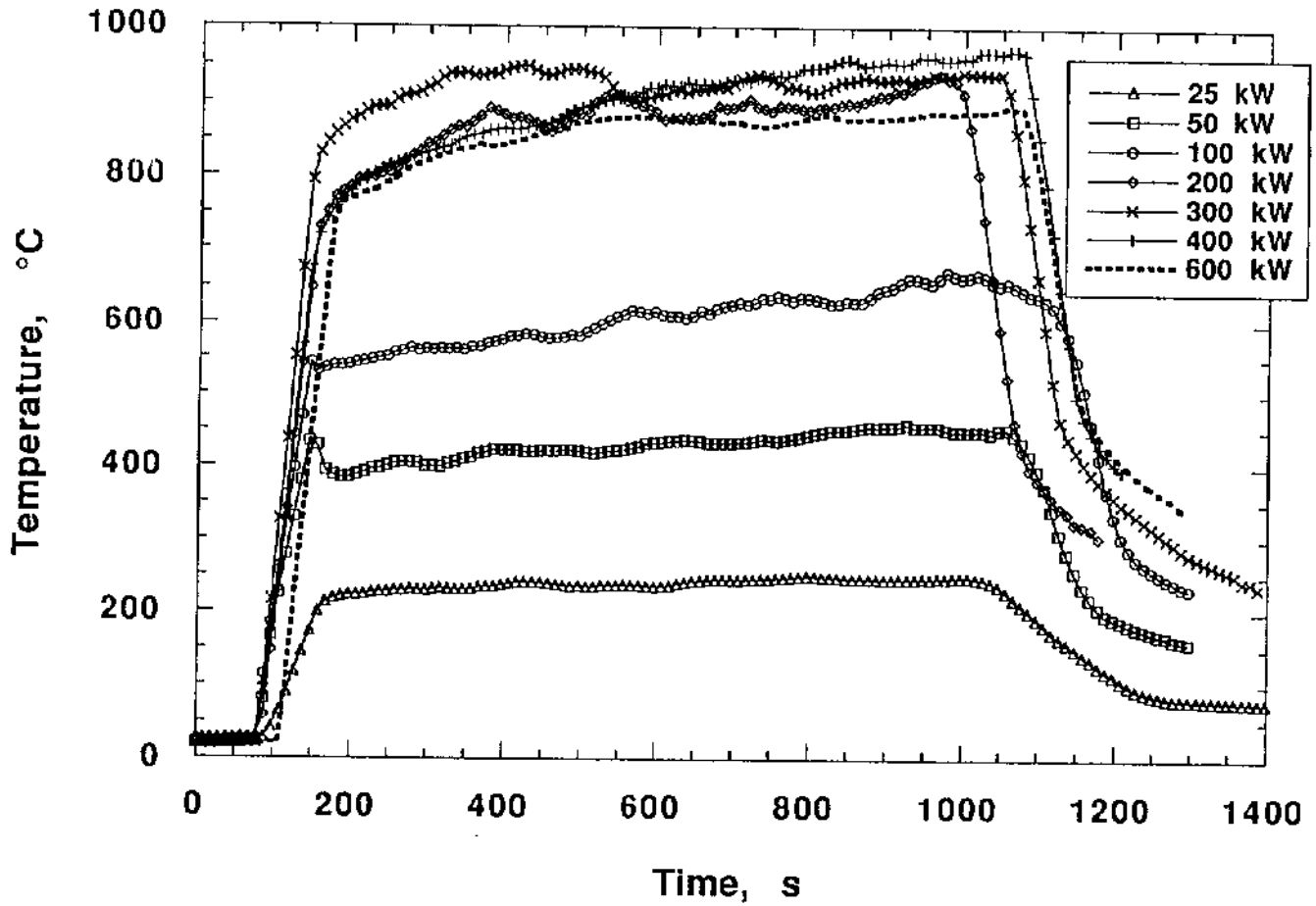

Figure 88. Temperatures for thermocouples located 80 cm above floor within enclosure for various heat-release-rate fires.

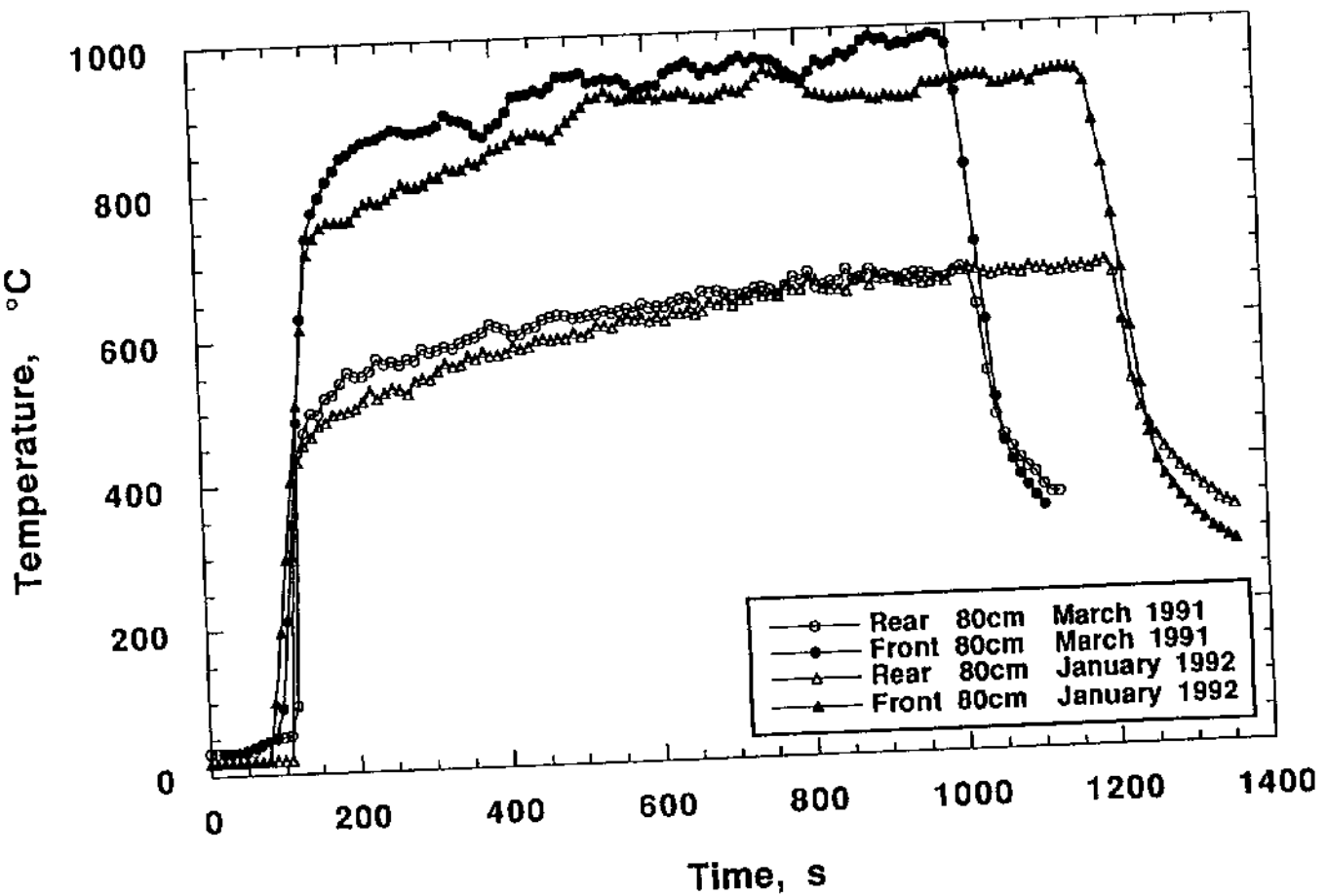

Figure 89. Front and rear temperatures, 80 cm elevation, for two 200 kW fires to demonstrate reproducibility.

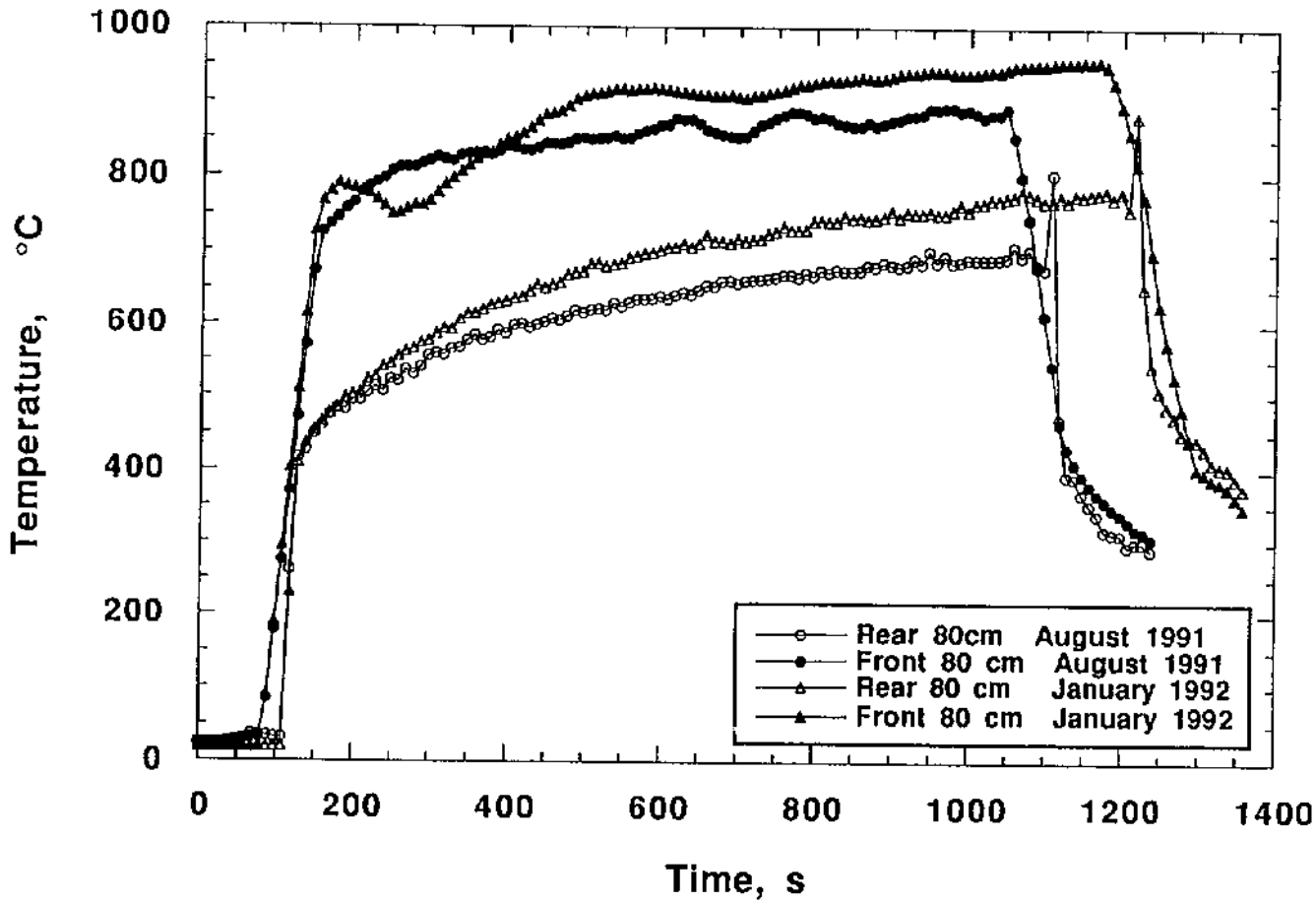

Figure 90. Front and rear temperatures, 80 cm elevation, for two 600 kW fires to demonstrate reproducibility.

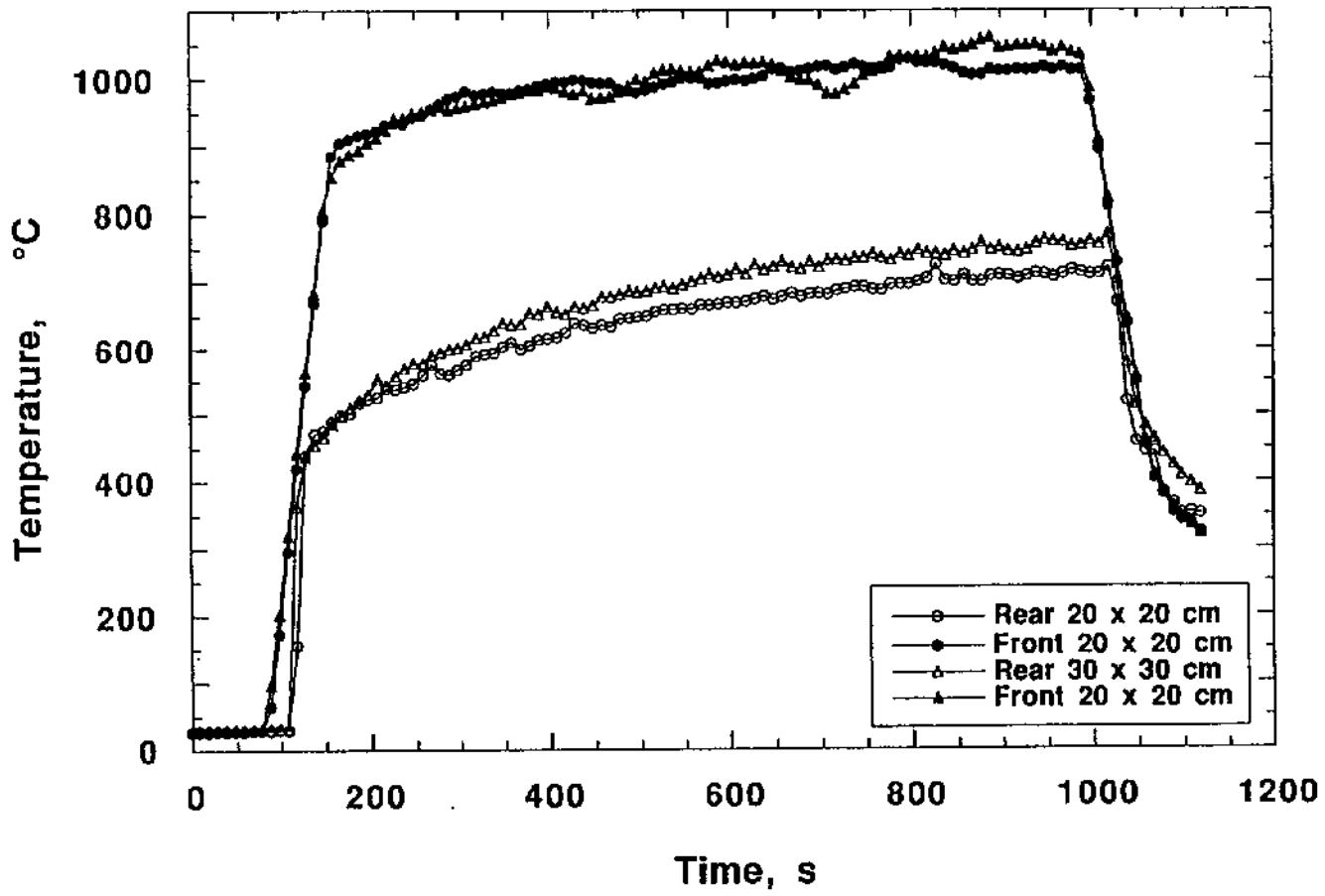

Figure 91. Front and rear temperatures, 80 cm elevation, for two 200 kW fires. Temperatures are for thermocouple trees positioned at 20 cm x 20 cm and 30 cm x 30 cm from rear corner of enclosure.

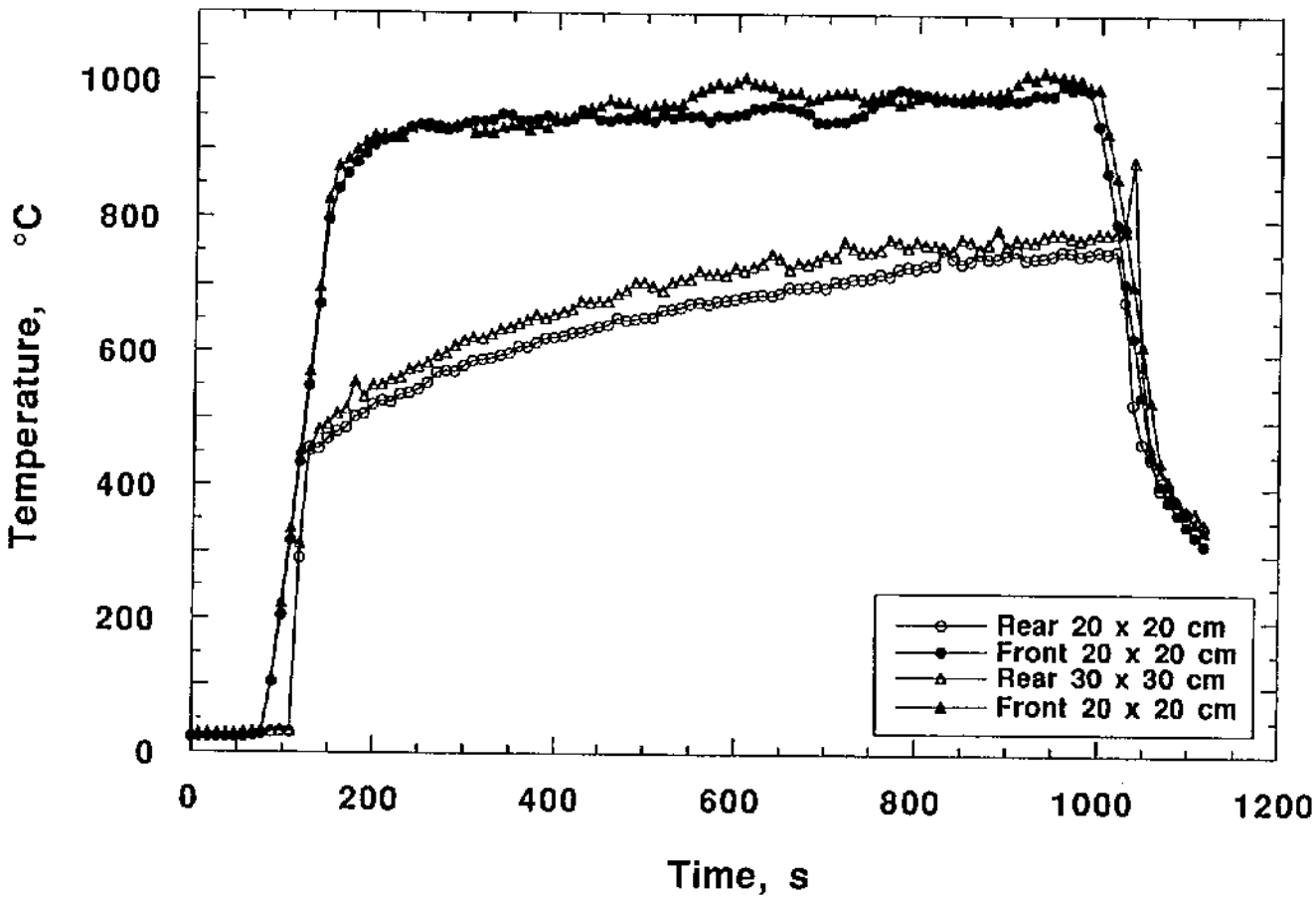

Figure 92. Front and rear temperatures, 80 cm elevation, for two 600 kW fires. Temperatures are for thermocouple trees positioned at 20 cm x 20 cm and 30 cm x 30 cm from rear corner of enclosure.

flow. The calculated ϕ_g for the natural gas burns ranged from 0.1 to 4.2 for HRRs of approximately 10 to 650 kW.

Figure 93 is a plot of time-averaged layer concentrations of oxygen as a function of ϕ_g. The oxygen levels in the rear of the enclosure fall to zero as ϕ_g approaches 1.0, but significant concentrations of oxygen are measured in the front for $\phi_g = 1$ and do not reach zero until ϕ_g is increased to approximately 1.5. Intuitively, oxygen levels should approach zero as ϕ_g reaches 1.0, i.e., stoichiometric burning. In the rear, the oxygen appears to be completely consumed as conditions in the rear start to become fuel rich. In the front however, the oxygen does not appear to be completely consumed as ϕ_g begins to exceed 1.0. This behavior is not well understood. It may be possible for oxygen concentrations to be greater than zero for $\phi_g > 1.0$ as was observed in low-temperature hood experiments [9,11,13]. But, the temperature in the front of the upper layer is much higher than the hood experiments and all the oxygen should react quickly with excess fuel [40]. One possible explanation for this observation is that additional oxygen is somehow introduced directly into the front of the upper layer, but not into the rear. As a result of this additional oxygen, the local equivalence ratio in the front would be lower than in the rear.

The trends observed in the global equivalence ratio were also observed for data collected with a new instrument, dubbed the phi-meter, designed to measure a local phi, ϕ_ℓ, for sampled gases [27]. While the global phi, ϕ_g, considers the total mass entering (fuel and air) and total mass exiting the enclosure, the phi-meter provides a point or local measurement of the equivalence ratio, ϕ_ℓ, at a specific sampling location. At a given location, the phi-meter determines what fraction of the mass in the upper layer at that location started as fuel and what mass originated in the air stream. During 24 burns, the phi-meter, was found to operate quite well and to provide reasonable estimates for ϕ_ℓ. The limited ϕ_ℓ data set (three points) for the rear of the upper layer is insufficient to provide additional insight into the behavior of upper layer. For the front of the upper layer, the oxygen

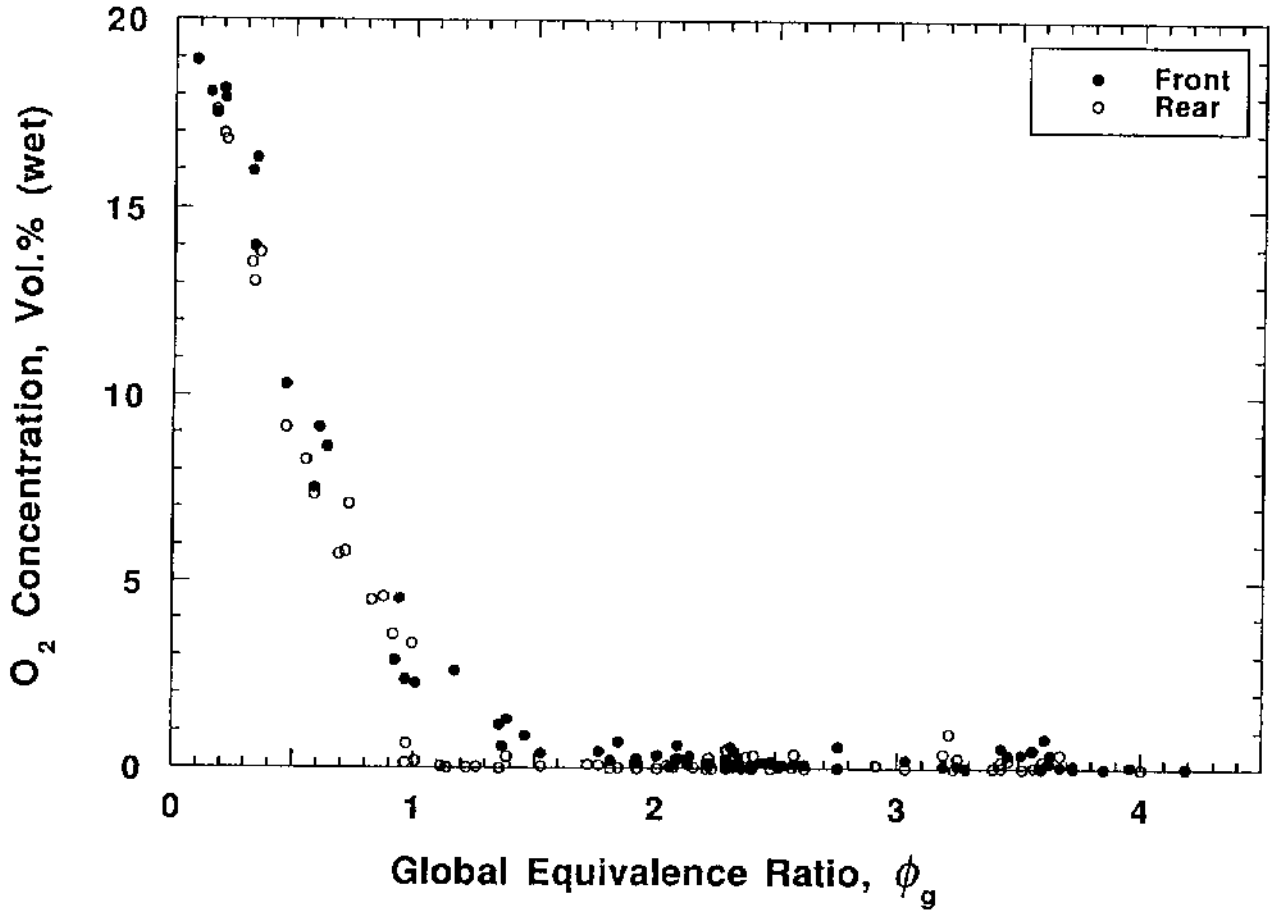

Figure 93. Front and rear oxygen concentrations versus global equivalence ratio. Each data point is the average of concentrations and equivalence ratios recorded between 300 and 900 seconds after ignition.

concentration versus equivalence ratio plots are very similar for ϕ_g and ϕ_ℓ (Figures 93 and 94). While the ϕ_ℓ plot indicates that the oxygen concentration approaches zero in the front of the enclosure for $\phi_\ell \approx 1.0$, the data is not nearly as conclusive as in the rear for ϕ_g where several data points are very near zero at $\phi_g = 1.0$. Since the O_2 concentrations approach zero as ϕ_ℓ exceeds 1.0 in the front, the front ϕ_ℓ appears to be slightly lower for a given fuel flow rate than the corresponding ϕ_g for the enclosure. This result is consistent with additional oxygen being introduced or injected directly into the front of the upper layer as discussed above.

Both the global and local equivalence ratios, ϕ_g and ϕ_ℓ, are plotted as a function of heat release rate in Figure 95. While the agreement between ϕ_g and ϕ_ℓ is quite good overall, the ϕ_ℓ values are a little lower for a HRR greater than 400 kW. Both ϕ_g and ϕ_ℓ pass through stoichiometric conditions, $\phi = 1.0$, at a HRR of about 200 kW. As discussed above, the front ϕ_ℓ appears lower than the ϕ_g for the enclosure. The limited data for ϕ_ℓ for the rear of the upper layer indicates that the equivalence ratio in the rear is lower than in the front. This behavior is not expected or understood and is not consistent with additional oxygen being injected directly into the front of the upper layer.

3.5 Hydrogen Grab-Bag Samples

A gas chromatograph was used to analyze grab-bag samples for hydrogen concentrations. Samples were collected in 2-liter Tedlar bags for different heat-release-rate fires and at different times during a specific burn. As shown in Table 1, measured hydrogen concentrations range from 1.1% to 2.9% for 250 kW and 550 kW fires, respectively. As the fire becomes fuel rich, the concentrations of products of incomplete combustion, such as H_2, CO, and unburned fuel, are expected to increase. The observation of CO and H_2 in the upper layer for $\phi_g > 1.0$ is consistent with this expectation.

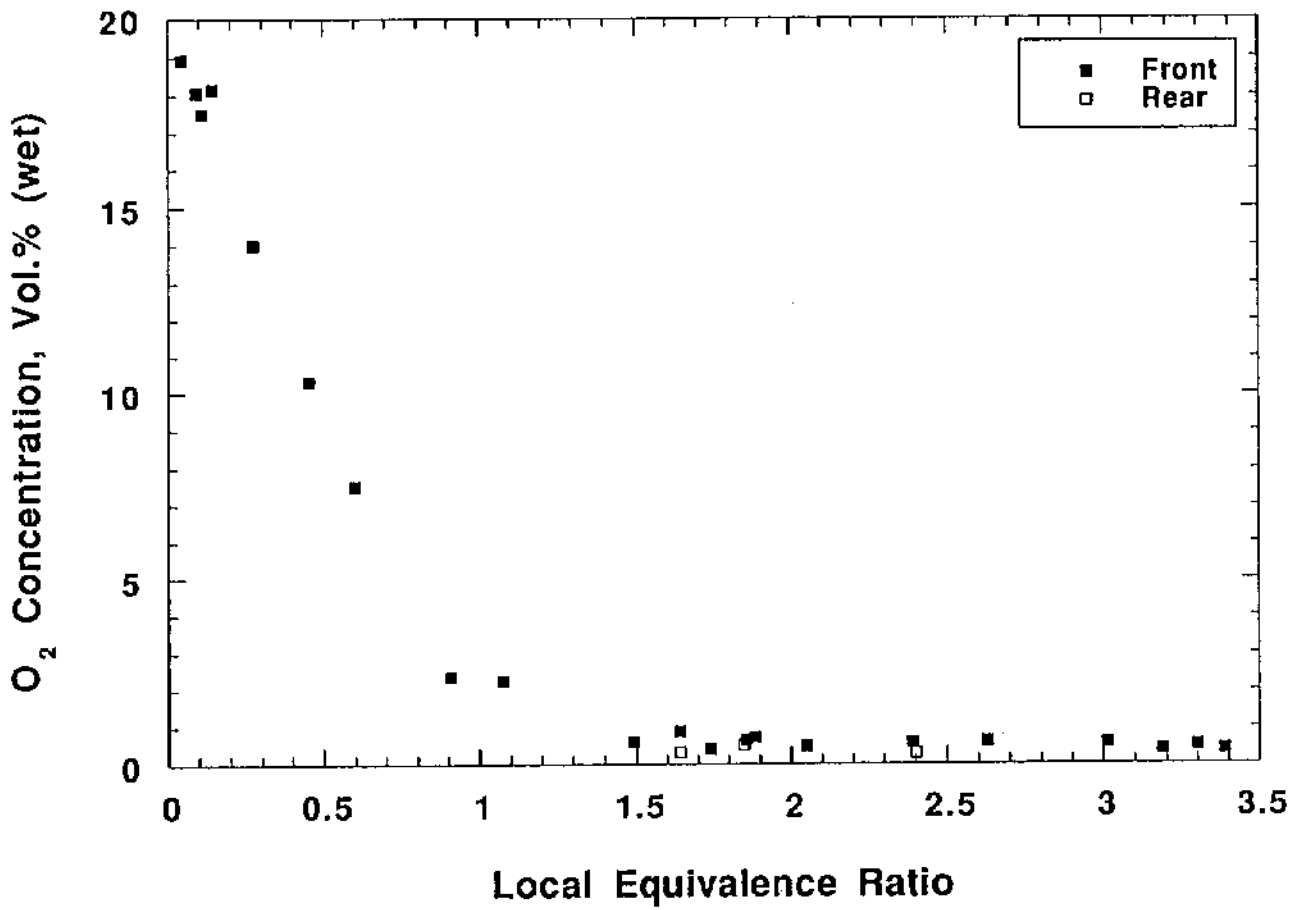

Figure 94. Front and rear oxygen concentrations versus local equivalence ratio (Phi-Meter measurements). Each data point is the average of concentrations and equivalence ratios recorded between 300 and 900 seconds after ignition.

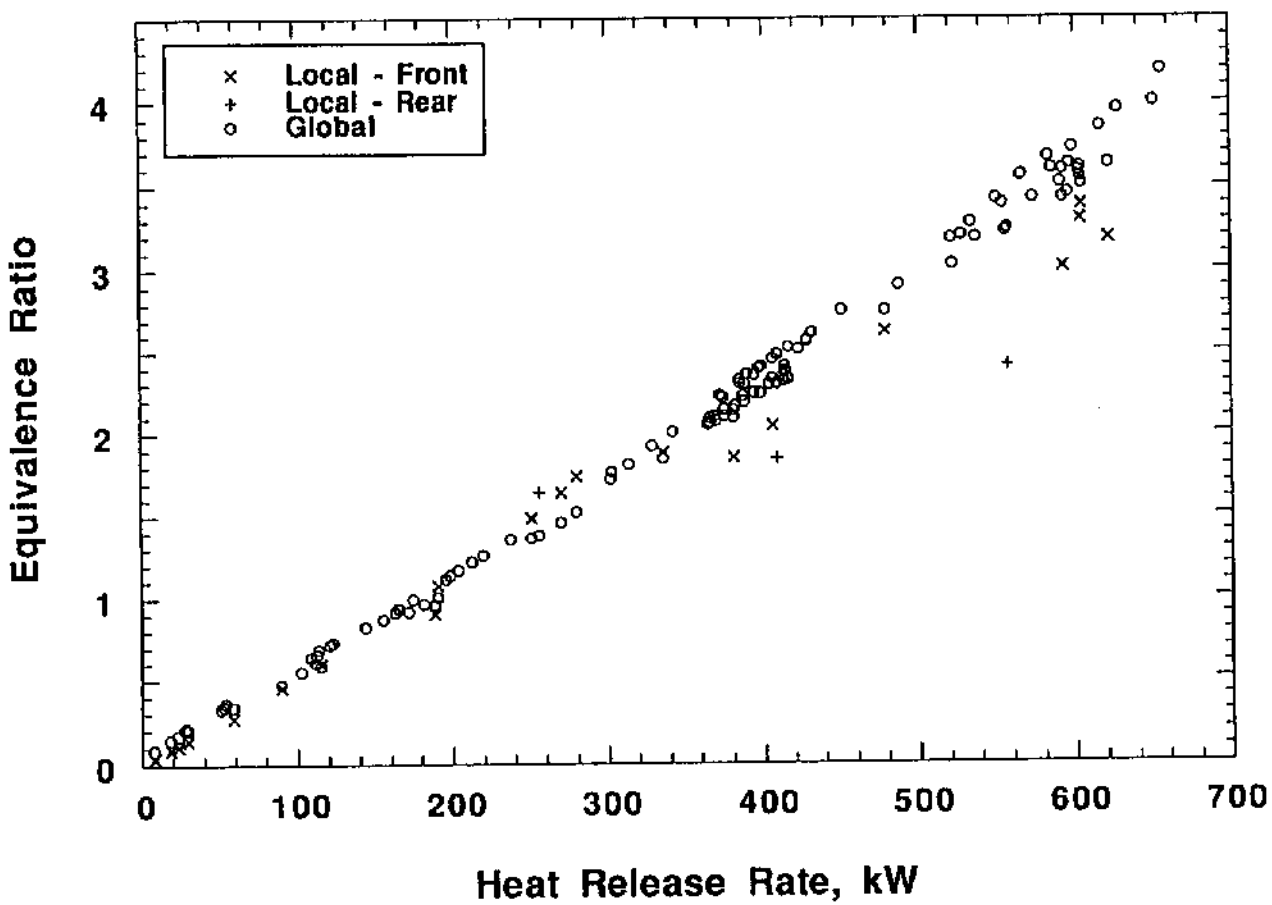

Figure 95. Global and local equivalence ratios versus heat release rate. Each data point is the average of equivalence ratios recorded between 300 and 900 seconds after ignition.

Table 1. Hydrogen Analysis of Grab-Bag Samples

Run ID Number	Heat Release Rate kW	Sample Time minutes	Hydrogen Conc. Vol% (Dry)	Probe Location
9173	250	10	1.1	Front
9272	400	7	2.5	Front
9272	400	12	2.9	Front
9280	400	12	1.8	Flame Sheet
9274	550	7	2.6	Front
9274	550	12	2.7	Front
9279	600	12	1.9	Flame Sheet

Notes:

1. Sample Time - time at which sample collection was initiated. Ignition of gas burner occurred at time = zero. Sampling period lasted approximately one minute.

2. Water-cooled probe was used to collect all samples.

3.6 Total Unburned Hydrocarbons

A total-unburned-hydrocarbon (TUH) analyzer was installed after approximately half the burns had been completed. The amount of data collected was limited by multiple operational problems. Initially the instrument was calibrated with 0.1% methane gas because this span gas was readily available. Unfortunately, the response of the instrument was extremely non-linear and the 0.1% methane was much too low for the underventilated fires. A higher concentration calibration gas, 3% methane, was procured and some data was collected, but further operational difficulties forced the instrument to be returned to the manufacturer for repair. Since the fraction of unburned hydrocarbons is expected to exceed 15% for 600 kW burns ($\phi_g \approx 4$), a third calibration gas, 10% methane, was obtained and further burns are planned to collect additional TUH data.

3.7 Narrow Door Burn Configuration

A limited number of small fires were conducted with the 48 cm door width of the RSE reduced to 1 cm while the height remained 81 cm. Due to the much lower HRR, temperatures in the enclosure did not exceed 400 °C and averaged about 300 °C. The upper layer was observed to form more slowly and the appearance or disappearance of individual gas species was more easily tracked. After ignition at 120 seconds for a 25 kW HRR fire, the oxygen began to drop immediately and simultaneously carbon dioxide started to appear (Figure 96). Carbon monoxide only began to appear in the upper layer after the oxygen concentration dropped below 7%. Because of the lower temperatures in the upper layer, CO and O_2 concentrations of 0.9% and 2% coexisted throughout much of the fire. The results of these burns are consistent with the concentrations observed by Morehart [13] for a low-temperature hood experiments for a range of fire sizes. Results for the two sets of measurements are compared in Table 2.

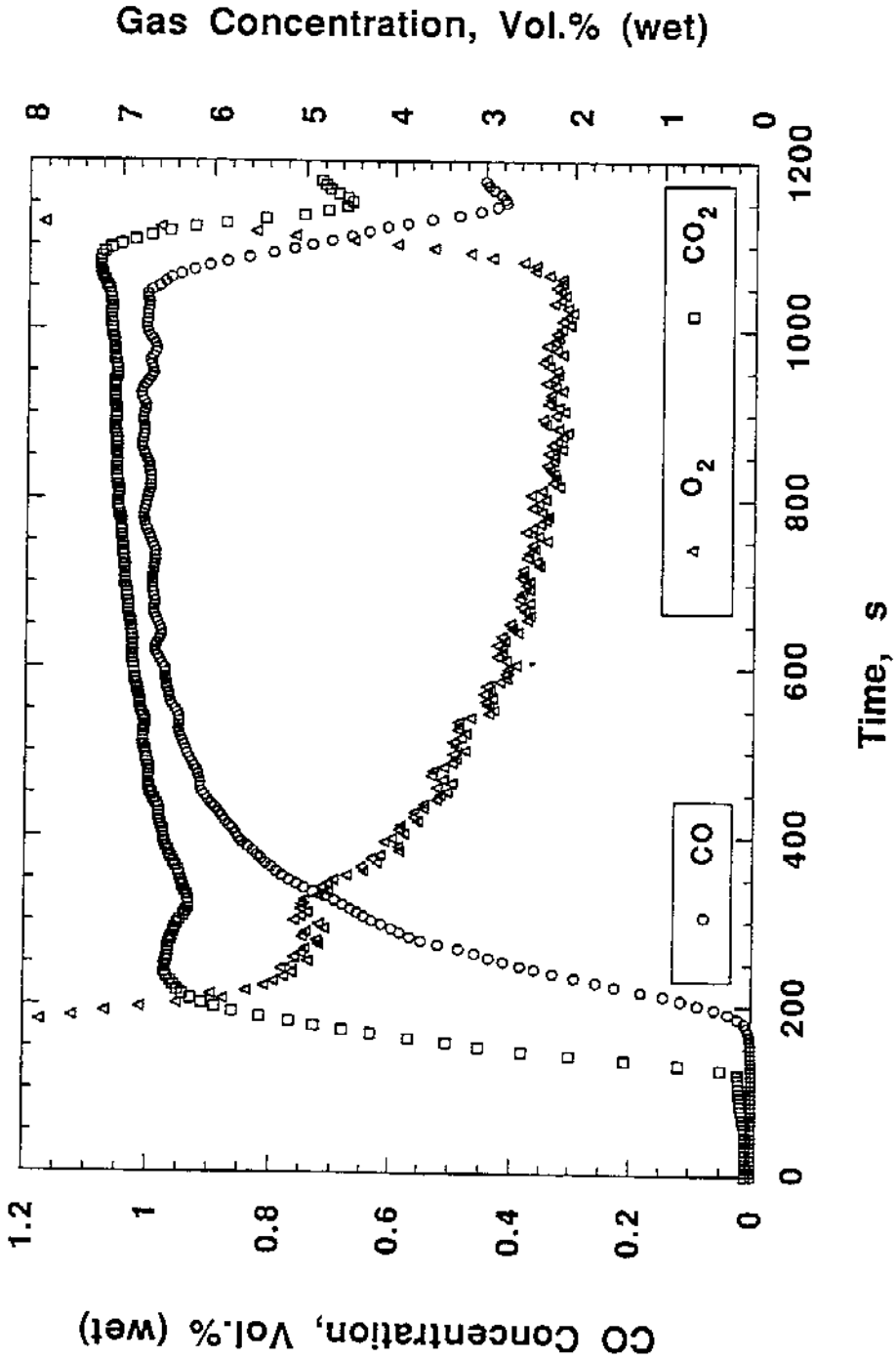

Figure 96. Carbon monoxide, carbon dioxide, and oxygen concentrations for a 25 kW fire with narrow door configuration.

Table 2. Upper-Layer Concentrations Observed in Narrow-Door Burns and Hood Fires.

HRR (kW)	ϕ_ℓ	Narrow-Door Configuration Burns			Hood Experiment (Morehart [13,14])		
		Concentration, Vol% (Wet)			Concentration, Vol.% (Wet)		
		CO	CO_2	O_2	CO	CO_2	O_2
7	0.5	0.003	4.7	10.0	0.00	5.1	9.6
10	0.7	0.23	6.5	6.5	0.35	6.2	7.0
15	1.2	0.8	7.1	3.9	1.3	6.9	3.8
25	1.5	1.0	7.3	2.1	1.5	6.9	2.5

During several of these fires, blue flames, which were not connected to the burner, were observed at different locations, including front, rear, upper and lower layer positions, within the enclosure. These "ghost" flames were approximately 25 cm x 10 cm and appeared sporadically throughout the burn. Sugawa et al. [41] have also observed ghosting flames when methanol, ethanol, and methane fires were burned in a compartment which was poorly ventilated and relatively cool - less than 150 °C (measured in upper-layer near ceiling).

3.8 Soot

For several enclosure configurations, the mass of soot collected on the hydrocarbon analyzer filter was recorded. Since the flow rate through the filter was measured before each burn, this rate was multiplied by the total burn time in order to estimate the total volume of smoke sampled. Dividing the mass of soot on the filter by the total sample volume provided an integrated soot mass

concentration. These mass concentrations, shown in Figure 97, should be viewed as qualitative and not quantitative because of uncertainties in the total smoke volume. Although the sample line to the hydrocarbon analyzer was heated, some wall losses were inevitable. The flow rate should be monitored throughout the entire burn since the smoke flow rate could be reduced as soot accumulates on the filter. For leaner conditions very little soot was observed. As the fires became underventilated, measured soot mass concentrations began to increase before leveling off at approximately 700 mg/m^3 as the HRR reached 300 kW.

3.9 Flashover Tests

Two crumpled balls and one flat piece of paper were placed on the enclosure floor as a crude measure of room flashover. Typically, the flat paper did not ignite, but pyrolyzed very quickly. The two paper balls, dubbed more-crumpled and less-crumpled, did ignite 1 to 6 minutes into each fire (Figure 98). The less-crumpled balls appeared to ignite slightly before the more tightly packed ones. As the HRR was increased, the time to ignition decreased and leveled off at about one minute. Interestingly, the leveling off in ignition time occurred for fires corresponding to underventilated conditions. Maximum upper-layer temperatures in these fires were roughly equivalent.

3.10 Cooled, Uncooled, and Through-the-Wall Probes

The upper-layer combustion gases were sampled using sample probes of three designs. In order to evaluate whether the probe design was affecting the measurement results, several head-to-head comparisons were conducted with two different designs sampling at the same location within the enclosure. The carbon monoxide and carbon dioxide concentrations for an uncooled and a cooled probe are plotted for a 400 kW fire in Figures 99 and 100, and the oxygen profiles for a similar 400 kW fire are shown in Figure 101. An oxygen meter sample line developed a leak during the first fire

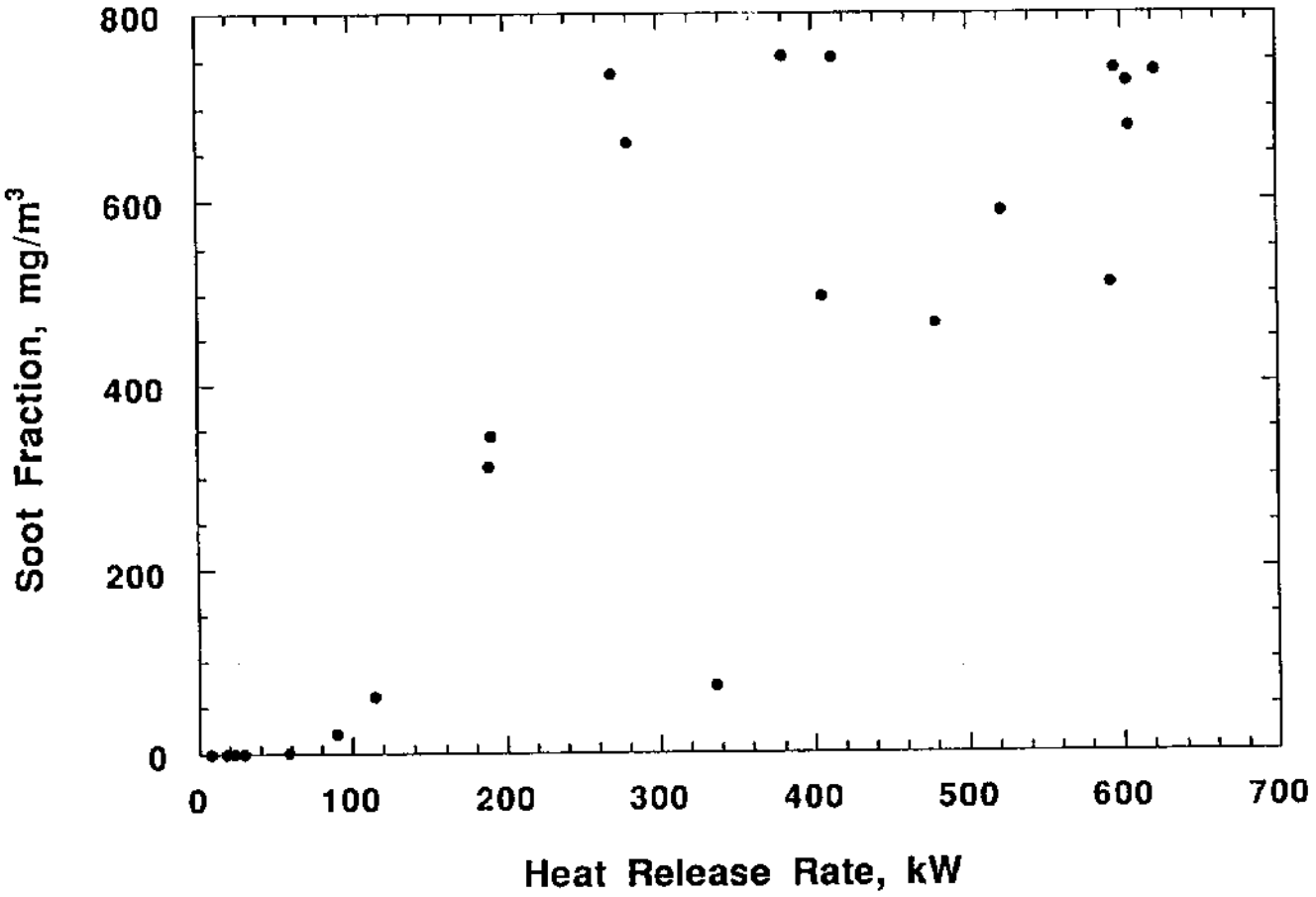

Figure 97. Calculated soot fraction versus heat release rate.

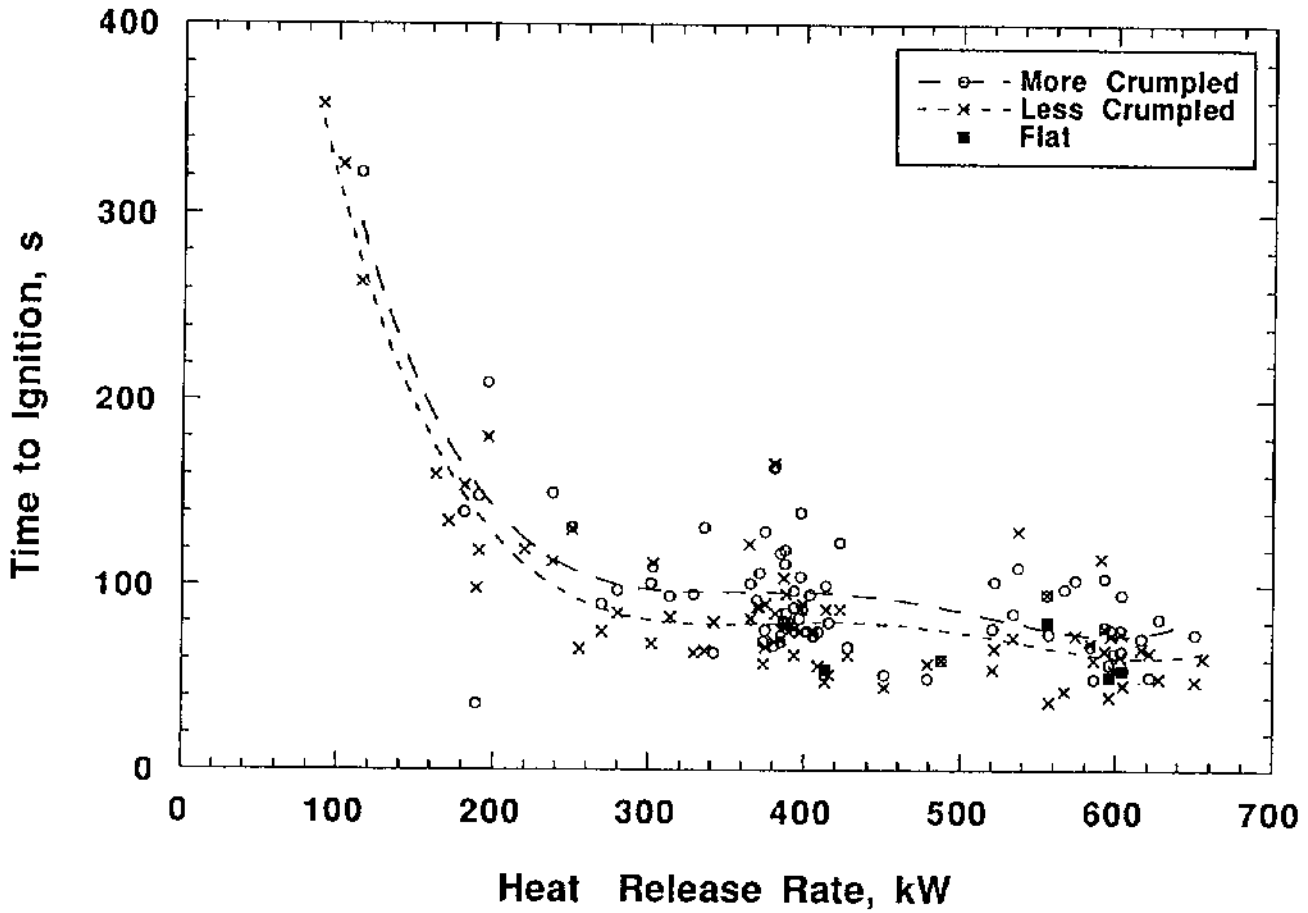

Figure 98. Ignition times for three "qualitative" flashover tests versus heat release rate.

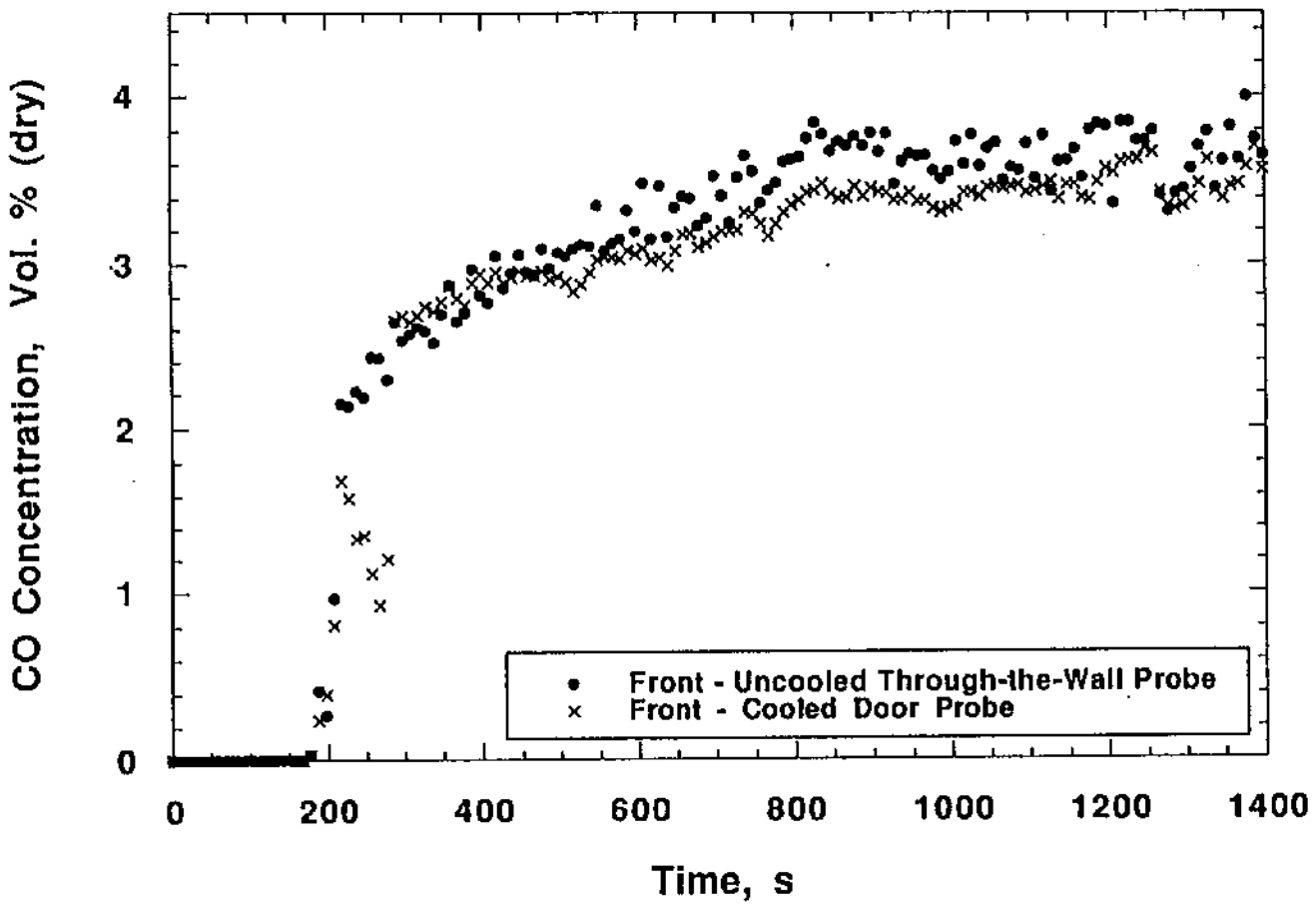

Figure 99. Carbon monoxide concentrations in the front of the upper layer for a 400 kW fire comparing cooled and uncooled probe measurements.

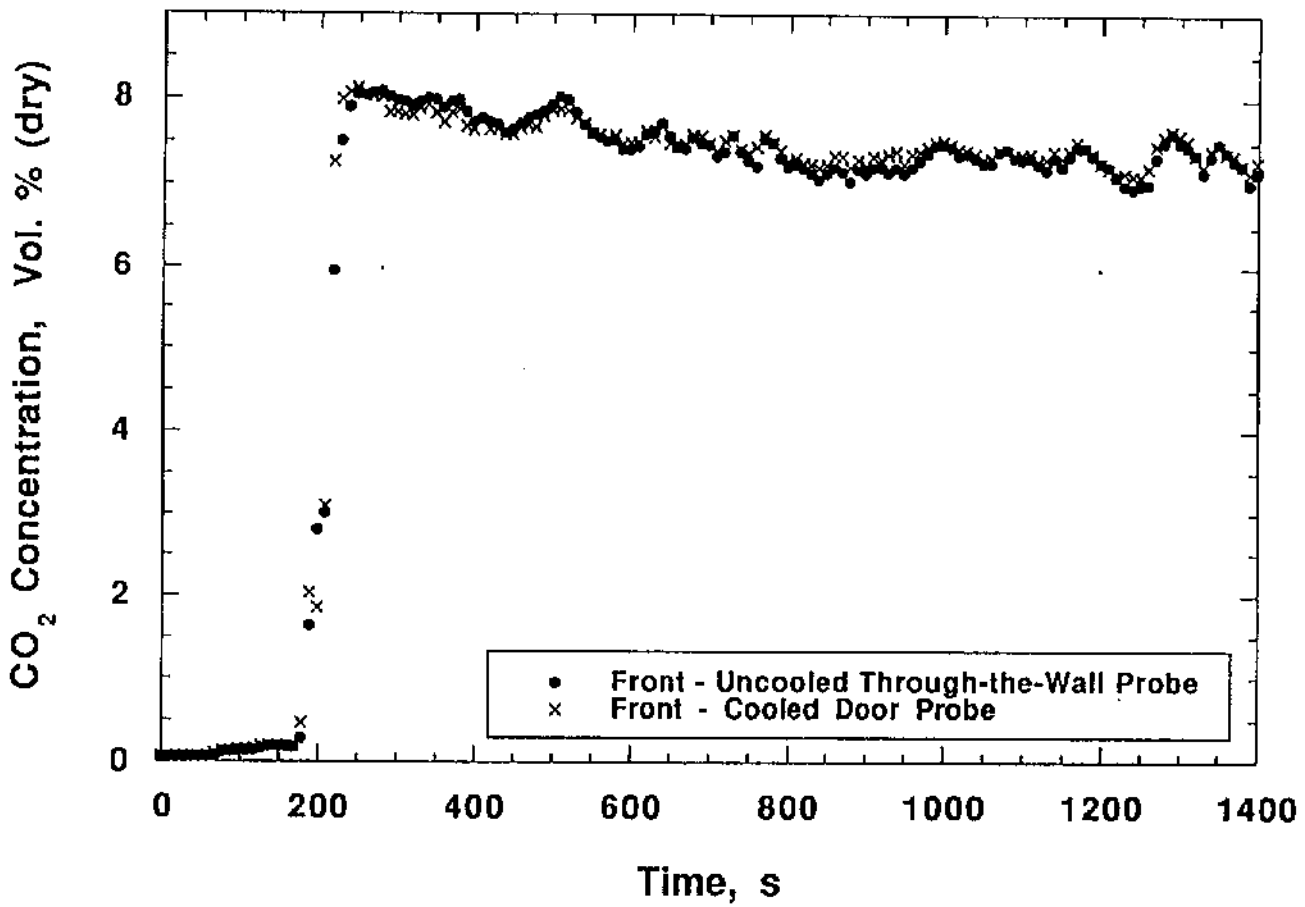

Figure 100. Carbon dioxide concentrations in the front of the upper layer for a 400 kW fire comparing cooled and uncooled probe measurements.

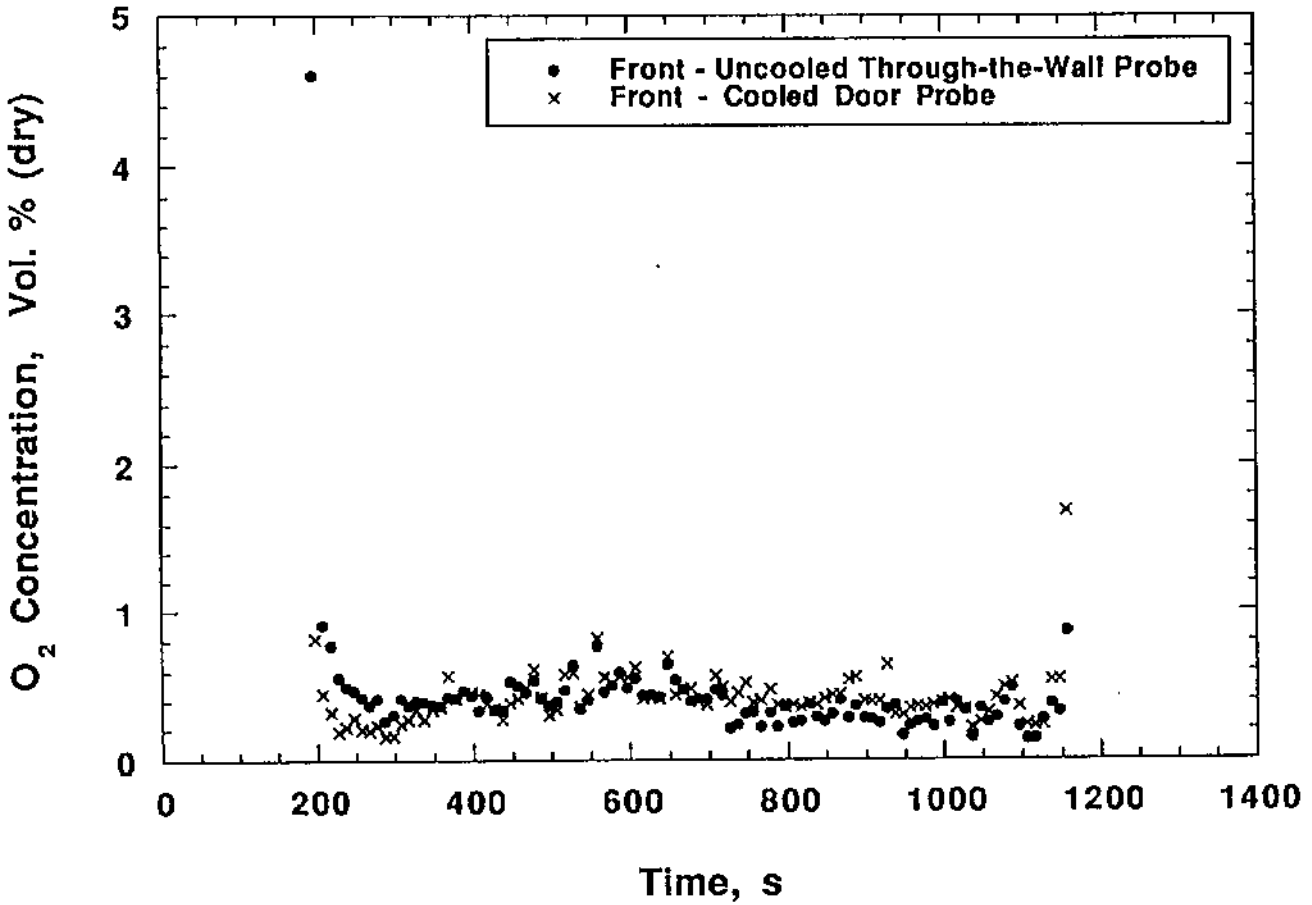

Figure 101. Oxygen concentrations in the front of the upper layer for a 400 kW fire comparing cooled and uncooled probe measurements.

and a carbon monoxide analyzer malfunctioned in the second fire. The concentrations of carbon monoxide and carbon dioxide are not significantly different for the cooled and uncooled probes. The oxygen was depleted to near-zero levels in both fires for each probe.

The front of the upper layer was also sampled head-to-head with through-the-wall and through-the-door uncooled probes. For a 600 kW fire, the CO_2 and O_2 concentrations for the uncooled doorway and through-the-wall probes are graphed in Figures 102 and 103. Difficulties with one of the carbon monoxide analyzers precluded a comparison of CO concentrations in the same fire. During another 600 kW fire, the front of the upper layer was sampled head-to-head with through-the-wall and cooled probes. For this second 600 kW fire, the CO concentrations for the cooled doorway and through-the-wall probes are graphed in Figure 104. These head-to-head probe comparisons indicate that the gas concentrations measured in the experiment do not depend significantly on the probe design.

3.11 Uncertainty Analysis

The combined standard uncertainty of the data can be evaluated by combining the random and systematic components of uncertainty. Uncertainties are grouped into two categories according to the method used to estimate them. Type A uncertainties are those which are evaluated by statistical methods, and Type B are those which are evaluated by other means[42]. Type B analysis of systematic uncertainties involves estimating the upper ($\overline{x}$ + a) and lower ($\overline{x}$ - a) limits for the quantity in question such that the probability that the value would be in the interval ($\overline{x} \pm$ a) is essentially 100 %. After estimating the random and systematic uncertainties by either Type A or B analysis, the uncertainties are combined in quadrature to yield the combined standard uncertainty. Multiplying the combined standard uncertainty by a coverage factor of two results in the expanded uncertainty which corresponds to a 95 % confidence interval (2σ).

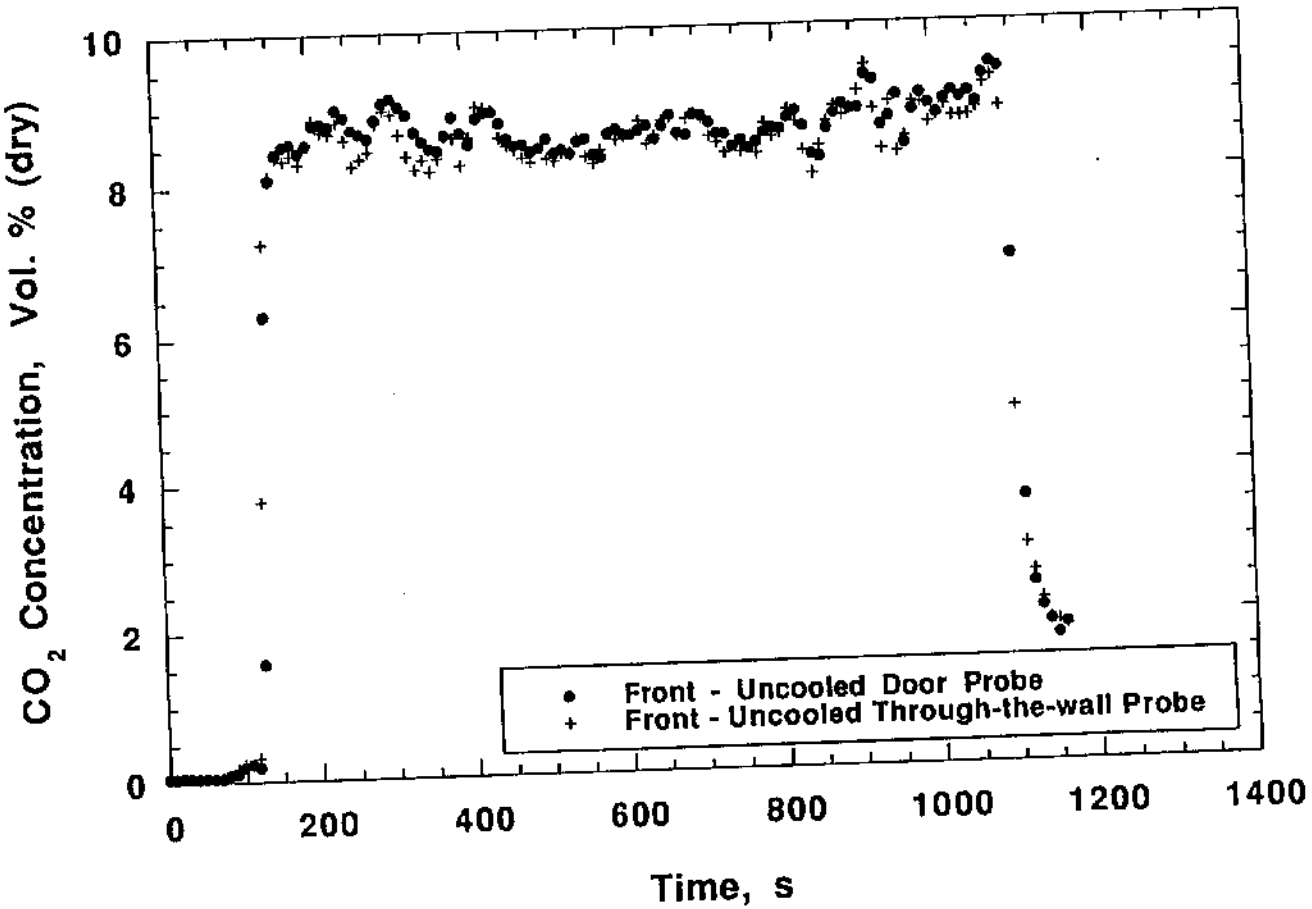

Figure 102. Carbon dioxide concentrations in the front of the upper layer for a 600 kW fire comparing through-the-wall and uncooled doorway probe measurements.

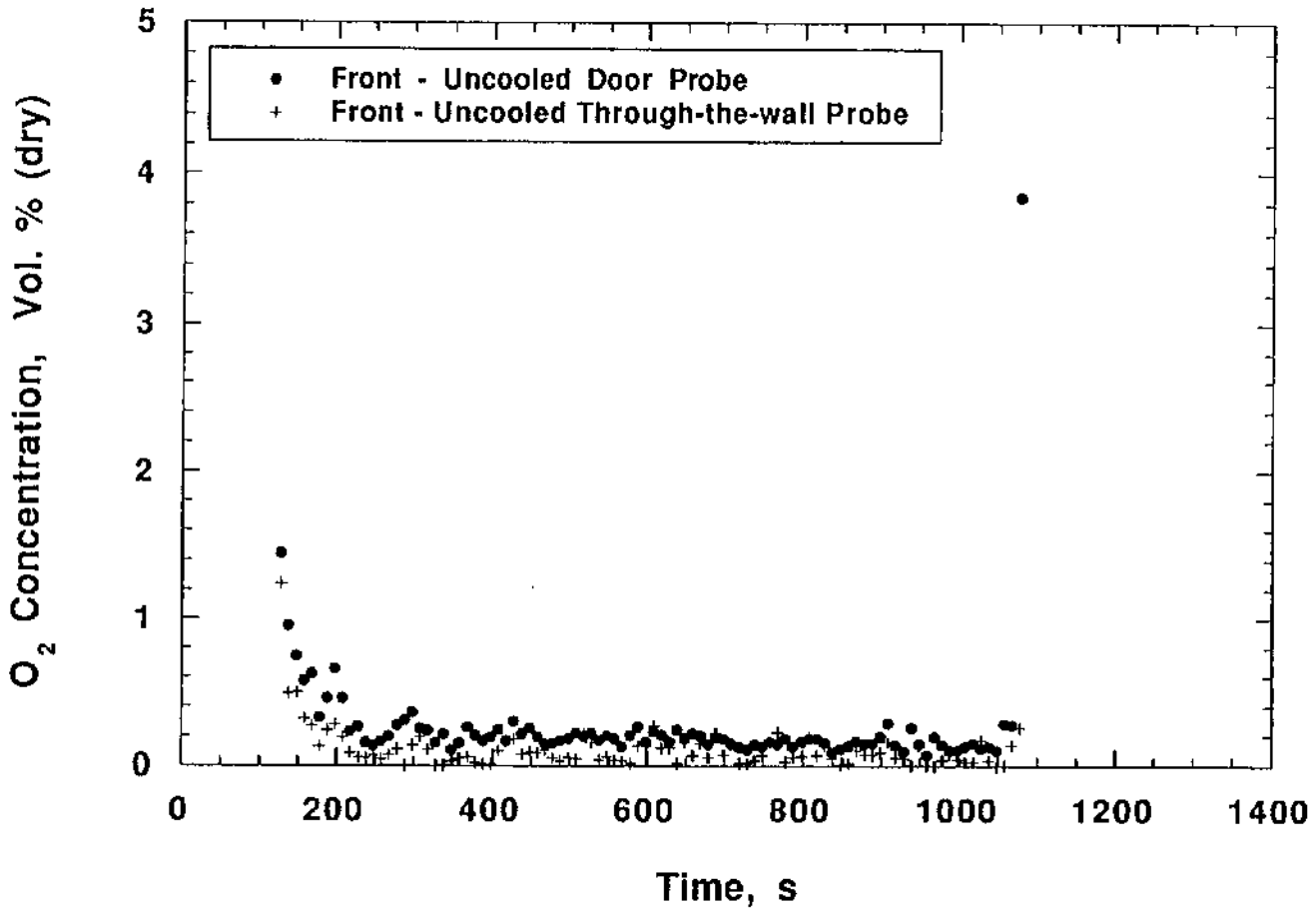

Figure 103. Oxygen concentrations in the front of the upper layer for a 600 kW fire comparing through-the-wall and uncooled doorway probe measurements.

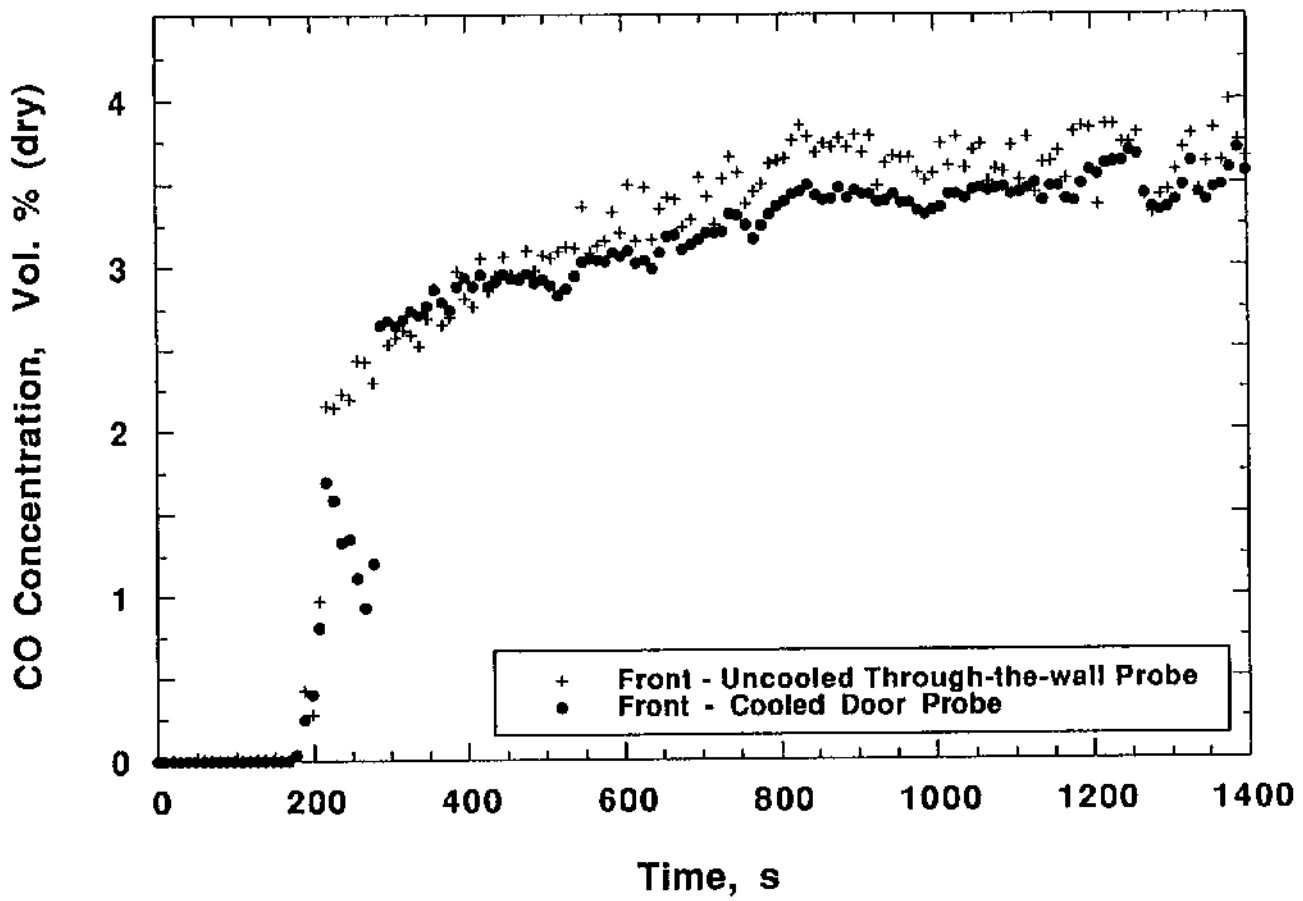

Figure 104. Carbon monoxide concentrations in the front of the upper layer for a 600 kW fire comparing through-the-wall and cooled doorway probe measurements.

For each fire, the flow rate of the natural gas fuel was monitored by diaphragm test meter and rotameter (as previously described in Section 2.3.5). For the diaphragm test meter, a Type B analysis included uncertainties in the natural gas line pressure, stopwatch operation, and volume of the test meter, as well as a random component. The analysis resulted in a combined standard uncertainty and an expanded uncertainty (2σ) of 3.1 % and 6.2 %, respectively. The uncertainty in the rotameter, the second method of monitoring the fuel flow rate, was significantly higher than the diaphragm test meter. Uncertainties in the rotameter scale and pressure, float position and density, and natural gas supply pressure and density were combined with the random component of uncertainty in a Type B analysis. This resulted in a combined standard uncertainty and expanded uncertainty (2σ) of ± 14 % and ± 28 %, respectively. These levels of uncertainty were consistent with the differences observed when the fuel flow rate calculated via the diaphragm test meter were compared to those computed from the rotameter measurements.

For each fire, the HRR was computed from the volumetric flow rate of the natural gas monitored by the diaphragm test meter and the heat of combustion and specific gravity obtained from the natural gas supplier. The combined standard uncertainty was estimated using a Type B analysis at ± 4.3 % for the heat release rate calculations. The expanded uncertainty (2σ) which represents the 95 % confidence interval, was assessed at ± 8.6 %.

The combined standard uncertainty was estimated as ± 0.12 % (gas volume percent, dry), ± 0.12 %, and ± 0.074 % in the carbon monoxide, carbon dioxide, and oxygen concentration measurements, respectively. Type A and B analyses were used to estimate uncertainties (O_2 and both CO and CO_2) associated with instrument repeatability, cold-trap dilution/mixing, analyzer zeroing, and analyzer spanning. The expanded uncertainty, ± 0.24 % (CO and CO_2) and ± 0.15 % (O_2), was obtained by multiplying the combined standard uncertainty by a coverage factor of two (2σ).

Estimating the uncertainty in the calculated water concentrations was more difficult than assessing the carbon monoxide, carbon dioxide, and oxygen concentration measurements. The largest single uncertainty in the water concentration calculations was the assumption that the water concentration was twice the carbon dioxide concentration. Toner et al.[12] and Morehart et al.[13] both reported carbon dioxide and water concentrations so the ratio of the water concentration divided by the carbon dioxide concentration was computed for each of their natural gas fueled fires. The resulting average water/carbon dioxide ratios were 2.5 ± .3 and 2.2 ± .2 for Toner et al. and Morehart et al., respectively. Considering the data of Toner et al. and Morehart et al., the systematic uncertainty in the water/carbon dioxide ratio was estimated to be ± 15 % which corresponds to about 3 % in gas volume percent concentration. This uncertainty in the water/carbon dioxide ratio was combined with the uncertainty in the carbon dioxide concentration in quadrature to yield the combined standard uncertainty of ± 3.1 % (gas volume percent) for the water concentrations. The expanded uncertainty ± 6.2 %, was obtained by multiplying the combined standard uncertainty by a coverage factor of two (2σ).

The combined standard uncertainty in the temperature measurements was estimated via Type B analysis at ± 7 %. The large number of thermocouples on the front and rear trees were replaced rather frequently and while the same technique was used to make each thermocouple junction or bead, the variation in bead size from thermocouple to thermocouple was difficult to estimate. The temperature measurements were not corrected for radiation losses because of the difficulty in estimating the surface area of each junction. The uncertainty due to the radiation losses was the largest component of uncertainty in the temperature measurements. For the temperature measurements near 1000 °C and 500 °C the combined standard uncertainty was ± 70 °C and ± 35 °C, respectively. Representing the 95 % confidence interval, the expanded uncertainty, ± 14 %, translated into reported temperatures of 1000 °C ± 140 °C or 500 °C and ± 70 °C.

For each fire, the global equivalence ratio was calculated from the flow of air into the enclosure and the composition and flow rate of the natural gas fuel. Using Type B analyses to combine the uncertainties in fuel mass flow rate (3.1 %) and the air flow rate (11 % see [36, 39]) resulted in estimates ± 7.5 % and ± 15 %, for the combined standard and expanded uncertainties, respectively. The composition of the natural gas fuel was used to calculate the ratio of air to fuel necessary for stoichiometric combustion for each fire.

The combined standard uncertainty for the local equivalence ratio as measured by the phi-meter was estimated by Babrauskas et al. [27] at ± 5.0 % to ± 1.4 % for a ϕ_ℓ range of 1.0 to 3.0, respectively. The corresponding expanded uncertainties in the ϕ_ℓ ranged from ± 10.0 % to ± 2.8 %.

The soot mass measurements were intended to produce qualitative results and made use of the soot collected on a filter upstream of the total unburned hydrocarbon analyzer as described previously (Section 3.8). Consequently the uncertainties associated with the sample flow rate and the losses in the sample extraction probe were not well characterized. The Type B analysis of the uncertainties resulted in a combined standard and expanded uncertainties of ± 77 % and ± 153 %, respectively.

4.0 Discussion

4.1 Reduced-Scale Enclosure Experiments

The reduced-scale enclosure experimental data provides insight into the conditions which exist over a wide range of HRR and ϕ_g, 7 to 650 kW and 0.2 to 4.2, respectively. These natural gas fire results show that there are significant differences in upper-layer temperatures and gas species concentrations between the front and rear of the enclosure. These differences are most evident for

fires having heat release rates sufficient to generate flashover conditions, HRR > 200 kW. The heat release rate used in this study to characterize a fire size includes combustion which occurs both inside and outside the enclosure. For fires larger than 200 kW, significant burning occurs outside the doorway. While this study refers to the two "standard" sampling locations in the upper layer as "front" or "rear", it is not clear how representative these locations are for the front and rear of the upper layer. The vertical and horizontal mapping data illustrate that gas species concentrations can vary significantly over small distances, vertical or horizontal, within the upper layer.

The geometry of the enclosure, including the door opening and the four walls, appears to impact significantly on how the fuel and air within the room mix, heat-up, and react. The walls, floor, and ceiling help to contain the energy of the fire and promote higher temperatures. During initial stages of these fires, upper- and lower-layer gas temperatures tend to increase rapidly with time. At longer times the rate of temperature increase slows and asymptotic values are approached. For underventilated burning, temperatures tend to increase during a fire and concentrations of CO and CO_2 also exhibit trends. Differences observed between the front and rear are consistent with the hypothesis that the fire plume, enclosure, and the door opening interact to generate flow patterns which inject additional air directly into the upper layer, primarily in the front of the enclosure. But, this interaction between the fire and enclosure is not well understood or characterized, so it remains a hypothesis that high levels of carbon monoxide are formed when additional air is introduced into the high-temperature, oxygen-depleted, and fuel-rich upper layer. The production of high levels of carbon monoxide appears to be a localized effect occurring only in the front portion of the upper layer.

The RSE fires differ from the earlier experiments of Beyler [9,11], Toner et al. [12], Morehart et al. [13], and Gottuk et al. [29] because the single doorway and four walls of the RSE induce specific flow patterns and reduce thermal radiation losses. These earlier experiments were

conducted under more idealized conditions where the upper layers were uniform except near the fire plume. Burning a variety of fuels, including natural gas and propane, Beyler, Toner et al., and Morehart et al., all utilized hoods to collect hot plume gases from fires burning in open laboratories. For these hood experiments, fires had access to air from all directions, i.e. the air flows to the fires were not impeded by walls or doorways. On the other hand, as occurs in many room fires, a single doorway in one of the RSE enclosure walls forced the cool fresh air to enter the RSE through the bottom of the opening while the hot combustion gases exited at the top of the doorway. Gottuk et al. burned wood, hexane, and polymethyl methacrylate (PMMA) in a four-walled enclosure designed in such a way that the inflowing air entered only along the floor and exhaust gases exited only through a window vent. While Gottuk et al.'s enclosure did include walls, the fires still had relatively unimpeded access to incoming air. While Gottuk's et al.'s apparatus did extend the hood experimental work by introducing an enclosure flow geometry, the configuration still excluded important phenomena, such as interactions between the upper layer and the incoming air flow or the fire plume and the incoming air flow.

The four walls of the RSE absorbed and reradiated thermal energy back to the upper layer and fire and this resulted in the RSE generating temperatures high enough to simulate post-flashover conditions in real room fires. Partly because the hoods lacked walls to capture the radiation, the hood experiments did not typically reach temperatures high enough to mimic post-flashover conditions. Although generating higher upper-layer temperatures than the hood experiments, the enclosure experiments of Gottuk et al. produced peak upper-layer temperatures of about 800 °C.

The RSE data provides insight into the gas species concentration and temperature non-uniformities of the upper layer, production and burnout of carbon monoxide, and validation of enclosure mixing models.

4.2 Gas Species Concentrations

Some findings of the RSE results are in good agreement with earlier research, but other aspects differ significantly. Carbon monoxide, carbon dioxide, oxygen, and water concentrations observed during natural gas fires by Toner et al. [12] and Morehart et al. [13] are plotted as a function of the upper-layer equivalence ratio in Figures 105 - 108. Although Beyler [9,11] investigated a wide range of fuels, he did not burn natural gas, but did examine propane fires for which results are included in Figures 105 - 108. The corresponding gas concentrations measured in the RSE for the front and rear sampling positions are graphed as a function of global phi, ϕ_g, in Figures 109 - 112.

The upper-layer oxygen concentrations in the front and rear of the RSE reached very low levels, 0.01 to 0.8%, at a ϕ_g of approximately 1.5 and 1.0, respectively. These concentrations are about the same as found for underventilated fires in the hood experiments of Toner et al. [12], but are lower than the oxygen levels observed in the experiments of Beyler [9,11] and Morehart et al. [13]. Although the RSE produced lower steady-state levels, the initial slope for the fall off of RSE oxygen concentration with increasing ϕ_g is consistent with those reported by Beyler, Toner et al., and Morehart et al. The steady-state oxygen concentrations observed by Beyler only drop to about 2% at a $\phi_g \approx 1.0$ and about 1% at a $\phi_g \approx 1.8$. However, Beyler studied relatively small fires (8 - 32 kW, propane) under a small and well insulated hood. Burning much larger fires (natural gas 20 - 200 kW), also under a small and well insulated hood, the oxygen concentrations of Toner et al. approached zero at an equivalence ratio of 1.0. Morehart et al.'s relatively large and uninsulated hood and medium sized fires (41 - 67 kW, natural gas) produced oxygen concentrations that only dropped to about 4% at a $\phi_g \approx 1.0$ and about 2% at a $\phi_g \approx 2.0$. Morehart et al. noted that their uninsulated-hood temperatures, ranging from about 425 to 530 K, were typically lower than the 500 to 875 K reported by Beyler and Toner et al. for rich burns. For a limited number of experiments

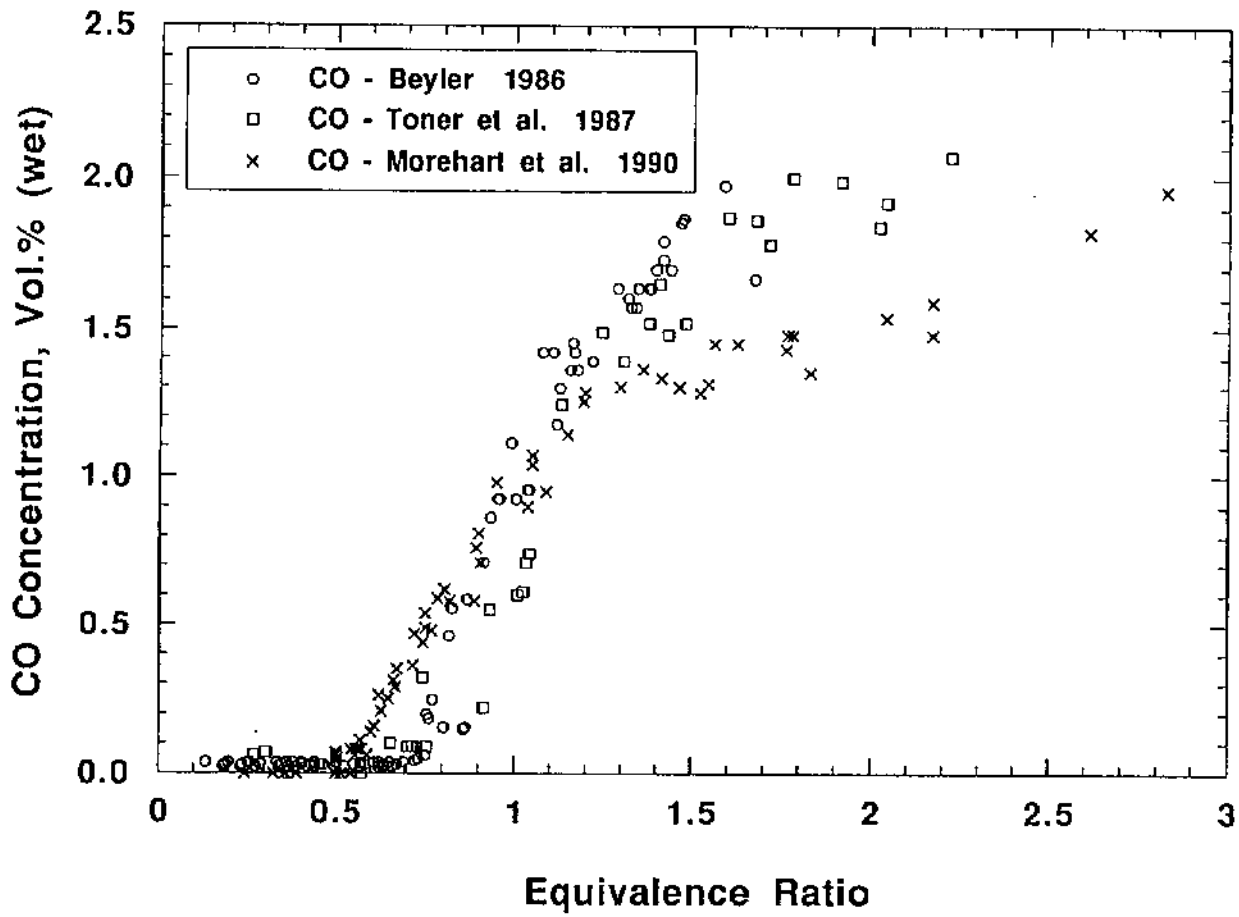

Figure 105. Carbon monoxide concentrations versus equivalence ratio from experiments by Beyler [11], Morehart et al. [13], and Toner et al. [12]. Beyler utilized propane as fuel while Morehart et al. and Toner et al. used natural gas.

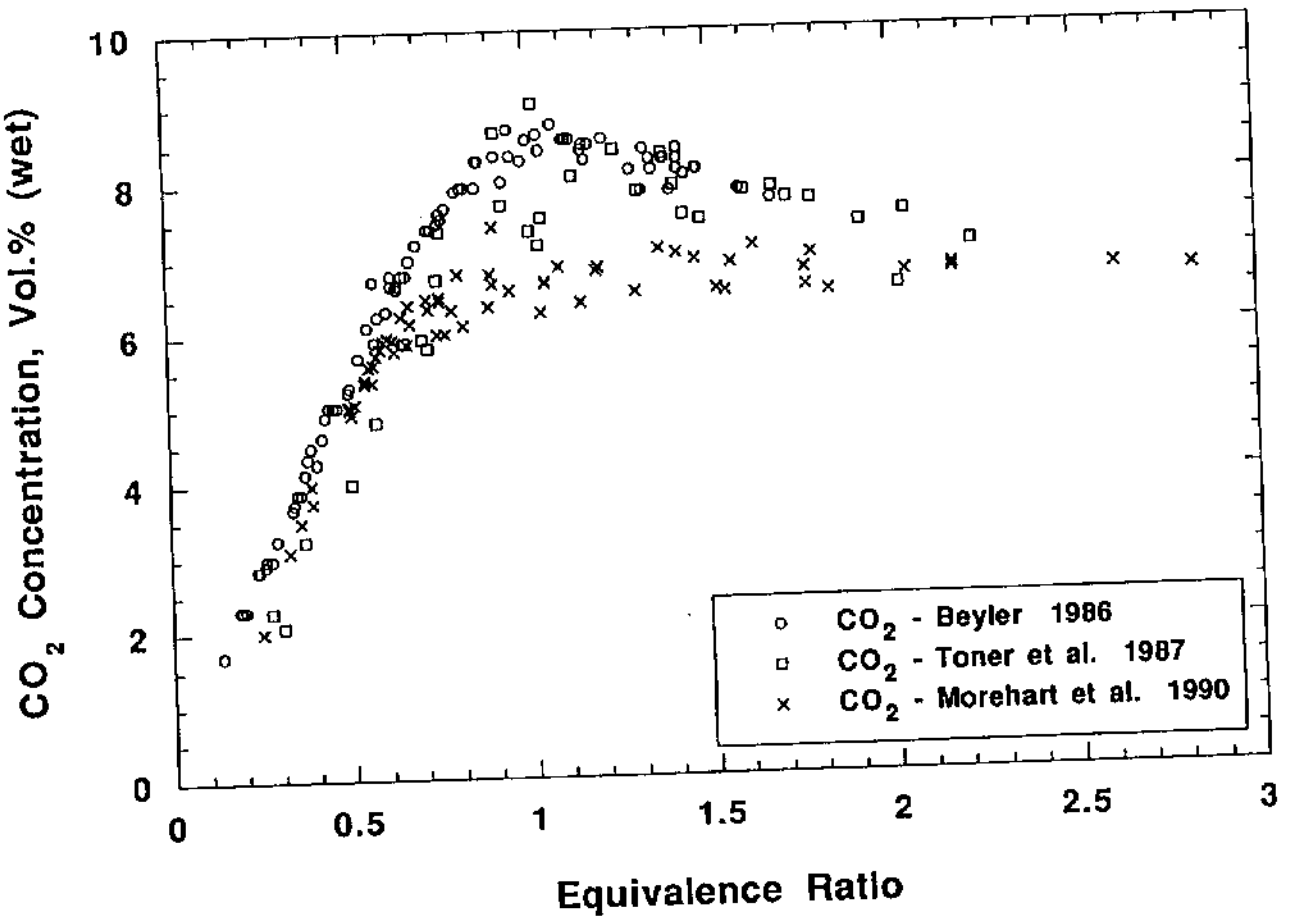

Figure 106. Carbon dioxide concentrations versus equivalence ratio from experiments by Beyler [11], Morehart et al. [13], and Toner et al. [12]. Beyler utilized propane as fuel while Morehart et al. and Toner et al. used natural gas.

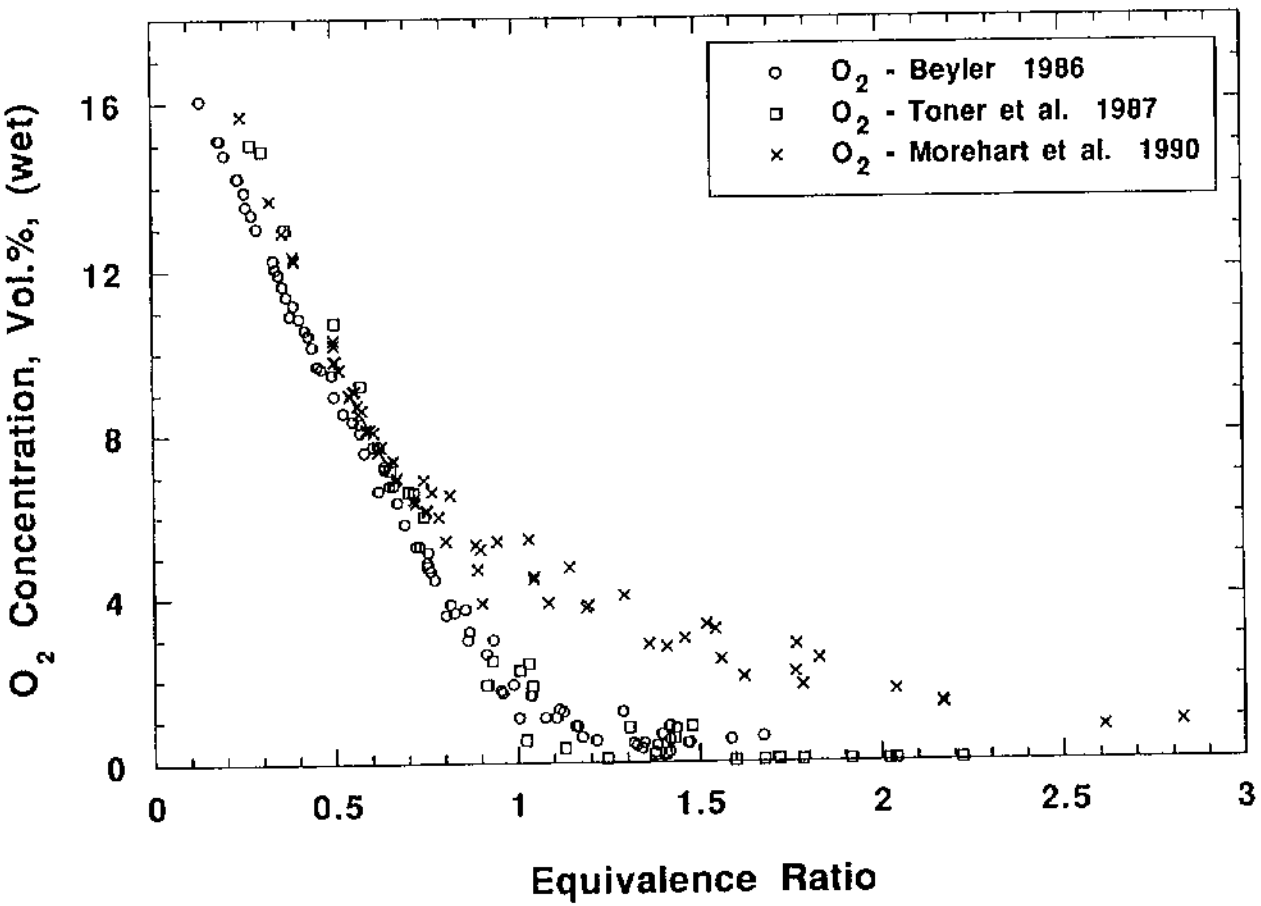

Figure 107. Oxygen concentrations versus equivalence ratio from experiments by Beyler [11], Morehart et al. [13], and Toner et al. [12]. Beyler utilized propane as fuel while Morehart et al. and Toner et al. used natural gas.

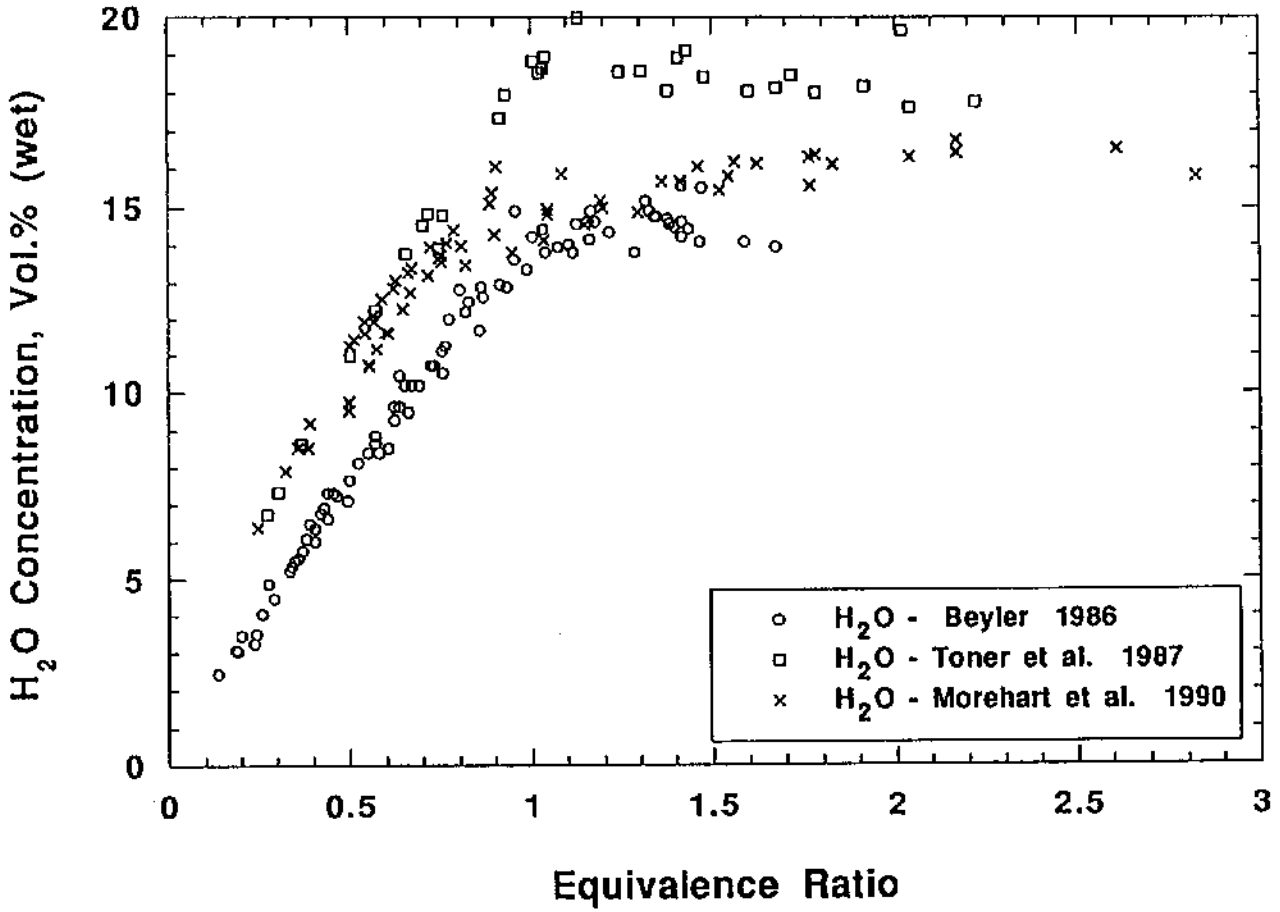

Figure 108. Water concentrations versus equivalence ratio from experiments by Beyler [11], Morehart et al. [13], and Toner et al. [12]. Beyler utilized propane as fuel while Morehart et al. and Toner et al. used natural gas.

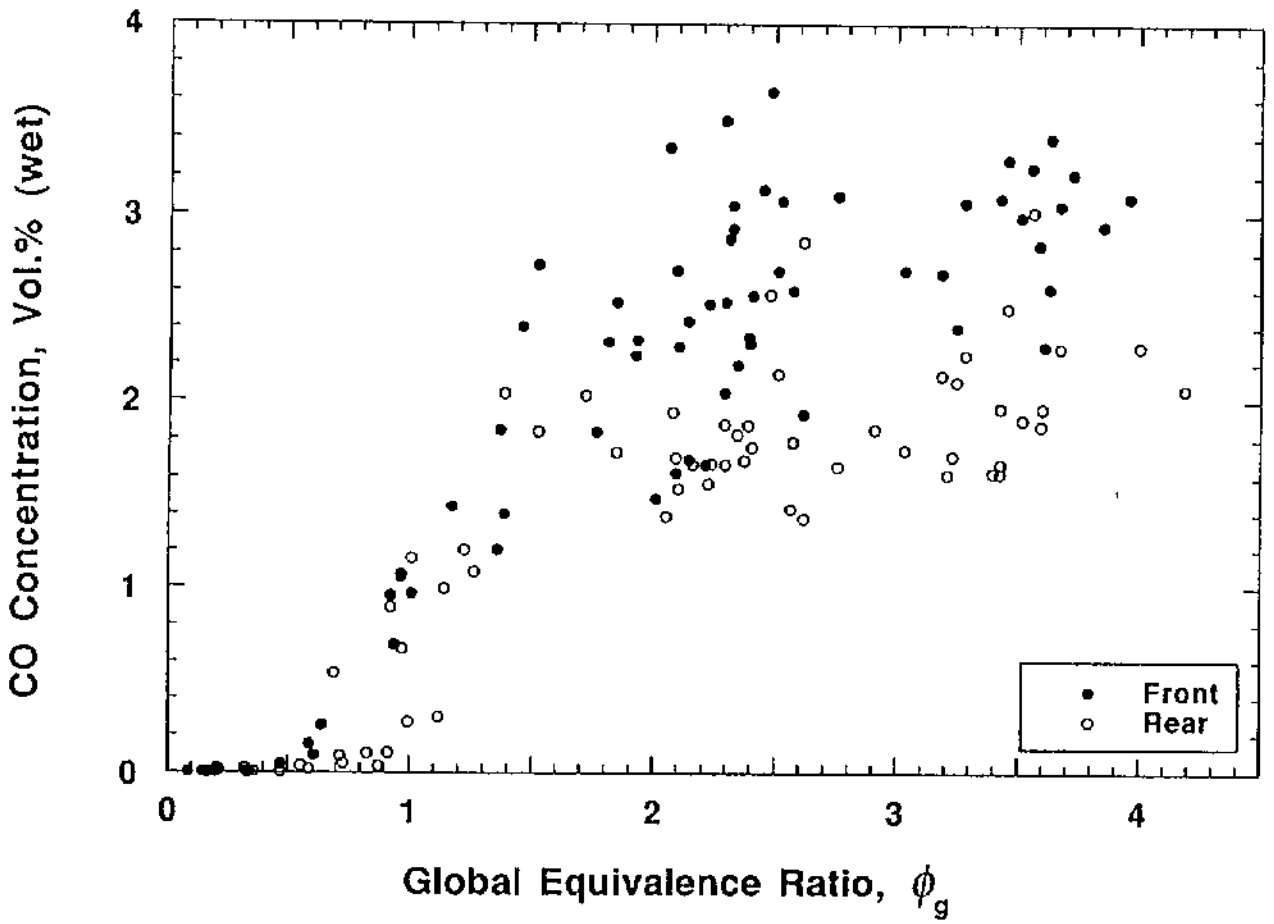

Figure 109. Front and rear CO concentrations versus global equivalence ratio observed in the reduced-scale enclosure. Each data point is the average of concentrations or equivalence ratios recorded between 300 and 900 seconds after ignition.

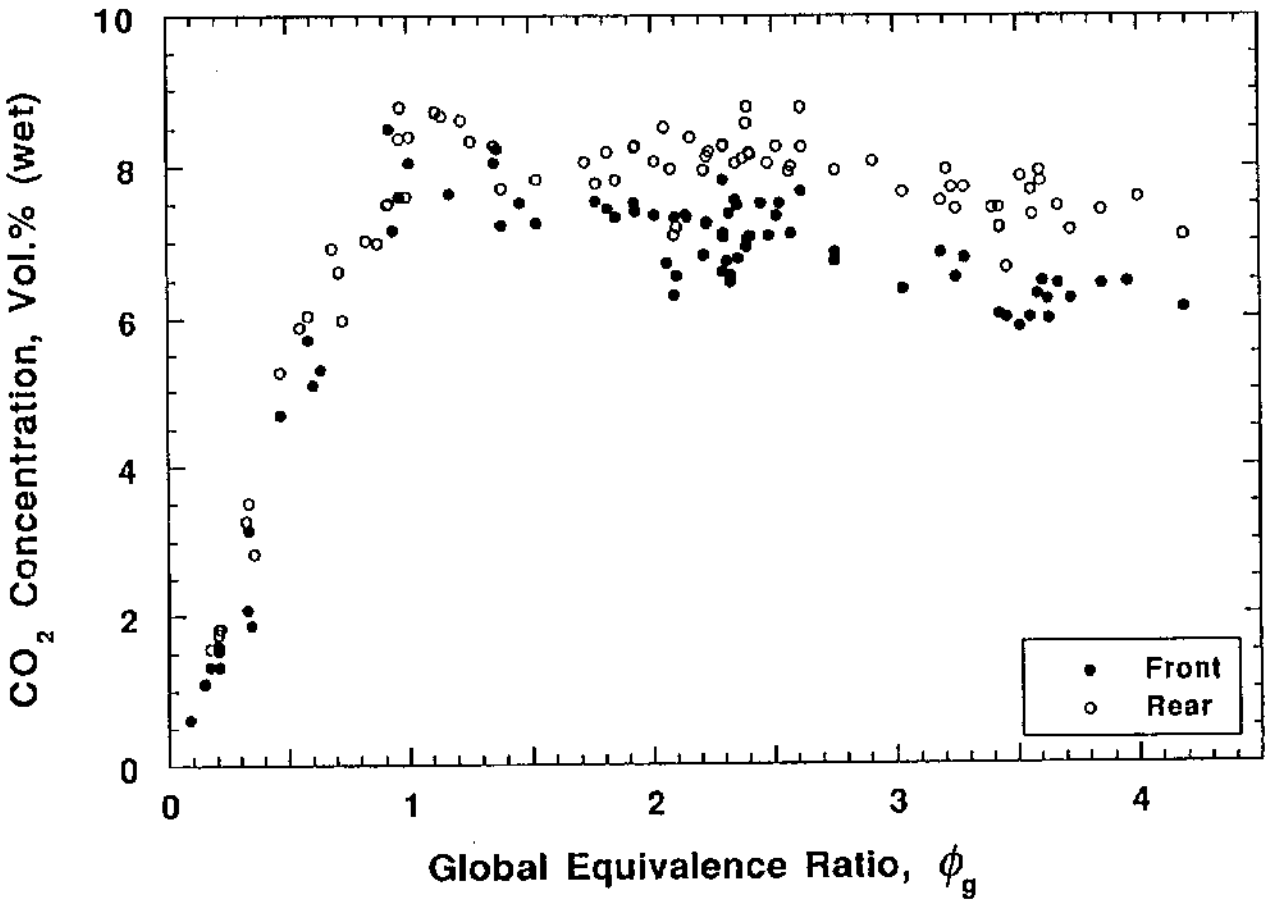

Figure 110. Front and rear CO_2 concentrations versus global equivalence ratio observed in the reduced-scale enclosure. Each data point is the average of concentrations or equivalence ratios recorded between 300 and 900 seconds after ignition.

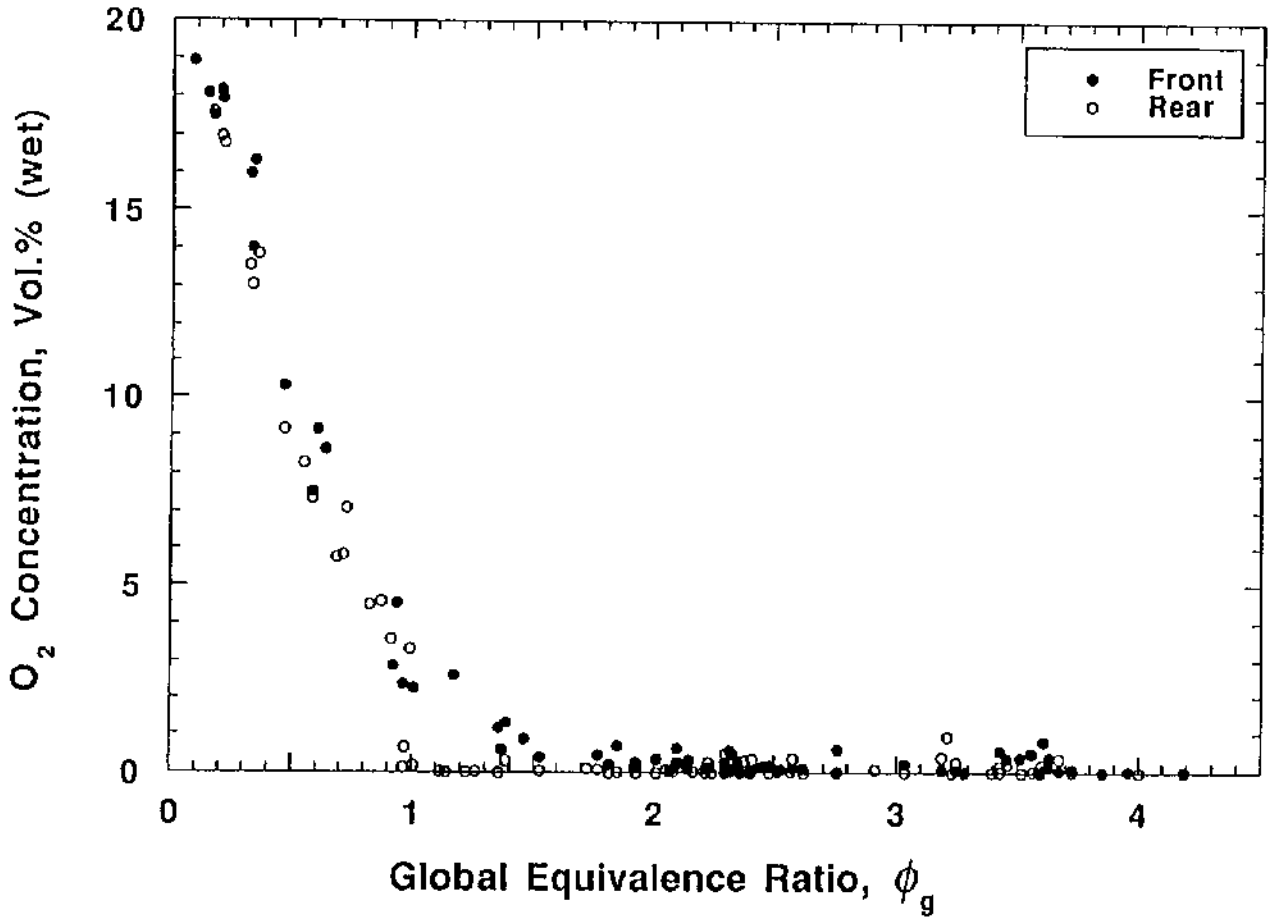

Figure 111. Front and rear O_2 concentrations versus global equivalence ratio observed in the reduced-scale enclosure. Each data point is the average of concentrations or equivalence ratios recorded between 300 to 900 seconds after ignition.

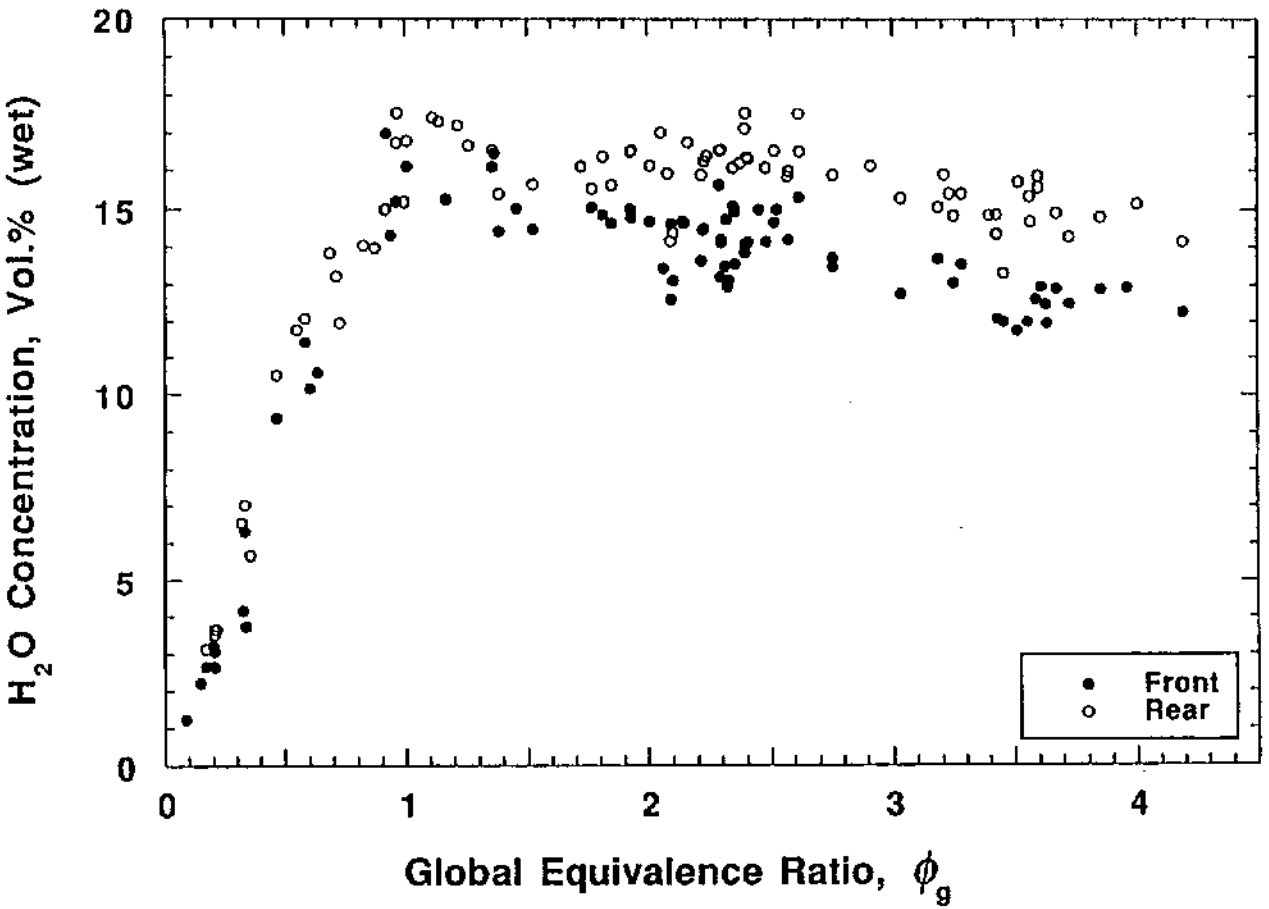

Figure 112. Front and rear water concentrations versus global equivalence ratio observed in the reduced-scale enclosure. Each data point is the average of concentrations and equivalence ratios recorded between 300 and 900 seconds after ignition.

Morehart et al. insulated the inside and outside of their hood. As the additional insulation increased the upper-layer temperature to about 675 K, the concentrations of oxygen dropped to approximately 1% for a $\phi_g \approx 1.5$. The higher temperatures and very low oxygen levels in both the RSE and Toner et al.'s experiments indicate that conditions in both experiments were similar.

Upper-layer carbon dioxide concentrations observed in the RSE are roughly the same as Toner et al., but higher than the levels reported by Morehart et al. The maximum RSE CO_2 concentration was 8.5 % which was observed in the rear of the RSE for approximately the same $\phi_g \approx 1.0$ where the O_2 concentration first approached zero. The RSE concentrations of CO_2 were significantly lower, about 0.5 % to 1 %, in the front. For fires with HRRs greater than 200 kW, average CO_2 concentrations were 6.9 % ± .6 and 7.9 % ± .5 for the front and rear, respectively. As the HRR in the RSE was increased to 650 kW or $\phi_g \approx 4.0$, the carbon dioxide levels tapered off to about 7%. The data of Toner et al. also peaked at about 8.5 % and then gradually decreased to 7% as ϕ_g was increased to 2.2. Morehart et al. observed lower values of CO_2 concentration which peaked at about 7% and decreased slightly to 6.5% as ϕ_g approached 2.8.

The upper-layer concentrations of water in the RSE enclosure were not measured directly, but were assumed to be twice the mole fraction (dry basis) of carbon dioxide (Figure 112). This assumption produces water concentrations which peak at about 20% for $\phi_g \approx 1.0$. The water level gradually tapers down from the peak to approximately 16% as ϕ_g approaches 3.0. These calculated values for the RSE are most consistent with the data of Toner et al. The water vapor concentrations of the Morehart et al. experiments are significantly lower as they begin to level off at about 14%, as ϕ_g approaches 1.0.

The asymptotic upper-layer CO concentrations (roughly 3 %) observed in the front region of the RSE are higher than the levels reported by Toner et al. and Morehart et al. The CO concentrations in the rear of the enclosure are significantly lower, 0.5% to 1 %, and are more

consistent with the concentrations of Toner et al. and Morehart et al. For fires with HRRs greater than 200 kW, average CO concentrations were 2.6 % ± .6 and 1.9 % ± .4 for the front and rear, respectively. In the RSE data, CO begins to appear for a ϕ_g of approximately 0.7. As ϕ_g was increased to 2.0, the carbon monoxide concentrations began to level off to values of roughly 2.0 % in the rear and 3.0 % in the front. Similar to the RSE data, the carbon monoxide in the studies of Toner et al. began to appear at $\phi_g \approx 0.75$. The CO reached a maximum of 2.0 % at $\phi_g \approx 2.0$ for Toner et al. The carbon monoxide observed by Morehart et al. appeared at lower ϕ_g ($\phi_g \approx 0.5$), and gradually increased to a maximum of 2.1% at a $\phi_g \approx 3.0$.

Overall it is remarkable how closely the plots of concentrations as a function of ϕ_g in the rear of the enclosure agree with those given by Toner et al. (see Figures 113 - 116). The agreement suggests that the gases in the rear of the enclosure were generated by a similar mechanism as those in the hood experiments of Toner et al.

The gas species concentrations did exhibit a distinct time dependent behavior. Typically over the course of a fire, the CO concentrations decreased in the rear and increased in the front of the upper layer. The CO trends were mirrored by increasing and decreasing trends in CO_2 in the rear and front, respectively. While the mass concentration of carbon in any form (CO, CO_2, soot) remained roughly constant, the conditions within the enclosure gradually changed during the fire causing a redistribution of the carbon between CO and CO_2.

Another time dependent behavior observed was the gradual thinning or "moving up of the layer" which was most apparent on the medium-sized fires ranging from 250 to 400 kW. In the rear of the enclosure, the interface between the upper and lower layers moved towards the ceiling during the burn effectively reducing the depth of the upper layer. The increase of O_2 (Figure 51) and decreases in CO and CO_2 (Figures 49 and 50) which are evident between the start and end of the fire at the rear sampling position are consistent with the layer becoming thinner and diluted with air

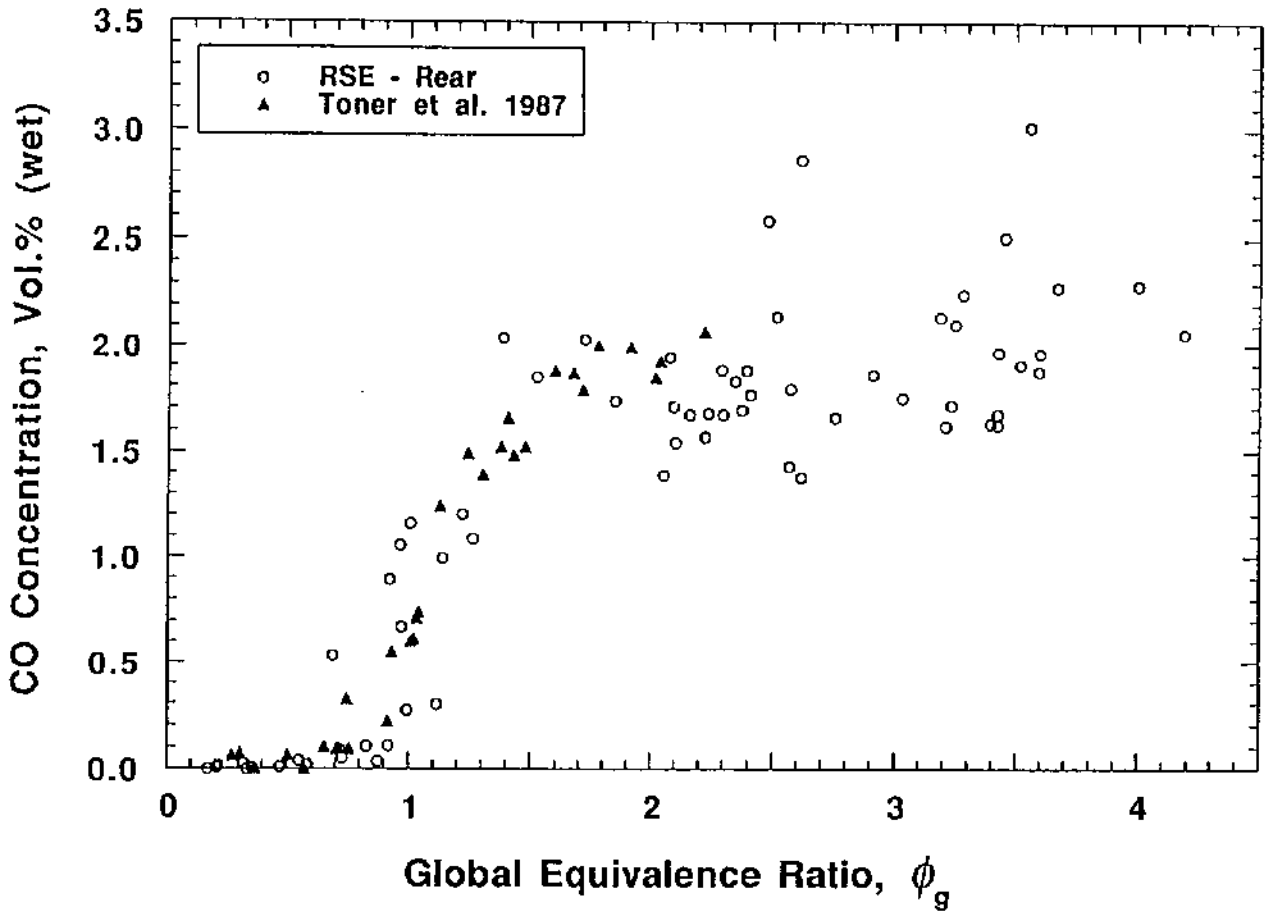

Figure 113. Carbon monoxide concentrations versus equivalence ratios for rear of enclosure and Toner et al. [12].

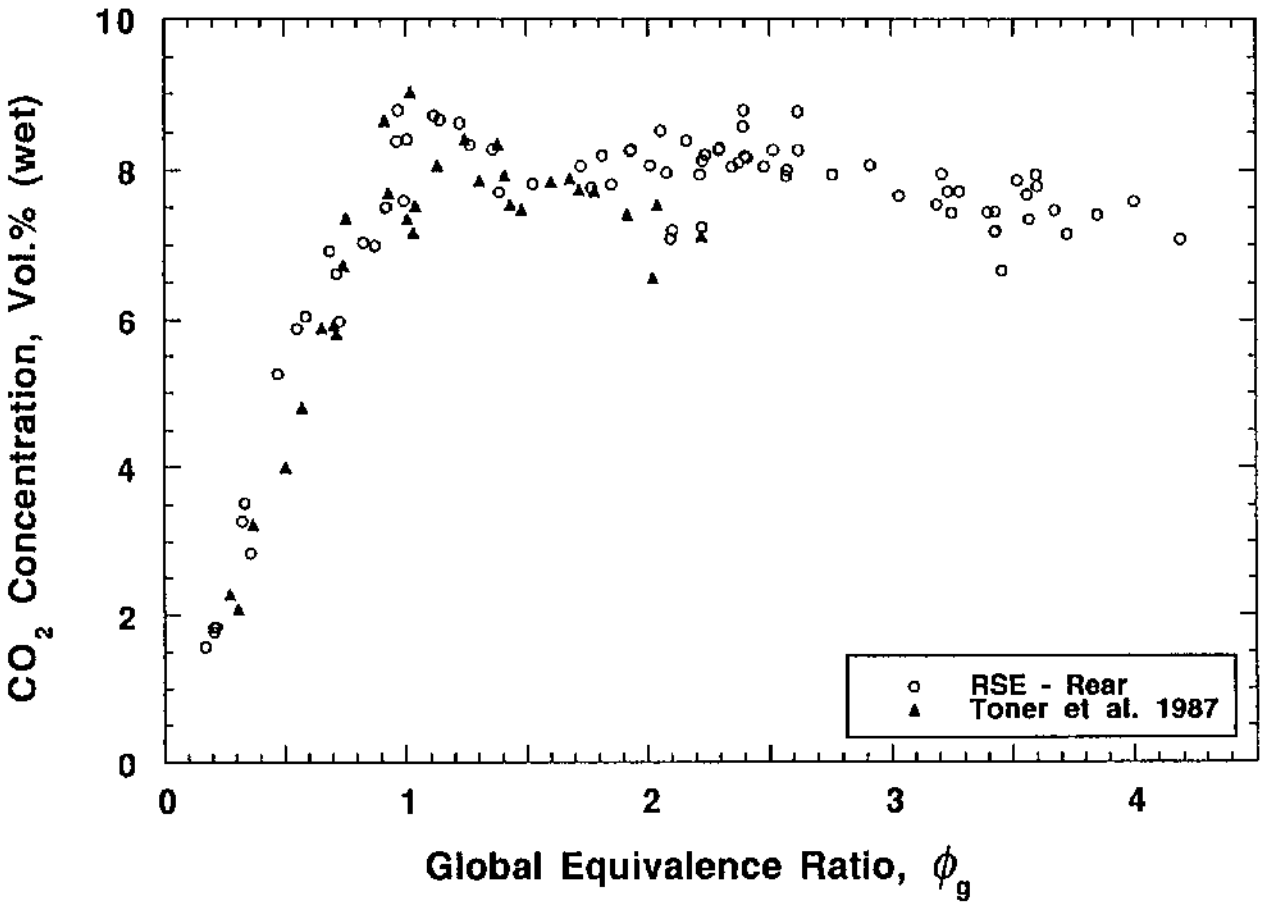

Figure 114. Carbon dioxide concentrations versus equivalence ratios for rear of enclosure and Toner et al. [12].

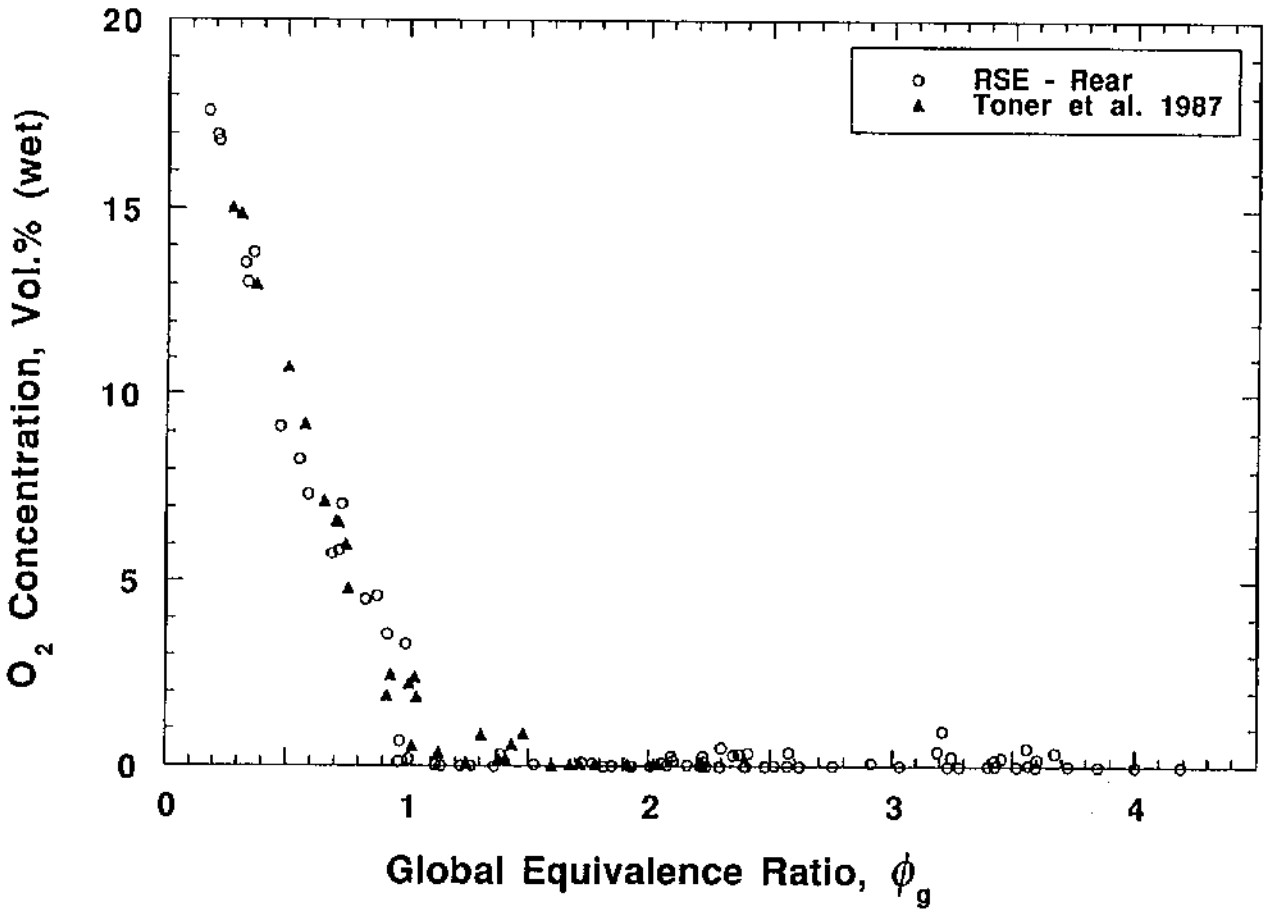

Figure 115. Oxygen concentrations versus equivalence ratios for rear of enclosure and Toner et al. [12].

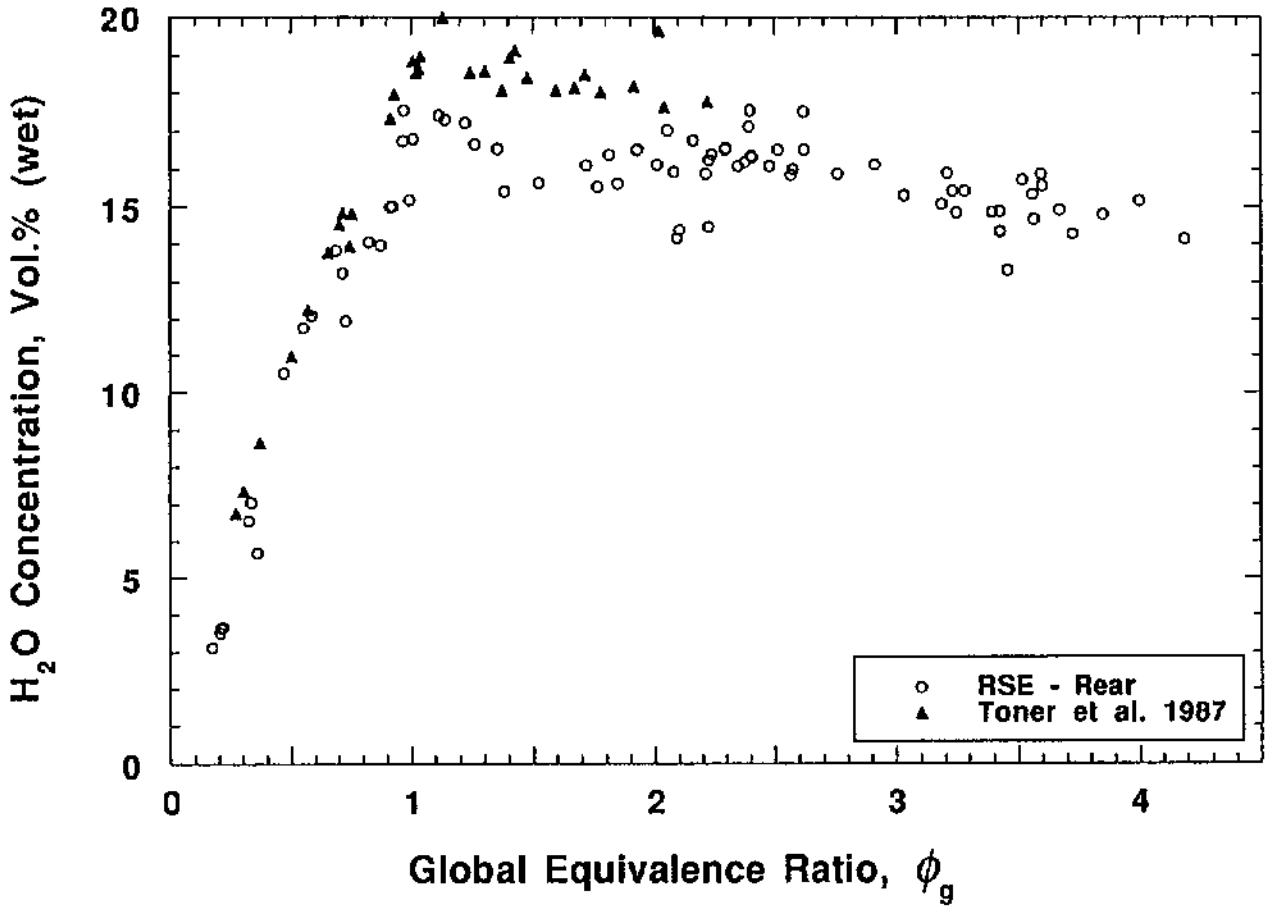

Figure 116. Calculated water concentrations versus equivalence ratios for rear of enclosure and Toner et al. [12].

from the lower layer. This intrusion of O_2 and dilution of CO and CO_2 for a 400 kW fire was only observed 30 cm from the ceiling but not at 10 cm or 20 cm below the ceiling.

While the mapping runs indicate that the upper layer tends to thin gradually during the course of some fires, they also demonstrate that a region of higher CO and lower CO_2 concentrations which occupies the front one-third of the upper layer in fires with HRRs > 300 kW. Even though CO concentrations within this region could be 50% higher than in the rear of the enclosure, the front and rear oxygen concentrations in the upper layer were both uniformly low in oxygen. The vertical mapping indicates that the upper layer just inside the door is relatively thick, approaching 30 cm for a 600 kW fire. Although there were not any vertical mapping runs conducted in the enclosure rear, the horizontal mapping runs and visual observations indicated that the layer is not as deep in the rear of the enclosure as it was approximately 15 cm thick. The vertical mapping runs demonstrated that the upper layer just inside the doorway (10 cm from front wall) was more uniform from ceiling to lower interface in the 600 kW fires than in the 250 kW fires.

The specific mechanism which allows the formation of a region of high concentration CO in the front of the RSE is not well understood. This region of high CO is a localized effect limited to the front of the upper layer. It is hypothesized that there is an interaction between the upper-layer environment, unburned fuel, and mixing caused by the fire centered within an enclosure. As the fire becomes fuel rich, additional fuel becomes available as unburned natural gas, its decomposition components and products of incomplete combustion, such as CO and H_2, reach the upper layer. Normally, this fuel would quickly react with oxygen to form carbon dioxide and water, but the oxygen concentrations are uniformly low throughout the upper layer. The high concentrations of carbon monoxide in the front of the enclosure indicate that some additional oxygen is being incorporated into the upper layer which subsequently reacts to generate primarily CO. Note that the close correspondence of combustion gas concentrations for rich burning in the rear of the enclosure and

the results of Toner et al. [12] indicates that no additional oxygen reaches the rear of the enclosure. On the other hand, additional oxygen was deliberately injected into the upper layer of some of Morehart et al.'s [13] hood experiments, but the carbon monoxide concentrations appeared essentially the same with and without the additional air being injected into the upper layer. While the region of high carbon monoxide was observed in reduced-scale enclosure fires with upper-layer temperatures that exceeded 900 °C, the hood experiments of Morehart et al. typically generated upper-layer temperatures less than 650 °C.

Pitts [40,43] used a detailed chemical kinetics model to characterize the reactor behavior of typical upper-layer combustion gases mixed with low concentrations of O_2. The model simulated various upper-layer reaction pathways over a range of temperatures and mixing scenarios which included plug-flow and perfectly stirred reactors. The results of this modeling effort included a) upper layer gases were unreactive for temperatures $\leq$ 400 °C, b) upper layer gases became reactive for temperatures $\geq$ 500 °C, c) products generated varied with temperature and for lean and rich conditions, e.g., for rich conditions the reactor generates CO in preference to CO_2. The modeling simulation demonstrates that the rich conditions and high temperatures of the upper layer for the current experiment will generate additional CO when O_2 is injected directly into the layer. The high temperatures observed in the front of the RSE relative to the rear are also consistent with the unburned fuel being partially oxidized to carbon monoxide with resulting heat release. If the oxidation of the CO releases energy to the front region of the upper layer, then temperatures should be elevated in the areas of high carbon monoxide concentration. The high-temperature region observed in the front of the enclosure is discussed in the next section.

Hydrogen concentrations of 2.9% in the front of the enclosure for rich conditions is consistent with underventilated burning. Hydrogen was also observed for underventilated conditions in the experiments of Morehart et al.[13].

4.3 Upper-Layer Temperature Nonuniformities

The upper layer is relatively uniform front to back at lower heat-release rates, but very significant differences in upper-layer temperatures are observed as the heat release rate exceeds 350 kW ($\phi \approx 2$). Temperatures in the front are 300 °C to 400 °C higher than in the rear. The rear thermocouple trees were placed at two different positions to investigate whether the temperature differences were caused by poor mixing near the walls. The temperature differences were still observed even when the thermocouple tree was repositioned 40% of the distance between the rear wall and the burner.

In the hood experiments [9 - 13], there were no walls to enclose the fires and prevent the radiative energy losses. These heat losses helped to reduce the upper-layer temperatures sufficiently to cause the upper layer gases to be significantly less reactive [40]. On the other hand, the walls, ceiling and floor of Gottuk et al.'s room [29] and the RSE trap the energy and result in higher upper-layer temperatures. The higher temperatures result in the production of additional carbon monoxide in the RSE and the enclosure of Gottuk et al. The increase in the CO level was less pronounced in the work of Gottuk et al. as compared to the front of the RSE, but was consistent with the temperature effect observed by Morehart et al. [13] after adding insulation to their hood. While re-radiation of energy from enclosure walls may help to explain some of the upper-layer temperature effects and thus the gas concentration differences in the hood and the enclosure studies, it does not account for the significant non-uniformities in temperature and gas composition in the RSE. However, as discussed earlier, if additional air was introduced only into the front region of the upper layer, the resulting oxidation of unburned fuel would release additional energy and would account for the increased upper-layer temperatures.

4.4 Enclosure Flow Patterns

The high temperatures and elevated carbon monoxide concentrations in the front region of the upper layer indicate that additional air is being introduced directly into the upper layer. The specific mechanism for injecting air into the upper layer in the RSE is not well characterized. Some insight may be obtained by qualitatively comparing the flow patterns of the RSE with the earlier hood and enclosure experiments.

It is very tempting to suggest that the asymmetrical inlet and exhaust flows of the RSE cause the flow patterns which inject or transport air directly into the front of upper layer. The flow fields induced by a fire plume entering an upper layer confined by a hood appear very different from the flow patterns generated by a fire within an enclosure. For the hood designs of Beyler, Toner et al., and Morehart et al., the air was symmetrically entrained into the fire from an open laboratory. The enclosure of Gottuk et al. introduced the air through slots in the floor in a manner similar to the hood experiments. The RSE walls and doorway forced the combustion air to enter asymmetrically from one side through the doorway. The hood experiments allowed the combustion products to exit around the perimeter of the collection hood. The enclosure of Gottuk et al. utilized a single window exhaust vent which introduced some asymmetry into the exhaust flow, but didn't seem to affect layer uniformity. The walls and doorway of the RSE would only allow the combustion products to exit through the door. The hood experiments featured symmetrical inlet and exhaust flows and the enclosure of Gottuk et al. included symmetrical inlet and asymmetric exhaust flows. Both the inlet and exhaust flows of the RSE were asymmetric.

The symmetry of the fire, entrained air, and exhaust flow in the hood experiments were very conducive to a well mixed and very uniform upper layer away from the fire plume as was experimentally found. It is interesting that Gottuk et al. specifically investigated the uniformity of the upper layer of their enclosure and reported a very uniform upper layer in terms of gas concentra-

tion and temperature. Is it coincidental that the high temperature, elevated carbon monoxide, and asymmetrical flows all occur in the front portion of the RSE? Mixing occurs along the layer interface as cool air enters the lower layer and hot combustion gas exits the RSE. However, this mixing should "burn" at the layer interface, not inject air into the layer. On the other hand, the cool air entering near the floor and hot combustion gases exiting near the ceiling may be combining with the fire plume to inject sufficient oxygen directly into the upper layer to create and maintain the high temperature region in the front one-third of the enclosure. Neither the mixing caused by the interaction between the fire plume, the cool air, and the exhaust gases or the mixing at the layer interface is present in the experiments of Gottuk et al. Further work, both experimental and modeling, will be necessary to identify the specific flow phenomena which may be transporting air directly into the front of the upper layer.

4.5 Carbon Monoxide Burnout Outside of Enclosure

The burnout of excess fuel and/or pyrolysis products as these gases exit the fire compartment is not well understood. In real fire scenarios, such as the Sharon, PA Townhouse fire [15], the unburned pyrolysis product, carbon monoxide, appeared to be the major toxicant for the victims which were remote from the room of fire origin. The conditions which are necessary for burnout of combustion products are not well characterized for real-fire or reduced-scale scenarios.

For fuel-rich cases in the RSE, the burnout of the residual fuel and products of incomplete combustion (e.g., CO and H_2) begins to occur as the hot upper-layer gases exit the enclosure. This process continues as the gases entrain air and enter the exhaust stack. By the time the upper-layer gases reach the exhaust-duct sampling instrumentation, almost all the remaining fuel has been oxidized. Therefore, the gases in the exhaust stack do not reflect the composition in the upper layer

within the enclosure. The sampling protocol must be carefully designed to insure proper representation of the fire conditions under investigation.

4.6 Narrow Door Burns

The narrow door configuration restricts the cool air flowing into the RSE and delays the formation of a stable upper layer. The depletion of oxygen and production of carbon monoxide occurs more slowly than in the open door configuration. Carbon monoxide was not detected until oxygen concentrations dropped to around 6%. For underventilated burning conditions, the CO, CO_2, and O_2 concentrations approached 2%, 8%, and 3% respectively. These levels agree quite well with the values reported by Morehart et al. They observed CO, CO_2, and O_2 levels of 2.1, 6.5 to 7.5, and 2.0 to 4.0%, respectively. This agreement indicates that the physical conditions which develop in the RSE with a narrow door are very similar to Morehart et al.'s fire plume entering their hood. The narrow door greatly reduces the vigorous mixing which normally occurs between the incoming air and the exiting hot gases. The similarity between the concentrations observed for the narrow door fires and the Morehart et al. hood experiments suggests that fires with a narrow doorway behave in manner similar to the low-temperature hood experiments, consistent with the low temperatures observed. Conversely, the difference observed between the hood experiments and the RSE study with a full doorway indicates that the fire plume entering a combustion layer contained by a hood does not adequately capture the physical mixing processes characteristic of vigorous compartment fires.

4.7 Global and Local Equivalence Ratios

Several researchers [12,13,38] have proposed correlating upper-layer gas concentrations with the global equivalence ratio, ϕ_g. The rear upper-layer gas concentrations of the enclosure were

consistent with the levels observed by Toner et al. suggesting the physical processes responsible were similar to those in the hood experiments. These similarities in gas concentrations indicate that under some conditions it may be feasible to correlate the upper-layer CO species concentrations in enclosure fires with the ϕ_g. But, the upper-layer gas concentrations observed in the front of the RSE are significantly higher than the earlier hood studies reported. These differences demonstrate that a correlation involving only ϕ_g will not allow prediction of upper-layer gas concentrations in all enclosure fire combustion environments.

As described earlier, the front temperatures in the RSE can be 300 °C to 400 °C higher than the rear temperatures. The present form of the ϕ_g correlation [38] does not account for the high temperature kinetics and/or mixing which injects air directly into the upper layer. For the lower temperatures of Beyler [9-11] and Morehart et al. [13,14], the ϕ_g may prove useful in correlating the gas species concentrations. But, as the temperatures exceed 800 °C, different chemical mechanisms and/or physical mixing phenomena appear to become increasingly important. Unless the ϕ_g concept is modified to incorporate temperature dependent kinetics and the entrainment or injection of air directly into the upper layer, it is unlikely to provide good predictions of gas species concentrations in high temperature compartment fire environments.

5.0 Conclusions

The formation of carbon monoxide during room or compartment fires has been investigated using natural gas fires burning within a reduced-scale enclosure. This series of 125 fires ranging in heat release rate and global equivalence ratio from 7 to 650 kW and 0.2 to 4.2, respectively, has demonstrated that the upper layer is non-uniform in temperature and gas species and that upper-layer

oxygen is depleted for underventilated fires with high-temperature upper layers. For fires having HRRs exceeding 400 kW ($\phi_g > 2$), carbon monoxide levels of up to 3.5 percent have been observed in the front of the upper layer near the doorway. Near-zero oxygen levels in the front and rear of the upper layer for underventilated burning indicate that oxygen entrained into the fire plume is completely reacted very quickly. Both the high temperatures and high carbon monoxide concentrations observed in the front of the upper layer as compared to the rear are consistent with additional oxygen being transported directly into the front portion of the upper layer for underventilated fires. This oxygen ultimately reacts with unburned fuel to form additional carbon monoxide instead of fully oxidized carbon dioxide consistent with the predictions of detailed chemical kinetic analyses. As the unburned fuel is oxidized, additional energy release is expected to occur consistent with the higher temperatures observed in the front of the RSE compared to the rear. The exact mechanism responsible for transporting oxygen directly into the front portion of the upper layer is not yet understood. The turbulent interaction between the cool incoming air, the exiting hot gases, and the fire plume must provide a mechanism. Additional mapping of temperature and gas species within the enclosure and flow modeling is required to provide verification of the hypothesis that oxygen is injected directly into the upper layer.

The results of these RSE fires clearly indicate that higher levels of carbon monoxide can be generated in post-flashover scenarios than suggested by hood experiments or enclosure studies designed to generate a stable two-layer structure. Current fire models, including the global equivalence concept, do not adequately simulate the temperature and gas species nonuniformities nor the high levels of carbon monoxide.

Acknowledgement

The authors would like to thank Vyto Babrauskas for designing the Reduced-Scale Enclosure, Emil Braun for the initial setup and instrumentation, and the Building 205 staff, Dick Zile, Roy McLane, Gary Roadarmel, and Lauren DeLauter, for their assistance in setting-up and performing the experiments.

6.0 References

[1] Karter Jr., Michael J. NFPA Reports on U.S. fire loss-1991. NFPA J. 86(5):32-38; 1992 September/October.

[2] Harland, W. Arthur.; and Anderson, Robert A. Causes of death in fires. Proceedings Smoke and Toxic Gases from Burning Plastics; January 6-7, 1982; London, England. 15/1-15/19.

[3] Harwood, Beatrice; and Hall, John R. What kills in fires: smoke inhalation or burns? Fire J. 83(3):29-34; 1989 May/June.

[4] Birky, M.M.; Halpin, B.M.; Caplan, Y.H.; Fisher, R.S.; McAllister, J.M.; Dixon, A.M. Fire fatality study. Fire and Materials, 3(4):211-217, 1979 December.

[5] Hill, I.R. Incapacitation and fires. American Journal of Forensic Medicine and Pathology, 10(1):49-53, 1989.

[6] Pitts, William M. Executive summary for the workshop on developing a predictive capability for CO formation in fires. Nat. Inst. Stand. and Tech. (U.S.) NISTIR 89-4093; 1989 April. 68 p.

[7] Pitts, William M. Long-range plan for a research project on carbon monoxide production and prediction. Nat. Inst. Stand. and Tech. (U.S.) NISTIR 89-4185; 1989 May; 40 p.

[8] Bukowski, R.W.; Peacock, R.D.; Jones, W.W.; Forney, C.L. HAZARD I - fire hazard assessment model. Nat. Inst. Stand. and Tech. (U.S.) Handb. 146 Vol.I and II; 1989 June. 580 p.

[9] Beyler, Craig L. Development and burning of a layer of products of incomplete combustion generated by a buoyant diffusion flame. Ph.D. Thesis. Cambridge, MA: Harvard University; 1983 September. 162 p.

[10] Beyler, Craig L. Major species production by solid fuels in a two layer compartment fire environment. Fire Safety Science--Proceedings of the First International Symposium, New York, NY: Hemisphere; 1991. 431-440.

[11] Beyler, Craig L. Major species production by diffusion flames in a two-layer compartment fire environment. Fire Safety Journal 10(1):47-56, 1986 January.

[12] Toner, S.J.; Zukoski, E.E.; Kubota, T. Entrainment, chemistry, and structure of fire plumes. Nat. Bur. Stand. (U.S.) NBS-GCR-87-528; 1987 April. 200 p.

[13] Morehart, J.H.; Zukoski, E.E.; Kubota, T. Species produced in fires burning in two-layered and homogeneous vitiated environments. Nat. Inst. Stand. and Tech. (U.S.) NIST-GCR-90-585; 1990 August. 259 p.

[14] Morehart, J.H.; Zukoski, E.E.; Kubota, T. Characteristics of large diffusion flames burning in a vitiated atmosphere. Fire Safety Science--Proceedings of the Third International Symposium. New York, NY: Hemisphere; 1993. 575-583.

[15] Levine, R.S.; Nelson, H.E. Full-scale simulation of a fatal fire and comparison of results with two multiroom models. Nat. Inst. Stand. and Tech.(U.S.) NISTIR 90-4268; 1990 August. 101 p.

[16] Fire tests - full-scale test for surface products. Draft International Standard ISO/DIS 9705. International Organization for Standardization. Geneva, Switzerland; 1991. 1-41.

[17] Proposed method for room fire test of wall and ceiling materials and assemblies. American Society for Testing and Materials. Philadelphia, PA; 1982 November. 1618-1638.

[18] Kawagoe, K. Fire behavior in rooms. Report of the Building Research Institute (Japan) BRI Report 27; 1958 September. 74 p.

[19] Gross, Daniel; Robertson, Alex F. Experimental fires in enclosures. Tenth Symposium (International) on Combustion; Pittsburgh, PA: The Combustion Institute; 1965. 931-942.

[20] Heskestad, Gunnar. Modeling of enclosure fires. Fourteenth Symposium (International) on Combustion; Pittsburgh, PA: The Combustion Institute; 1972. 1021-1030.

[21] Quintiere, James G. Scaling applications in fire research. Fire Safety Journal; 15(1):3-29; 1989.

[22] Sensenig, D.L.; Parker, W.J.; New concept for rate of heat release measurements by oxygen consumption," paper presented at the Eastern Section, The Combustion Institute, Eastern States Section Meeting, Miami Beach, FL, November 1978.

[23] Huggett, Clayton. Estimation of rate of heat release by means of oxygen consumption measurements. Fire and Materials, 4(2):61-65, 1980 June.

[24] Seery, Daniel J.; Zabielski, Martin F. Comparisons between flame species measured by probe sampling and optical spectrometry techniques. Combustion and Flame 78(1):169-177; 1989.

[25] Orloff, L.; de Ris, J.; Delichatsios, M.A. Chemical modeling of gaseous species in turbulent fires. Factory Mutual Research Corp. (U.S.) Tech. Rep. FMRC J.I.OKOJ2.BU; 1985 August. 37 p.

[26] Schoenung, S.M.; Hanson, R.K. CO and temperature measurements in a flat flame by laser absorption spectroscopy and probe techniques. Combustion Science and Technology; 24(5):227-237; 1981 January.

[27] Babrauskas, Vytenis; Parker, William J.; Mulholland, George W.; Twilley, William H. Phi-meter: a simple fuel-independent instrument for monitoring combustion equivalence ratio. Rev. Sci. Instrum. 65(7):2367-2375; 1994 July.

[28] Gottuk, Daniel T.; Roby, Richard J.; Beyler, Craig L. A study of carbon monoxide and smoke yields from compartment fires with external burning. Twenty-Fourth Symposium (International) on Combustion; Pittsburgh, PA: The Combustion Institute; 1992. 1729-1735.

[29] Gottuk, Daniel T.; Roby, Richard J.; Peatross, Michelle J.; Beyler, Craig L. Carbon monoxide production in compartment fires. Journal of Fire Protection Engineering 4(4):133-150; 1992 October.

[30] Roby, Richard J.; Beyler, Craig L. Compartment fire combustion dynamics. Nat. Inst. Stand. and Tech. (U.S.) NIST/BFRL Grant 60NANB1D1176 Quarterly Report; December 1, 1991 - March 1, 1992; 17 p.

[31] Basic rotameter principles. Fischer & Porter Company (U.S.) Variable area flowmeter handbook. Vol. 1. Catalog 10A1021; Warminster, PA; 1982. 11 p.

[32] Rotameter calculations. Fischer & Porter Company (U.S.) Variable area flowmeter handbook. Vol. 2. Catalog 10A1022; Warminster, PA; 1982. 15 p.

[33] Breese, J. Newton; Peacock, Richard D. A user's guide for RAPID, reduction algorithms for the presentation of incremental fire data. Nat. Bur. Stand. (U.S.) NBS-SP 722; 1986 August. 188 p.

[34] Peacock, Richard D.; Breese, J. Newton; Forney, Cheryl L. A users guide for RAPID, version 2.3. Nat. Inst. Stand. and Tech.(U.S.) NIST-SP 798; 1991 January. 105 p.

[35] Janssens, Marc; Tran, Hao C. Data reduction of room tests for zone model validation. Journal of Fire Sciences 10:528-555; 1992 November/December.

[36] Johnsson, Erik L.; Bryner, Nelson P.; Pitts, William M. Fire-induced mass flow into a reduced-scale enclosure. Submitted to Journal of Fire Protection Engineering for publication.

[37] Roby, Richard J.; Beyler, Craig L. Compartment fire combustion dynamics. Nat. Inst. Stand. Tech.(U.S.) NIST/BFRL Grant 60NANB1D1176 Quarterly Report; December 1, 1991 - March 1, 1992. 17 p.

[38] Cooper, Leonard Y. A model for predicting the generation rate and distribution of products of combustion in two-layer fire environments. Nat. Inst. Stand. Tech.(U.S.) NISTIR 90-4403; 1990 September. 47 p.

[39] Weast, Robert C., ed. Components of Atmospheric Air. CRC Handbook of Chemistry and Physics; Boca Raton, FL; 1979. F-211.

[40] Pitts, William M. Reactivity of product gases generated in idealized enclosure fire environments. Twenty-Fourth Symposium (International) on Combustion; Pittsburgh, PA: The Combustion Institute; 1992. 1737-1746.

[41] Sugawa, Osami; Kawagoe, Kunio; Oka, Yasushi; Ogahara, Iichi Burning behavior in a poorly ventilated compartment fire. Fire Science & Technology 9(2):5-14; 1989.

[42] Taylor, Barry N.; Kuyatt, Chris E. Guidelines for evaluating and expressing the uncertainty of NIST measurement results. Nat. Inst. Stand. Tech.(U.S.) NIST-TN 1297; 1994 September. 20 p.

[43] Pitts, William M. Application of thermodynamic and detailed chemical kinetic modelling to understanding combustion product generation in enclosure fires. To appear in Fire Safety Journal.

7.0 Appendices

Appendix A. $Ah^{1/2}$ Enclosure Ventilation Scaling Calculations

A fire in a room or compartment will usually form two layers. The hot and more buoyant combustion gases collect near the top of the enclosure and begin to exit near the top of any opening in the compartment walls. As the hot gases exit the room, the pressure within the enclosure drops slightly and cool air begins to enter at the bottom of the opening. The flow entering or exiting the room is a function of the pressure differential and the cross-sectional area of the opening. The velocity through an orifice can be described as proportional to the cross-sectional area and to the square root of the pressure difference. The theoretical air-flow rate derived by Kawagoe [18] is proportional to the $Ah^{1/2}$ ventilation parameter later utilized by Gross and Robertson [19], Heskestad [20], and Quintiere [21]. While the flow area is described by A, the cross-sectional area of the opening, the pressure difference is incorporated via h, the height of the vent.

Although there may be different methods to implement the $Ah^{1/2}$ convention into scaling the ventilation opening for an enclosure fire, Gross and Robertson normalized the ventilation parameter by the square of a geometric similarity factor, S. This study used the same normalization factor to scale the RSE door opening.

$$A_2(h_2)^{1/2} = S^2 \cdot A_1(h_1)^{1/2} \qquad \text{(A-1)}$$

where A_1 = area of vent, m^2 = (width of vent) · h_1 — Enclosure 1 (ISO/ASTM)

h_1 = height of vent, m — Enclosure 1 (ISO/ASTM)

A_2 = area of vent, m^2 = (width of vent) · h_2 — Enclosure 2 (RSE)

h_2 = height of vent, m — Enclosure 2 (RSE)

S = geometric similarity scaling factor = 0.4 for the 2/5ths scale RSE

The full-size ISO/ASTM room is 2.44 m wide by 2.44 m tall, and 3.66 m deep [16,17]. The door opening is 0.76 m wide and 2.03 m tall and is centered horizontally on one of the square walls. The ISO/ASTM enclosure width, height, and depth dimensions and only the height of the door are scaled linearly by multiplying the geometric scaling factor time the dimension. The reduced-scale dimensions are tabulated in Table 3.

The vent or door opening for the ISO/ASTM room has area, $A_1 = 1.54\ m^2$, and height, $h_1 = 2.03$ m. Inserting the values of A_1, h_1, S, and h_2 into Equation A-1 results in a RSE door width, $A_2 = 0.48$ m.

Table 3. ISO/ASTM Room and Reduced-Scale Enclosure Dimensions.

	ISO/ASTM Room		Geometric Scaling Factor, S		Reduced-Scale Enclosure
Room Width, m	2.44	x	0.4	=	0.98
Room Height, m	2.44	x	0.4	=	0.98
Room Depth, m	3.66	x	0.4	=	1.46
Vent Height, m	2.03	x	0.4	=	0.81 = h_2
Vent Area, m^2	1.54	x	0.4^2 x $2.03^{1/2}/ 0.81^{1/2}$ (from Equation A-1)		= 0.39 = A_2
Vent Width, m	0.76		0.39 / 0.81 (Vent Area/Vent Height = Vent Width)		= 0.48

Appendix B. Natural Gas Analysis

Composition of natural gas was obtained by contacting the local gas supplier. Natural gas was delivered to the experimental facility via pipeline. Sampling was completed at the nearest pumping station. The following example is from a gas analysis requested on January 22, 1992. Heat of combustion, specific gravity, and analysis of specific components are routinely provided by the supplier.

A spreadsheet software package, EXCEL, was used to process the gas analysis data and compute some useful quantities. The number of moles oxygen required is calculated assuming complete combustion with the stoichiometric amount of oxygen for each hydrocarbon. The moles of air required are computed with the assumption that air is 20.9% oxygen. The ratio of $[(\text{fuel/air})_{\text{stoichiometric}}]$ is tabulated and used later in the calculation of the equivalence ratio, ϕ.

GAS ANALYSIS 22JAN92.EXC

Retrieval Date: Jan. 22, 1992
Analysis Date: Jan. 22, 1992
Analysis Type: Average of last 24 hours ending 8 am

1. Heat of Combustion

Dry	1037.2	BTU/ft^3	38.6	MJ/m^3
Wet	1019.2	BTU/ft^3	38.0	MJ/m^3

2. Specific Gravity

relative to air 0.5892

3. Analysis

	Volume Percent	Moles O2 Required
Methane	95.25	1.9050
Ethane	2.56	0.0896
Propane	0.48	0.0240
n-Butane	0.10	0.0065
Isobutane	0.09	0.0059
Isopentane	0.04	0.0032
n-Pentane	0.03	0.0024
Hexane and above	0.08	0.0076
Carbon Dioxide	0.96	0.0
Nitrogen	0.39	0.0
Total	**99.98**	**2.0442**

Moles of Air Required - 9.7806

$(Fuel/Air)_{STOICH}$ = 0.060242

GAS ANALYSIS 22JAN92.EXC

Natural Gas Analysis

Washington Gas Light Company
Milan Skarka
703-750-4821

Natural Gas Supplier
Columbia Gas

Notes:

Natural Gas + Moles O_2 Required = CO_2 + H_2O

Calculate number of Moles O_2 Required by assuming complete combustion with stoichiometric amount of oxygen for each hydrocarbon, ie. C_2H_6 or ethane, would require 3.5 moles of O_2 for complete combustion.

Assume air is 20.9% O_2, and therefore

Moles O_2 Required / 0.209 = Moles Air Required

Density of air is 1.205 kg/m^3

Mass Basis for phi requires the ratio $(fuel/air)_{STOICH}$

and we have the molar ratio $(fuel/air)_{STOICH}$

1 mole FUEL / moles of AIR Required

but we would prefer to deal in mass units, so may convert using grams/mole of fuel and grams/mole of air, or we may recognize that the specific gravity of natural gas relative to air is the mass ratio of natural gas to air. Simply multiplying the specific gravity by the molar ratio should provide the desired mass ratio

(1 mole FUEL / moles of AIR Required) x Specific Gravity = $(Fuel/Air)_{STOICH}$

Appendix C. Rotameter Calculations

The rotameters which were used to monitor the natural gas flow rate were designed for measuring air flow rates. It was necessary to correct the air flow rate to reflect the true gas flow rate. The manufacturers of rotameters provide relationships which can be used to convert the flow rates from air to other gas [31,32]. The following equations

$$Q_{fuel} = Q_{air} \sqrt{\left(\frac{\rho_{float} - \rho_{gas}}{\rho_{float} - \rho_{air}} \frac{\rho_{air}}{\rho_{gas}} \right)} \quad (1)$$

where

Q_{fuel} = flow rate of fuel, m^3/s

ρ_{gas} = density of gas, kg/m^3

$$\rho_{gas} = SG_{gas} * \rho_{air} * \left(\frac{p + p_o}{p_o} \right) \quad (2)$$

SG_{gas} = specific gravity of natural gas (provided by gas supplier)

p = pressure of natural gas, kiloPascal

p_o = atmospheric pressure (101.325 kPa)

Q_{air} = flow rate of air m^3/s (rotameter flow rate)

ρ_{float} = density of float, kg/m^3 (stainless steel = 8027 kg/m^3)

ρ_{air} = density of air, kg/m^3 (1.205 kg/m^3 at 22 °C and 760 mm Hg).

And the volumetric flow rate was then converted to mass flow rate,

$$\dot{M}_{fuel} = Q_{fuel} * \rho_{gas} \quad (3)$$

$\dot{M}_{fuel}$ = mass flow rate of fuel, kg/s.

And the heat release rate (J/s) was calculated using the heat of combustion (J/kg),

$$Heat\ Release\ Rate = H_{comb} * \dot{M}_{fuel}, \quad Joules/s \quad (4)$$

H_{comb} = heat of combustion , J/kg.

A spreadsheet software package, EXCEL, was used to process the mass flow rate for the rotameter and the diaphragm test meter. Example, Run RSE9245, is from 200 kW natural gas burn on January 21, 1992.

RSE9245.exl

Run ID = **RSE9245**

Test Data

Data Set	Rotameter SCFH	Rotameter m3/s	Diaphragm Test Meter Time s	Volume ft3	Volume m3	Pressure psi	Pressure kPa
1	460	0.00362	54.8	5	0.142	13.5	93.1
2	470	0.00370	55.2	5	0.142	13.8	95.1
3	490	0.00385	54.2	5	0.142	14.5	100.0
4	470	0.00370	54.9	5	0.142	13.8	95.1
5	470	0.00370	54.9	5	0.142	13.8	95.1
Average	467.5	0.00368	54.8	5	0.142	13.88	95.7

Properties

Specific Gravity Natural Gas (ref Air at 22 C and 760 mm) = 0.5892

Density - Air = 1.205 kg/m^3

Density - Float = 8027.2 kg/m^3

Density of Natural Gas (corrected for flow pressure) = 1.3805 kg/m^3

Heat of Combustion (Saturated) = 1019.2 BTU/ft^3 = 38.0 MJ/m^3

Results

	Rotameter	Diaphragm Test Meter
Mass Flow Rate - kg/s	0.00340	0.00567

$$\frac{\text{(Rotameter - Diaphragm Test Meter)}}{\text{Rotameter}} \times 100 = -4.87\%$$

Heat Release Rate - kW	182	191

Appendix D. RAPID Data Analysis - .DTA File

Example is from a 200 kW natural gas burn on January 21, 1992. RAPID software retrieves raw data from a data (.DTA) file for processing. This example file has 5 zero scans, 10 span scans, and 10 data scans. The complete raw data file for this burn consisted of 142 scans collected at 10 second intervals. Each scan forms a separate record which begins with date and time. Within each scan record, each data channel is identified, C001 through C055, and the voltage signal (volts) follows each channel identifier. Each channel is separated from other channels by an "X" delimiter. An "EOR" marks the end of each scan. The specific format for data input is detailed in the RAPID User's Manuals [33,34].

RSE9245 01/21/92 EOR
TIME 21 Jan 1992 10:10:13 X Zero SCAN
C001 4.03852E-02 XC002 5.01042E+00 XC003 2.36823E-02 XC004 5.01128E+00 XC005 2.18060E-03 XC006 5.01134E+00 XC007 8.17150E-03 XC008 2.55493E-02 X
C009 9.79220E-02 XC010 1.21953E-01 XC011 9.48723E-01 XC012 -9.81000E-05 XC013 5.03000E-04 XC014 8.20000E-06 XC015 6.22600E-02 XC016 5.01043E+00 X
C017 -2.66800E-04 XC018 -3.74610E-03 XC019 -2.95100E-04 XC020 9.60000E-05 XC021 9.64000E-05 XC022 6.36200E-04 XC023 2.92400E-04 XC024 -2.10562E-02 X
C025 7.28400E-04 XC026 7.23500E-04 XC027 7.14200E-04 XC028 6.99200E-04 XC029 6.76100E-04 XC030 6.64800E-04 XC031 6.77500E-04 XC032 6.81400E-04 X
C033 6.95500E-04 XC034 7.07300E-04 XC035 7.15500E-04 XC036 7.21600E-04 XC037 7.33500E-04 XC038 7.29600E-04 XC039 7.32700E-04 XC040 7.42300E-04 X
C041 7.42900E-04 XC042 7.41800E-04 XC043 7.43400E-04 XC044 7.33500E-04 XC045 7.34200E-04 XC046 7.34000E-04 XC047 7.34400E-04 XC048 6.81300E-04 X
C049 7.00000E-04 XC050 7.14300E-04 XC051 7.43500E-04 XC052 7.48000E-04 XC053 7.63400E-04 XC054 7.36100E-04 XC055 7.41400E-04 XEOR
TIME 21 Jan 1992 10:10:33 X Zero SCAN
C001 3.77186E-02 XC002 5.01049E+00 XC003 2.47598E-02 XC004 5.01125E+00 XC005 1.94410E-03 XC006 5.01127E+00 XC007 3.79630E-03 XC008 2.00253E-02 X
C009 1.00166E-01 XC010 1.23105E-01 XC011 9.45249E-01 XC012 -1.16700E-04 XC013 -6.71000E-05 XC014 -4.50000E-06 XC015 6.15757E-02 XC016 5.01043E+00 X
C017 -2.61600E-04 XC018 -4.68530E-03 XC019 -2.88600E-04 XC020 9.62000E-05 XC021 9.70000E-05 XC022 6.41800E-04 XC023 2.91600E-04 XC024 -1.29760E-03 X
C025 7.26300E-04 XC026 7.24800E-04 XC027 7.16200E-04 XC028 6.99800E-04 XC029 6.70900E-04 XC030 6.62000E-04 XC031 6.78800E-04 XC032 6.83300E-04 X
C033 6.95400E-04 XC034 7.01800E-04 XC035 7.11100E-04 XC036 7.19400E-04 XC037 7.30900E-04 XC038 7.27100E-04 XC039 7.32100E-04 XC040 7.43200E-04 X
C041 7.45200E-04 XC042 7.41600E-04 XC043 7.43800E-04 XC044 7.33800E-04 XC045 7.35200E-04 XC046 7.35000E-04 XC047 7.35300E-04 XC048 6.81300E-04 X
C049 6.99900E-04 XC050 7.14400E-04 XC051 7.44300E-04 XC052 7.48300E-04 XC053 7.63900E-04 XC054 7.34700E-04 XC055 7.37200E-04 XEOR
TIME 21 Jan 1992 10:10:44 X Zero SCAN
C001 4.01599E-02 XC002 5.01048E+00 XC003 2.59051E-02 XC004 5.01122E+00 XC005 2.58430E-03 XC006 5.01123E+00 XC007 7.16720E-03 XC008 2.93196E-02 X
C009 1.07622E-01 XC010 1.21615E-01 XC011 9.44073E-01 XC012 -1.07700E-04 XC013 -5.22100E-04 XC014 6.00000E-06 XC015 5.86531E-02 XC016 5.01045E+00 X
C017 -4.21000E-04 XC018 -5.29710E-03 XC019 -2.98600E-04 XC020 9.44000E-05 XC021 9.32000E-05 XC022 6.39800E-04 XC023 2.90700E-04 XC024 -9.05300E-04 X
C025 7.27300E-04 XC026 7.24300E-04 XC027 7.09500E-04 XC028 6.92600E-04 XC029 6.65300E-04 XC030 6.59100E-04 XC031 6.75300E-04 XC032 6.81700E-04 X
C033 6.89900E-04 XC034 6.99200E-04 XC035 7.05900E-04 XC036 7.06900E-04 XC037 7.16300E-04 XC038 7.18800E-04 XC039 7.30100E-04 XC040 7.40400E-04 X
C041 7.43700E-04 XC042 7.40900E-04 XC043 7.43900E-04 XC044 7.33200E-04 XC045 7.34800E-04 XC046 7.34000E-04 XC047 7.33700E-04 XC048 6.82400E-04 X
C049 6.99000E-04 XC050 7.14300E-04 XC051 7.44300E-04 XC052 7.48100E-04 XC053 7.63600E-04 XC054 7.34700E-04 XC055 7.36900E-04 XEOR
TIME 21 Jan 1992 10:11:02 X Zero SCAN
C001 4.06434E-02 XC002 5.01052E+00 XC003 2.63598E-02 XC004 5.01129E+00 XC005 2.34170E-03 XC006 5.01137E+00 XC007 3.56820E-03 XC008 9.38660E-03 X
C009 9.91806E-02 XC010 1.22615E-01 XC011 9.44071E-01 XC012 -1.06900E-04 XC013 3.93500E-04 XC014 3.67000E-05 XC015 5.80851E-02 XC016 5.01050E+00 X
C017 -3.29000E-04 XC018 -5.99450E-03 XC019 -2.79800E-04 XC020 9.48000E-05 XC021 9.17000E-05 XC022 6.42100E-04 XC023 2.88400E-04 XC024 1.30800E-03 X
C025 7.26800E-04 XC026 7.23600E-04 XC027 7.10100E-04 XC028 6.90400E-04 XC029 6.64600E-04 XC030 6.59200E-04 XC031 6.75700E-04 XC032 6.82800E-04 X
C033 6.86500E-04 XC034 6.90600E-04 XC035 6.98700E-04 XC036 7.02100E-04 XC037 7.13900E-04 XC038 7.05000E-04 XC039 7.21800E-04 XC040 7.38500E-04 X
C041 7.42900E-04 XC042 7.40600E-04 XC043 7.42300E-04 XC044 7.33300E-04 XC045 7.33600E-04 XC046 7.33200E-04 XC047 7.32300E-04 XC048 6.81000E-04 X
C049 6.99900E-04 XC050 7.14600E-04 XC051 7.44700E-04 XC052 7.49100E-04 XC053 7.64000E-04 XC054 7.35300E-04 XC055 7.36700E-04 XEOR
TIME 21 Jan 1992 10:11:12 X Zero SCAN
C001 4.38823E-02 XC002 5.01043E+00 XC003 2.48578E-02 XC004 5.01129E+00 XC005 2.51300E-03 XC006 5.01127E+00 XC007 -8.14200E-04 XC008 3.14769E-02 X
C009 1.12346E-01 XC010 1.21847E-01 XC011 9.44073E-01 XC012 -8.79000E-05 XC013 1.06800E-04 XC014 1.12000E-05 XC015 5.58143E-02 XC016 5.01051E+00 X
C017 -4.01500E-04 XC018 -6.73740E-03 XC019 -2.69300E-04 XC020 9.59000E-05 XC021 9.41000E-05 XC022 6.42200E-04 XC023 2.85200E-04 XC024 1.56340E-03 X
C025 7.27000E-04 XC026 7.24100E-04 XC027 7.10700E-04 XC028 6.91900E-04 XC029 6.66300E-04 XC030 6.61100E-04 XC031 6.74800E-04 XC032 6.82800E-04 X
C033 6.88000E-04 XC034 6.93000E-04 XC035 6.98500E-04 XC036 7.01000E-04 XC037 7.18500E-04 XC038 7.16200E-04 XC039 7.25800E-04 XC040 7.39500E-04 X
C041 7.42800E-04 XC042 7.40300E-04 XC043 7.42100E-04 XC044 7.32200E-04 XC045 7.33100E-04 XC046 7.31900E-04 XC047 7.31000E-04 XC048 6.81600E-04 X
C049 7.00100E-04 XC050 7.14700E-04 XC051 7.43700E-04 XC052 7.49100E-04 XC053 7.63600E-04 XC054 7.35200E-04 XC055 7.39700E-04 XEOR
TIME 21 Jan 1992 10:17:29 X Span SCAN
C001 9.30170E+00 XC002 -1.24000E-05 XC003 1.04501E+01 XC004 8.40000E-06 XC005 9.80590E+00 XC006 1.13000E-05 XC007 5.77540E-03 XC008 7.75197E+00 X
C009 8.68581E+00 XC010 1.20841E-01 XC011 1.66327E+00 XC012 -5.75000E-05 XC013 7.87900E-04 XC014 2.77000E-05 XC015 8.69213E+00 XC016 -1.71000E-05 X
C017 2.09502E-01 XC018 2.73501E+00 XC019 3.12750E-01 XC020 7.64700E-04 XC021 7.61400E-04 XC022 6.62300E-04 XC023 7.51500E-04 XC024 -5.65900E-04 X
C025 7.10600E-04 XC026 6.97000E-04 XC027 6.80900E-04 XC028 6.76600E-04 XC029 6.65600E-04 XC030 6.58000E-04 XC031 6.67600E-04 XC032 6.67800E-04 X
C033 6.74800E-04 XC034 6.77600E-04 XC035 6.79900E-04 XC036 6.83100E-04 XC037 6.90100E-04 XC038 6.85000E-04 XC039 6.89400E-04 XC040 6.98400E-04 X
C041 7.05200E-04 XC042 7.10600E-04 XC043 7.20100E-04 XC044 7.16700E-04 XC045 7.22500E-04 XC046 7.24100E-04 XC047 7.25500E-04 XC048 6.94600E-04 X
C049 7.11000E-04 XC050 7.20900E-04 XC051 7.40400E-04 XC052 7.40600E-04 XC053 7.51600E-04 XC054 7.31500E-04 XC055 7.29800E-04 XEOR

TIME 21 Jan 1992 10:18:18 X Span SCAN
C001 9.29008E+00 XC002 -1.14000E-05 XC003 1.04475E+01 XC004 8.50000E-06 XC005 9.80522E+00 XC006 1.12000E-05 XC007 6.80670E-03 XC008 7.75843E+00 X
C009 8.69344E+00 XC010 1.20679E-01 XC011 1.67724E+00 XC012 -6.14000E-05 XC013 8.14600E-04 XC014 3.73000E-05 XC015 8.68484E+00 XC016 -1.81000E-05 X
C017 2.09570E-01 XC018 2.54704E+00 XC019 3.13267E-01 XC020 7.63600E-04 XC021 7.61300E-04 XC022 6.62600E-04 XC023 7.47800E-04 XC024 1.63131E-02 X
C025 7.07600E-04 XC026 6.92000E-04 XC027 6.77200E-04 XC028 6.69400E-04 XC029 6.60500E-04 XC030 6.53700E-04 XC031 6.59900E-04 XC032 6.63800E-04 X
C033 6.65600E-04 XC034 6.69100E-04 XC035 6.75900E-04 XC036 6.79400E-04 XC037 6.86200E-04 XC038 6.84800E-04 XC039 6.86600E-04 XC040 6.95700E-04 X
C041 7.00100E-04 XC042 7.03400E-04 XC043 7.14300E-04 XC044 7.11400E-04 XC045 7.17700E-04 XC046 7.23000E-04 XC047 7.25500E-04 XC048 6.96300E-04 X
C049 7.11100E-04 XC050 7.21500E-04 XC051 7.39400E-04 XC052 7.40400E-04 XC053 7.50400E-04 XC054 7.28400E-04 XC055 7.28600E-04 XEOR
TIME 21 Jan 1992 10:18:27 X Span SCAN
C001 9.28959E+00 XC002 -1.17000E-05 XC003 1.04569E+01 XC004 8.30000E-06 XC005 9.80594E+00 XC006 1.06000E-05 XC007 -2.21270E-03 XC008 7.74671E+00 X
C009 8.68601E+00 XC010 1.20937E-01 XC011 1.67832E+00 XC012 -7.22000E-05 XC013 8.00000E-04 XC014 2.39000E-05 XC015 8.67981E+00 XC016 -1.86000E-05 X
C017 2.09467E-01 XC018 1.58138E+00 XC019 3.13479E-01 XC020 7.64200E-04 XC021 7.60900E-04 XC022 6.61400E-04 XC023 7.48300E-04 XC024 1.22999E-02 X
C025 7.06800E-04 XC026 6.92200E-04 XC027 6.78600E-04 XC028 6.69700E-04 XC029 6.59600E-04 XC030 6.54400E-04 XC031 6.59600E-04 XC032 6.60800E-04 X
C033 6.64700E-04 XC034 6.65900E-04 XC035 6.72300E-04 XC036 6.75100E-04 XC037 6.85300E-04 XC038 6.82900E-04 XC039 6.86700E-04 XC040 6.94500E-04 X
C041 7.00000E-04 XC042 7.05000E-04 XC043 7.15900E-04 XC044 7.14000E-04 XC045 7.18600E-04 XC046 7.24000E-04 XC047 7.26100E-04 XC048 6.97200E-04 X
C049 7.11900E-04 XC050 7.21400E-04 XC051 7.38700E-04 XC052 7.39100E-04 XC053 7.50400E-04 XC054 7.28100E-04 XC055 7.29000E-04 XEOR
TIME 21 Jan 1992 10:18:36 X Span SCAN
C001 9.29264E+00 XC002 -1.26000E-05 XC003 1.04444E+01 XC004 7.80000E-06 XC005 9.80655E+00 XC006 1.10000E-05 XC007 5.11010E-03 XC008 7.73212E+00 X
C009 8.69568E+00 XC010 1.20895E-01 XC011 1.68183E+00 XC012 -5.93000E-05 XC013 8.02800E-04 XC014 6.70000E-06 XC015 8.69708E+00 XC016 -1.84000E-05 X
C017 2.09510E-01 XC018 2.42522E+00 XC019 3.13469E-01 XC020 7.64200E-04 XC021 7.61800E-04 XC022 6.59100E-04 XC023 7.49700E-04 XC024 9.63100E-03 X
C025 7.06700E-04 XC026 6.91800E-04 XC027 6.76300E-04 XC028 6.69200E-04 XC029 6.59700E-04 XC030 6.54200E-04 XC031 6.60000E-04 XC032 6.62500E-04 X
C033 6.67300E-04 XC034 6.69500E-04 XC035 6.73500E-04 XC036 6.77900E-04 XC037 6.87800E-04 XC038 6.83800E-04 XC039 6.86900E-04 XC040 6.95800E-04 X
C041 7.03400E-04 XC042 7.06700E-04 XC043 7.17000E-04 XC044 7.14800E-04 XC045 7.19500E-04 XC046 7.23300E-04 XC047 7.25700E-04 XC048 6.96200E-04 X
C049 7.10500E-04 XC050 7.21200E-04 XC051 7.38700E-04 XC052 7.38200E-04 XC053 7.49600E-04 XC054 7.27100E-04 XC055 7.28600E-04 XEOR
TIME 21 Jan 1992 10:18:45 X Span SCAN
C001 9.29452E+00 XC002 -1.26000E-05 XC003 1.04530E+01 XC004 7.00000E-06 XC005 9.80620E+00 XC006 1.05000E-05 XC007 -5.93000E-05 XC008 7.75860E+00 X
C009 8.69162E+00 XC010 1.20996E-01 XC011 1.68298E+00 XC012 -5.52000E-05 XC013 8.22800E-04 XC014 2.76000E-05 XC015 8.69475E+00 XC016 -1.98000E-05 X
C017 2.09531E-01 XC018 1.80696E+00 XC019 3.13581E-01 XC020 7.62900E-04 XC021 7.59300E-04 XC022 6.58400E-04 XC023 7.48300E-04 XC024 1.13921E-02 X
C025 7.05800E-04 XC026 6.91500E-04 XC027 6.76300E-04 XC028 6.67400E-04 XC029 6.59200E-04 XC030 6.53400E-04 XC031 6.59800E-04 XC032 6.61500E-04 X
C033 6.66400E-04 XC034 6.69400E-04 XC035 6.72700E-04 XC036 6.75500E-04 XC037 6.86700E-04 XC038 6.82500E-04 XC039 6.86000E-04 XC040 6.94800E-04 X
C041 7.02600E-04 XC042 7.05500E-04 XC043 7.15900E-04 XC044 7.13400E-04 XC045 7.18700E-04 XC046 7.22600E-04 XC047 7.25700E-04 XC048 6.96300E-04 X
C049 7.10900E-04 XC050 7.21300E-04 XC051 7.38900E-04 XC052 7.38500E-04 XC053 7.49700E-04 XC054 7.27200E-04 XC055 7.28200E-04 XEOR
TIME 21 Jan 1992 10:30:22 X Span SCAN
C001 3.39737E-02 XC002 5.01037E+00 XC003 2.94705E-02 XC004 5.01111E+00 XC005 1.10769E-01 XC006 5.01118E+00 XC007 2.06472E-01 XC008 1.25628E-02 X
C009 2.76701E-01 XC010 1.22801E-01 XC011 4.13681E+00 XC012 -1.68600E-04 XC013 2.11009E-01 XC014 1.94000E-05 XC015 2.23908E-01 XC016 5.01045E+00 X
C017 6.63907E-01 XC018 2.52144E+00 XC019 -3.86000E-05 XC020 7.50200E-04 XC021 7.49800E-04 XC022 6.19800E-04 XC023 7.31200E-04 XC024 -6.97790E-03 X
C025 6.92800E-04 XC026 6.75300E-04 XC027 6.56700E-04 XC028 6.58700E-04 XC029 6.37100E-04 XC030 6.30800E-04 XC031 6.39800E-04 XC032 6.50800E-04 X
C033 6.58300E-04 XC034 6.58400E-04 XC035 6.60500E-04 XC036 6.61900E-04 XC037 6.69600E-04 XC038 6.68300E-04 XC039 6.74900E-04 XC040 6.88900E-04 X
C041 6.95200E-04 XC042 7.01200E-04 XC043 7.09000E-04 XC044 7.08500E-04 XC045 7.12500E-04 XC046 7.17500E-04 XC047 7.20900E-04 XC048 6.23600E-04 X
C049 6.27400E-04 XC050 6.56300E-04 XC051 6.74700E-04 XC052 6.84000E-04 XC053 7.26500E-04 XC054 6.90700E-04 XC055 7.03600E-04 XEOR
TIME 21 Jan 1992 10:30:30 X Span SCAN
C001 3.29181E-02 XC002 5.01040E+00 XC003 2.97377E-02 XC004 5.01124E+00 XC005 1.10516E-01 XC006 5.01127E+00 XC007 2.17562E-01 XC008 3.09615E-02 X
C009 2.82304E-01 XC010 1.22809E-01 XC011 4.13681E+00 XC012 -1.41600E-04 XC013 2.11431E-01 XC014 -1.43000E-05 XC015 2.26269E-01 XC016 5.01041E+00 X
C017 6.63879E-01 XC018 2.99966E+00 XC019 -1.15000E-05 XC020 7.48600E-04 XC021 7.46600E-04 XC022 6.19000E-04 XC023 7.29000E-04 XC024 -1.01000E-05 X
C025 6.91800E-04 XC026 6.74000E-04 XC027 6.55500E-04 XC028 6.55900E-04 XC029 6.35300E-04 XC030 6.26000E-04 XC031 6.42100E-04 XC032 6.53800E-04 X
C033 6.60600E-04 XC034 6.61100E-04 XC035 6.63600E-04 XC036 6.63900E-04 XC037 6.70100E-04 XC038 6.66700E-04 XC039 6.73200E-04 XC040 6.84900E-04 X
C041 6.89800E-04 XC042 6.93800E-04 XC043 7.01200E-04 XC044 7.01000E-04 XC045 7.08500E-04 XC046 7.15600E-04 XC047 7.19500E-04 XC048 6.31600E-04 X
C049 6.40400E-04 XC050 6.56700E-04 XC051 6.74800E-04 XC052 6.79300E-04 XC053 7.24000E-04 XC054 7.01300E-04 XC055 6.98800E-04 XEOR
TIME 21 Jan 1992 10:30:38 X Span SCAN
C001 3.07668E-02 XC002 5.01033E+00 XC003 2.72669E-02 XC004 5.01119E+00 XC005 1.07754E-01 XC006 5.01123E+00 XC007 2.00748E-01 XC008 2.53704E-02 X
C009 2.79964E-01 XC010 1.22531E-01 XC011 4.13680E+00 XC012 -1.29300E-04 XC013 2.08101E-01 XC014 -4.11000E-05 XC015 2.26656E-01 XC016 5.01041E+00 X
C017 6.64045E-01 XC018 3.22059E+00 XC019 -2.25000E-05 XC020 7.50900E-04 XC021 7.49600E-04 XC022 6.20500E-04 XC023 7.29900E-04 XC024 4.31800E-03 X

C025 6.94300E-04 XC026 6.80700E-04 XC027 6.61300E-04 XC028 6.56900E-04 XC029 6.36400E-04 XC030 6.29300E-04 XC031 6.43200E-04 XC032 6.54700E-04 X
C033 6.59300E-04 XC034 6.60700E-04 XC035 6.62000E-04 XC036 6.60600E-04 XC037 6.67200E-04 XC038 6.63100E-04 XC039 6.70000E-04 XC040 6.80800E-04 X
C041 6.85500E-04 XC042 6.90000E-04 XC043 6.97700E-04 XC044 6.94600E-04 XC045 7.02700E-04 XC046 7.12000E-04 XC047 7.19700E-04 XC048 6.30200E-04 X
C049 6.31000E-04 XC050 6.53000E-04 XC051 6.75800E-04 XC052 6.75800E-04 XC053 7.24800E-04 XC054 7.03500E-04 XC055 6.90100E-04 XEOR
TIME 21 Jan 1992 10:30:47 X Span SCAN
C001 3.02767E-02 XC002 5.01033E+00 XC003 2.47251E-02 XC004 5.01126E+00 XC005 1.07943E-01 XC006 5.01124E+00 XC007 2.01512E-01 XC008 2.49758E-02 X
C009 2.68962E-01 XC010 1.22761E-01 XC011 4.13681E+00 XC012 -1.49700E-04 XC013 2.07669E-01 XC014 -8.41000E-05 XC015 2.25291E-01 XC016 5.01039E+00 X
C017 6.64097E-01 XC018 2.29922E+00 XC019 -2.07000E-05 XC020 7.52900E-04 XC021 7.50400E-04 XC022 6.20800E-04 XC023 7.33200E-04 XC024 6.01600E-04 X
C025 6.95800E-04 XC026 6.82700E-04 XC027 6.64800E-04 XC028 6.57500E-04 XC029 6.39300E-04 XC030 6.32300E-04 XC031 6.40000E-04 XC032 6.52800E-04 X
C033 6.56700E-04 XC034 6.58000E-04 XC035 6.59900E-04 XC036 6.59400E-04 XC037 6.67600E-04 XC038 6.65200E-04 XC039 6.70100E-04 XC040 6.80600E-04 X
C041 6.85600E-04 XC042 6.91800E-04 XC043 7.01000E-04 XC044 6.97000E-04 XC045 7.03900E-04 XC046 7.13400E-04 XC047 7.20700E-04 XC048 6.37100E-04 X
C049 6.27200E-04 XC050 6.45200E-04 XC051 6.69300E-04 XC052 6.69600E-04 XC053 7.24400E-04 XC054 6.92500E-04 XC055 6.94700E-04 XEOR
TIME 21 Jan 1992 10:30:55 X Span SCAN
C001 2.98267E-02 XC002 5.01030E+00 XC003 2.86449E-02 XC004 5.01109E+00 XC005 1.08750E-01 XC006 5.01114E+00 XC007 2.01549E-01 XC008 3.45143E-02 X
C009 2.70407E-01 XC010 1.22818E-01 XC011 4.13681E+00 XC012 -1.79000E-04 XC013 2.07964E-01 XC014 -9.22000E-05 XC015 2.21852E-01 XC016 5.01030E+00 X
C017 6.64236E-01 XC018 2.68831E+00 XC019 -3.99000E-05 XC020 7.54900E-04 XC021 7.52200E-04 XC022 6.18200E-04 XC023 7.34900E-04 XC024 5.28130E-03 X
C025 6.96300E-04 XC026 6.81500E-04 XC027 6.65800E-04 XC028 6.59100E-04 XC029 6.40200E-04 XC030 6.34100E-04 XC031 6.42400E-04 XC032 6.52300E-04 X
C033 6.58600E-04 XC034 6.60300E-04 XC035 6.62500E-04 XC036 6.60800E-04 XC037 6.68600E-04 XC038 6.62500E-04 XC039 6.71800E-04 XC040 6.86300E-04 X
C041 6.92500E-04 XC042 6.95100E-04 XC043 7.03800E-04 XC044 7.01100E-04 XC045 7.06300E-04 XC046 7.13100E-04 XC047 7.17600E-04 XC048 6.41300E-04 X
C049 6.34000E-04 XC050 6.50500E-04 XC051 6.76300E-04 XC052 6.75200E-04 XC053 7.22800E-04 XC054 6.90000E-04 XC055 7.13300E-04 XEOR
TIME 21 Jan 1992 10:31:31 X Data SCAN
C001 3.28929E-02 XC002 5.01023E+00 XC003 2.34487E-02 XC004 5.01127E+00 XC005 1.08550E-01 XC006 5.01118E+00 XC007 2.00856E-01 XC008 1.72226E-02 X
C009 2.69311E-01 XC010 1.23062E-01 XC011 4.13680E+00 XC012 -2.03400E-04 XC013 2.10637E-01 XC014 -1.11500E-04 XC015 2.21188E-01 XC016 5.01022E+00 X
C017 6.64523E-01 XC018 1.82226E+00 XC019 -1.47000E-05 XC020 7.45600E-04 XC021 7.47400E-04 XC022 6.22300E-04 XC023 7.32900E-04 XC024 -5.61910E-03 X
C025 6.96700E-04 XC026 6.82600E-04 XC027 6.65200E-04 XC028 6.60200E-04 XC029 6.46000E-04 XC030 6.39500E-04 XC031 6.50800E-04 XC032 6.56000E-04 X
C033 6.58200E-04 XC034 6.59400E-04 XC035 6.61700E-04 XC036 6.61100E-04 XC037 6.67900E-04 XC038 6.66300E-04 XC039 6.72800E-04 XC040 6.83300E-04 X
C041 6.89700E-04 XC042 6.95300E-04 XC043 7.05200E-04 XC044 7.03000E-04 XC045 7.06300E-04 XC046 7.14900E-04 XC047 7.20200E-04 XC048 6.44000E-04 X
C049 6.33400E-04 XC050 6.47800E-04 XC051 6.65900E-04 XC052 6.68100E-04 XC053 7.23700E-04 XC054 7.01600E-04 XC055 7.11300E-04 XEOR
TIME 21 Jan 1992 10:31:38 X Data SCAN
C001 3.20178E-02 XC002 5.01032E+00 XC003 2.24080E-02 XC004 5.01123E+00 XC005 1.07702E-01 XC006 5.01120E+00 XC007 2.06938E-01 XC008 3.23502E-02 X
C009 2.79130E-01 XC010 1.23040E-01 XC011 4.13681E+00 XC012 -1.66400E-04 XC013 2.10561E-01 XC014 -9.39000E-05 XC015 2.21033E-01 XC016 5.01037E+00 X
C017 6.64892E-01 XC018 1.69826E+00 XC019 -3.11000E-05 XC020 7.51200E-04 XC021 7.48900E-04 XC022 6.26100E-04 XC023 7.32300E-04 XC024 4.77590E-03 X
C025 6.96500E-04 XC026 6.83600E-04 XC027 6.66800E-04 XC028 6.62000E-04 XC029 6.47600E-04 XC030 6.42800E-04 XC031 6.51800E-04 XC032 6.56100E-04 X
C033 6.61200E-04 XC034 6.62700E-04 XC035 6.64700E-04 XC036 6.64300E-04 XC037 6.68500E-04 XC038 6.65800E-04 XC039 6.69700E-04 XC040 6.81600E-04 X
C041 6.90000E-04 XC042 6.95800E-04 XC043 7.03700E-04 XC044 7.02900E-04 XC045 7.06400E-04 XC046 7.13300E-04 XC047 7.20200E-04 XC048 6.47500E-04 X
C049 6.36600E-04 XC050 6.46800E-04 XC051 6.71000E-04 XC052 6.61000E-04 XC053 7.23700E-04 XC054 7.02800E-04 XC055 7.10800E-04 XEOR
TIME 21 Jan 1992 10:31:48 X Data SCAN
C001 3.24925E-02 XC002 5.01025E+00 XC003 3.04957E-02 XC004 5.01121E+00 XC005 1.07590E-01 XC006 5.01116E+00 XC007 2.17760E-01 XC008 2.83652E-02 X
C009 2.80856E-01 XC010 1.22657E-01 XC011 4.13681E+00 XC012 -1.77200E-04 XC013 2.10609E-01 XC014 -8.08000E-05 XC015 2.21214E-01 XC016 5.01026E+00 X
C017 6.65453E-01 XC018 2.18737E+00 XC019 -3.20000E-05 XC020 7.50200E-04 XC021 7.50000E-04 XC022 6.26200E-04 XC023 7.33500E-04 XC024 -3.85760E-03 X
C025 6.96200E-04 XC026 6.81000E-04 XC027 6.64700E-04 XC028 6.62300E-04 XC029 6.49300E-04 XC030 6.43900E-04 XC031 6.54800E-04 XC032 6.55800E-04 X
C033 6.60500E-04 XC034 6.64100E-04 XC035 6.66000E-04 XC036 6.66100E-04 XC037 6.71100E-04 XC038 6.68000E-04 XC039 6.72500E-04 XC040 6.83100E-04 X
C041 6.92400E-04 XC042 6.96400E-04 XC043 7.06100E-04 XC044 7.05000E-04 XC045 7.08600E-04 XC046 7.15800E-04 XC047 7.20600E-04 XC048 6.43300E-04 X
C049 6.46700E-04 XC050 6.53200E-04 XC051 6.73900E-04 XC052 6.75300E-04 XC053 7.23200E-04 XC054 7.04000E-04 XC055 7.06100E-04 XEOR
TIME 21 Jan 1992 10:31:58 X Data SCAN
C001 3.39124E-02 XC002 5.01029E+00 XC003 2.56873E-02 XC004 5.01134E+00 XC005 1.08162E-01 XC006 5.01127E+00 XC007 2.03594E-01 XC008 2.52915E-02 X
C009 2.78247E-01 XC010 1.23039E-01 XC011 4.13681E+00 XC012 -1.40200E-04 XC013 2.11053E-01 XC014 -3.51000E-05 XC015 2.26454E-01 XC016 5.01019E+00 X
C017 6.65865E-01 XC018 2.41436E+00 XC019 -2.64000E-05 XC020 7.53800E-04 XC021 7.51900E-04 XC022 6.23800E-04 XC023 7.36300E-04 XC024 4.75550E-03 X
C025 6.95700E-04 XC026 6.81800E-04 XC027 6.65200E-04 XC028 6.61500E-04 XC029 6.51100E-04 XC030 6.44300E-04 XC031 6.51500E-04 XC032 6.54700E-04 X
C033 6.58900E-04 XC034 6.61400E-04 XC035 6.62900E-04 XC036 6.65000E-04 XC037 6.73100E-04 XC038 6.69300E-04 XC039 6.74600E-04 XC040 6.85700E-04 X
C041 6.91600E-04 XC042 6.97000E-04 XC043 7.06200E-04 XC044 7.05900E-04 XC045 7.11900E-04 XC046 7.16800E-04 XC047 7.18100E-04 XC048 6.48900E-04 X
C049 6.46900E-04 XC050 6.50900E-04 XC051 6.69800E-04 XC052 6.68900E-04 XC053 7.22600E-04 XC054 7.06100E-04 XC055 7.07300E-04 XEOR

TIME 21 Jan 1992 10:32:08 X - Data SCAN
C001 3.08204E-02 XC002 5.01029E+00 XC003 2.74176E-02 XC004 5.01120E+00 XC005 1.06586E-01 XC006 5.01111E+00 XC007 2.15726E-01 XC008 2.48870E-02 X
C009 2.77316E-01 XC010 1.22567E-01 XC011 4.13681E+00 XC012 -1.75700E-04 XC013 2.08135E-01 XC014 -3.65000E-05 XC015 2.30220E-01 XC016 5.01022E+00 X
C017 6.65987E-01 XC018 2.28713E+00 XC019 -3.39000E-05 XC020 7.51500E-04 XC021 7.51200E-04 XC022 6.25600E-04 XC023 7.36600E-04 XC024 -6.69270E-03 X
C025 6.99000E-04 XC026 6.82600E-04 XC027 6.66200E-04 XC028 6.62800E-04 XC029 6.52200E-04 XC030 6.47100E-04 XC031 6.53800E-04 XC032 6.57800E-04 X
C033 6.58400E-04 XC034 6.58400E-04 XC035 6.59400E-04 XC036 6.57300E-04 XC037 6.63300E-04 XC038 6.62100E-04 XC039 6.67200E-04 XC040 6.74700E-04 X
C041 6.85200E-04 XC042 6.91300E-04 XC043 7.02600E-04 XC044 7.03100E-04 XC045 7.09800E-04 XC046 7.16500E-04 XC047 7.21300E-04 XC048 6.42200E-04 X
C049 6.45500E-04 XC050 6.50100E-04 XC051 6.67700E-04 XC052 6.63300E-04 XC053 7.23200E-04 XC054 7.03500E-04 XC055 7.14300E-04 XEOR
TIME 21 Jan 1992 10:32:18 X - Data SCAN
C001 2.89924E-02 XC002 5.01021E+00 XC003 2.69236E-02 XC004 5.01129E+00 XC005 1.07697E-01 XC006 5.01126E+00 XC007 2.15406E-01 XC008 1.56362E-02 X
C009 2.83761E-01 XC010 1.23537E-01 XC011 4.13681E+00 XC012 -1.88100E-04 XC013 2.08003E-01 XC014 -3.56000E-05 XC015 2.31111E-01 XC016 5.01026E+00 X
C017 6.66469E-01 XC018 1.96815E+00 XC019 -1.72000E-05 XC020 7.58300E-04 XC021 7.57200E-04 XC022 6.27600E-04 XC023 7.42800E-04 XC024 1.25680E-03 X
C025 7.01800E-04 XC026 6.82800E-04 XC027 6.66900E-04 XC028 6.63500E-04 XC029 6.53500E-04 XC030 6.48400E-04 XC031 6.53400E-04 XC032 6.57100E-04 X
C033 6.56800E-04 XC034 6.57800E-04 XC035 6.59800E-04 XC036 6.59600E-04 XC037 6.66700E-04 XC038 6.64100E-04 XC039 6.68200E-04 XC040 6.76800E-04 X
C041 6.86800E-04 XC042 6.91700E-04 XC043 7.03700E-04 XC044 7.05300E-04 XC045 7.11500E-04 XC046 7.17500E-04 XC047 7.20800E-04 XC048 6.46500E-04 X
C049 6.44200E-04 XC050 6.54100E-04 XC051 6.67000E-04 XC052 6.68200E-04 XC053 7.22700E-04 XC054 7.01300E-04 XC055 7.16100E-04 XEOR
TIME 21 Jan 1992 10:32:28 X - Data SCAN
C001 3.42527E-02 XC002 5.01030E+00 XC003 2.02950E-02 XC004 5.01112E+00 XC005 1.09826E-01 XC006 5.01115E+00 XC007 2.05764E-01 XC008 2.83398E-02 X
C009 2.88701E-01 XC010 1.22824E-01 XC011 4.13681E+00 XC012 -1.62900E-04 XC013 2.08068E-01 XC014 -3.27000E-05 XC015 2.37432E-01 XC016 5.01027E+00 X
C017 6.66413E-01 XC018 2.36759E+00 XC019 -1.88000E-05 XC020 7.48900E-04 XC021 7.49800E-04 XC022 6.29500E-04 XC023 7.37400E-04 XC024 9.08400E-04 X
C025 7.00500E-04 XC026 6.83200E-04 XC027 6.67500E-04 XC028 6.64100E-04 XC029 6.54300E-04 XC030 6.50200E-04 XC031 6.55100E-04 XC032 6.60300E-04 X
C033 6.61300E-04 XC034 6.62800E-04 XC035 6.65900E-04 XC036 6.64400E-04 XC037 6.72800E-04 XC038 6.75600E-04 XC039 6.81200E-04 XC040 6.91600E-04 X
C041 7.08700E-04 XC042 7.06500E-04 XC043 7.29600E-04 XC044 7.26000E-04 XC045 7.24900E-04 XC046 7.26900E-04 XC047 7.28600E-04 XC048 6.49800E-04 X
C049 6.46300E-04 XC050 6.57900E-04 XC051 6.80700E-04 XC052 6.90300E-04 XC053 7.23300E-04 XC054 7.18600E-04 XC055 7.49100E-04 XEOR
TIME 21 Jan 1992 10:32:38 X - Data SCAN
C001 3.30090E-02 XC002 5.01033E+00 XC003 2.95100E-02 XC004 5.01121E+00 XC005 1.13917E-01 XC006 5.01120E+00 XC007 2.03186E-01 XC008 2.48083E-02 X
C009 2.95029E-01 XC010 1.23001E-01 XC011 4.13681E+00 XC012 -1.85500E-04 XC013 2.11607E-01 XC014 -3.07000E-05 XC015 2.43123E-01 XC016 5.01023E+00 X
C017 6.66204E-01 XC018 3.71142E+00 XC019 6.93000E-05 XC020 7.49200E-04 XC021 7.50100E-04 XC022 6.25500E-04 XC023 7.37200E-04 XC024 1.52850E-03 X
C025 7.15500E-04 XC026 6.98400E-04 XC027 6.74900E-04 XC028 6.65600E-04 XC029 6.55000E-04 XC030 6.50800E-04 XC031 6.56100E-04 XC032 6.61000E-04 X
C033 6.62700E-04 XC034 6.64000E-04 XC035 6.67800E-04 XC036 6.67000E-04 XC037 6.78600E-04 XC038 6.80600E-04 XC039 6.87700E-04 XC040 7.01400E-04 X
C041 7.12700E-04 XC042 7.15900E-04 XC043 7.31300E-04 XC044 7.31200E-04 XC045 7.34700E-04 XC046 7.40400E-04 XC047 7.39400E-04 XC048 6.50700E-04 X
C049 6.49800E-04 XC050 6.57900E-04 XC051 6.73700E-04 XC052 6.78700E-04 XC053 7.22300E-04 XC054 7.62000E-04 XC055 7.59300E-04 XEOR
TIME 21 Jan 1992 10:32:48 X - Data SCAN
C001 3.33917E-02 XC002 5.01035E+00 XC003 2.64368E-02 XC004 5.01126E+00 XC005 1.12514E-01 XC006 5.01126E+00 XC007 2.01649E-01 XC008 2.28836E-02 X
C009 3.23350E-01 XC010 1.22621E-01 XC011 4.13681E+00 XC012 -1.74300E-04 XC013 2.08891E-01 XC014 8.30000E-06 XC015 2.60477E-01 XC016 5.01034E+00 X
C017 6.66451E-01 XC018 2.32499E+00 XC019 5.81000E-05 XC020 7.51600E-04 XC021 7.49100E-04 XC022 6.24800E-04 XC023 7.36100E-04 XC024 -1.37440E-03 X
C025 7.28400E-04 XC026 7.04700E-04 XC027 6.75900E-04 XC028 6.69000E-04 XC029 6.56900E-04 XC030 6.50900E-04 XC031 6.59200E-04 XC032 6.63400E-04 X
C033 6.64600E-04 XC034 6.66100E-04 XC035 6.69600E-04 XC036 6.70500E-04 XC037 6.77800E-04 XC038 6.80100E-04 XC039 6.86700E-04 XC040 6.97700E-04 X
C041 7.25200E-04 XC042 7.39200E-04 XC043 7.52000E-04 XC044 7.54100E-04 XC045 7.55600E-04 XC046 7.64100E-04 XC047 7.67900E-04 XC048 6.51600E-04 X
C049 6.49100E-04 XC050 6.57200E-04 XC051 6.73100E-04 XC052 6.88000E-04 XC053 7.24300E-04 XC054 7.72700E-04 XC055 7.85000E-04 XEOR
TIME 21 Jan 1992 10:32:58 X - Data SCAN
C001 3.36657E-02 XC002 5.01027E+00 XC003 2.68823E-02 XC004 5.01110E+00 XC005 1.10069E-01 XC006 5.01116E+00 XC007 2.08221E-01 XC008 3.11383E-02 X
C009 3.37745E-01 XC010 1.21739E-01 XC011 4.13680E+00 XC012 -1.93700E-04 XC013 2.07978E-01 XC014 -4.70000E-06 XC015 2.83985E-01 XC016 5.01032E+00 X
C017 6.66236E-01 XC018 2.36205E+00 XC019 1.20000E-05 XC020 7.54400E-04 XC021 7.51900E-04 XC022 6.24200E-04 XC023 7.36900E-04 XC024 7.26030E-03 X
C025 7.45700E-04 XC026 7.09800E-04 XC027 6.76400E-04 XC028 6.70300E-04 XC029 6.58400E-04 XC030 6.52200E-04 XC031 6.59300E-04 XC032 6.62800E-04 X
C033 6.64300E-04 XC034 6.66900E-04 XC035 6.69300E-04 XC036 6.67700E-04 XC037 6.74500E-04 XC038 6.74000E-04 XC039 6.84100E-04 XC040 7.02900E-04 X
C041 7.38500E-04 XC042 7.56000E-04 XC043 7.71500E-04 XC044 7.76400E-04 XC045 7.72100E-04 XC046 7.88000E-04 XC047 7.87900E-04 XC048 6.38900E-04 X
C049 6.40400E-04 XC050 6.47700E-04 XC051 6.71900E-04 XC052 6.93100E-04 XC053 7.23800E-04 XC054 8.11000E-04 XC055 8.11400E-04 XEOR

Appendix E. Instrumentation Hook-Up Sheet

An instrumentation hook-up sheet was prepared each time an instrument, thermocouple, or span gas was changed. This sheet was then incorporated into the control file, .CTL, to reduce the data. The example Hook-Up Sheet is from Run 9265 which was conducted on February 4, 1992.

Hook-Up Sheet

Date 4FEB92

Run ID RSE9265

Channel Number		Analyzer Description	Sampling Range(s)
1.	CO	Defor	2/10 %
2.	Ch.1	Range Marker	5/0 volts
3.	CO	Defor	2/10 %
4.	Ch.8	Range Marker	5/0 volts
5.	CO2	Defor	1/5 %
6.	Ch.9	Range Marker	5/0 volts
7.	O2	Taylor	0.836 V = 20.9%
8.	CO	Defor	3/12 %
9.	CO2	Defor	4/20 %
10.	Pressure, MKS		1 V = 13.32 pa
11.	O2	Servomex	0-21 %
12.	CO2	LIRA #34678	0-10 %
13.	O2	Taylor	0.836 V = 20.9%
14.	CO	LIRA #34753	0-5 %
15.	CO2	Defor	4/20 %
16.	Ch.15	Range Marker	5/0 volts
17.	O2	Taylor	0.209 V = 20.9%
18.	Velocity Probe		2" H2O = 10 V
19.	TUH	Rosemount	311 mv = 3.11 %
20.	T/C		
21.	T/C		
22.	T/C, ambient Temp		
23.	T/C, QR, GWM		
24.	T/C		
25.	T/C		
26.	T/C		
27.	T/C		
28.	T/C		
29.	T/C		
30.	T/C		
31.	T/C		
32.	T/C		
33.	T/C		
34.	T/C		
35.	T/C		
36.	T/C		
37.	T/C		
38.	T/C		
39.	T/C		
40.	T/C		
41.	T/C		
42.	T/C		
43.	T/C		
44.	T/C		
45.	T/C		
46.	T/C		
47.	T/C		
48.	T/C,	Aspirated	
49.	T/C,	"	
50.	T/C,	"	
51.	T/C,	"	
52.	T/C,	"	
53.	T/C,	"	Door Lintel
54.	T/C		
55.	T/C		

Location	Span	Span Gas	Span Reading
RSE Probe #2	1	9.32	93.2
Exh Stk		1.77	17.7
Exh Stk		4.53	45.3
RSE Probe #1			
RSE Probe #1	1	9.32	93.2
RSE Probe #1	1	17.4	17.4
RSE Front Right			
Exh Stk			
Phimeter			
RSE Probe #2			
Phimeter			
RSE Probe #2	1	17.4	17.4
Phimeter			
Exh Stk			
RSE Probe #1			
Bottom Exh Stk			
Top Exh Stk			
Back of Data Acq Box			
Mezzanine Exh Stk			
Rear Corner 8 cm from floor			
" 24 cm "			
" 44 cm "			
" 56 cm "			
" 68 cm "			
" 80 cm "			
" 96.5 cm "			
Front Corner 8 cm from floor			
" 24 cm "			
" 40 cm "			
" 44 cm "			
" 48 cm "			
" 52 cm "			
" 56 cm "			
" 60 cm "			
" 64 cm "			
" 68 cm "			
" 72 cm "			
" 76 cm "			
" 80 cm "			
" 84 cm "			
" 88 cm "			
" 92 cm "			
" 96.5 cm "			
Doorway 3" / 7.62 cm from floor			
" 9" / 22.86 cm "			
" 15" / 38.1 cm "			
" 21" / 53.34 cm "			
" 27" / 68.58 cm "			
" 31" / 78.74 cm "			
RSE Sample Probe #2			
RSE Sample Probe #1			

Appendix F. RAPID Data Analysis - .CTL File

Example is from a 200 kW natural gas burn on January 21, 1992. The RAPID software utilizes a control (.CTL) file to identify each channel, specify how each data channel will be processed, and rename the data for output. In this example, 55 channels were scanned every 10 seconds (Appendix D). The .CTL is developed for each burn from the hook-up sheet (Appendix E). The specific format of each statement or command is detailed in the RAPID User's Manuals [33,34].

```
  5   0   0   0  20   1   0   0
  4   1   1   1   0   5
FC RSE Burn Series 21JAN92 RSE9245 Nat Gas 200kW Probe #1 4"-S wall,11"-W wall
and 4" from ceiling
  00 1Time  Elapsed time                                        (s)
  01 2CO-4  Room      CO   Defor   Probe #2 Upper Layer      (Vol %)
    0     Linear calibration, Span 1
  02 2CO-4R Marker Channel          Hi Range 0-10% Low 0-2%
  03 2CO-1  Exh Stack  CO   Defor                             (Vol %)
    0     Linear calibration, Span 1
  04 2CO-6R Marker Channel          Hi Range 0-12% Low 0-3%
  05 2CO2-1 Exh Stack  CO2  Defor                             (Vol %)
    0     Linear calibration, Span 1
  06 2CO2-6RMarker Channel          Hi Range 0-20%  Low 0-4%
  07 2O2-6  Room      O2   Taylor  Probe #1 Upper Layer      (Vol %)
    0     0.836V = 20.9%
  08 2CO-6  Room      CO   Defor   Probe #1 Upper Layer      (Vol %)
    0     Linear calibration, Span 1
  09 2CO2-6 Room      CO2  Defor   Probe #1 Upper Layer      (Vol %)
    0     Linear calibration, Span 1
  10 2DPres Differential Pressure Across Compartment Opening      (Pa)
    0     1 torr = 10 volts or 13.332 pascals/volt
  11 2O2-1  Exh Stack  O2   Servomex, Span 2                  (Vol %)
  12 2CO2-5 Phimeter   CO2  Lira    Probe #1 Upper Layer      (Vol %)
  13 2O2-4  Room      O2   Taylor  Probe #2 Upper Layer      (Vol %)
    0     0.836V = 20.9%
  14 2CO-5  Phimeter   CO   Lira    Probe #1 Upper Layer      (Vol %)
  15 2CO2-4 Room      CO2  Defor   Probe #2 Upper Layer      (Vol %)
    0     Linear Calibration, Span 1
  16 2CO2-4RMarker Channel          Hi Range 0-20% Low 0-4%
  17 2O2-5  Phimeter   O2   Taylor  Probe #1 Upper Layer      (Vol %)
    0     0.2095V = 20.95%
  18 2GASVELBi-directional velocity probe  2 inches = 10 V      (m/s)
  19 2TUH-5 Total Unburned Hydrocarbon Probe #1 Upper Layer     (Vol %)
    0     Linear Calibration, Span 1
  20 2TCBOT Temperature at bottom of stack                    (Deg C)
  21 2TCTOP Temperature at top of stack                       (Deg C)
  22 2RMTEMPAmbient temperature at back of box                (Deg C)
  23 2TCMEZ Temperature 8 feet into stack mezzanine T/C       (Deg C)
  24 2TC965RRear  Thermocouple Tree, 96.5 cm from floor       (Deg C)
  25 2TC800RRear  Thermocouple Tree, 80   cm from floor       (Deg C)
  26 2TC680RRear  Thermocouple Tree, 68   cm from floor       (Deg C)
  27 2TC560RRear  Thermocouple Tree, 56   cm from floor       (Deg C)
  28 2TC440RRear  Thermocouple Tree, 44   cm from floor       (Deg C)
  29 2TC240RRear  Thermocouple Tree, 24   cm from floor       (Deg C)
  30 2TC080RRear  Thermocouple Tree,  8   cm from floor       (Deg C)
  31 2TC080FFront Thermocouple Tree,  8   cm from floor       (Deg C)
  32 2TC240FFront Thermocouple Tree, 24   cm from floor       (Deg C)
  33 2TC400FFront Thermocouple Tree, 40   cm from floor       (Deg C)
  34 2TC440FFront Thermocouple Tree, 44   cm from floor       (Deg C)
  35 2TC480FFront Thermocouple Tree, 48   cm from floor       (Deg C)
  36 2TC520FFront Thermocouple Tree, 52   cm from floor       (Deg C)
  37 2TC560FFront Thermocouple Tree, 56   cm from floor       (Deg C)
  38 2TC600FFront Thermocouple Tree, 60   cm from floor       (Deg C)
  39 2TC640FFront Thermocouple Tree, 64   cm from floor       (Deg C)
  40 2TC680FFront Thermocouple Tree, 68   cm from floor       (Deg C)
  41 2TC720FFront Thermocouple Tree, 72   cm from floor       (Deg C)
  42 2TC760FFront Thermocouple Tree, 76   cm from floor       (Deg C)
  43 2TC800FFront Thermocouple Tree, 80   cm from floor       (Deg C)
  44 2TC840FFront Thermocouple Tree, 84   cm from floor       (Deg C)
  45 2TC880FFront Thermocouple Tree, 88   cm from floor       (Deg C)
  46 2TC920FFront Thermocouple Tree, 92   cm from floor       (Deg C)
  47 2TC965FFront Thermocouple Tree, 96.5 cm from floor       (Deg C)
  48 2TC076DDoor Vertical Center Line,  7.62 cm from floor    (Deg C)
  49 2TC229DDoor Vertical Center Line, 22.86 cm from floor    (Deg C)
  50 2TC381DDoor Vertical Center Line, 38.1  cm from floor    (Deg C)
  51 2TC533DDoor Vertical Center Line, 53.34 cm from floor    (Deg C)
  52 2TC686DDoor Vertical Center Line, 68.58 cm from floor    (Deg C)
  53 2TC787DDoor Vertical Center Line, 78.74 cm from floor    (Deg C)
  54 2TCPR1 Thermocouple in Gas probe #2 for upper layer      (Deg C)
  55 2TCPR2 Thermocouple in Gas probe #1 for upper layer      (Deg C)
                                                             999
```

```
   1.0
   1.0
                                                    999
SKIP=(S1Z5R5S5)16
GAS%        Convert gas analyzers from voltage to volume percent
11
1  3    Z  R       9.32   X  Defor     CO   Room Upper Layer P#2
3  3    Z  10.     10.0   X  Defor     CO   Exhaust Stack
5  3    Z  R       4.89   X  Defor     CO2  Exhaust Stack
7  3    Z          20.95  X  Taylor    O2   Room Upper Layer P#1
8  3    Z  R       9.32   X  Defor     CO   Room Upper Layer P#1
9  3    Z  R       17.4   X  Defor     CO2  Room Upper Layer P#1
11 3    Z          20.95  X  Servomex  O2   Exhaust Stack
13 3    Z          20.95  X  Taylor    O2   Room Upper Layer P#2
15 3    Z  R       17.4   X  Defor     CO2  Room Upper Layer P#2
17 3    Z  .20952  20.95  X  Taylor(Phi)O2  Room Upper Layer P#1
19 3    Z  R       3.11   X  Rosemount TUH  Room Upper Layer P#1
COMPUTE     Defor Readings
4
8*(((((4>1.)-1.)/(4-1.))*.25)+((((4<1.)-1.)/(4-1.))*1.))     X CO  P#1
9*(((((6>1.)-1.)/(6-1.))*.20)+((((6<1.)-1.)/(6-1.))*1.))     X CO2 P#1
1*(((((2>1.)-1.)/(2-1.))*.20)+((((2<1.)-1.)/(2-1.))*1.))     X CO  P#2
15*(((((16>1.)-1.)/(16-1.))*.2)+((((16<1.)-1.)/(16-1.))*1.)) X CO2 P#2
DELAY       Time for gas to travel down exhaust stack to instruments
1
03  05  11  18  21  00  12.6 X
DELAY       Time for gas to travel from P#1 to instruments - New Defors
1
07  $1  $2  00  10.7  X
DELAY       Time for gas to travel from P#2 to instruments - Old Defors
1
$3  13  $4  00  11.4  X
TC
1
20 55 X
VELOCITY
1
18  49.74   Z  3  1  21  X
PRESSURE
1
10  0.121947  13.332 X
SMOOTH      Thermocouple Readings
23
31  00  5  X
32  00  5  X
33  00  5  X
34  00  5  X
35  00  5  X
36  00  5  X
37  00  5  X
38  00  5  X
39  00  5  X
40  00  5  X
41  00  5  X
42  00  5  X
43  00  5  X
44  00  5  X
45  00  5  X
46  00  5  X
47  00  5  X
48  00  5  X
49  00  5  X
50  00  5  X
51  00  5  X
52  00  5  X
53  00  5  X
MASS-FLOW-3   Calculate mass flow of gas in exhaust stack for HRR calculation
18 0.18 21 .9 1.0 22  X
HEAT-RATE     Calculate heat release rate from stack measurements
11 $28 1 5 1 3 0 1.105 13600 X
GAS-FLOW      Mass flow rate of CO through stack
1 22 'CO' X
3 18 21 0.18 28. X
COMPUTE     Yield of CO
1
```

```
$30/0.0035669 X Assumes fuel mass burning rate of 3.5669 g/s
INTEGRATE     Total CO Produced
1
$30 000 X
GAS-FLOW      Mass flow rate of CO2 through stack
1 22  'CO2' X
5 18 21 0.18 44. X
COMPUTE       Yield of CO2
1
$33/0.0035669 X Assumes fuel mass burning rate of 3.5669 g/s
INTEGRATE     Total CO2 produced
1
$33 000 X
INTEGRATE     Total heat released through the stack
1
$29 000 X
SPECIFY       Reuse total heat release channel
$36  X
COMPUTE       Convert the total heat release from kJ to MJ
1
$36 / 1000.0  X
HOT/COLD      Interface calculations based on FRONT thermocouple tree
1  1  1 .9652  X
31  32  33  34  35  36  37  38  39  40  41  42  43  44  45  46  47   X
.08  .24 .4 .44 .48 .52 .56 .6 .64 .68 .72 .76 .8 .84 .88 .92 .9652  X
HOT/COLD      Interface calculations based on REAR thermocouple tree
1  1  1  .9652  X
30     29     28     27     26     25     X
0.08   0.24   0.44   0.56   0.68   0.80  X
COMPUTE       The molar CO/CO2 ratios
3
$1 / $2   X   Compartment analyzers P#1
$3 / $4   X   Compartment analyzers P#2
3 / 5     X   Exhaust Stack analyzers
MASS-FLOW-2   At Burn Room Opening
0.4826  0.81026  0.9652  1  1  1  22 .0035669 .73 .001 X
$5 $6 $7 $8 $9 $10 $11 $12 $13 $14 $15 $16 $17 $18 $19 $20 $21 X
.06 .24 .40 .44 .48 .52 .56 .6 .64 .68 .72 .76 .8 .84 .88 .92 .9652  X
$22     $23     $24     $25     $26     $27  X
0.0762  0.2286  0.381  0.5334  0.6858  0.7875  X
COMPUTE   Global Equivalence Ratio
1
0.0035669 / ( .060242 * $48 ) X
MASS-FLOW     At Burn Room Opening
0.4826  0.81026  0.9652  1  1  1  10  0.0254  22 .68 .73 .001 X
$5 $6 $7 $8 $9 $10 $11 $12 $13 $14 $15 $16 $17 $18 $19 $20 $21 X
.06 .24 .40 .44 .48 .52 .56 .6 .64 .68 .72 .76 .8 .84 .88 .92 .9652  X
$22     $23     $24     $25     $26     $27  X
0.0762  0.2286  0.381  0.5334  0.6858  0.7875  X
22  X
COMPUTE       Point equivalence ratio calculated from phimeter data
1
1. + (.6683 - .2096)/(1. - 17/100.)*(7. + 17/100.)/(7. + .6683)/.2096*(1. + .143
*.6683 + .011*17/100.)/(1. + .143*17/100. + .011*.6683) - 17/100./.2096*(1. - .2
096)/(1. - 17/100.)  X
COMPUTE       Total of CO2 and CO combined
2
$1 + $2  X
$3 + $4  X
SMOOTH        Heat release rate
1
$29  00  5  X
RENAME
  $1   CORM1 CO  HI Ranges for Defor in room, upper layer P#1     (Vol %)
  $2   CO2RM1CO2 HI Ranges for Defor in room, upper layer P#1     (Vol %)
  $3   CORM2 CO  HI Ranges for Defor in room, upper layer P#2     (Vol %)
  $4   CO2RM2CO2 HI Ranges for Defor in room, upper layer P#2     (Vol %)
  $5   T08FS T/C    8 cm from floor Front smoothed              (Deg C)
  $6   T24FS T/C   24 cm     "          "                       (Deg C)
  $7   T40FS T/C   40 cm     "          "                       (Deg C)
  $8   T44FS T/C   44 cm     "          "                       (Deg C)
  $9   T48FS T/C   48 cm     "          "                       (Deg C)
  $10  T52FS T/C   52 cm     "          "                       (Deg C)
  $11  T56FS T/C   56 cm     "          "                       (Deg C)
  $12  T60FS T/C   60 cm     "          "                       (Deg C)
```

```
$13  T64FS T/C   64 cm    "        "          (Deg C)
$14  T68FS T/C   68 cm    "        "          (Deg C)
$15  T72FS T/C   72 cm    "        "          (Deg C)
$16  T76FS T/C   76 cm    "        "          (Deg C)
$17  T80FS T/C   80 cm    "        "          (Deg C)
$18  T84FS T/C   84 cm    "        "          (Deg C)
$19  T88FS T/C   88 cm    "        "          (Deg C)
$20  T92FS T/C   92 cm    "        "          (Deg C)
$21  T96FS T/C  96.5 cm   "        "          (Deg C)
$22  T07AD T/C  7.62 cm   "  Aspirated door smoothed    (Deg C)
$23  T22AD T/C 22.86 cm   "        "          (Deg C)
$24  T38AD T/C  38.1 cm   "        "          (Deg C)
$25  T53AD T/C 53.34 cm   "        "          (Deg C)
$26  T68AD T/C 68.58 cm   "        "          (Deg C)
$27  T78AD T/C 78.74 cm   "        "          (Deg C)
$28  MFLOW Mass flow rate of gas through stack          (kg/s)
$29  HRR  Heat release rate through stack               (kW)
$30  MFCO  Mass flow rate of CO through stack           (kg/s)
$31  YLDCO CO yield in stack                           (kg/kg)
$32  TOTCO Total CO produced                           (kg)
$33  MFCO2 Mass flow rate of CO2 through stack         (kg/s)
$34  YLDCO2CO2 yield in stack                          (kg/kg)
$35  TOTCO2Total CO2 produced                         (kg)
$37  TOTHRRTotal heat released through stack           (MJ)
$38  FrTCH Interface height based on rear TC tree      (m)
$39  FrTCUTTemperature above the neutral plane for rear TC tree (Deg C)
$40  FrTCLTTemperature below the neutral plane for rear TC tree (Deg C)
$41  RrTCH Interface height based on front TC tree     (m)
$42  RrTCUTTemperature above the neutral plane for front TC tree(Deg C)
$43  RrTCLTTemperature below the neutral plane for front TC tree(Deg C)
$44  RAT01 CO/CO2 ratio in the compartment P#1
$45  RAT02 CO/CO2 ratio in the compartment P#2
$46  RATEX CO/CO2 ratio in the exhaust stack
$47  DTCNP Door neutral plane height                   (m)
$48  DTCMI Flow into compartment                       (kg/s)
$49  DTCMO Flow out of compartment                     (kg/s)
$50  GLOEQ Global Equivalence Ratio
$51  DTCNPPDoor neutral plane height from pressure     (m)
$52  DTCMIPFlow into compartment from pressure         (kg/s)
$53  DTCMOPFlow out of compartment from pressure       (kg/s)
$54  PntEQ Point equivalence ratio
$55  CO2CO1CO2 + CO sum P#1                           (Vol %)
$56  CO2CO2CO2 + CO sum P#2                           (Vol %)
$57  SmHRR Smoothed heat release rate                 (kW)
                                        999
END
```

Appendix G. Run Operation Sheet

An operation sheet was completed for each burn. The location or position of the sample probes, thermocouple trees, and flashover tests were recorded. The flow rate data, both rotameter and diaphragm test meter, were recorded periodically throughout each burn. The example is from a 200 kW burn, Run RSE 9245, completed on January 21, 1992.

Reduced Scale ASTM Enclosure Burn Series

Fuel

TEST ID RSE 9245
Date 21JAN92

Estimated HRR 200 kWatts
Natural Gas 460 SCFH
Liquid _____ liters
_____ kg
Solid _____ kg
_____ kg

Humidity Wet 50.5°F
Dry 64 °F

Thermocouple Tree Location
Front 8 x 8 " E & S wall
Rear 8 x 8 " W & N wall

Sample Probe #1 Location
Thru wall
☒ Front ☐ Rear
☒ Left ☐ Right
☒ Inside ☐ Outside
4 " from ~~ft or~~ S wall
11.5 " from W ~~or E~~ wall
3.5 " from ceiling ~~or floor~~

Sample Probe #2 Location
☐ Front ☒ Rear
☒ Left ☐ Right
☒ Inside ☐ Outside
11.5 " from N ~~or S~~ wall
11.5 " from W ~~or E~~ wall
4 " from ceiling ~~or floor~~

Defors

Flashover Tests -
8.5" x 3" Paper
12 x 12 " E & S wall
Less Crumpled 8.5 x 11" (LC)
8 x 20 " W & S wall
More Crumpled 8.5 x 11" (MC)
12 x 16 " W & S wall

Time (min)	Comments	Gas Flowrates RM SCFH	DTM	Press psi	Vol ft3	Time sec	Chamber Top Temp C
0	DATA ON - BKGRND						21
1	PILOT ON						
3	GAS ON	460	10	13.5/13.4	5	54.8	23
	Videotaped						
6		470	7	13.8/13.8	5	55.2	26
10	2-3% O_2 thru wall probe	490	8	14.5/14.4	5	54.2	38
13		470	8	13.8/13.8	5	54.9	51
16		470	7	13.8/13.6	5	54.9	63
20	GAS OFF						80
21	PILOT OFF						
23	DATA OFF						

3:59 ○ LC ● MC 4:29

☐ pyrolized

Humidity Wet 51 °F
Dry 66 °F